WADC TECHNICAL REPORT 52-204
VOLUME I
SUPPLEMENT 1

AD0066250

HANDBOOK OF ACOUSTIC NOISE CONTROL

Volume I. Physical Acoustics

Supplement 1

EDITORS

STEPHEN J. LUKASIK

A. WILSON NOLLE

BOLT BERANEK AND NEWMAN INC.

WRIGHT AIR DEVELOPMENT CENTER

20020611094

$\mathcal{M}$

HANDBOOK OF ACOUSTIC NOISE CONTROL

Volume I. Physical Acoustics

Supplement 1

EDITORS

STEPHEN J. LUKASIK

A. WILSON NOLLE

BOLT BERANEK AND NEWMAN INC.

APRIL 1955

WRIGHT AIR DEVELOPMENT CENTER
AIR RESEARCH AND DEVELOPMENT COMMAND
UNITED STATES AIR FORCE
WRIGHT-PATTERSON AIR FORCE BASE, OHIO

FOREWORD

This report was prepared by the firm of Bolt Beranek and Newman Inc. under Contract No. AF 33(600)-23901 and supplemental agreement No. 1 for the Wright Air Development Center. The work was supported by funds available under RDO 695-63 "Vibration, Sonic and Mechanical Action on Air Force Personnel". Technical supervision of the preparation of the report was the responsibility of Major Horace O. Parrack, United States Air Force, Aero Medical Laboratory, Research Division, Wright Air Development Center, Wright-Patterson Air Force Base, Ohio.

WADC TR 52-204

ABSTRACT

The Handbook of Acoustic Noise Control is intended to provide an overall view of the problem of the control of acoustic noise. Since the publication of the first two volumes, the need for their revision has become apparent. In some cases, material has been added to enlarge the coverage of original sections. In others, sections have been completely re-written to present the latest experimental or theoretical information available.

With ever-increasing interest and activity in acoustic noise control, published procedures must, of necessity, lag behind the newest thinking in the field. There are few areas of the noise control problem where the present answers are the "best". As the operational requirements for noise control devices change and as new or more powerful sound sources appear in our advancing technology, better answers will have to be found. In presenting these revised sections, an attempt is being made to keep up with our expanding knowledge.

This supplement contains additions and revisions to Volume I which treated the generation and control of various types of noise sources. Similarly, Volume II, which analyzed the interaction between noise and man, is being supplemented. These supplements, together with the unchanged sections of Volumes I and II, provide a unified view of noise control problems.

PUBLICATION REVIEW

This report has been reviewed and is approved.

FOR THE COMMANDER:

JACK BOLLERUD
Colonel, USAF (MC)
Chief, Aero Medical Laboratory
Directorate of Research

TABLE OF CONTENTS

LIST OF ILLUSTRATIONS

INTRODUCTION

This section briefly describes the changes that have been made to Volume I WADC TR 52-204, Handbook of Acoustic Noise Control. The changes are essentially either of two basic types. In some cases, new sections have been added on subjects not covered in Volume I. More often, however, the new sections reflect changes in theory or practice which made a reorganization of the material desirable. In one case, the new material was of a somewhat different nature and was simply appended to the existing section. These changes are detailed below to aid the reader in recognizing the relative status of the old and new section. It will be noted that the revision has proceded on a section-by-section basis. This has necessitated certain changes in the figure and equation numbering conventions which are also indicated below.

All of Chapter 4 has been revised although the bulk of the changes are in Sec. 4.1 which makes up the main part of the chapter. The discussion of propeller noise has been reorganized around the existing theory. Both rotational noise and vortex noise have been treated and N. A. C. A. charts constructed from the Gutin theory are given. The design procedure based on the empirical PWL chart is essentially unchanged although its extension to other than three blade propellers involves a somewhat greater uncertainty than indicated in the original section. Chiefly, the empirical chart works in the transonic and supersonic tip speeds where available theory is not as well developed. Also, the two spectrum charts have been replaced by a single curve which is similar to the transonic tip speed case of the original section.

Section 6.3a adds to the empirical information on axial flow compressors presented in Sec. 6.3 The new section discusses the physical principles involved in noise generation by an axial flow compressor. It contains a short statement of the theoretical results to date and illustrates them with a calculation of the absolute sound pressure level for a compressor of given operating conditions. The previous empirical design procedure is still applicable. Nothing new is presented on centrifugal compressors.

Section 6.5 on ventilating fans and noise from ventilating systems is new. There is no section in Volume I to which it corresponds.

The sections on wall construction and floating floors in Volume I have been greatly expanded and reorganized around existing theory. However, the original sections are still correct in what they say and they form a good introduction to the more detailed discussion of the revised Secs. 11.2 and 11.3. In particular, Sec. 11.3 on the Insulation of Impact Sound corresponds only roughly to the original Sec. 11.3 dealing with floating floors. The original section has more architectural details which may be useful to the reader.

The new section on the transmission of sound through cylindrical shells is intended to replace completely the original section in Volume I. Research in this field is continuing, however, and more experimental and theoretical information may be expected in the future.

Section 12.1 on the specification of sound absorptive properties of materials is new. It replaces the very short introductory section in Vol. I which simply listed several topics to be discussed in connection with the control of airborne sound.

The section on the attenuation of sound in lined ducts (Sec. 12.2) has been greatly expanded. Several different theoretical procedures for calculating the attenuation, each of various degrees of accuracy and usefulness are presented, and all the available empirical information is summarized. A tabular summary of the various procedures is given. This revised section is intended to replace the original section in Volume I completely.

Section 12.6a discusses the use of acoustic resonators in free space. Since the original section discussed resonators attached to ducts, the subject matter of the old and new sections are complementary rather than overlapping.

Finally, Section 12.9 presents a new design procedure for the prediction of acoustic shielding by an obstacle. Although it is based on the same diffraction theory as the original section, several modifications found necessary in actual practice have been introduced.

Because the total number of equations, figures, etc. in each revised section do not, in general, equal the corresponding number in the section replaced, a new identification scheme has been used. Previously equations, figures, tables and references were numbered consecutively through a chapter and were identified by chapter and/or a serial number. Now all identification numbers refer to both chapter and section in addition to a serial number. For example, the fifth equation in Ch. 12, occurring say in Sec. 2 is now numbered Eq. (12.2.5) while previously it would be numbered simply Eq. (12.5). References, instead of being a single number, such as Ref. (7) now contain a section identification also; the fourth reference is Sec.11.5 and is now numbered (5.4). Finally, a letter a following a section designation indicates that the section does not replace the previous section, but merely supplements it, e.g., Sec. 12.6a. Figure, equation, table and reference numbers then contain the letter also, e.g., Fig. 12.6a.5.

A list of errata to Volume I is given at the end of this volume.

CHAPTER 4

AIRCRAFT PROPELLERS AND RECIPROCATING ENGINES

4.1 Propeller Noise

Introduction. The propeller, rather than the engine, is the chief source of noise in the usual reciprocating-engine aircraft of 200 horsepower or more. For this reason, considerable work has been done toward explaining the action of this important noise source. The problem has not as yet been treated rigorously from a theoretical standpoint, but the approximate analysis which has been done has proved satisfactory for engineering purposes in the case of propellers operating at subsonic blade speeds and not too close to obstacles. Also, the approximate analysis shows clearly the role played by the various parameters which are important in propeller noise generation, including particularly horsepower, thrust, tip speed, diameter, and number of blades. The results of this analysis are given here. Measurements are cited and comparisons between theory and experiment are shown where possible. Equations and charts for engineering calculations are given. Their use is explained in a numerical example at the end of the section.

Gutin's Theory of Rotational Propeller Noise. A rotating propeller blade at constant speed carries with it a steady pressure distribution. Hence, any non-axial point, fixed in space with reference to the aircraft, experiences a periodic pressure variation, generally of complex wave form, always having the blade passage frequency as the fundamental. This periodic pressure variation is an acoustic disturbance, and is known as the rotational noise. For points lying in, or very nearly in, the volume swept out by the propeller blades, and for cases where there is negligible overlap of the pressure distributions of adjacent blades, the pressure disturbance due to a multiple-blade propeller can be approximated simply as a repetition, at the appropriate frequency, of the disturbance due to the passage of an isolated blade. (In other words, for such near points, the pressure disturbance at a given time is due to the nearest blade, the influence of the more distant blades being negligible.) To this approximation, the acoustic disturbance very near the propeller can be simply expressed, and the disturbance at more distant points can then be calculated by integrating the signal propagated from all regions near the propeller. To facilitate this calculation, the disturbance is considered to radiate from a zero-thickness disk in the region swept out by the propeller. This

is the basis for Gutin's analysis of the rotational pro-
peller noise 1.1/. The Gutin analysis does not consider
nonperiodic disturbances (principally vortex noise), which
are produced by an actual propeller along with the periodic
rotational noise. These will be considered later. The
analysis assumes that the forward speed of the propeller is
small compared to the speed of sound.

Gutin's analysis proceeds by writing expressions for
the reaction on the air of the time-dependent thrust and
drag forces due to a single rotating propeller blade. These
forces are then expressed as a Fourier series; the funda-
mental frequency is the blade passage frequency $n\alpha$ where n
is the number of blades in the propeller and α is the
rotational frequency in radians/sec. The force exerted on
the air by a rotating blade also depends on the thrust dis-
tribution along the blade. In the Fourier expansion, the
sine function is approximated by its argument $mn\alpha t$ where m
is the harmonic number and t is the time. This is justified
provided that the discussion is restricted to a suitably
small value of the product of number of blades and of har-
monic number, and provided that the portions of the blade
near the hub (which produce a relatively small part of the
air forces) are ignored. Gutin also shows that his
expressions, which are in no case valid for high harmonics,
are correct when the air forces are not uniformly distributed
over the width of the blade.

Expressions for the aerodynamic disturbance in the
propeller disk having now been established, the next step
is to compute the resultant acoustic effect at external
points. The coordinates shown in Fig. 4.1.1 are used.
From hydrodynamics, we can immediately write the velocity
potential $\emptyset$ for the resultant sound field from the known
forces acting on the air due to the rotating propeller
blade 1.2/. The sound pressure is the time derivitive of
the velocity potential. That is, for an air density ρ,
the sound pressure p is $\rho d\emptyset/dt$. While this gives the
desired acoustic solution in principle, some simplifica-
tions are desirable for ease in calculation. Gutin
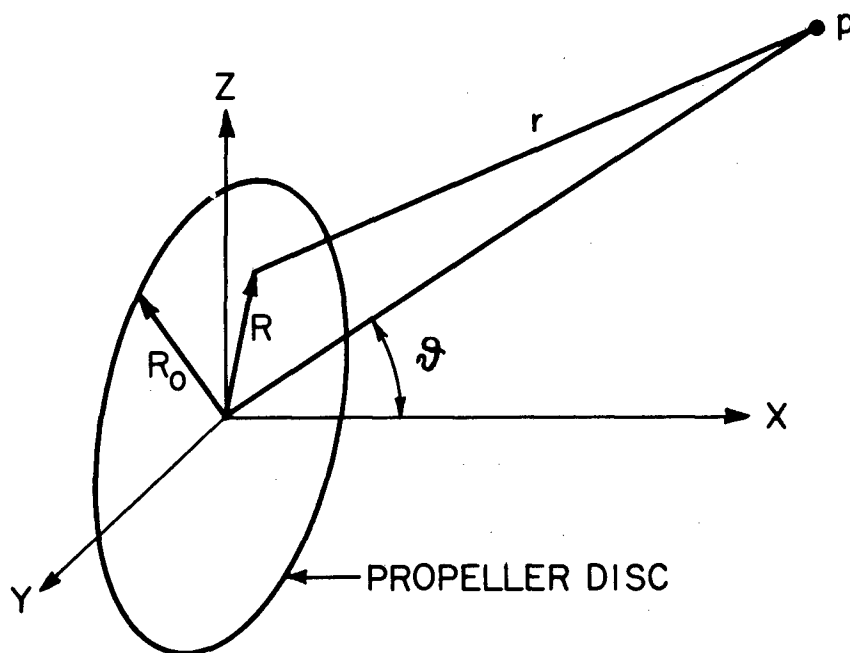
FIGURE 4.1.1

Coordinate systems used in calculation of noise
radiated by a propeller.

---

restricts the point of observation to the xy plane, with-
out loss of generality, and also restricts r to values
much greater than the propeller diameter. The latter
stipulation will make the succeeding work inapplicable to
the near field, so that the results under this restriction
will not apply to noise levels within the aircraft itself.

WADC TR 52-204   3

It is desirable to put the result in a form which does not demand detailed knowledge of the distribution of thrust and torque along the blade. This is achieved approximately by considering the total thrust P and the total torque M to act at effective mean radii R_1 and R_2 respectively. The sound pressure becomes

$$p = \frac{m\omega_1}{2\pi cr} [-P \cos \nu J_{mn}(kR_1 \sin \nu) + \frac{ncM}{\omega_1 R_2^2} J_{mn}(kR_2 \sin \nu)] .$$

$$(4.1.1)$$

The radian fundamental frequency is ω_1, c is the velocity of sound, J_{mn} is the Bessel function of order mn and $k = \omega/c$ where ω is the frequency of the m th harmonic of ω_1. Gutin further shows that, for the lower harmonics produced by propellers having a "small" number of blades, both R_1 and R_2 are approximately equal to R_c, the radius corresponding to the point of resultant thrust for a single blade, which is of the order of 0.7 or 0.8 of the propeller radius R_o. This leads to the final simplified result,

$$p = \frac{m\omega_1}{2\pi cr} [- P \cos \nu + \frac{ncM}{\omega_1 R_c^2} J_{mn} (kR_c \sin \nu)]$$

$$(4.1.2)$$

This expression is a sum of two terms, the first of which is the thrust term, and the second of which is the torque term. The torque is proportional to the input power, W, through the relation

$$W = M \alpha \qquad (4.1.3)$$
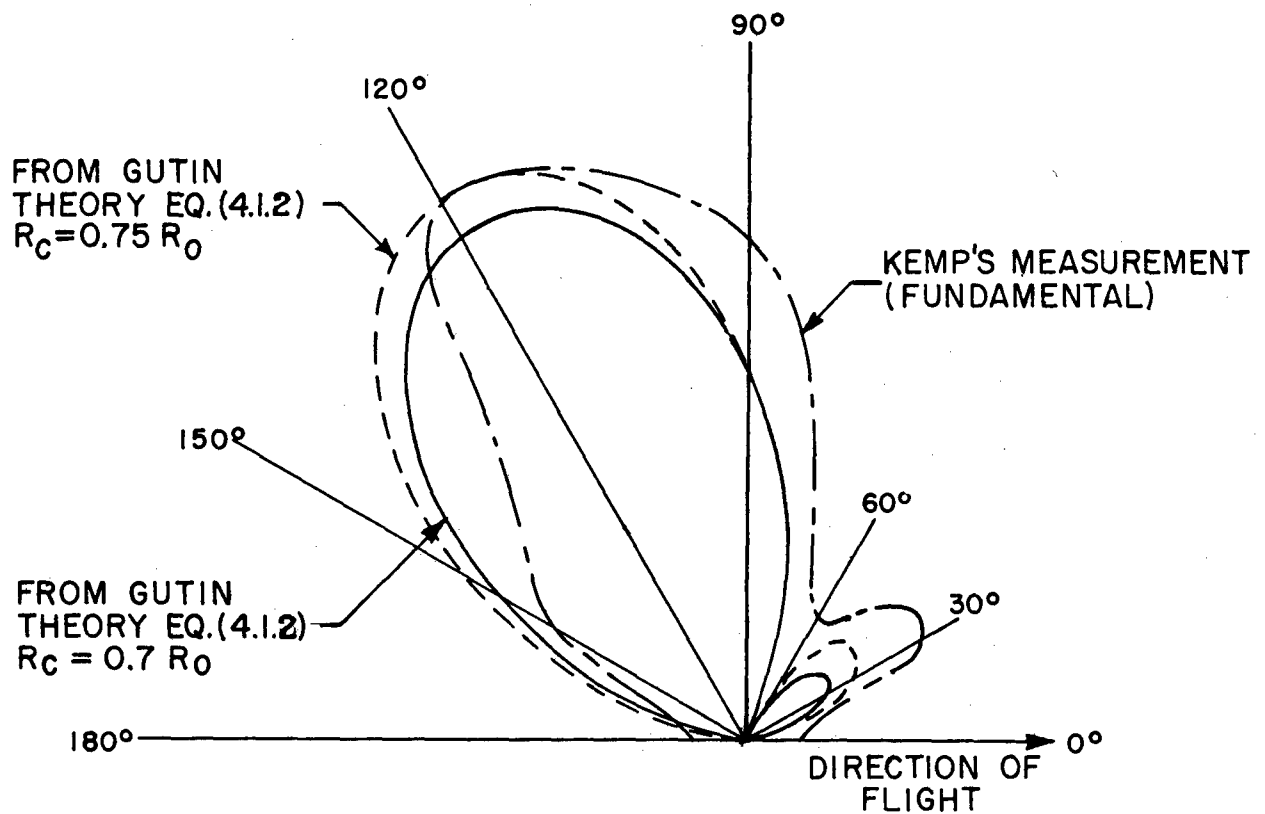
Figure 4.2.1

Calculated and measured distributions of fundamental-frequency sound pressure from a propeller. The measurements are by Kemp 1.4/. The calculations are from the Gutin equation (4.1.2), for values of R_c equal to 0.7 R_o and to 0.75 R_o.
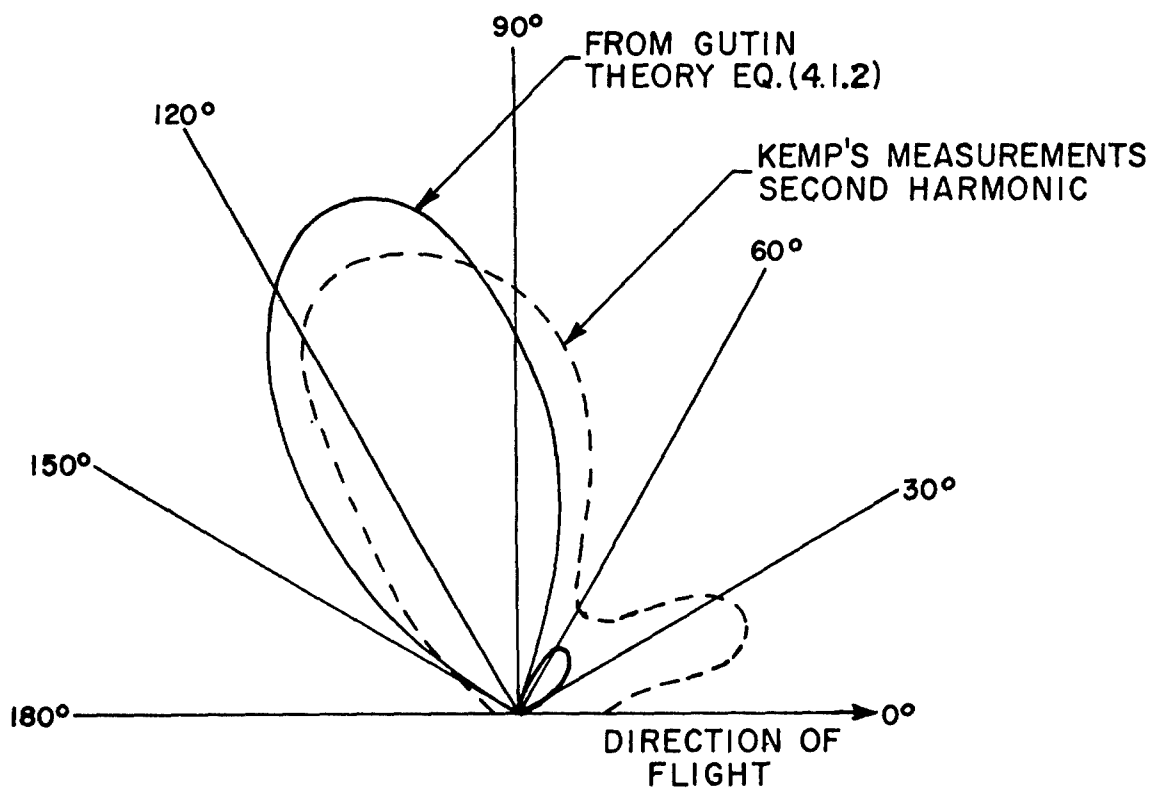
FIGURE 4.1.3

Calculated and measured distributions of second-harmonic sound pressure from a propeller. The measurements are by Kemp 1.4/. The calculations are from the Gutin equation, (4.1.2), with $R_c = 0.75\ R_o$

The thrust P is related to the input power by an aerodynamic relation which Gutin gives in the form

$$P = (2\rho S W^2 \eta^2)^{1/3} \qquad (4.1.4)$$

where S is the area of the propeller disk and η is an efficiency factor estimated to equal about 0.75.

Gutin calculated the expected polar distribution of radiated sound for the first two harmonics, for the following situation: Two-blade propeller, radius 2.25 meters, 1690 kg thrust, 515 kgm torque, 13.9 rev/sec. The results were compared with experimental data for this situation as taken by Paris 1.3/ and by Kemp 1.4/, with values of both 0.7 and 0.75 being tried for R_c/R_o. The comparison with the Kemp results is shown in Figs. 4.1.2 and 4.1.3. The agreement is fair for the fundamental, but appears to deteriorate for higher harmonics. This would be expected from the nature of the assumptions made in the derivation. Fortunately, the fundamental usually constitutes the greatest single contribution to the sound output. Gutin's calculations showed slightly better agreement with the Paris data (fundamental only).

The general features of the polar patterns in Figs. 4.1.2 and 4.1.3 are found in virtually all cases of noise generation by a propeller free of obstacles. The torque term results in an acoustic pressure pattern which is zero on the propeller axis and maximum in the propeller plane. The thrust term results in an acoustic pressure which is somewhat smaller than the maximum torque contribution (this need not always be true), and which is zero in the plane of the propeller as well as on the axis. The two contributions are out of phase for positions in front of the propeller, but in phase for positions to the rear. The combined effect of the two terms is a radiation pattern having symmetry of rotation, which is zero on the propeller axis and which is maximum at a position some 15° behind the propeller plane.

N.A.C.A. Propeller Noise Charts Based on Gutin's Equation. No propeller noise analysis is available which does not include at least some of the approximations made by Gutin. Fortunately, the simplified Gutin relation,

Eq. (4.1.2), seems to give the maximum overall sound pressure in the far field of a propeller to an accuracy sufficient for the usual requirements of noise-control engineering, at least for those propellers operating at subsonic tip speeds which are currently in use.

A convenient set of propeller-noise charts has been computed from the Gutin relation by Hubbard 1.5/ under the auspices of the N.A.C.A. These are reproduced in part in Figs. 4.1.4 through 4.1.9. The independent variables are input horsepower, propeller diameter, number of blades, and rate of rotation or Mach number of the blade tip. The result is read from the charts as sound pressure level at a distance of 300 feet, at a position 105° removed from the forward propeller axis (approximately the position of maximum sound pressure in ordinary cases). The sound pressure contributions from the first four harmonics have been added on an energy basis to give this result; hence, the values obtained are closely representative of overall sound pressure level, since ordinarily the contributions of the higher harmonics drop off rapidly.

Analysis of a typical propeller radiation pattern shows that the sound pressure level in the direction of maximum output is about five db above the space-average value. Hence, 5 db should be subtracted from the chart values to obtain the space-average sound pressure level at a distance of 300 ft. Adding 55 db to the N.A.C.A. chart values gives approximately the power level of the propeller as a noise source.

The Gutin result is found in the N.A.C.A. publications by Hubbard 1.5/ and others in the form and symbols of Eq. (4.1.5). This is adapted to simple engineering computation.

$$p = \frac{169.3 m B D M_t}{2sA} \left[\frac{P_H}{c(0.8M_t)^2} - T \cos \beta \right] J_{mB}(0.8mBM_t \sin \beta).$$

$$(4.1.5)$$
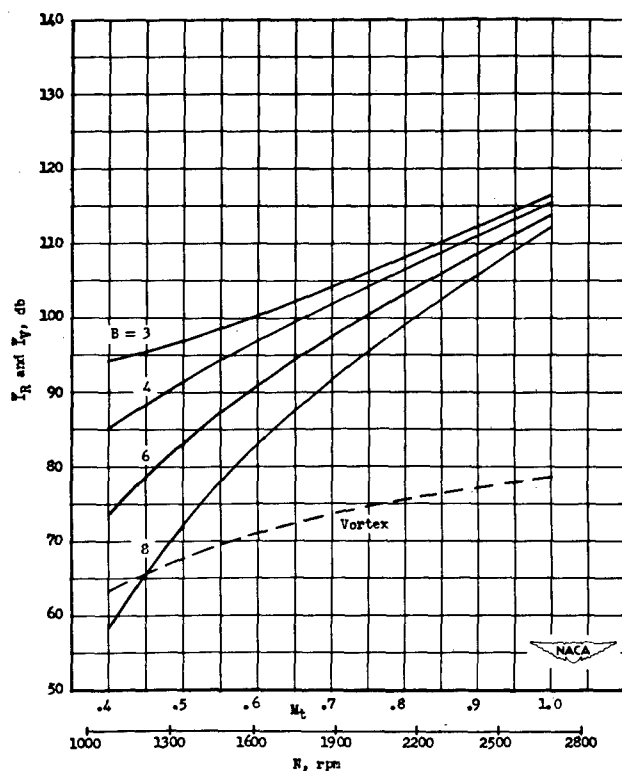
D = 8 ft   Propeller Diameter   D = 12 ft
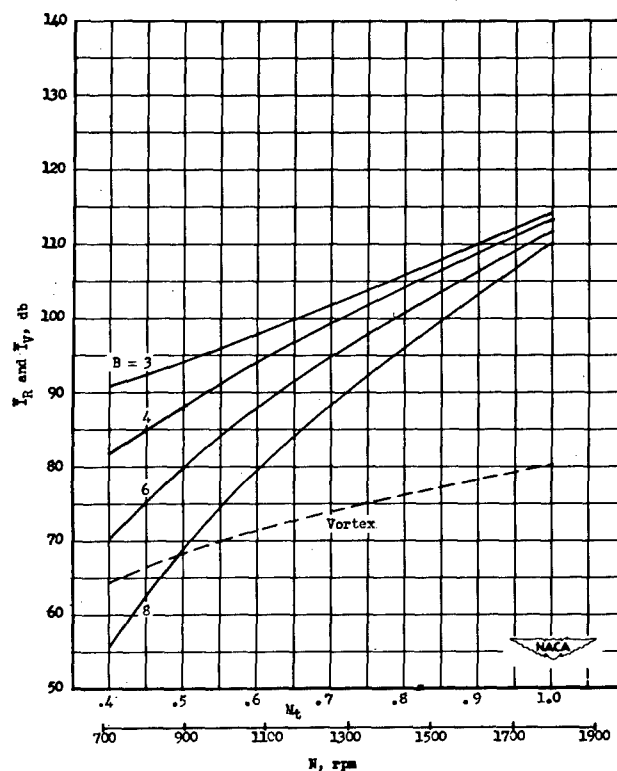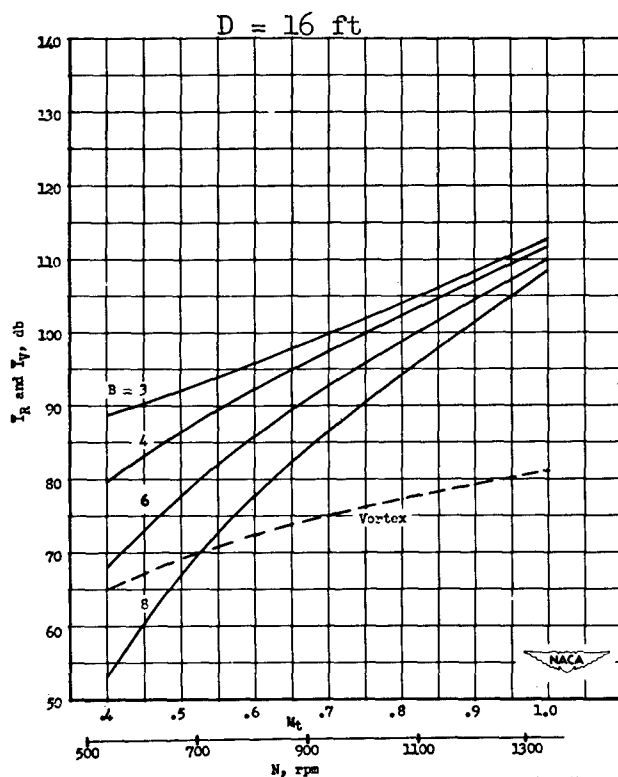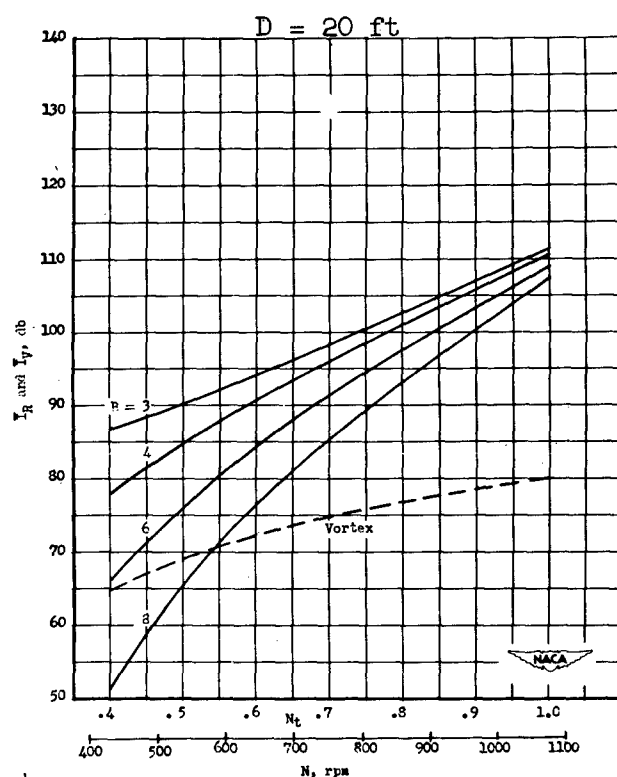
D = 16 ft   D = 20 ft

FIGURE 4.1.4

Overall rotational propeller sound pressure level, at 1000 horsepower input, as a function of tip Mach number and number of blades, for various propeller diameters (solid-line curves). The values are for 300 ft distance, in a direction 105° from the forward axis. To obtain the approximate acoustic power level of the propeller add 55 db to the result. The broken-line curves are estimated levels due to vortex noise. From Ref. (1.5).

Propeller Diameter

D = 8 ft

D = 12 ft

D = 16 ft

D = 20 ft

FIGURE 4.1.5

Same as Fig. 4.1.4, but for 2000 horsepower input.

Propeller Diameter
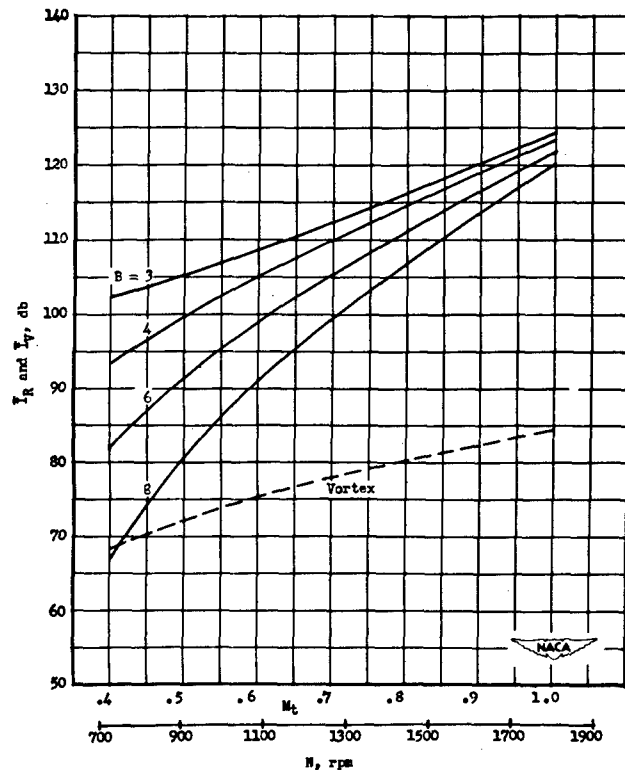
D = 8 ft

D = 12 ft

D = 16 ft

D = 20 ft

FIGURE 4.1.6

Same as Fig. 4.1.4, but for 4000 horsepower input.

Propeller Diameter
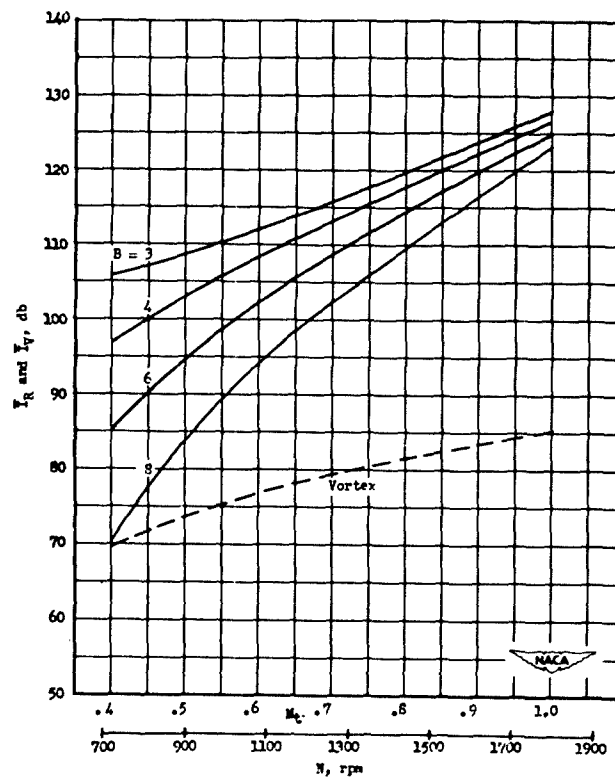
D = 8 ft

D = 12 ft

D = 16 ft

D = 20 ft

FIGURE 4.1.7

Same as Fig. 4.1.4, but for 6000 horsepower input.

Propeller Diameter
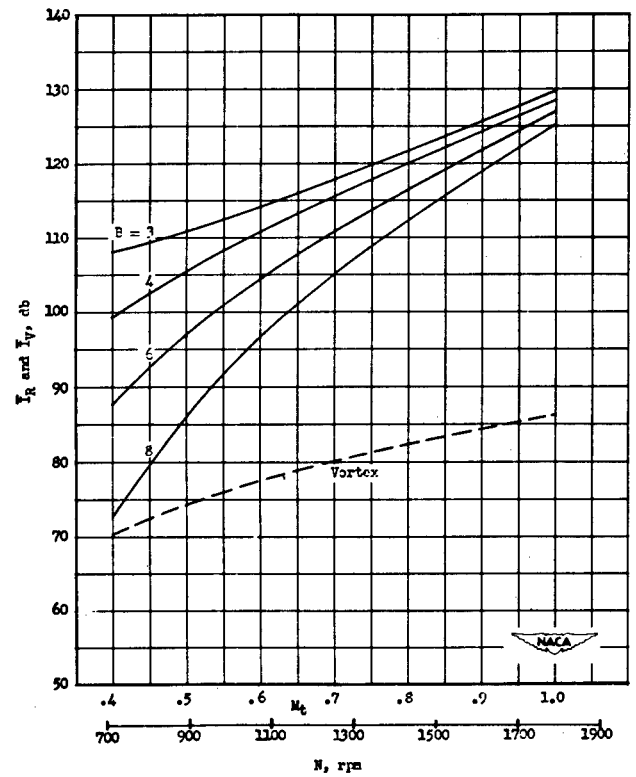
D = 8 ft

D = 12 ft

D = 16 ft

D = 20 ft

FIGURE 4.1.8

Same as Fig. 4.1.4, but for 8000 horsepower input.

Propeller Diameter

D = 8 ft D = 12 ft
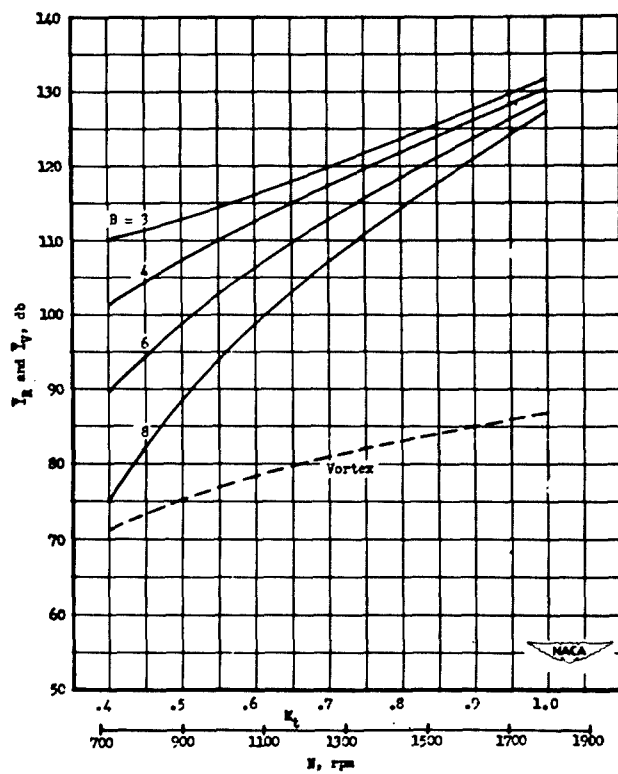
D = 16 ft D = 20 ft

FIGURE 4.1.9

Same as Fig. 4.1.4, but for 10,000 horsepower input.

Here m is the harmonic number; B, number of blades; D, propeller diameter, ft; M_t, tip Mach number; s, distance from propeller hub to observer, ft; A, propeller disk area, sq ft; P_H, input horsepower; T, thrust in pounds; β, angle between forward propeller axis and line of observations. The effective radius has been taken as 0.8 of the total.

In Hubbard's calculations, the thrust is derived from the input horsepower by a relation equivalent to the one used by Gutin, Eq. (4.1.4), except that a revised value of the constant gives thrust values which are 0.78 of those computed by Gutin's procedure. The procedure used by Hubbard is said to be approximately correct for propellers operating near the stall condition.

The sound pressure levels given in the N. A. C. A. charts include an estimated contribution from the non-periodic vortex noise, which ordinarily constitutes a small portion of the total propeller noise power. The basis for calculation of the vortex noise will be discussed later. The broken lines in the charts indicate the estimated levels of vortex noise only.

Effect of Number and Shape of Blades on the Rotational Noise. Two of the most important parameters which can be altered in the propeller with a certain amount of flexibility are the number and shape of the blades. It is readily visualized that the number of the blades determines the frequency of the fundamental blade passage tone. On the other hand, it can be shown that the intensity of the sound will decrease as the number of blades is increased.

A qualitative explanation for the reduction of sound output by an increase of the number of blades can be given on the basis of the phase cancellation of the several component forces. A simple example is given by the generation
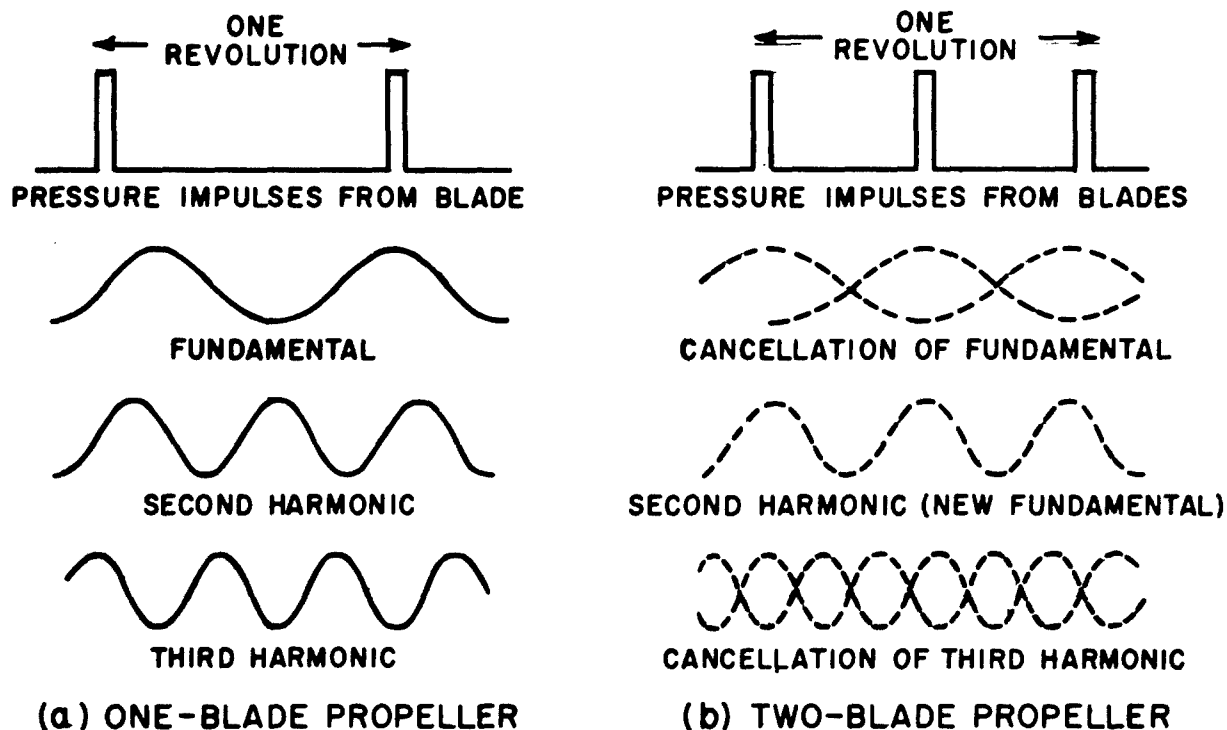
FIGURE 4.1.10

Illustration of the acoustic pressure components
developed by a one-blade propeller, and of the cancella-
tion of the odd harmonics of the original signal when
a second blade is added.

of sound by a propeller consisting of one blade only. The corresponding aerodynamic force is shown in Fig. 4.1.10. In that figure the Fourier components have also been represented (not to scale). In Figure 4.1.10 the case of a two-blade propeller is considered. The Fourier components of the force shown in this figure indicate that the odd harmonics (with reference to the original one-blade propeller) cancel, while the even harmonics are reinforced. A quantitative calculation shows that the net effect, however, is an overall decrease in the sound intensity. For the special case in which the tip speed, the thrust, and the input horsepower are kept constant, while the blades are redesigned and increased in number, the acoustic effect can be seen directly from Eq. (4.1.5). The quantity which varies is mB [J_{mB} (0.8mBM_t sin β)]. Examination of tables of Bessel functions shows that, for typical values of the variables, this quantity decreases rapidly as mB increases.

The effect of the blade width can be particularly important for the higher harmonics. In the Gutin approximation, the force produced in the propeller plane by the passage of an individual blade is treated as an impulse. This is equivalent to assigning the propeller blade a negligible width. Regier 1.6/ has evaluated the spectrum distribution corresponding to several more nearly realistic force-time characteristics, as shown in Fig. 4.1.11. All of these distributions have equal areas under the curves, and thus exert equal forces on the propeller. The horizontal line for the zero-width blade corresponds to the uniform Fourier amplitudes in the Gutin approximation; the other curves show the new distributions which replace this one in the case of finite blade width. It is apparent that increasing the width of the blade, while the thrust is kept constant, decreases the intensity of the radiated sound through reductions in the amplitudes of the higher harmonics.

The role played by the number and kind of blades in the total noise radiated by a propeller is illustrated in a series of experiments by Beranek, Elwell, Roberts, and Taylor 1.7/. The experiments consisted in measuring the noise radiated in flight, by certain aircraft of less than 200 horsepower, for propellers of two, three, four, and six blades. The propellers exerted approximately
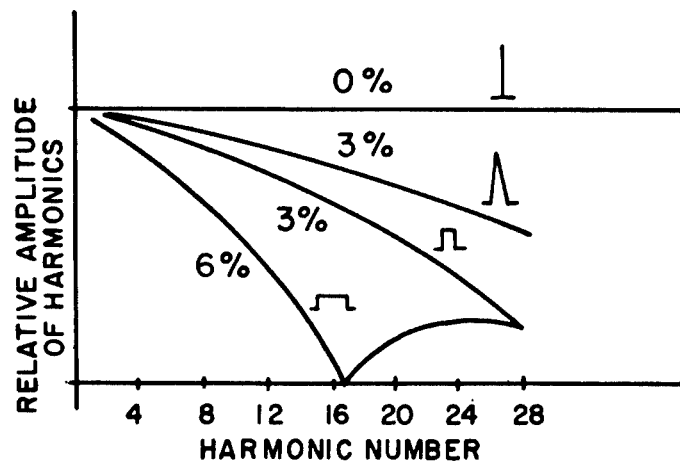
FIGURE 4.1.11

Effect of the shape of the force distribution
around a propeller blade on the harmonic content
of propeller rotational noise (for points near the
propeller plane). All distributions have the
same area. The number refers to the duration of
the pulse as a percentage of the time for a full
revolution.

equal thrusts and were of nearly the same diameter. The results may be summarized approximately by the statement that the intensity if lowered 6 db for each doubling of the number of blades in the propeller, the input power and the speed of rotation remaining fixed.

Hicks and Hubbard 1.8/ measured the noise from small propellers of two, four, and seven blades under controlled conditions, and compared the measured sound levels with calculations from the Gutin equation. A selection of typical results is given in Table 4.1.1. The sound pressure levels refer to a point 30 ft from the propeller hub, in open air, in a direction 105° from the forward propeller axis. The blade angle is 16.5°.

TABLE 4.1.1

MEASURED SOUND PRESSURE LEVELS FROM 4-FOOT DIAMETER PROPELLERS AND CALCULATED LEVELS FROM THE GUTIN EQUATION - REFERENCE 1.8

Number of Blades	Tip Mach Number	Input Horse-power	SPL by Wave Analyzer Method	Overall SPL by Wide-Band Measure-ment	SPL of Rotational Noise, from Gutin Equation
			db	db	db
2	0.3	3.5	79.6	85.8	83.8
	.5	20.5	95.9	95.9	98.0
	.7	65.8	111.4	110.4	111.1
	.9	148.2	123.4	121.6	123.0
4	0.3	6.0	75.8	81.9	65.8
	.5	34.2	94.3	96.9	90.9
	.7	110.0	110.6	111.5	110.5
	.8	167.8	116.8	116.4	---
7	0.3	10.7	68.8	78.3	38.4
	.5	53.0	85.0	89.9	80.9
	.64	124.0	99.2	100.0	98.6

The results by the wave analyzer method refer to the square root of the sum of the squares of the amplitudes for the first five harmonics of the blade passage frequency. This method therefore measures the level of the periodic rotational noise, provided that the effect of other noise components falling within the pass band of the wave analyzer (25 cps) is negligible. The calculated values represent the square root of the sum of the squares of the individual calculated amplitudes for the first five harmonics.

For each propeller, the SPL measured by the wave analyzer method and that measured by the wide-band method in the range of Mach numbers above about 0.6, are both closely equal to the value predicted by the Gutin theory. This means that the noise at the higher Mach numbers is almost entirely of the rotational type, and that its overall level under these conditions is adequately predicted by Gutin's equation. Thus, as far as operation at the higher Mach numbers is concerned, theory and experiment agree as to the amount of reduction in noise level which is obtained by increasing the number of propeller blades and reducing the tip speed. For example, in Ref. 1.8 it is found that for a tip Mach number of 0.7, 66 horsepower can be absorbed by the 2-blade propeller with a 16.5° attack angle, and 76 horsepower by the 7-blade propeller with a 10° attack angle. Although the horsepower is nearly the same, the second configuration gives a wide-band sound pressure level of 101 db, as compared to 110 db for the first. The calculated values are 100 db and 111 db.

In the results for each propeller configuration in Table 4.1.1, the overall SPL at the lower Mach numbers is greater than the SPL by the wave analyzer method, which is in turn greater than the calculated value from the Gutin equation. These effects are explained at least partially by the additional observation that the sound at the lower Mach numbers consists mostly of

nonperiodic vortex noise rather than periodic rotational noise. In the theory of vortex noise, which is discussed at the end of this section, it is shown that this should occur, because vortex noise decreases less rapidly than rotational noise as the tip speed is reduced. The data in Ref. 1.8 do not show conclusively whether or not the Gutin theory remains approximately correct for rotational noise alone at the lower Mach numbers, since it is not certain at what point the wave analyzer results begin to represent vortex noise. These experiments seem to show, however, that the Gutin equation predicts overall propeller noise to adequate engineering accuracy under those operating conditions where rotational noise is dominant.

Deming's Extension of the Gutin Theory. Deming 1.9/ attempted to improve upon the Gutin approximations by including the finite thickness of the propeller blades in the analysis, and by introducing the concept of distributed aerodynamic forces, instead of assuming the force concentrated at one value of the radius. It was hoped that considering the finite thickness of the blades would improve the accuracy of the calculations for the higher harmonics, for which the assumption that the propeller thickness is much less than the wavelength of the radiated sound is not justified. Deming also performed a careful series of experiments. It was found that the particular improvements which he had made in the Gutin theory did not yield results appreciably different from Gutin's, but that the experimental work showed a greater disagreement with the theory than Gutin had originally suggested. Figure 4.1.13 shows a comparison between Gutin's and Deming's calculations, together with Deming's measurements.

The Effect of Forward Speed upon Propeller Rotational Noise. The Gutin equation must be modified, when it is desired to find the noise radiated by a propeller moving forward in the air, to take into account the fact that the forward speed· alters the effective acoustic path length from an element in the propeller disk to the point of observation. Garrick and Watkins 1.10/ have worked out the necessary changes in the theory. Their result for the

far field is given in Eq. (4.1.6). The point of observation remains in a fixed position relative to the moving propeller.

$$p = \frac{m\omega_1}{2\pi c\sqrt{x^2+\beta^2 y^2}}\left[T\left(M + \frac{x}{\sqrt{x^2+\beta^2 y^2}}\right)\frac{1}{\beta^2} - Q\frac{Bc}{\omega_1 R_c^2}\right]J_{mB}\left(\frac{m\omega_1 y R_c}{x\sqrt{x^2+\beta^2 y^2}}\right)$$

$$(4.1.6)$$

In this equa..ion, m is the harmonic number; ω_1, fundamental frequency in radians/sec; c, speed of sound; β denotes $\sqrt{1 - M^2}$; M, Mach number for forward speed; T, thrust; Q, torque; B, number of blades; R_c, effective blade radius; x,y, coordinates as in Fig. 4.1.1. Setting β equal to unity gives a result equivalent to Eq. (4.1.2) or Eq. (4.1.5) for a statically operated propeller.

It is found from Eq. (4.1.6) that the effect of increasing the forward speed, for a propeller operating at constant thrust, is to increase the noise output and to alter the directional distribution in a somewhat complicated fashion. Garrick and Watkins also give equations for computing the near field of the propeller with forward speed.

The effect of increasing the forward speed under conditions of constant thrust corresponds to a hypothetical case which is of less practical interest than the effect of increasing the forward speed and allowing the thrust to decrease in the manner of an actual propeller. Apparently this decrease of thrust will usually cause the noise of an actual propeller to decrease with increasing forward

---

FIGURE 4.1.12

Comparison of observed sound pressure distribution around a propeller with Gutin's and Deming's theories. Measured distribution, _____; Gutin's prediction -----; Deming's modified result, __ _ __ _. Part A, fundamental frequency; Part B, second harmonic; Part C, third harmonic; Part D, fourth harmonic .

FIRST HARMONIC
(A)

SECOND HARMONIC
(B)

THIRD HARMONIC
(C)

FOURTH HARMONIC
(D)
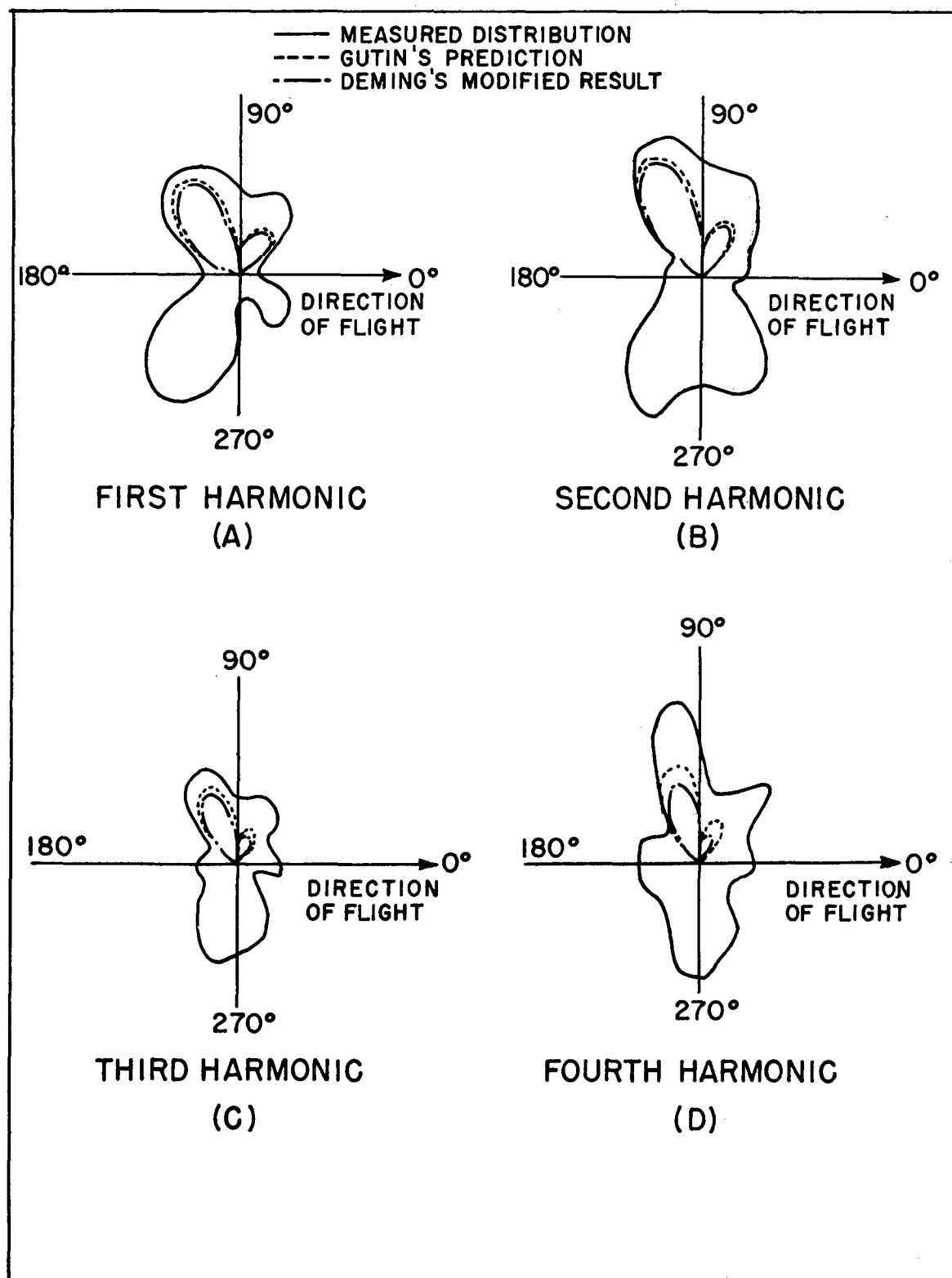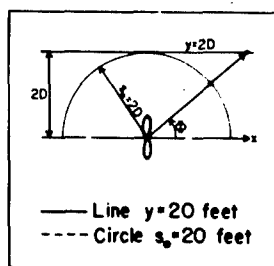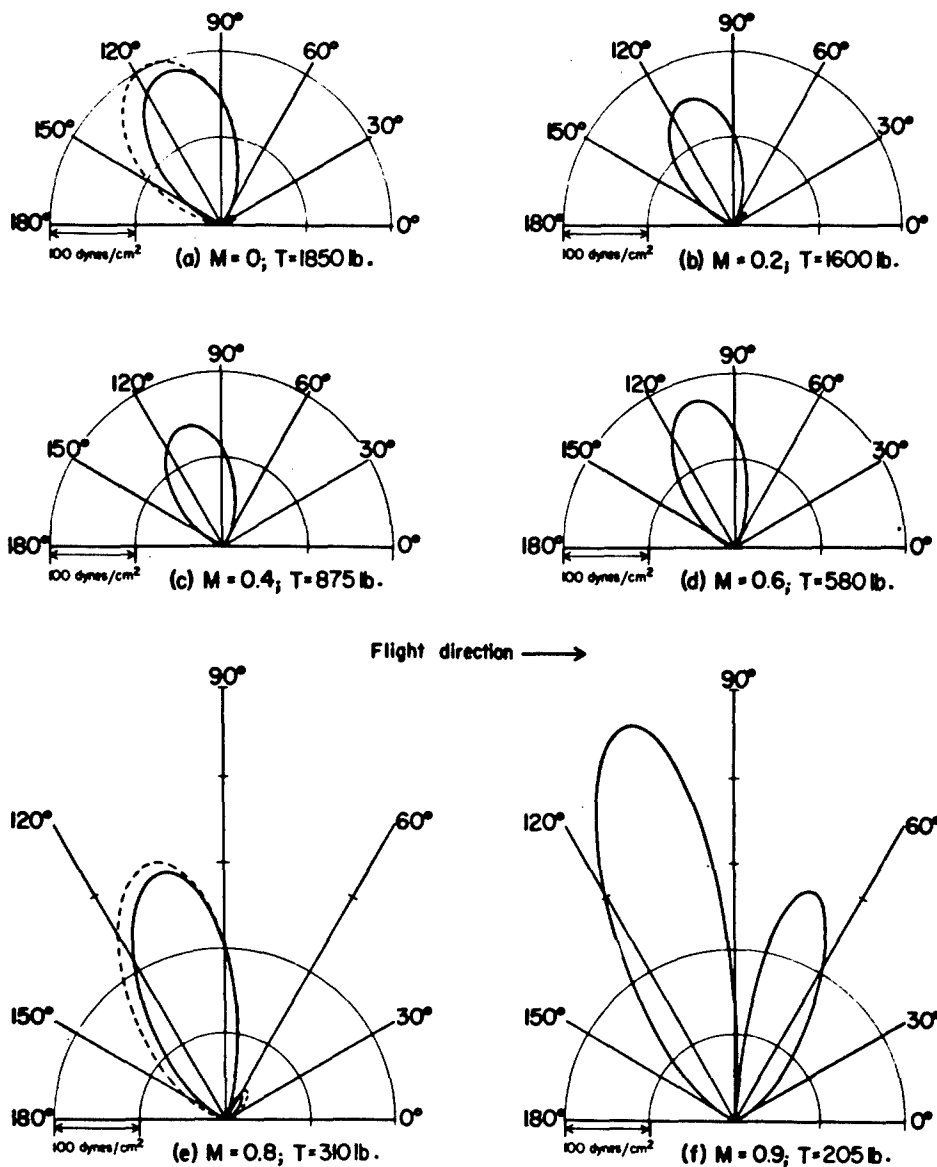
FIGURE 4.1.13

Polar diagrams of the distribution of rms sound pressure for a 2-blade,
10-foot diameter propeller, for various values of forward-speed Mach
number, M. Solid lines, values along a line 20 ft from the axis and
parallel to it. Broken lines, true polar patterns at constant radial
distance of 20 ft. The blade angle is always adjusted so that the input
is 815 horsepower at a torque of 2680 lb-ft. The thrust values are
shown in the figure. From Ref. 1.10.

speed up to Mach numbers of about 0.4. Garrick and Watkins have calculated the noise output of a two-blade propeller for various forward speeds, with the thrust values taken from actual aerodynamic measurements. The results are shown in Fig. 4.1.13. The initial drop of noise output as the forward speed increases is confirmed in a measurement by Regier 1.11/, who found that the overall noise developed by a light trainer airplane in normal flight is 6 db less than that produced by the same airplane in static ground operation.

As a practical matter, the distinction between the Gutin relation and the modified equation for the case of forward flight, Eq. (4.1.6), may be neglected for forward speeds up to $M = 0.3$. At this speed, the value of β has dropped only to 0.95, from the value 1.00 corresponding to static operation. Therefore, within this range, the effect of forward speed may be represented adequately by making the appropriate changes in the thrust value used in the original Gutin approximation.

Noise Levels Very Near a Propeller. Calculation of the noise levels near a propeller by Gutin's method requires that some of the convenient geometric approximations be omitted and that more complicated integrations be carried out. These calculations have been done by Hubbard and Regier 1.11/ for several cases. The work of Garrick and Watkins on the moving propeller, described above, also pertains largely to the near field.

Hubbard and Regier found that near-field calculated sound pressures, for the first few harmonics, were in good agreement with experiments performed with model propellers of diameters 48 to 85 inches, the range of propeller-tip Mach numbers being 0.45 to 1.00. The observed pressure increases very rapidly as the measuring point is brought close to the propeller tips; this behavior corresponds closely to what would be observed if the propeller tip were the effective noise source in the very near field. The distribution of sound pressure in the propeller plane can be expressed conveniently in terms of d/D, where d is distance from the propeller tips, and D is the propeller diameter, for a given propeller shape and given rotational speed. On this basis, good agreement was obtained between observations taken near the full-sized propellers, and extrapolated results of the model studies.

The sound pressure ahead of the propeller plane is out of phase with that behind the propeller plane in most cases where the near field was investigated. A plane wall (simulating a fuselage) placed just behind the microphone, parallel to the propeller axis, and 0.083 of a propeller diameter from the tips, doubles the pressure reading for a given location by reflection, but does not seem to react on the acoustic behavior of the propeller. (This conclusion might not hold if the wall were brought much closer to the propeller tips.)

Input power and tip speed are of primary importance in determining the near field. At the lower tip-speed Mach numbers, the sound pressure for given tip speed and input power is reduced by using a propeller with a greater number of blades, but this difference virtually disappears at Mach 1.0. At constant power, the pressure amplitudes of the lower harmonics tend to decrease, and of the higher harmonics to increase, as the tip speed is increased. The difference in sound pressure produced by square and rounded tips is found to be very slight, with the square tips producing about 1.0 db higher SPL than the round, in a very restricted region near the propeller plane. Also, blade width is found to have no important effect.

Further, Hubbard and Regier compared their more accurate near-field calculations with the results obtained by using the Gutin equation for the near field, in the plane of the propeller. It is found that the Gutin equation under-estimates the SPL in this situation. Apparently the discrepancy becomes less than 2 db when the distance from the propeller tips is greater than one propeller diameter, so that the Gutin equation is sufficiently accurate for many purposes at distances greater than this.

Where it is desired to know the overall sound pressure level of propeller noise immediately within an airplane cabin, at a location near the propeller tips, the experimental findings of Rudmose and Beranek 1.13/ may be used. They analyzed data taken within some 50 types of aircraft of the period 1941-1945; in seven types, a systematic study of the parameters which influence the low-frequency propeller noise was made.

The following generalizations were made:

(a) The SPL increases by about 2.7 db for each increase of 100 ft/sec in propeller tip speed.

(b) The SPL increases by approximately 5.5 db for each doubling of the horsepower per engine.

(c) The SPL increases rapidly as the clearance between the propeller tips and the fuselage is decreased below 8 inches, but becomes relatively independent of this clearance when the value is above 20 inches.

(d) Propellers with blunt tips produce more noise by several db than propellers with fine pointed tips. The results are summarized in Eq. (4.1.7).

$$SPL = 102 + \frac{43}{d} - \frac{24}{d^2} + 18.3 \log \frac{HP}{600} + 0.027(V_o - 700) \cdot$$

$$(4.1.7)$$

Here d is the minimum propeller-fuselage distance in inches, HP is the horsepower delivered to each propeller, and V_o is the propeller-tip speed in ft/sec. This equation is intended to give the SPL in each octave band below 150 cps, existing within a typical cabin, at about 2 ft from the wall, in a section of the airplane within 6 ft of the plane of the near propellers, there being no bulkhead between the observation point and the propeller plane. The relation represents data for two- and four-engine aircraft, and refers primarily to 3-blade propellers. Subsonic tip speeds are assumed. The authors found that approximate noise levels for 4-blade and 2-blade propellers could be obtained from the same equation by multiplying the actual horsepower per engine by 3/4 and 3/2, respectively, before inserting the horsepower value in the equation. The amount by which the overall propeller SPL in the cabin exceeds the above octave-band value seems to be at least 3 db in all cases, and more usually of the order of 5 db. This figure will increase with increasing tip speed because of the rising preponderance of high harmonics, mentioned by Hubbard and Regier.

The Rudmose-Beranek experimental results can be reconciled fairly effectively with the theoretical analysis. The increase of SPL by 5.5 db for each doubling of input power agrees closely with the predictions of the propeller charts, Figs. 4.1.4 - 4.1.9, which show that this effect is generally 5 to 6 db per power doubling. The increase of SPL at the rate of 2.7 db per 100 ft/sec. increase of tip speed, as reported by Rudmose and Beranek for the low frequencies, is somewhat less than that predicted in Figs. 4.1.4 - 4.1.9, where the effect is about 20 to 30 percent greater than this, for three-blade propellers. This discrepancy is qualitatively reasonable, however, because the charts include the combined effect of four harmonics, and it is known that the effect of tip speed goes up with increasing harmonic number. The critical effect of clearance between the propeller tip and the fuselage is predicted in the analysis and measurements by Hubbard and Regier 1.12/. The final observation of Rudmose and Beranek, that propellers with fine pointed tips produce a lower cabin sound level, is superficially in contradiction to the findings of Hubbard and Regier, but can probably be interpreted to mean that an extreme change of blade shape, in this sense, causes the effective sound source for fine tip blades to be located further in from the tip of the propeller. The absolute levels given by Eq. (4.1.7) are considerably lower than those given by free-space propeller theory, since Eq. (4.1.7) includes the noise reduction afforded by a typical cabin.

Dual-Rotating Propellers. Hubbard 1.14/ has applied Gutin's analysis to dual-rotating propellers, and has found reasonably good agreement with the results of experiments on a model unit comprised of two, two-blade, 4-ft diameter propellers. The sound field no longer has circular symmetry about the propeller axis, but instead has maxima in the directions of blade overlap. These maxima of sound pressure correspond closely to the amplitude which would be produced by a single propeller having the same number of blades as the total in the tandem unit. The intervening pressure minima have amplitudes corresponding closely to the output of one of the dual propellers only. If the two propellers rotate at slightly different speeds, the pattern of maxima and minima then rotates, and the sound reaching the observer is consequently amplitude modulated. When the number of blades is not the same in the front and rear units, this modulation is

found only for harmonics which are integral multiples
of both fundamental frequencies; for example, the lowest
modulated harmonic of a three-blade, two-blade dual-rotat-
ing propeller is the sixth. The case of tandem propellers
operating side by side was also investigated, and similar
phenomena were found. The results thus far mentioned are
not critically affected by the separation of the propellers.

An additional signal, the "mutual interference noise",
is developed when the spacing of the dual-rotating elements
is made small. This noise component appears to be a maxi-
mum on the forward axis of rotation, where the rotational
noise is small, and has a fundamental frequency equal to
the blade passage frequency. The mutual interference
noise is undetectable at positions near the propeller plane,
where the rotational noise is strong, and apparently
consitutes only a small fraction of the total power
radiated by the propeller. The pressure amplitude of this
additional noise component varies as the propeller power
and as the cube of the tip speed, according to measure-
ments on the axis. The effect of spacing is critical; in
Hubbard's experiment, the mutual interference noise is
the predominant signal on the forward axis at a spacing of
6 3/4", but is not detectable with certainty at a spacing
of 12".

The Effect of Struts on Propeller Noise. While no
theoretical analysis has been made of the effect of a
strut near the propeller plane, the experimental evidence
indicates that a much more serious disturbance is produced
by a strut ahead of the propeller than by one behind.
This question was examined in the work on dual-rotating
propellers described above. No strut effect was reported
for the tractor propeller, which was supported by a strut
placed behind. The pusher propeller (supported by a strut
ahead) was found to give 3 db higher overall SPL than the
tractor when the pusher strut clearance was 11.75 inches,
and about 7 db higher SPL than the tractor when this
clearance was 5.75 inches. The effect is nearly independent
of tip speed.

An increase of noise resulting from a strut ahead of
the propeller was also reported by Roberts and Beranek
1.15/ in a series of experiments on quieting of a pusher
amphibian. The total noise power radiated by this air-
plane was greater than that from a tractor airplane operat-
ing at greater power and tip speed. The sound level

measured from the pusher did not drop off sharply to the rear as it does for a tractor airplane, and as the Gutin theory predicts. Whereas the noise output of a tractor airplane for specified power and tip speed can be decreased by increasing the number of propeller blades, in at least qualitative agreement with the Gutin theory, the pusher airplane was found to become noisier as the number of blades was increased above four.

Supersonic Tip Speeds and Empirical Propeller Noise Chart. The Gutin theory of rotational noise and its various modifications are all restricted to subsonic tip speeds. At present, the knowledge of propeller noise generation for supersonic tip speeds is restricted to experimental findings. In general, the experimental data show that there is no discontinuous change in noise output as the propeller goes into the supersonic range. At or near the beginning of the supersonic range, however, the noise power output becomes nearly independent of tip speed, as shown in N. A. C. A. experiments 1.16/ on a model propeller, the sound output of which was in good agreement with the Gutin theory in the subsonic range. A less extensive series of measurements by a commercial laboratory (unpublished), on full-scale propellers, seems to indicate that the noise output for supersonic tip speeds also becomes relatively independent of input power. This statement is based upon observations of 10- and 16-ft diameter propellers in the range 800 to 2000 horsepower.

In the absence of a suitable theory of noise generation in the range of supersonic tip speeds, the empirical chart in Fig. 4.1.14 has been prepared as an approximate

---

FIGURE 4.1.14

Propeller noise chart, constructed from experimental data, showing the approximate acoustic power level for tip speeds into the supersonic range. The chart applies to 3-blade propellers, of diameter approximately 12 ft. Power levels for 2- and 4-blade propellers lie approximately 2 db above and below the chart values, respectively. For operating conditions to the upper right of the broken line, propeller noise usually exceeds the exhaust noise from a reciprocating engine, but for operating conditions to the lower left, exhaust noise may predominate (see Sec. 4.3).
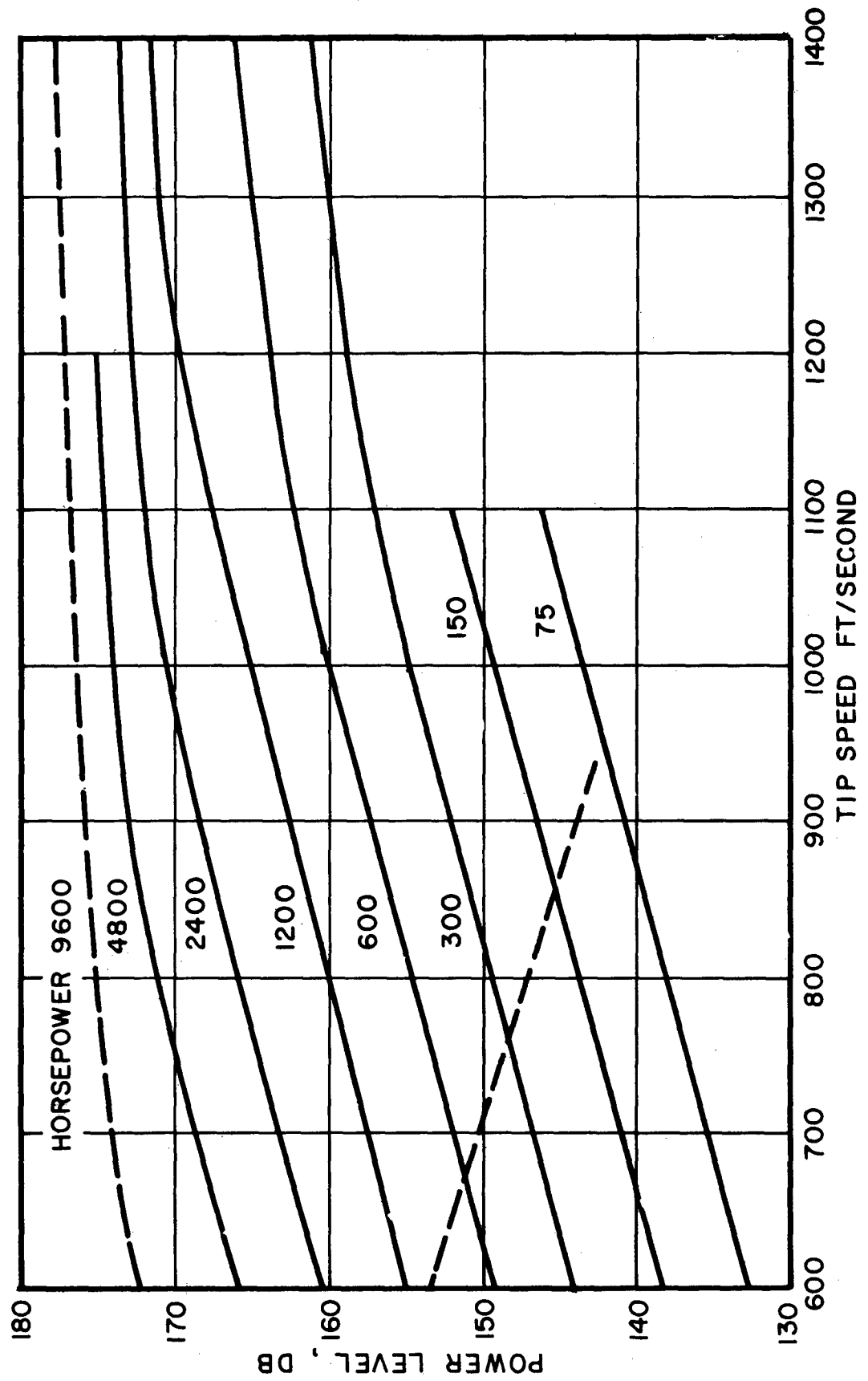
summary of existing information. This chart gives the
overall power level of the propeller when the input horse-
power and the tip speed are known. The information for
tip speeds of 1000 ft/sec and greater was taken from the
two sources mentioned above. The subsonic portion of the
chart is arbitrarily drawn to have the dependence on tip
speed and input power which was reported by Rudmose and
Beranek for low frequencies, as shown in Eq. (4.1.7); on
the basis of propeller noise theory, slightly greater
effect of tip speed might be argued. The absolute
values indicated by the subsonic curves are determined
in part by the low-speed portions of the data on large
propellers mentioned above, and in part by several mea-
surements of ground and flight operation of actual aircraft
under known conditions. Where measurements were taken with
a microphone very near the ground and within 50 ft of the
source, pressure doubling at the microphones was assumed,
and 6 db was subtracted from the SPL reading. Where the
microphone was 200 ft or more from the source, so that
ground attenuation might be more important, this reflection
correction was arbitrarily reduced to 3 db. To get the
power level for an outdoor propeller from the SPL measured
in one direction, use was made of the typical propeller
directivity curve shown in Fig. 4.1.15. The individual data
points used to make the chart are generally consistent
with the final chart values within 4 db. The extension
of the curves into the supersonic range is determined by
very few measurements and is therefore tentative.

The chart in Fig. 4.1.14 does not show the effect
of propeller diameter or of number of blades. The chart
is an approximate average of data for propellers of two,
three, and four blades, and is most nearly correct for
three blades. Very roughly, values for propellers of two
and four blades lie 2 db above and below the chart values,
respectively. The chart is most nearly correct for pro-
pellers of diameter 12 ft; for 3-blade, 12-ft propellers,
the subsonic portions of this chart are generally in agree-
ment with the charts based on Gutin's equation, Figs. 4.1.4
through 4.1.9, within 3 db. For propellers of about this
size, the empirical chart in Fig. 4.1.14 may be used in
lieu of the detailed charts for engineering predictions.
Either this chart or the detailed charts, properly applied,
should predict overall static propeller noise within $\pm$ 5 db
in most instances.

Parkins and Purvis 1.17/ have measured maximum sound levels beneath a number of types of 2- and 4-engine aircraft immediately after takeoff, and have reduced their results to a standard distance. If it is assumed that the aircraft as a whole has approximately the same directivity as a propeller*, so that the maximum SPL is approximately 5 db above the space-average value, and if it is assumed that the noise powers from the propellers on a given airplane are additive, these data can be reduced to give the power level of a single propeller under take-off conditions. It is found that the power levels obtained in this way are typically 8 db lower than those predicted by the chart in Fig. 4.1.14. Therefore, 8 db should be subtracted from the chart values to obtain power levels for flight conditions following takeoff. This correction is in the expected direction, inasmuch as the chart refers to static operation, for which noise generation is greatest.

The Spectrum of Propeller Noise. The theories of propeller noise do not give a generally successful treatment of the frequency distribution of the sound energy. The success of the theories in predicting overall sound power is attributable partly to the fact that a large part of the energy radiated is found in the first few harmonics of rotational noise. The theoretical calculations of rotational noise generally underestimate the amplitudes of the higher harmonics. Moreover, a large part of the high-frequency energy often comes from vortex noise, the amplitude of which is not rigorously predictable at present. Theoretical considerations of both rotational and vortex noise agree qualitatively, however, that the high-frequency energy increases relative to the low-frequency energy as the propeller tip speed is increased (at least, in the subsonic range).

---

* Some unpublished measurements of the polar sound distribution for an airplane operating on the ground show that this assumption is reasonable. The observed distribution is similar to that in Fig. 4.1.13, which is for a propeller on a test stand, except that the sound levels behind the actual airplane do not fall off as rapidly for points toward the front of the plane.

OVERALL SOUND PRESSURE LEVEL IN GIVEN DIRECTION RELATIVE TO SPACE AVERAGE, DECIBELS
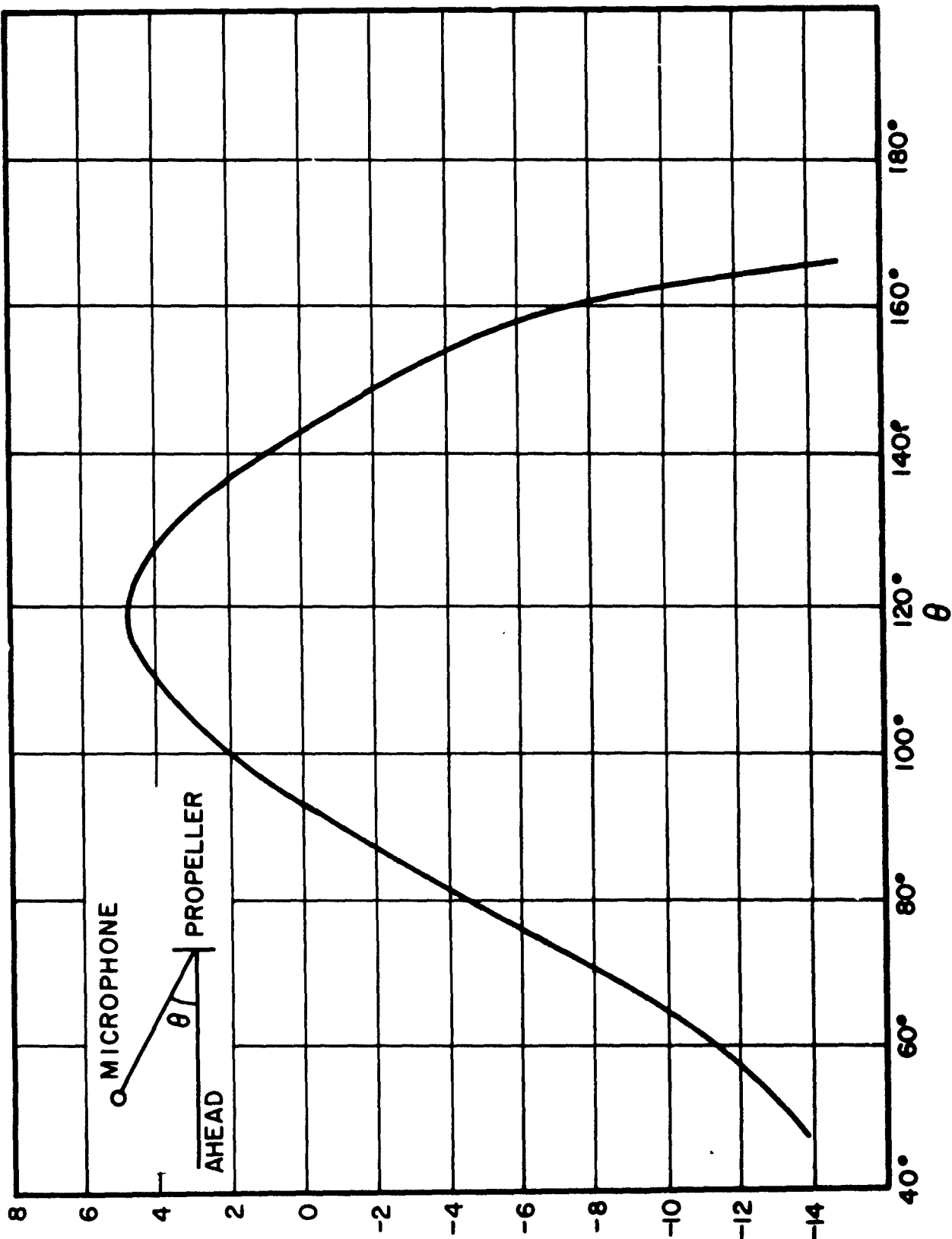
The octave-band spectra measured immediately beneath several types of transport airplanes shortly after takeoff, presumably under full-power operation, are shown in Fig. 4.1.16. The information is from Ref. 1.17. There is a remarkable similarity in the results for the several airplanes, except that the two-engine airplane (of considerably lower horsepower than the others) gives relatively less noise in the two highest octave bands. The arbitrary curve drawn in this figure is a suggested design curve for engineering prediction of the propeller noise spectrum under takeoff conditions, for transport airplanes. It is assumed that the observed noise from a propeller-driven aircraft at takeoff is due to the propellers. The results shown here will be duplicated only in measurements taken fairly near the aircraft and over a hard surface. Because atmospheric and terrain attenuation of sound rise with increasing frequency, spectra measured over absorbing terrain, or at a distance of the order of thousands of feet, will have appreciably lower relative levels in the highest bands than those shown. The relative high-frequency content of propeller sound also decreases upon change from takeoff to cruising operating conditions, but data are not available to show precisely the extent of the effect.

Vortex Noise. It has been generally assumed that the nonperiodic part of the propeller noise (ordinarily less than the periodic part) is associated with the shedding of vortices (eddies) in the wake of the moving

---

FIGURE 4.1.15

Directivity pattern computed from overall SPL for a propeller on an outdoor test stand. The directivity is the difference in db between observed SPL in a given direction and the SPL which would be observed with non-directional radiation of the same total sound power. Computed from data in Ref. 1.16.

FREQUENCY BAND – CPS

RELATIVE POWER LEVEL, DB

O STRATOCRUISER
X CONSTELLATION
+ DC – 6
● DC–3(TWO-ENGINE)
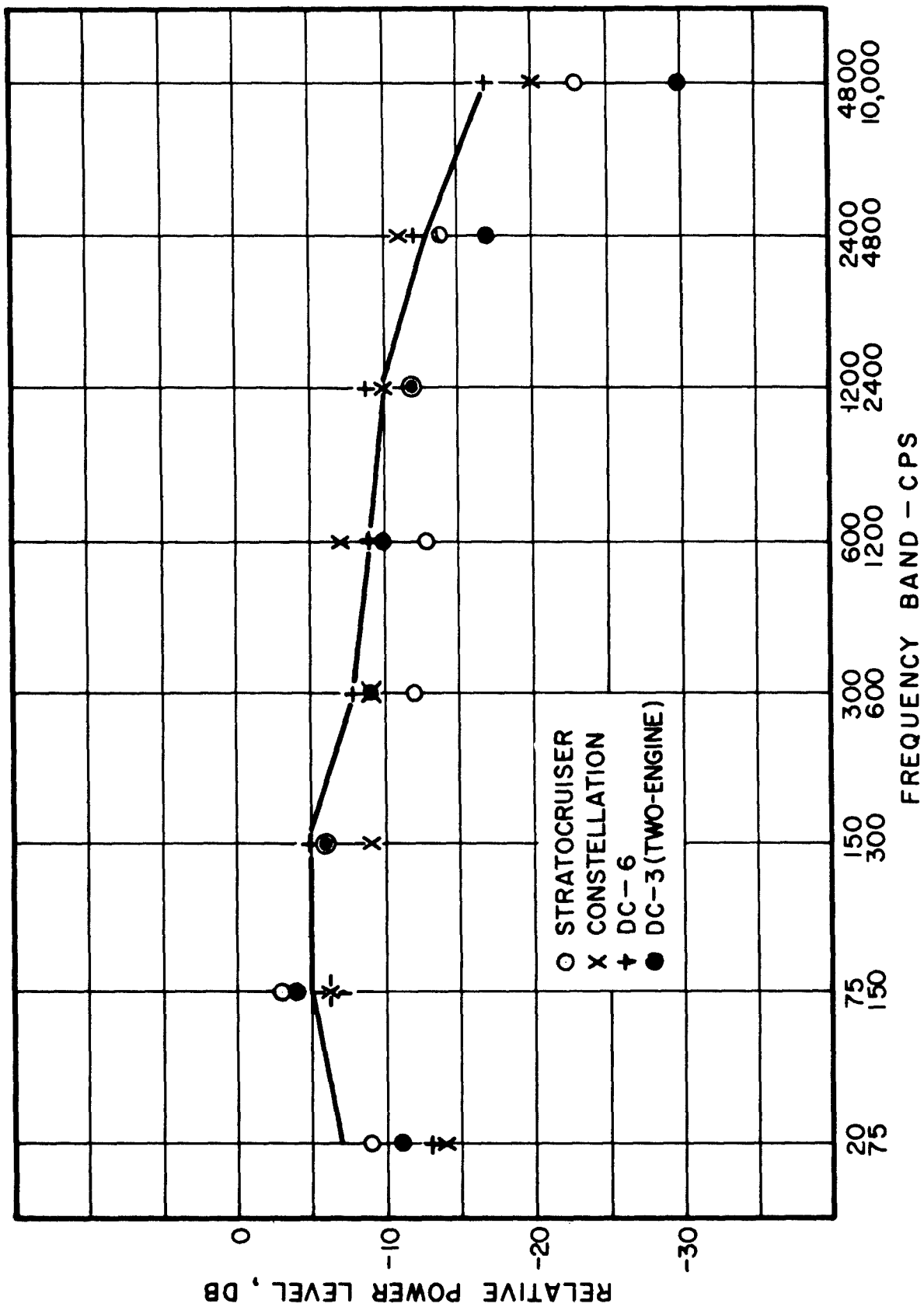
blade. These vortices are a normal consequency of the instability of fluid flow past an object of more or less cylindrical shape. Under idealized conditions, the vortices form and tear away from the obstacle in regular fashion, to form a Karman vortex trail 1.18/ as shown in Fig. 4.1.18. While pressure fluctuations are registered by a detector placed in the trail, it can be proved that the vortices in the trail cannot radiate sound; their pressure distributions fall off very rapidly with distance. The sound radiated by the vortex shedding process must arise from the immediate vicinity of the obstacle, as in the region AO'O"B, and must be the result of the pressure impulses which occur whenever the flow system of a vortex is suddenly torn from the obstacle.

Some idea of the process is given by dimensional analysis. The intensity of an acoustic wave is given by

$$I = p^2/\rho c \qquad (4.1.8)$$

where ρ is the fluid density, and c the speed of sound. Let the acoustic pressure p be measured in units of $1/2\ (\rho u^2)$, where u is the flow velocity past the obstacle, which can be expressed in terms of the Mach number, $M = u/c$. Then the intensity is

$$I = B\frac{\rho u^4}{c} \qquad (4.1.9)$$

where B is a coefficient which may be a function of the Reynolds number, $Re = \rho u \ell /\mu$ of the Mach number M, or ℓ /r, where ℓ is some dimension of the body and r the distance to the point of observation, and also of $\Theta, \emptyset$, the azimuth and zenith angles of the point of observation with respect to some reference axes. The symbol μ denotes the viscosity coefficient of air.

FIGURE 4.1.16

Propeller noise spectra measured beneath several types of 2- and 4-engine airplanes immediately after takeoff. Data from Ref. 1.17. The chart shows the amount by which the power level for each octave band differs from the overall power level. The curve is a suggested basis for engineering estimates of the spectrum for transport airplanes under takeoff conditions.

For large distances, the law of conservation of energy will require that the intensity fall off with the square of the distance, as expressed by the next relation

$$B(Re, \frac{\ell}{r}, M, \Theta, \emptyset) = \frac{\ell^2}{r^2} B' (Re, M, \Theta, \emptyset) \quad .$$

(4.1.10)

Furthermore, the Mach number effect must occur as a multiplier, since the sound intensity must vanish for incompressible fluids ($c \longrightarrow \infty$). Thus, the preceding equation may be rewritten as

$$B = \frac{\ell^2}{r^2} \left(\sum_n M^n \right) B'' (Re, \Theta, \emptyset)$$

(4.1.11)

where the Mach number effect has been generalized as a power series in M. An approximate solution will be sought by retaining one term of the series. It can be shown that the exponent $n = 1$ corresponds to a simple source, and $n = 2$ to a dipole. The simple source may be ruled out on the basis that the observed radiation is directional, or through a theoretical argument which shows it to be inconsistent with the aerodynamic flow situation. With the exponent $n = 2$, it is evident that the sound intensity will vary as u^6. When the directional function for a dipole is inserted, the final expression for the intensity is

$$I = \alpha \ (Re) \ \frac{\cos^2\Theta}{r^2} \ A\rho \ \frac{u^6}{c^3} \quad .$$

(4.1.12)

Here A, the projected area of the obstacle in the

direction of fluid flow, has been written instead of ℓ^2. The coefficient α (Re) cannot be determined from dimensional analysis alone. In the case of a propeller blade, it is found that the dipole radiation pattern has its maxima on the propeller axis.

While the noise generated by vortex shedding is not periodic in ordinary practical situations, the rate of shedding vortices is in principle a constant in the case of steady flow around a uniform cylinder. Strouhal argued by dimensional analysis that the frequency of vortex shedding from a cylinder is

$$f = K \frac{u}{d} \qquad\qquad (4.1.13)$$

where d is the diameter. He found an experimental value of K of about 0.185. This quantity is actually a function of the Reynolds number, and is 0.18 for Reynolds numbers from 10^3 to 3×10^4.
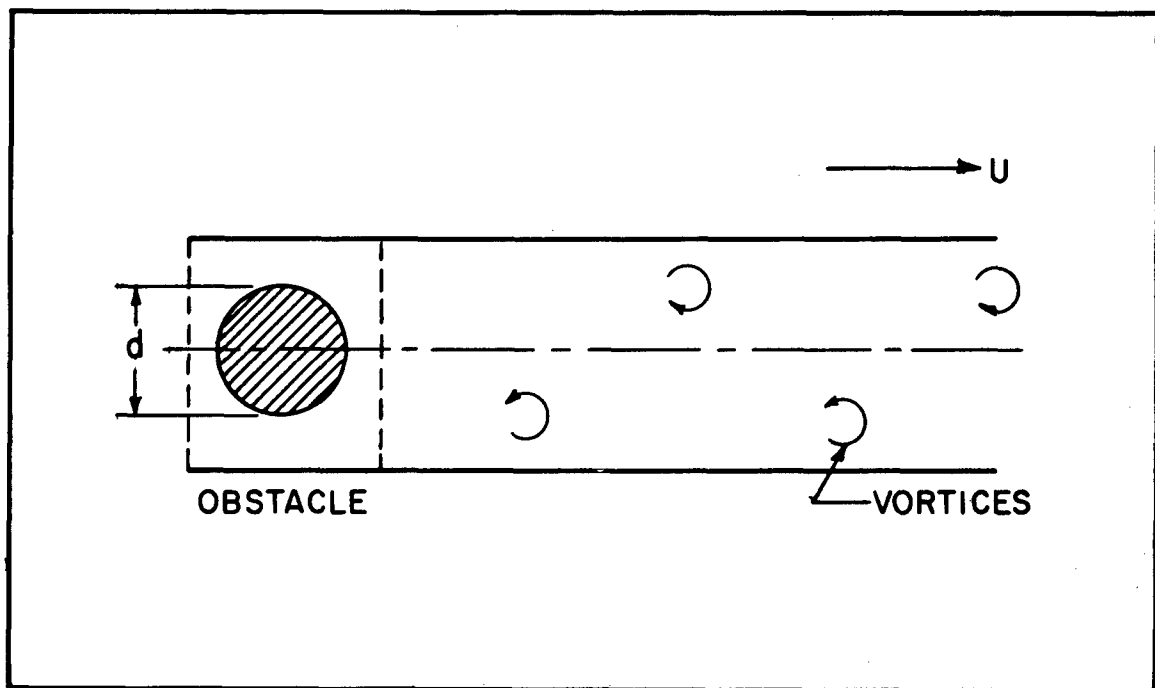
FIGURE 4.1.17

Idealized Karman's vortex trail.

Evaluation of Vortex Noise Intensity. The knowledge
of vortex noise is not yet entirely satisfactory from a
quantitative standpoint. Stowell and Deming 1.19/ experi-
mented with a device in which circular rods, rather than
blades, projected from a rotating hub, and found the inten-
sity of the radiated sound to be proportional to the
projected area A and to the sixth power of the velocity,
as predicted by Eq. (4.1.12). In a later N.A.C.A. experi-
ment 1.20/, the constant of proportionality was evaluated
from measurements on a helicopter blade. On this basis,
Hubbard adopted the engineering equation below to give the
overall intensity level (essentially equal to SPL) of vor-
tex noise at a distance of 300 ft from a propeller, presum-
ably for those directions where the sound is strongest.

$$ IL = 10 \, \log_{10} \frac{k A_B V_{0.7}^6}{10^{-16}} \qquad (4.1.14) $$

The value of k is given by 3.8×10^{-27}. The symbol $V_{0.7}$
denotes section velocity at 0.7 of full radius, in ft/sec;
A_B denotes total plan area of blades, which is roughly
proportional to the area A of Eq. (4.1.12) if consistent
operating conditions somewhat below stall are assumed.
The relation Eq. (4.1.19) is the basis for the broken-line
curves showing vortex noise in Figs. 4.1.4-4.1.9. Hubbard
estimates these tentative results as being correct within
$\pm$ 10 db for conditions below stall, and points out that
the vortex noise may increase by 10 db when the propeller
is operated under stalled conditions.

The uncertainty in the present evaluation of vortex
noise may be explained in part by recalling that the
coefficient in Eq. (4.1.12) is a function of the Reynolds
number. Evaluations currently available were made at
Reynolds numbers much smaller than those found in pro-
peller applications. Experiments at high Reynolds numbers
necessarily bring in rotational noise and are therefore
more difficult in that the rotational and vortex noise
contributions must be separated. Moreover, propeller
blades may operate at Reynolds numbers greatly exceeding
10^5, the value at which laminar flow in the boundary
layer is replaced by turbulent flow. Completely turbulent
flow generates broad-band noise through mechanisms other
than vortex shedding, and the vortex noise analysis does
not apply rigorously.

The Spectrum of Vortex Noise. The rotating-rod experiments of Stowell and Deming 1.19/ and others give spectra in which most of the noise energy is located in the frequency range given by the Strouhal formula, Eq. (4.1.13). (The formula gives a range of values rather than a single value in the case of a rotating rod, since the section velocity varies continuously from the hub to the tip.) Noise energy is observed over the entire audible range, however, as illustrated by oscillograms given in Ref. 1.5. There is some evidence of peaks in the spectrum at harmonics of the Strouhal frequencies. The spectral distribution of the noise needs further investigation.

Practical Importance of Vortex Noise. It appears that vortex noise never constitutes a significant portion of the distant sound produced by heavily loaded propellers, operating at tip speeds of 900 ft/sec or more. Thus, it is not necessary to consider vortex noise in connection with takeoff operation of transport airplanes, and it is unlikely that vortex noise is important even in the sound produced by transports under cruising conditions.

The intensity of rotational noise is much more sensitive to tip speed and to blade loading (angle of attack) than that of vortex noise. Consequently, it is always possible, by reducing the tip speed and possibly the angle of attack, to reach a condition where the propeller sound consists largely of vortex noise rather than rotational noise. Vortex noise thus becomes the limiting factor when an attempt is made to reduce propeller noise by reducing the tip speed and increasing the number of blades. This point was discussed in an earlier paragraph.

An Example of Calculating Propeller Noise. Given the following propeller data, it is desired to estimate

(a) the SPL near the ground (hard surface) at 500 ft distance;

(b) the SPL at that point in the 600-1200 cps band: Four propeller blades; tip speed 900 ft/sec (approximately Mach 0.9); 2000 horsepower input.

From Fig. 4.1.5, the power level is 112 + 55 = 167 db. The direction-averaged SPL at 500 ft distance, in free space, would be the power level less 10 log $[4\pi(500)^2]$, which gives 102 db. Near the hard ground, pressure doubling raises the SPL by 6 db to give 108 db, still on a direction-averaged basis. If the typical directional distribution of Fig. 4.1.15 is assumed, the SPL in the propeller plane (90°) is 1 db less than the direction-average value, which yields 107 db. This is answer (a).

The given conditions resemble takeoff operation for a large airplane. Therefore the spectral distribution in Fig. 4.1.16 should apply. According to this figure, the SPL in the 600-1200 cps band is approximately 9 db below the overall SPL, which gives 99 db as answer (b).

Sometimes it is necessary to estimate sound pressure levels external to a test cell, with the propeller operating inside. For a cell which has no sound-absorbing treatment, and which has openings looking out in a horizontal direction front and rear, a first approximation to low-frequency sound levels is obtained by making a calculation as given above, and using the space-averaged value, since the cell disturbs the normal directionality of the propeller. For higher frequencies, the cell openings must be assigned the directionality of a stack opening, and in general a proper allowance must be introduced for sound-absorbing treatment. These topics are reserved for later chapters.

The calculations above could also have been started by reference to the empirical propeller-noise chart, Fig. 4.1.14, which is approximately correct for large propellers of two to four blades. This chart gives a power level of 167.5 db, from which about 2 db should be subtracted to correct from three to four blades, giving a power level of approximately 166 db. All results would then be less by one db than those obtained above.

4.2 Noise from Aircraft Reciprocating Engines

Reciprocating engine noise has been studied less extensively than propeller noise, because the maximum noise levels produced by propeller-driven aircraft, under full-throttle conditions, are usually attributable to the propeller. The tentative generalizations given below concerning engine noise are made on the basis of a few observations (Refs. 1.13 and 1.7); also a ground airplane test; and unpublished results of tests on an 800 horsepower engine in a dynamometer test cell).

1. The noise developed by a reciprocating engine is produced almost exclusively by the exhaust, with possible exceptions in cases where unusually effective mufflers are used.

2. The noise energy of the lowest-frequency exhaust component of a reciprocating engine is approximately proportional to the total power developed. Quantitatively, the power level of this exhaust component for an engine without exhaust mufflers is not less than

Power level of lowest frequency component =

$$122 + 10 \log_{10} (\text{horsepower}).$$

$$(4.2.1)$$

On theoretical grounds, the horsepower value used in Eq. (4.2.1) should include mechanical losses in the engine. However, these are usually not known. In cases where the mechanical losses are large, they must be included.

3. The lowest-frequency exhaust component of importance usually has a frequency equal to the number of exhaust discharges per second (two discharges occurring simultaneously are counted as one). This frequency is usually below 300 cps.

4. Usually the spectral distribution of noise energy is approximately as follows: The power level in the octave band containing the lowest-frequency exhaust component lies about 3 db below the overall power level. The levels in octave bands above this one decrease at about 3 db per octave of increasing frequency. No significant noise is produced in octave bands below the one containing the lowest-frequency exhaust component. These conditions may be typical of engines operated at cruising conditions, and of small engines (150 horsepower and less).

5. In the case of an engine of 800 horsepower operated at full throttle, a uniform octave-band spectrum has been observed (equal power levels in the octave band containing the lowest-frequency exhaust component and all higher octave bands). This may be typical of larger engines under full-power conditions. In this case the overall power level is about 8 db larger than that of the lowest frequency exhaust component.

6. Directional effects are much smaller for engine noise than for propeller noise. The total variation in SPL with direction is about 6 db for the lower-frequency components of engine noise. This statement probably holds for high frequencies also in the case of an isolated engine, but no detailed measurements for high frequencies are available. In the case of an engine mounted on an airplane, the high frequency directivity will be affected by shadowing produced by the airplane structure.

Simple relations for the overall power level of an engine without mufflers are obtained by combining statements 2, 4, and 5. For the case of small engines (150 horsepower or less), or engines operated under cruising conditions, the relation is

Overall power level $= 125 + 10 \log_{10}$ (horsepower).

(4.2.2)

For the case of a large engine operated at full load, the relation if

$$\text{Overall power level} = 130 + 10 \log_{10} (\text{horsepower}).$$

<div align="right">(4.2.3)</div>

For example, according to Eq. (4.2.2), the overall power level is 152 db for engines delivering 500 horse-power under cruising conditions. According to Eq. (4.2.3), the overall power level is 160 db for an engine delivering 1000 horsepower at full load.

4.3 Total External Noise of Aircraft with Reciprocating Engines

According to Secs. 4.1 and 4.2, the overall noise level of a propeller increases by approximately 5.5 db per horsepower doubling (plus 2.7 db or more for each increase of 100 ft/sec in tip speed), whereas the overall noise level of an engine increases at approximately 3 db per horsepower doubling. It follows from these principles that the predominant noise source in a propeller-driven aircraft with very large engine power will be the propeller, but that engine noise will predominate when the power is low.

This expectation appears to be borne out in the results of a survey 3.1/ of take-off noise level of various airplanes ranging from 65 to 5800 horsepower. In this survey the microphone was located in the propeller plane at a distance of 500 ft from the center of the runway. At this microphone position the sound received from both engine and propeller has approximately the space-average value, so that directional effects may be neglected. It is found that the observed sound levels for aircraft with more than 150 horsepower agree with values predicted from the empirical propeller chart, Fig. 4.1.14, to the accuracy of the chart. For airplanes of 150 horsepower and less, the overall noise levels exceed those predicted from the propeller chart, but are in approximate agreement with levels for engine noise as given by Eq. (4.2.2). There are, however, other take-off noise data 1.7/ for aircraft with less than 200 horse-power which are in agreement with propeller noise figures rather than with estimated noise figures. The reason for the discrepancy is not known.

Polar plot with radial axis labeled in db: 80, 90, 100, 110. Angular labels: 0°, 30°, 30°, 60°, 60°, Left wing, Right wing, 120°, 120°, 150°, 150°, Tail.
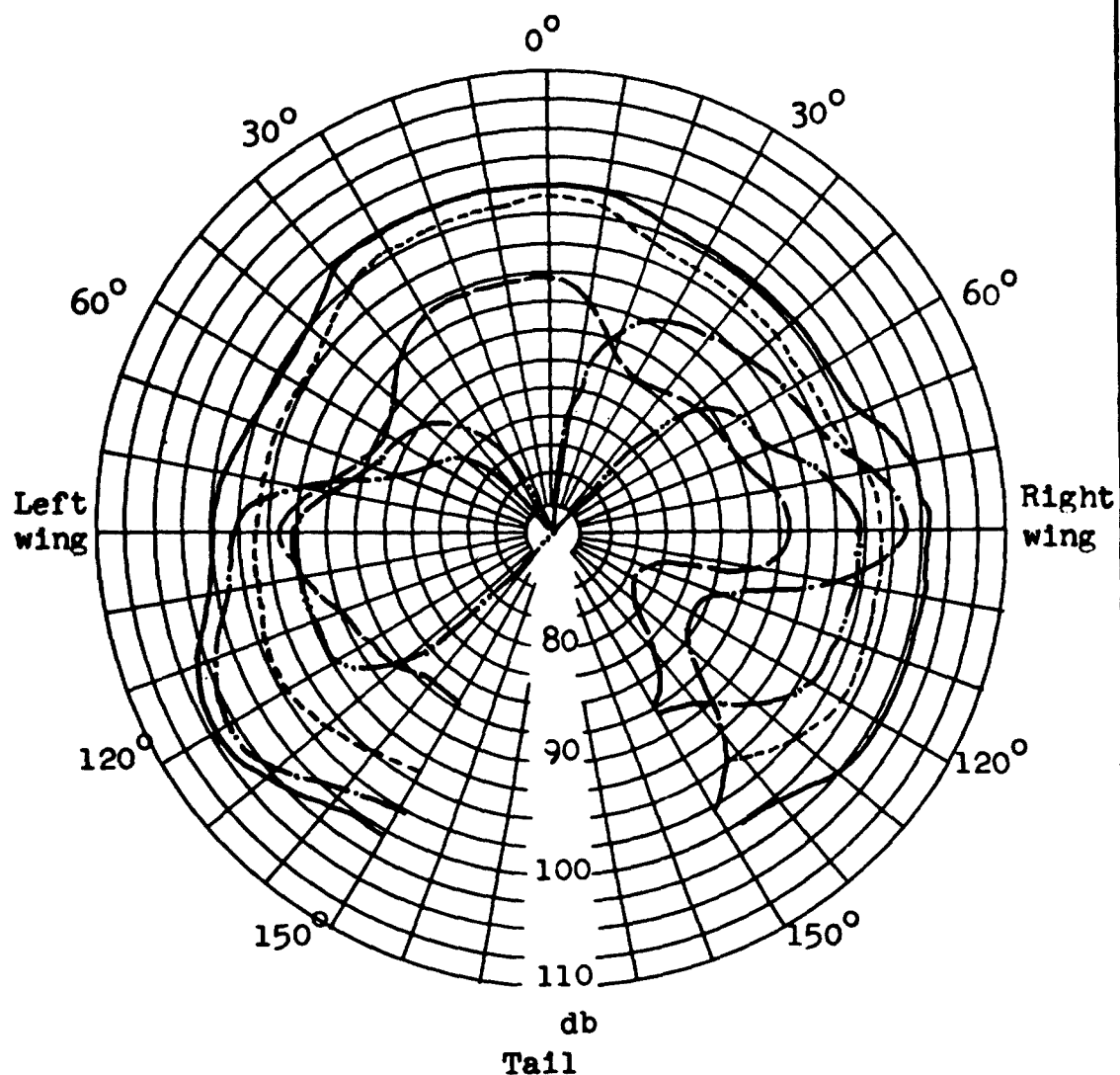
Engine	Average frequency		Propeller	Average frequency
Fundamental — — — —	97		Fundamental — — — — —	65
Second harmonic	195		Second harmonic — — — —	130
			Third harmonic — — — —	
		Overall level ———————	

A convenient approximate expression for the overall power level of various aircraft under take-off conditions has been deduced from the data of Ref. 3.1. This relation is

$$\left(\begin{array}{c}\text{Overall power} \\ \text{level take-off}\end{array}\right) = 121 + 12 \log_{10} \left(\begin{array}{c}\text{Total take-off} \\ \text{horsepower of} \\ \text{aircraft}\end{array}\right)$$

$$(4.3.1)$$

It happens that under the particular conditions found in take-off it is not necessary to consider propeller tip speed explicitly. Since the tip speed is not considered in Eq. (4.3.1), this relation cannot be applied to operating conditions differing materially from takeoff.

The broken line drawn across the empirical propeller noise chart, Fig. 4.1.14, divides the chart approximately into a region in which the propeller is the major noise source for an entire aircraft (upper right-hand portion) and a region in which the engine is the major noise source (lower left-hand portion). This line is constructed by computing, for various values of total horsepower, the tip speed at which the overall propeller noise power level equals the overall engine noise power level given by Eq. (4.2.2) is assumed. Operating data for small single-engine aircraft often fall in the region in which engine noise is important (lower left). All data used in deriving this dividing line represent average trends from which results for a particular aircraft may differ by as much as 5 db as regards either engine noise or propeller noise. Therefore, the line as drawn on the chart will not indicate accurately under what conditions propeller noise is dominant in a particular aircraft. Also, the results are averages for reciprocating engine aircraft as commercially produced up to 1952, and do not apply to specially constructed units in which noise control measures are incorporated. It has been shown that overall aircraft noise can be reduced significantly by use of propellers with an increased number of blades and by use of exhaust mufflers 1.6/.

FIGURE 4.3.1

Directional distribution of SPL for certain discrete-frequency components of airplane noise. Measurements 50 ft from hub; ground test at cruising power. Two-blade propeller; 1940 rpm; direct drive; 97 horsepower; blunt tips, speed 646 ft/sec. (From Fig. 27a of Ref.1.7).

The preceding remarks on total aircraft noise refer to the space average of sound output. This concept is inherent in the definition of power level. In general, actual observation made in the propeller plane will agree approximately with space-average results. The directivity patterns of engine and propeller must be considered in predicting noise levels observed in other directions. A typical situation is illustrated in Fig. 4.3.1, which shows the variation with azimuth angle of measured overall sound level and/or the levels of selected propeller and engine noise components for a particular small airplane. These results were obtained by operating the airplane at cruising power on the ground and by placing the microphone in various locations 50 ft from the propeller hub, and approximately at the hub level.

The tentative conclusions regarding external noise or reciprocating-engine aircraft are summarized below.

1. For large aircraft, the overall PWL for either cruising or take-off conditions is approximately equal to the overall PWL for propeller noise which may be estimated by the methods given at the end of Sec. 4.1.

2. For aircraft of 150 horsepower or less, it appears that the overall PWL under cruising or takeoff conditions is approximately that given for the engine by Eq. (4.2.2).

3. The SPL in the propeller plane is approximately that which would be produced by a non-directional source having the stated overall PWL.

4. The overall PWL for various aircraft under takeoff conditions is given approximately by Eq. (4.3.1).

5. The observed noise for positions directly ahead of or directly behind, the aircraft is approximately the engine noise alone having a PWL given by Eq. (4.2.2) or (4.2.3).

6. The observed SPL for positions from 20° to 30° behind the propeller plane has the greatest preponderance of propeller components. An approximate indication of the overall SPL for this region may be obtained, for either cruise or takeoff conditions by adding 5 db to the value obtained by using the overall propeller PWL (Sec. 4.1) and proceeding as for a non-directional source.

References

(1.1) Gutin, L., "Uber das Schallfeld einer rotierenden Luftschraube," Phys. Zeits. der Sowjetunion 9, 57-71 (1936). The following is a translation into English: Gutin, L., "On the Sound Field of a Rotating Propeller," National Advisory Committee for Aeronautics, TM 1195 (1948).

(1.2) Lamb, H. Hydrodynamics, Dover Edition (New York), pp. 501 ff.

(1.3) Paris, E. T., "On the Sound Generated by a Rotating Aircrew" Phil. Mag. 13 99-111 (1932).

(1.4) Kemp, S. F., "Some Properties of the Sound Emitted by Airscrews" Proc. Phys. Soc. (London) 44 151-165 (1932).

(1.5) Hubbard, H. H., "Propeller Noise Charts for Transport Airplanes," National Advisory Committee for Aeronautics, TN 2968 (1953).

(1.6) Regier, A. A., and Hubbard, H. H., "Status of Research on Propeller Noise and Its Reduction," J. Acoust. Soc. Am. 25, 395-404 (1953).

References (cont.)

(1.7) Beranek, Elwell, Roberts, and Taylor, "Experiments in External Noise Reduction of Light Airplanes," National Advisory Committee for Aeronautics, TN 2079 (1950).

(1.8) Hicks, C. W., and Hubbard, H.H., "Comparison of Sound Emission from Two-Blade, Four-Blade, and Seven-Blade Propellers," National Advisory Committee for Aeronautics, TN 1354 (1947).

(1.9) Deming, A. F., "Propeller Rotation Noise Due to Torque and Thrust" J. Acoust.Soc. Am. $\underline{12}$, 173-182 (1940).

(1.10) Garrick, I.E., and Watkins, C.E., "A Theoretical Study of the Effect of Forward Speed on the Free-Space Sound-Pressure Field Around Propellers," National Advisory Committee for Aeronautics, TN 3018 (1953).

(1.11) Regier, A. A., "Effect of Distance on Airplane Noise," National Advisory Committee for Aeronautics, TN 1353 (1947).

(1.12) Hubbard, H.H., and Regier, A.A., "Free-Space Oscillating Pressures Near the Tips of Rotating Propellers," National Advisory Committee for Aeronautics, Rept. 996 (1950).

(1.13) Rudmose, H.W., and Beranek, L.L., "Noise Reduction in Aircraft", J. Aero. Sci. $\underline{14}$, 79-96 (1947).

(1.14) Hubbard, H.H., "Sound from Dual-Rotating and Multiple Single-Rotating Propellers," National Advisory Committee for Aeronautics, TN 1654 (1948).

(1.15) Roberts, J.P., and Beranek, L.L., "Experiments in External Noise Reduction of a Small Pusher-Type Amphibian Airplane," National Advisory Committee for Aeronautics, TN 2727 (1952).

(1.16) Hubbard, H.H., and Lassiter, L.W., "Sound from a Two-Blade Propeller at Supersonic Tip Speeds," National Advisory Committee for Aeronautics, Rept. 1079 (1952).

References (cont.)

(1.17)   Parkin and Purvis. Article on take-off noise of aircraft, supposed to be in Acustica in 1954.

(1.18)   Lamb, H., Hydrodynamics, Dover Edition (New York), pp. 224 ff.

(1.19)   Stowell, E. Z., and Deming, A. F., "Vortex Noise from Rotating Cylindrical Rods," National Advisory Committee for Aeronautics, TN 519 (1935).

(1.20)   Hubbard, H. H., and Regier, A. A., "Propeller Loudness Charts for Light Airplanes," National Advisory Committee for Aeronautics, TN 1358 (1947).

(3.1)   Institute of Aeronautical Sciences, "External Sound Levels of Aircraft", Preprint No. 126.

6.3a Noise-Generating Mechanisms in Axial-Flow Compressors

An axial-flow compressor consists of a sequence of multiple-blade propellers (rotors) operating within a duct. Several stators, which are essentially non-rotating propellers, are placed between successive rotors, and possibly at the ends of the array. Since the axial-flow compressor is made up of propellers, the mechanisms of noise generation are very similar to those for aircraft propellers as discussed in the revised Sec. 4.1. A familiarity with parts of that section will be assumed in the present discussion.

The theory of propeller noise generation predicts that the periodic sound component (i.e. the rotational noise) has zero amplitude on the propeller axis. This is because any point on the axis is, at all times, a fixed distance from the steady rotating pressure pattern associated with any one of the blades, and hence experiences no time-varying pressure, or sound. If this concept is extended to the axial-flow compressor, it appears that there should be no propagation of sound down the duct axis. A theoretical calculation confirms that no sound energy from rotational noise will be propagated down the duct, provided that the rotors, the stators, and the duct all have perfect circular symmetry. There will be, however, a large-amplitude pressure disturbance in the plane of each rotor having the characteristics of an array of dipoles, one for each rotor vane. This disturbance does not excite plane waves of sound in the duct, but does excite high-order modes, the amplitude of which falls to practically negligible values within one duct diameter on either side of the rotor. The theory of the sound-pressure distribution in higher modes has been worked out in detail.

In addition to periodic noise, the compressor rotor will generate nonperiodic vortex noise in the manner of an airplane propeller. No phase cancellation of vortex noise is possible, because of its nonperiodic nature, and the vortex noise is therefore radiated down the duct. As indicated in Sec. 4.1, the sound power radiated as vortex noise is proportional to the projected blade area in the direction of motion, and to the sixth power of the blade speed.

Where the duct, the stators, or the rotors, do not have perfect axial symmetry, rotational noise will be propagated down the duct as airborne sound. Since this effect

depends upon departures from the nominal symmetrical design, it is difficult to make any general predictions. However, case vibrations, as discussed below, are important for usual compressor design; asymmetry effects are of secondary importance compared to these.

The preceding considerations apply to sound within the duct which is completely airborne. In addition, structure-borne sound is important. The pressure disturbances around the rotor blade tips apply oscillating dipole forces to the compressor case immediately about the rotors. The effect is similar to that of vibrational forces developed on an airplane fuselage in the vicinity of the propeller. The case vibration will cause the rotational noise to propagate along the duct walls. If vibration breaks are installed near the compressor, this has little effect on noise levels at a distance down the duct. In the absence of vibration breaks, this structure-borne sound may be the major source of noise within the duct at a distance from the compressor.

The vibration of the case in the immediate vicinity of the rotors is responsible for most of the external noise from the compressor. This external noise is largely periodic. The noise chart for axial-flow compressors, Fig. 6.7, refers to the generation of external noise by the compressor, and not to the generation of noise within the duct. The effective power levels given in the chart were obtained by finding the total power delivered externally, on the basis of a multiple-point survey.* Since the external sound is largely rotational noise, it is predicted theoretically that the level should increase by 5 to 6 db per horsepower doubling, in agreement with Fig. 6.5. It is difficult to calculate the absolute level of the external sound theoretically because this involves the vibrations of elastic plates (the case) under complicated boundary and excitation conditions. However, under simplifying assumptions, some theoretical results may

---

*   Note that in the case of axial-flow compressors, the power levels as given in Sec. 6.3 refer to the noise external to the compressor. On the other hand, the power levels for centrifugal compressors refer to the noise inside the compressor ducts, so that the transmission loss of the duct walls must be taken into account to obtain the external noise.

be obtained. They are not intended to replace the empirical results of Sec. 6.3 but to give further quantitative insight into the problem.

It is possible to identify three important mechanisms that contribute to the intensity of the blade rotation noise:

(1) Blade rotation itself, as in the case of a propeller in free space.

(2) Aerodynamic interaction of the blades and stators.

(3) Fluid flow between the blade tips and the compressor case.

Only the mechanism associated with (1) has been evaluated theoretically; preliminary calculations indicate that (2) and (3) are of secondary importance. In order to evaluate (1), it has been assumed that the distribution of the thrust force along the blades is independent of the distance along the blades. Further, it has been assumed that the blade width and thickness is very small, so that the thrust force is concentrated on blade lines and so that volume change effects of the air as the blade passes may be neglected. Then, the mean pressure in the plane of rotation is found to be:

$$p_1 = \frac{\Delta P}{4\pi} \left(\frac{\delta + 1}{\delta - 1} \quad \ln \delta \right)^{1/2} \qquad (6.3a.1)$$

where p_1 is the rms pressure for the fundamental frequency

ΔP is the pressure rise across the plane of rotation

δ is the ratio of the inside compressor radius R_o, to the hub radius R_h.

The fundamental frequency is given by

$$f_1 = \frac{N \ (\text{RPM})}{60} \quad , \text{cps} \qquad (6.3a.2)$$

where N is the number of blades. Harmonics of the funda-
mental frequency are generated also. The pressure for the
harmonics depends upon the assumed force versus time
character at each element of the blade disc; for the
assumption used in Eq. (6.3a.1), equal magnitudes are pre-
dicted for all the harmonics in the plane of rotation.
(Note that this result does not agree with the empirical
information given in Sec. 6.3, in which the second harmonic
is estimated to be the frequency of maximum radiation.)

The theoretical results above may be used to predict
the excitation of the compressor case, and thus the sound
radiated from the case. As an example, consider the
following problem:

$$\Delta P = 60" \; H_2O \text{ per stage}$$

$$\text{Number of stages } = 3$$

$$\text{Distance between stages } = 3"$$

$$R_o = 13"$$

$$R_h = 60$$

$$RPM = 7200$$

$$HP = 1350$$

Then, for each stage,

$$p_1 = 1.2 \times 10^4 \text{ dynes/cm}^2$$

or

$$SPL = 155 \text{ db } \underline{re} \; .0002 \text{ dyne/cm}^2$$

at

$$f_1 = 7200 \text{ cps}$$

The transmission loss (TL) of the compressor case is a
measure of the radiation for a given pressure excitation.
Assume the case is of cylindrical construction and about
1/4" thick. Then the TL is about 30 db. The resulting
pressure outside the case is thus about 125 db per stage.
According to the assumed thrust distribution, this value
of SPL is valid for all the harmonics as well as the funda-
mental. All three stages, however, are operating in
definite phase relation. Thus conservative practice dic-
tates that the combined sound pressure for the three
stages just outside the case is the sum of the sound
pressures from each stage, giving SPL = 125 db + 20 log 3
= 135 db.

It is instructive to compare the above estimate with the values predicted by the empirical relations given in Sec. 6.3. Figure 6.7 yields a PWL value of 135 db for the frequency of maximum output (the second harmonic). The relevant area for converting the PWL to SPL is not accurately known, but may be assumed to vary between about 2 sq ft (corresponding to the cross-sectional area between the hub and the case) and about 5 sq ft (corresponding to the surface area of the case in the vicinity of the blades). Thus the resulting SPL is between 128 db and 132 db, in reasonable agreement with the value calculated above from Eq. (6.3a.1).

Section 6.3 also indicates a method for estimating the spectrum below the fundamental frequency. Using the information given in Sec. 4.1 on vortex noise*, the spectrum below the fundamental may be calculated. The result is also in reasonable agreement with the empirical result from Sec. 6.3.

---

*   In order to use the information, account has to be taken of the different drag coefficients and Reynolds' number for the present example and the experiments quoted therein.

6.5 Noise from Ventilating Fans and Ventilation Systems

Experimentally Measured Power Levels and Spectra. The acoustic power level of a ventilating fan in a duct may be determined from the average sound pressure across the duct passage. The measurements must be made at locations at least several fan diameters away from the fan and the sound pressure must be the result of acoustic energy traveling away from the source, i.e., the reflection of the sound back from the more distant portions of the duct should be negligible. The power level for a fan in open air, or for the back side of a fan which is connected to a duct on one side only, can be determined from measurements of the sound pressure at several points on a surface in space which surrounds the source. This survey must be performed in the absence of reflecting objects. The basic principles of both of these methods are discussed in Chapter 3.

The first method, which relates to a fan operating in a duct, may be applied successfully when the duct is very long and has sufficient sound attenuation to prevent reflections at all frequencies which are of importance, or when the duct is connected to a non-reflective termination specially designed for use in laboratory measurements of fan noise. A laboratory system having a non-reflective termination, as described by Beranek, Reynolds and Wilson 5.1/, is shown in Fig. 6.5.1. A recommended modification of this system, for future measurements is given in the reference.

Measurements performed with this laboratory system on fans of both vaneaxial and centrifugal types, with input power up to six horsepower, have led to the following conclusions 5.1, 5.2, 5.3/.

1. The spectrum for centrifugal fans falls off rapidly with increasing frequency. The decrease of power level between successive octave bands is 5 db.

2. The spectrum for vaneaxial fans is nearly uniform for octave bands 20-75 cps to 1200-2400 cps, inclusive, but decreases in the higher bands.
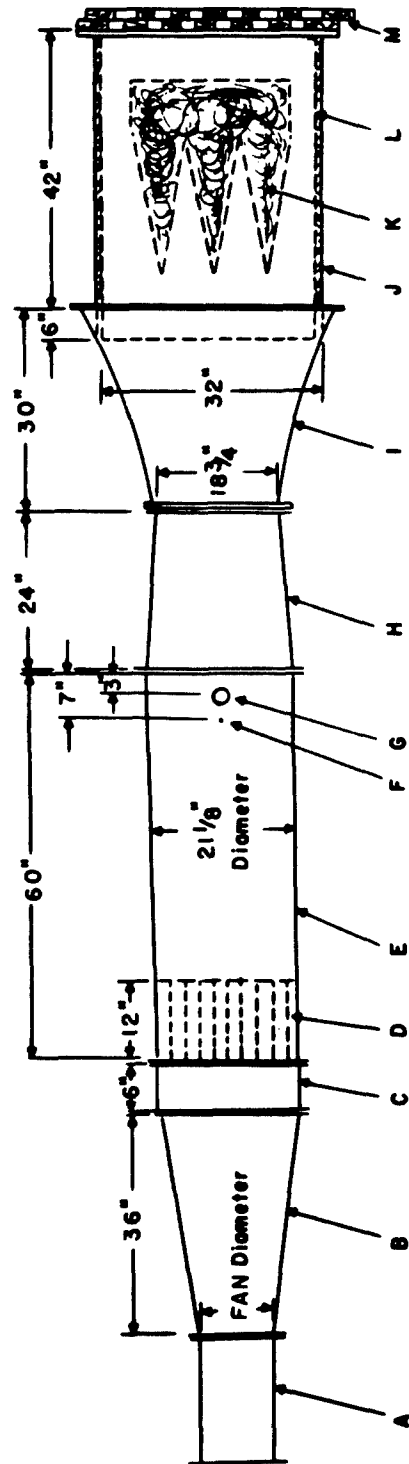
FAN AND DUCT SYSTEM

3. The spectra on inlet and outlet sides of a fan are similar, except that a narrow peak protruding above the broad-band noise by 6 db or less at the blade fundamental frequency, may be observed on the inlet side, but is scarcely observable in the exhaust.

4. The spectra and the power level are not significantly changed by varying the back pressure on the fan.

5. The exhaust spectrum is nearly independent of speed below the rated maximum.

6. The open inlet to the fan has very nearly the same directional properties as a piston of the same size.

7. Reversing a vaneaxial fan has no significant effect on the sound output.

The summary spectra resulting from the study are shown in Fig. 6.5.2 where the ordinate indicates octave band power level relative to the overall power level. The shaded zones show the latitude within which variations may be expected according to the individual fan design and operating speed.

FIGURE 6.5.1

Laboratory system for measuring noise delivered to a duct by one side of a ventilating fan.

A - fan
B - conical adapter
C - canvas vibration-isolation coupling
D - straightening vanes
E - measuring section
F - manometer location
G - microphone opening
H - adapter
I - exponential horn section
J - acoustic termination
K - three acoustic wedges, each 8" x 24" base, 6 lb/ft^3 Fiberglas
L - Fiberglas lining, 6 lb/ft^3, 1" thick
M - adjustable back-pressure panels 5.1/

It has been found that the overall acoustic power level is determined by the mechanical power delivered to the fan. The relationship given in Ref. 5.2 is based on measurements made on two centrifugal fans. In order to cover a range of input mechanical power, the fan speed was varied. It was found that the PWL varied as 20 log HP when the speed of a single fan was decreased below the rated maximum value. Since the horsepower depends on the 5/2 power of the angular velocity of the fan in the range near the rated load, the acoustic PWL varies as 50 log rpm. However, when the PWL's of a series of different fans having different maximum rated horsepower are compared, a different dependence of PWL on input mechanical power is observed. In this case, the PWL for fans operating at their rated horsepower varies as 10 log HP. That is, the PWL increases by only 3 db per doubling of horsepower in the second case but as 6 db per horsepower doubling in the first case.

From Ref. 5.3, the overall PWL, for different fans operating near their maximum rated horsepower, is

$$PWL = 100 + 10 \log_{10} HP \qquad db. \qquad (6.5.1)$$

For the case where the speed of a single fan is varied, Eq. (7) of Ref. 5.1 is still valid. However, the corrections and limitations to the data of Ref. 5.2, as discussed in Ref. 5.3 should be consulted. In particular, the constant 120.4 db should be 114 db.

It should be noted that a reduction in noise can be obtained by using a fan having a maximum rated input power larger than necessary for the job to be done and then operating it at lower than rated power. The power level delivered to the exhaust duct alone or the input duct alone is approximately 3 db less than the total PWL given by Eq. (6.5.1)

Ventilation System Noise Level in a Room. When the ventilating fan communicates with a room through a section of duct, the duct opening in the room becomes a source of sound which, in any given octave band, has the same power level as one side of the fan, less the attenuation introduced by the duct in that band. The methods for finding the attenuation of sound in an acoustically treated duct are discussed in Sec. 12.2. Thus, when the properties of the fan and of the duct are known, the sound pressure level

in the room may be found by the methods which are employed in any case where a sound source of known properties is present. A method of calculating the level in the room is discussed in Sec. 3.5. The quantities which enter into the calculation are:

1. the power level of the source in the desired frequency band

2. the directivity factor, Q, of the source in this frequency band, in the direction of the observer

3. the distance, r (ft) between the observer in the room and the source

4. the room constant, R in sq ft.

The room constant R is equal to $S\bar{\alpha}/(1-\bar{\alpha})$ where S is the area of the room boundaries in sq ft and $\bar{\alpha}$ is the average value of the absorption coefficient*. Ordinarily, the chamber absorption coefficient is used. (Sec. 12.1)

The accompanying charts facilitate evaluation of some of these quantities 5.1/. The effective directivity factor for the source at low frequencies is affected by the location at which the duct enters the room. Four cases may be distinguished conveniently, as shown in Fig. 6.5.3. A duct which opens in the center of the room volume (Case A) is assumed to radiate nondirectionally, as into open space, at low frequencies. This corresponds to a low-frequency value of 1.0 for Q. At the other extreme, radiation from an opening in the corner (Case D) is restricted to one octant in space, with a minimum value of 8 for Q. At sufficiently high frequencies the directivity in all cases approaches that of a piston of radius a, but in practice the directivity factor on the axis rarely rises above 50. The axial directivity factor for each of the four cases is plotted as a function of a dimensionless frequency parameter in Fig. 6.5.4. The quantity a is equal to the radius of a circular duct opening, or to $L/\sqrt{\pi}$ for a square opening of width L. For a rectangular

---

*   This quantity is called α in Chapter 3.

TYPICAL FAN SPECTRA

OCTAVE BAND FREQUENCIES IN CYCLES PER SECOND

OCTAVE BAND LEVEL RELATIVE TO
TOTAL POWER LEVEL IN DECIBELS
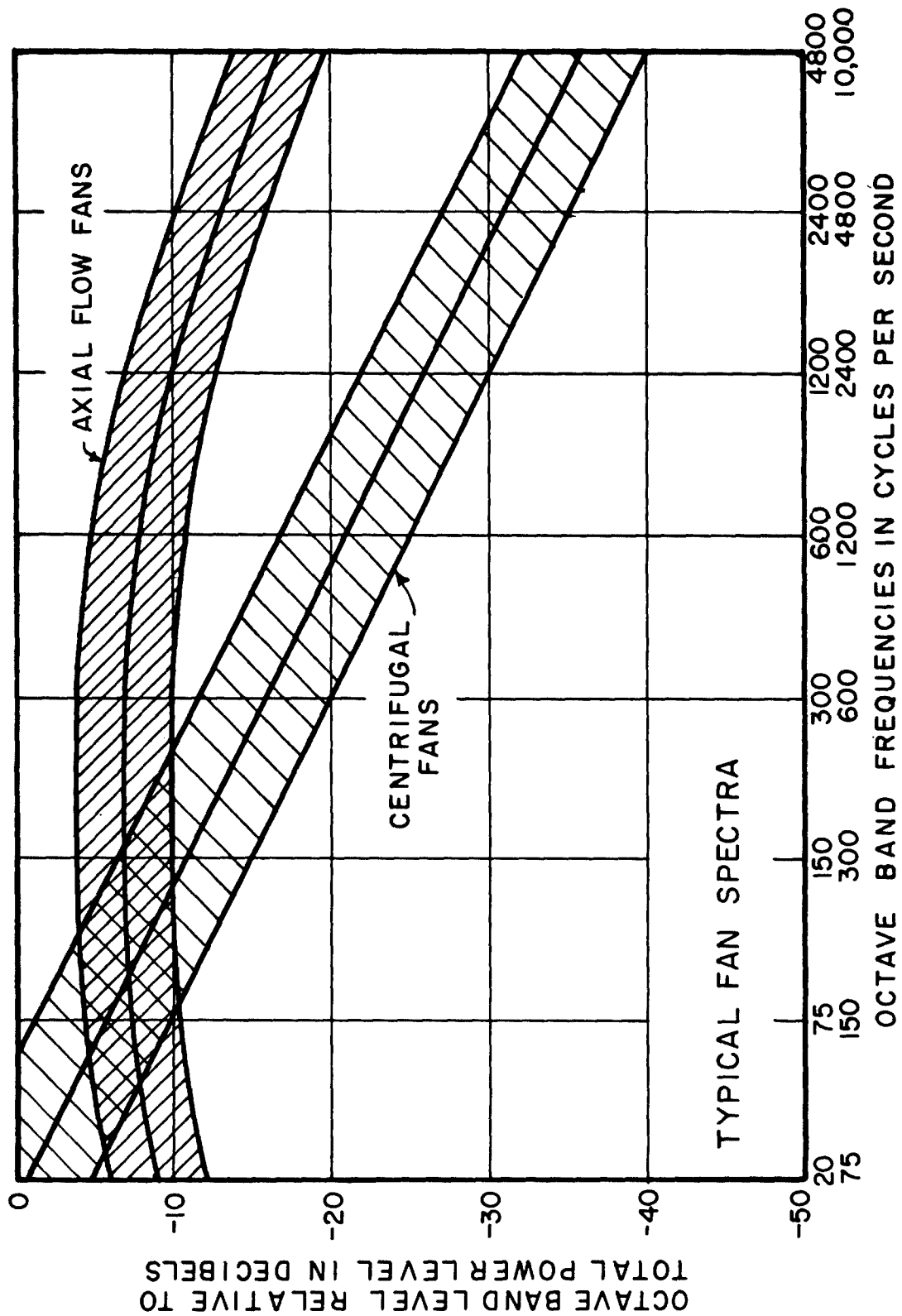
opening of widths L_x, L_y, the value of Q lies between the values for the corresponding square openings. The large values of Q for high frequencies represent beaming of the sound in the axial direction, perpendicular to the plane of the opening. The off-axis values of Q are much smaller at high frequencies; for example, if the opening is in the center of a wall, the value of Q for the direction 45° from the axis is approximately 2 at all frequencies.

In some cases an accurate calculation is not required, or information regarding the absorption coefficient of the walls may be insufficient for accurate calculation. In these cases, an approximate value of the room constant, R, may be obtained by characterizing the room as "live" ($\bar{\alpha}$ = 0.05) or "dead" ($\bar{\alpha}$ = 0.4) or by some intermediate designation, and by using the value of $\bar{\alpha}$ thus selected with the known wall area. If the room shape is specified, the wall area is uniquely related to the volume; for example, in a cubical enclosure the wall area is six times the two-thirds power of the volume. On this basis, the chart of Fig. 6.5.5 has been constructed to give values of the room constant as a function of room volume for four values of the average absorption coefficient which cover the range "dead" to "live". While the chart is derived for a cubical enclosure, it may be used for ordinary rooms, but is not applicable to extreme cases such as that of a long corridor.

Grille Noise. In calculating the noise produced in a room by a ventilating system, it is necessary to consider not only noise generated directly by the fan, but air-flow noise produced at the grille opening into the room. No extensive measurements of grille noise are available. The following tentative relations, which indicate how the PWL of noise from a grille is expected to vary with flow velocity and with pressure drop across the grille, are given in the Heating Ventilating Air Conditioning Guide 5.4/.

FIGURE 6.5.2

Typical octave band spectra for vaneaxial and centrifugal fans. Shaded areas show the expected spread as a result of variations in details of fan and blade design and speed 5.1, 5.3/.
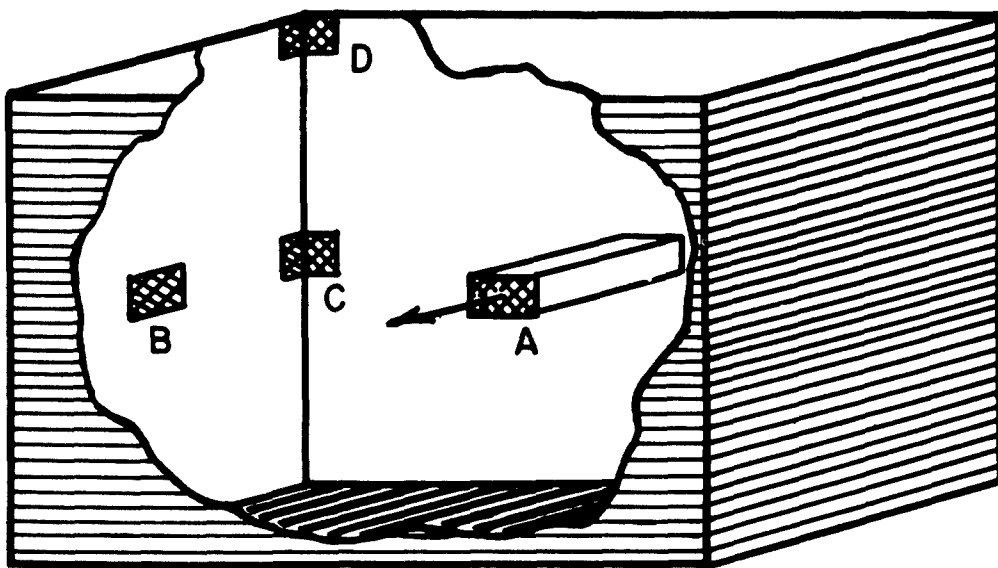
Figure 6.5.3

Illustration of four positions for duct opening in a
room, for which the directivity factor is given in
Fig. 6.5.4. Ref. 5.1.

$$\text{PWL change in db} = 50 \log_{10} (V_2/V_1) \qquad (6.5.2)$$

V_1 and V_2 are flow velocities on the two sides of the grille

$$\text{PWL change in db} = 25 \log_{10} (P_2/P_1) \qquad (6.5.3)$$

P_1 and P_2 are the pressures on the two sides of the grille. Also, on the basis of very limited data, a typical value of SPL at the grille is 48 db for a pressure drop of 0.1 in. water. If this figure is accepted for use with Eq. (6.5.3), the power level for one side of the grille is

$$\text{PWL} = 73 + 10 \log_{10} A + \log_{10} P \qquad (6.5.4)$$

where A is the grille area in sq ft and P is the pressure drop in inches of water. In view of the limited evidence on which this relation is based, it is preferable to work from experimental measurements on a grille of type similar to the one in question, rather than to use the above equations, when this is possible.

Available data on grille noise give no detailed information on the spectrum of the noise. Until adequate data are available, it is suggested that Curve D of Fig. 6.11 for noise due to air flow through a valve be used in estimating the grille noise spectrum.

Example of Estimating Ventilation System Noise in a Room. The application of these principles is now illustrated by numerical example. Suppose that it is desired to estimate the SPL in octave bands, for a location of 10 ft in front of the grille opening, under the conditions which are listed below. Assuming it has been established that the air flow noise at the grille will not exceed allowable limits, we now estimate noise due directly to the fan.

Room Data: Volume 10^5 cu ft. Medium-live in the lower two octave bands, and medium-dead in the higher frequency bands. The corresponding values of the room constant, from Fig. 6.5.5, are 2300 sq ft for the lower two bands and 4400 sq ft for higher bands.

Connecting Duct: Length of duct, 40 ft. The total attenuation of the duct, when split into several parallel sections each with individual acoustical lining, is assumed to be as shown in Table 6.5.1. The grille opening is near the center of a room wall, and is 4 ft square.

A – GRILLE AT CENTER OF ROOM
B – GRILLE AT CENTER OF WALL
C – GRILLE AT CENTER OF EDGE
D – GRILLE AT CORNER

APPROACHES
Q = 50 AS A
PRACTICAL
LIMIT

DIRECTIVITY FACTOR Q

$$ka = \frac{2\pi fa}{c} = \frac{2\pi a}{\lambda}$$
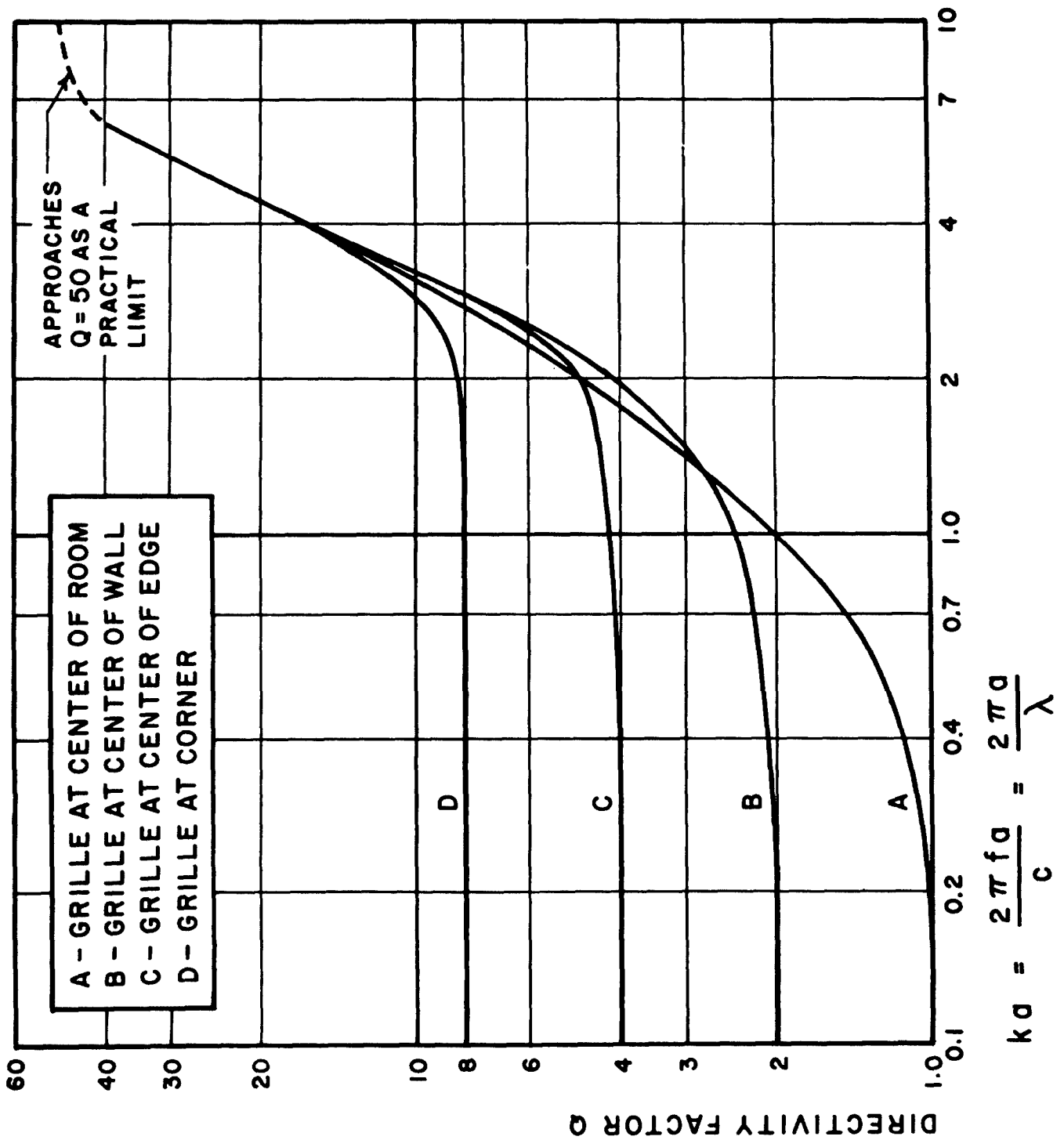
Fan: Centrifugal fan operated at its rated power of 5 HP. From Eq. (6.5.1), the total PWL is estimated as 107 db, and the PWL affecting the duct on one side of the fan only is then 104.

From Fig. 6.5.2, which gives the limits of the spectrum to be expected, we derive the effective power levels in the individual bands from the overall PWL of 104 db. The individual band power levels are shown in Table 6.5.1.

The axial directivity values are obtained from Fig. 6.5.4 for an opening 4 ft square, at the frequencies corresponding to the centers of the octave bands. These directivity (Q) values are also listed in the table.

The values of relative SPL at a distance of 10 ft from the opening are found from Figs. 6.3.3, 6.3.4, and 6.3.5 or from Eq. (3.10), for each band, by use of the appropriate room constant (R) and directivity factor (Q) already determined. These relative SPL values would be numerically equal to the SPL figures at the point of observation if the grille opening acted as a source whose PWL was zero db in each band.

Actual values of SPL in each band, at the desired point 10 ft in front of the grille, are obtained by subtracting the duct loss from the sum of the band PWL of the fan and the relative SPL. These actual values of SPL are listed in the final column of Table 6.5.1.

The resulting SPL spectrum falls off very rapidly with increasing frequency in the lowest few octave bands. This effect is often found in ventilation noise problems. In the present example, this is the combined result of the slope of the centrifugal fan spectrum and the extreme slope of the duct attenuation function in the lower frequency bands.

FIGURE 6.5.4

The directivity factor on the axis (perpendicular to the plane of the opening) for the four duct opening locations of Fig. 6.5.3. Speed of sound, c; λ, wavelength; f, frequency in cps; a, radius of circular opening or (width $/\sqrt{\pi}$) for a square opening 5.1/.
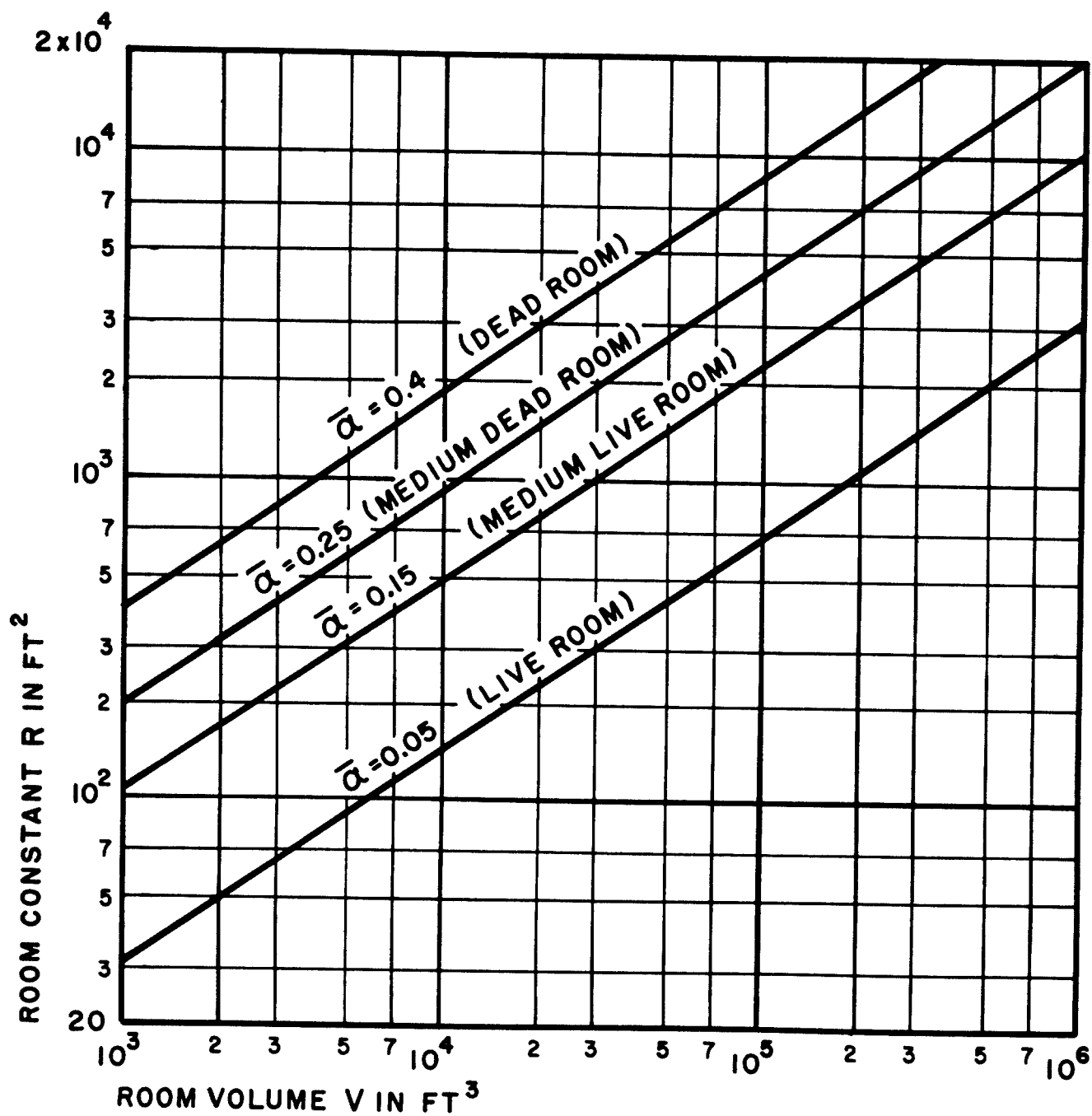
Usually, the designer is given the characteristics of the fan and the allowable sound pressure levels in the room, and the problem becomes one of finding the attenuation that must be provided in the duct system so that the allowable levels will not be exceeded. The methods for obtaining this attenuation are considered in Chap. 12. In many cases, an elaborate treatment must be used if the sound pressure level is to be substantially reduced in the low-frequency bands.

Relation to Other Air Flow Devices as Noise Sources. The same basic phenomena are responsible for noise generation in a wide variety of fluid flow devices. These phenomena include the mechanisms by which energy of flow is converted into heat and into random acoustical energy in the process of turbulence, and the mechanisms by which the air flow can be modulated to give an acoustic signal having a periodic waveform, as in a fan, propeller, turbine, or other device with rotating blades. An understanding of these phenomena enables the engineer to utilize principles of noise reduction in the basic design of ventilation equipment.

FIGURE 6.5.5

The room constant as a function of room volume, for average absorption coefficient categories "live" to "dead". This assumes that the relation between wall area and volume is approximately that for a cubical room, but may be applied in usual cases where the room shape is not extreme.5.1/

TABLE 6.5.1

CALCULATION OF SOUND PRESSURE LEVELS PRODUCED BY A VENTILATING SYSTEM

Octave Band cps	Source PWL in Band db	Q Directivity Factor on Axis of Opening	R Room Factor	Relative SPL-10' in Front of Opening (Eq 3.10)	Duct Loss db	Resulting Band SPL, db, 10' in Front of Opening
20-75	102	2	2300	-25 db	7	70
75-150	98	3	2300	-24	12	62
150-300	93	9	4400	-21	45	27
300-600	88	40	4400	-15	50	23
600-1200	82	50	4400	-14	50	18
1200-2400	78	50	4400	-14	50	14
2400-4800	73	50	4400	-14	50	9
4800-10000	68	50	4400	-14	50	4

References

(5.1)   Beranek, L. L., Reynolds, J. L., and Wilson,K.E.
        "Apparatus and Procedures for Predicting Ventila-
        tion System Noise", J. Acous. Soc. Am. <u>25</u>,
        313-321 (1953).

(5.2)   Peistrup, C. F., and Wesler, J. E., "Noise of
        Ventilating Fans", J. Acous. Soc. Am. <u>25</u>,
        322-326 (1953).

(5.3)   Beranek, L. L., Kamperman, G. W., Allen, C. H.
        "Noise of Centrifugal Fans" (to be published
        in the J. Acoust. Soc. Am.)

(5.4)   <u>Heating Ventilating Air Conditioning Guide 1953</u>
        (Vol. 31), (Am. Soc. Heating and Ventilating
        Engrs., New York, 1953), pp. 901-902; also
        earlier editions of this guide.

11.2 Insulation of Airborne Sound by Rigid Partitions

General Remarks. Since our ear is an airborne sound receiver, the best insulation from noise radiated into the air is to interrupt the direct sound path by a rigid partition. This then forces the sound to become structure-borne sound for some part of the way.

This partition may surround the source or the receiver in all directions (Fig. 11.2.1a and 1b) or it may separate a large room into two rooms (Fig. 11.2.2). In the second case, the area of the partition wall S is only a part of the area S_1 of the source room and the area S_2 of the receiving room. By multiplying S_1 and S_2 by the corresponding mean absorption coefficients of the source room and the receiver-room, we obtain the so-called absorption powers A_1 and A_2. If we now consider as given the power of the source P_o we may ask for the mean sound pressure p_2 in the receiver room, or for the corresponding energy density E_2 (energy /unit volume) which is proportional to the square of p_2.

We split the problem into the following steps. Due to the source of power P_o, the energy density E_1 in the source room is

$$E_1 = 4P_o/cA_1 \qquad (11.2.1)$$

where c is the velocity of sound in air. (These and the following formulae are based on the assumption that the sound is distributed randomly over all regions and directions in the room). The energy density E_1 determines the power P_1 striking the wall under test

$$P_1 = cSE_1/4 = P_oS/A_1 \quad . \qquad (11.2.2)$$

Notice that P_1 can and usually will be much greater than P_o, because the reflected energy in the souce room is included in P_1. As a result of the power P_1 being incident on the wall, there is a transmitted power P_2. This process is influenced only by the construction of the wall and is characterized by the transmission coefficient defined by
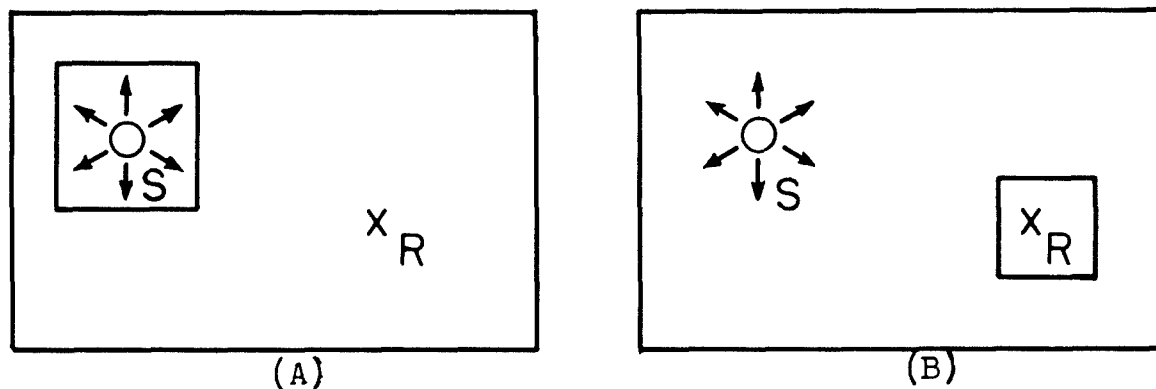
FIGURE 11.2.1

Two possible ways of shielding a receiver R from a sound source S in the same room. In (A) the source is enclosed by a rigid partition while in (B), the receiving space is enclosed.
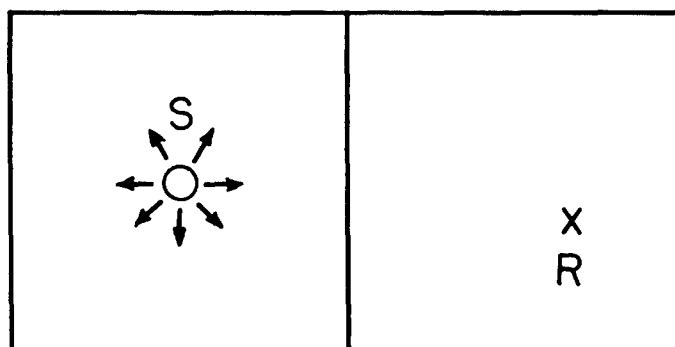
FIGURE 11.2.2

A more common situation where the source and receiver are separated by a partition dividing the space in two.

$$P_2 = \tau P_1 = \tau cSE_1/4 = \tau SP_c/A_1 \quad .$$

$$(11.2.3)$$

Finally, P_2 results in an energy density E_2 in the receiving room for which we require

$$E_2 = \frac{4P_2}{cA_2} = \frac{4P_1}{cA_2} = (S/A_2)\,E_1 = 4S\,\tau\,P_o/cA_1A_2 \quad .$$

$$(11.2.4)$$

The equation relating E_2 and P_o demonstrates the existence of reciprocity; it states that if you hear a neighbor, he hears you just as well.

But this general law only regards the physical part of the problem. When the physiological part is introduced, reciprocity may not hold. Suppose a masking noise exists in one room. Then the sound of speech transmitted from a neighboring (quiet) room may be masked completely; but in the quiet room, the noise level is much lower (corresponding to the reduction of the noise by the wall) and speech which is louder than the noise in the source room will, after transmission through the wall, still be heard very clearly in the neighboring rooms.

The principle of reciprocity also may not be applicable from the physical point of view if we do not regard the power of the sound source P_o as the given quantity but the energy density E_1 in the source room. This is the case in the usual measuring techniques for air-borne sound insulation where we compare E_1 and E_2 by measuring the sound pressure at several points in both rooms. In this case we get from Eq. (11.2.4)

$$\tau = E_2 A_2/E_1 S \quad . \qquad (11.2.5)$$

This means that in order to find τ we have not only to compare E_1 and E_2 but we have to measure S and A_2. Here

we get different ratios of energy density depending on which we choose to call the source and the receiving room.

The absorption power A_2 may be evaluated from the measurement of the reverberation time T_2 in the receiving room using Sabine's formula

$$A_2 = 0.05\ V_2/T_2 \qquad (11.2.6)$$

where A_2 and V_2 are the room absorption and room volume in units of sq ft and cu ft respectively.

Since we are usually trying to minimize the amount of sound energy transmitted to another room, we are interested in values of τ as small as possible. For characterizing the quality of sound insulation, it is more useful to define a reciprocal quantity and, since this quantity varies between 10 and 10^8, we define a logarithmic measure called the Transmission Loss (TL) as

$$TL = 10\ \log 1/\tau \quad . \qquad (11.2.7)$$

Calculated in this way, the TL is expressed in decibels*. At first it was assumed that this logarithmic scale would also correspond to our subjective valuation of sound intensity which we call loudness. Although this is not actually the case, we may say to a first approximation, that each increment of 9 db in TL is equivalent to halving the loudness.

---

* This quantity is internationally used, but is called "transmission loss" in America only. For a European Code, the British proposed to call it reduction factor "R". In Germany the quantity is called "Schalldammzahl" and the letter K is used. Kosten (Netherlands) proposed the name "insulation" and the symbol i.

In the same way, the quantity

$$NR = 10 \log E_1/E_2 \text{ db} \qquad (11.2.8)$$

may be called the noise reduction (NR). With modern measurement equipment this quantity can be measured directly. Then Eq. (11.2.5) in the logarithmic form is

$$TL = NR + 10 \log S/A_2. \qquad (11.2.9)$$

The noise reduction to be expected with a given construction is

$$NR = TL - 10 \log S/A_2. \qquad (11.2.9a)$$

Note that the noise reduction depends on the area of the separating wall. The smaller this area is, the lower the transmission loss which will be tolerated.

The last remark is of special importance if the partition consists of two parallel parts, for instance a heavy wall and a door. It would be too expensive to give the door the same TL as the wall. Since the door, however, has only a small surface S_2 compared to the surface of the whole wall $S_1 + S_2$ the power entering the second room, consisting here of two parts,

$$P_2 = cE_1 \; (\tau_1 S_1 + \tau_2 S_2)/4$$

$$(11.2.10)$$

will not be increased very much if τ_2 is higher than τ_1. The resulting loss of TL is given by

$$\Delta (TL) = 10 \log \frac{\tau_1 S_1 + \tau_2 S_2}{\tau_1 (S_1 + S_2)} \; .$$

$$(11.2.11)$$

If we chose a value for this quantity, we might calculate for the difference between both kinds of partitions

$$(TL)_2 - (TL)_1 = 10 \log \tau_1/\tau_2 = -10 \log [10^{\Delta/10}(1+S_1/S_2)-S_1/S_2].$$

$$(11.2.12)$$

In Figure 11.2.3 this difference is plotted as a function of the ratio S_1/S_2 for $\Delta = 1$ and $\Delta = 3$ db.

Now we may discuss the influence of the absorption power in the receiving room. For measurements, we prefer rooms with small absorption power. In this case the measured NR may be greater than the quantity we wish to measure, the TL. In the case of a closed box installed in a large, noisy room (Fig. 11.2.1b), all walls are transmitting. Then A_2/S is equal to the mean absorption coefficient and therefore is always smaller than 1. In this case the NR is smaller than the TL. If, for example, it is possible to make $\alpha_2 = A_2/S = 0.5$ (which is a rather high value), we get from Eq. (11.2.9a)

$$NR = TL - 3 \text{ db} \qquad (11.2.13)$$

provided that these statistical formulae are valid for absorption coefficients which are so high. If we have $\alpha_2 = 0.25$, we get

$$NR = TL - 6 \text{ db}. \qquad (11.2.14)$$

We see that proper absorption in the receiving room has some advantage. In particular, very small amounts of absorption power must be avoided. If, in the limit, the absorption power in the receiving room is equal to the transmissivity of the surface S only, i.e., by $A_2 = \tau S$, then we find from Eq. (11.2.5), $E_2 = E_1$, or no transmission loss at all. This result may easily be understood from the standpoint of energy balance. If the receiving room and the wall itself present no energy losses, then the wall may have an arbitrarily high TL; as steady-state is reached, the energy density at both sides of the common wall is the same. On the other hand, even large amounts of absorbing material in the receiving room cannot result in a high noise reduction. The most we can expect is to get a free-field condition in which we have

near the wall, instead of Eq. (12.2.4)

$$E_2 = P_2/cS = \tau E_1/4$$

or

$$NR = TL + 6 \text{ db} . \qquad (11.2.15)$$

At a greater distance from the wall, the sound level will fall off faster than the inverse square relation for a free field. But excluding this very unusual (and expensive) case, we may summarize the last results by saying: some amount of absorbing power in the receiving room is necessary. An absorption power equal to half the surface of the separating wall may easily be reached, even in a closed box, but further amounts of absorption never would bring more than a 9 db increase in energy density ratio.

    Therefore, we see that we only get high sound level differences with constructions of high TL.

    Since the TL depends on frequency, it is not realistic to give only a mean value. Such a mean value can be at best a very crude order of magnitude estimate of effectiveness. In order to define such a mean value, one must first decide on the limits of the frequency range, the quantity we would like to average and the particular frequencies at which one measures values to average. In the European code of sound insulation measurements, the lowest frequency is given by 100 cps and the highest by 3200 cps. Below 100 cps measuring becomes very uncertain and, fortunately, the sensitivity of our ears is small. Above 3200 cps insulation is so good, generally, that we seldom have trouble. The frequency scale is logarithmic. This corresponds to the common use of octave steps or third-octave-steps and may be justified by the similar distribution of response for different frequencies on the basilar membrane in the inner ear. The most difficult question is to say what should be averaged. It is usual to average the transmission loss and therefore in the following $[TL]_m$ means the TL averaged between 100 and 3200 cps over a logarithmic scale.

    But we must realize that this kind of averaging is justified only if the loudness or the rate of nervous impulses per unit of time is proportional to the sound level.

We know that this assumption is not valid, but if we try
to take into account the loudness function, the average
TL will depend on the spectrum of the sound in the source
room. However, this is the situation we have if we want
to make conclusions concerning the subjective effect of
noise.

Therefore, it is better to consider the TL of a wall
as a set of values or a curve plotted over a logarithmic
frequency scale than to characterize it by a single value.

Single Wall

1. Relationship between the Transmission Coefficient and
the Transmission Impedance. In the following, we define
as a single wall each partition at which the normal velo-
city at the source side v_1 and the normal velocity at the
back side v_2 (and the velocities of all points between
them) are equal. Thus

$$v_1 = v_2 = v \quad . \qquad (11.2.16)$$

This does not require that the wall is of homogeneous
construction. It may consist of different sheets, e.g.,
plaster, brick, plaster. It may even contain holes.
There are many inhomogeneous constructions which work as
a single partition, at least in the low and middle fre-
quency region. But there are also constructions, as, for
example, concrete poured between plates of cemented wood-
shavings and plastered at both sides which would be
called single walls from a standpoint of construction but
which acoustically show the behavior of multiple partitions
in the most of the frequency region. On the other hand,
even for a homogeneous plate there exists a frequency

FIGURE 11.2.3

The loss in TL as a result of building a wall
with an area S_1 of a construction having $[TL]_1$
and an area S_2 of a construction having $[TL]_2$.
The ordinate gives the necessary TL of the
"insert" (i.e. door, window, etc.) when the
relative size of the wall and insert are known
and when the maximum tolerable loss of the total
TL has been chosen.
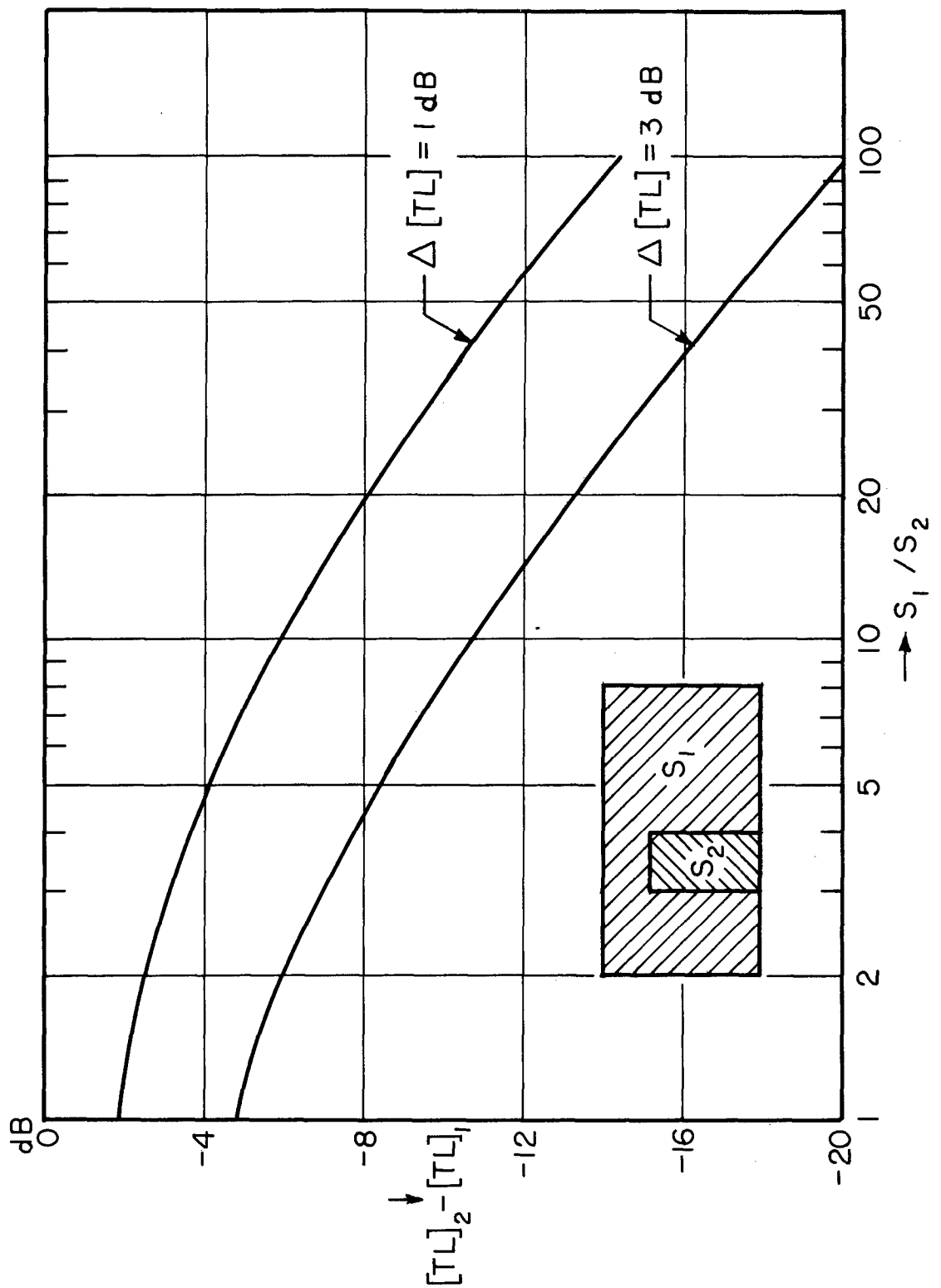
limit, above which the assumption of Eq. (11.2.16) loses its validity. This limit is reached when the thickness becomes larger than a tenth of the wavelength for the longitudinal wave in the wall. But in most cases of practical interest, this happens above the frequency region in which we are interested.

Assuming Eq. (11.2.16) is true, we may characterize the wall by its "transmission impedance" Z_τ which we define as the ratio of the pressure difference between inner and outer wall to the normal velocity

$$Z_\tau = (p_1 - p_2)/v_n \quad . \qquad (11.2.17)$$

It is to be expected that this quantity is dependent on frequency. This means that, in general, we have to consider all the quantities in Eq. (11.2.17) as complex, involving not only amplitudes but also phases. The transmission impedance differs from the so-called wall impedance

$$Z_w = p_1/v_n \qquad (11.2.18)$$

which characterizes the boundary condition for the source room by the term p_2/v_1. In the case of a wave radiated at the angle ϑ, which is the angle of incidence at the source side, Z_w is given by*

$$p_2/v_n = \rho c/\cos \vartheta \quad . \qquad (11.2.19)$$

---

* Practically, the difference between Z_τ and Z_w is much greater; in order to get the absorption coefficient using Z_w, we have to take into account also all losses which are given by heat conduction and friction, especially if the surface is porous. But for the calculation of transmission, these effects have no remarkable influence. Thus, if the wall is covered with a layer of fiberglas, we may split the whole problem into one of absorption and one of transmission.

The dimensionless transmission coefficient depends on the ratio of the impedances defined by Eqs. (11.2.17) and (11.2.19)

$$\tau = 1 / \left| 1 + Z_\tau \cos \vartheta / \rho c \right|^2$$

(11.2.20)

It is clear that the transmission must become total ($\tau = 1$) if the transmission impedance vanishes. This means that the pressures are equal at both sides of the wall. The transmission is zero if the transmission impedance tends to infinity.

We see that, in general, τ depends on the angle of incidence, even if Z_τ is independent of ϑ. This means that the transmission loss we observe experimentally, where the sound is impinging the wall at different angles, depends on the particular angular distribution of the sound. Also one must realize that a given surface S only subtends the area $S \cos \vartheta$ in the direction of the incident wave. (See Fig. 11.2.4). Therefore, when averaging τ over different plane waves, we have to multiply τ with the weighting factor $\cos \vartheta$. Hence

$$\overline{\tau} = \frac{1}{n} \sum_{k=1}^{n} \tau_k \cos \vartheta_k .$$

(11.2.21)

For a statistical sound distribution, as we may have in the case of testing a wall between two reverberant rooms, we may assume that the sound is equally distributed over all directions. This requires the introduction of another weighting factor $\sin \vartheta$ because the region between ϑ and $\vartheta + d\vartheta$ cuts out a zone of a sphere $2\pi \sin \vartheta \, d\vartheta$. Then we get for the average statistical transmission coefficient

$$\overline{\tau} = \frac{\int_{o}^{\pi/2} \tau \cos \vartheta \sin \vartheta \, d\vartheta}{\int_{o}^{\pi/2} \cos \vartheta \sin \vartheta \, d\vartheta} = 2 \int_{o}^{\pi/2} \tau \cos \vartheta \sin \vartheta \, d\vartheta .$$

(11.2.22)

This may also be written

$$\overline{\tau} = \int_o^1 \tau\, d(\cos^2 \vartheta) = \int_o^1 \tau\, d(\sin^2 \vartheta) \qquad (11.2.22a)$$

which is more convenient since τ always appears as a
function of $\cos \vartheta$ or $\sin \vartheta$ or even $\sin^2 \vartheta$ directly. Such
averaging becomes more and more dependent on the accuracy
of the assumption of random distribution of angles of
incidence the higher the TL of the wall.

2. The "mass law". The TL of any single wall depends chiefly
on the mass per unit area* In general light constructions

---

* This law was first found experimentally by
Richard Berger in 1910 and is sometimes called
"Berger's Law" in the German literature.
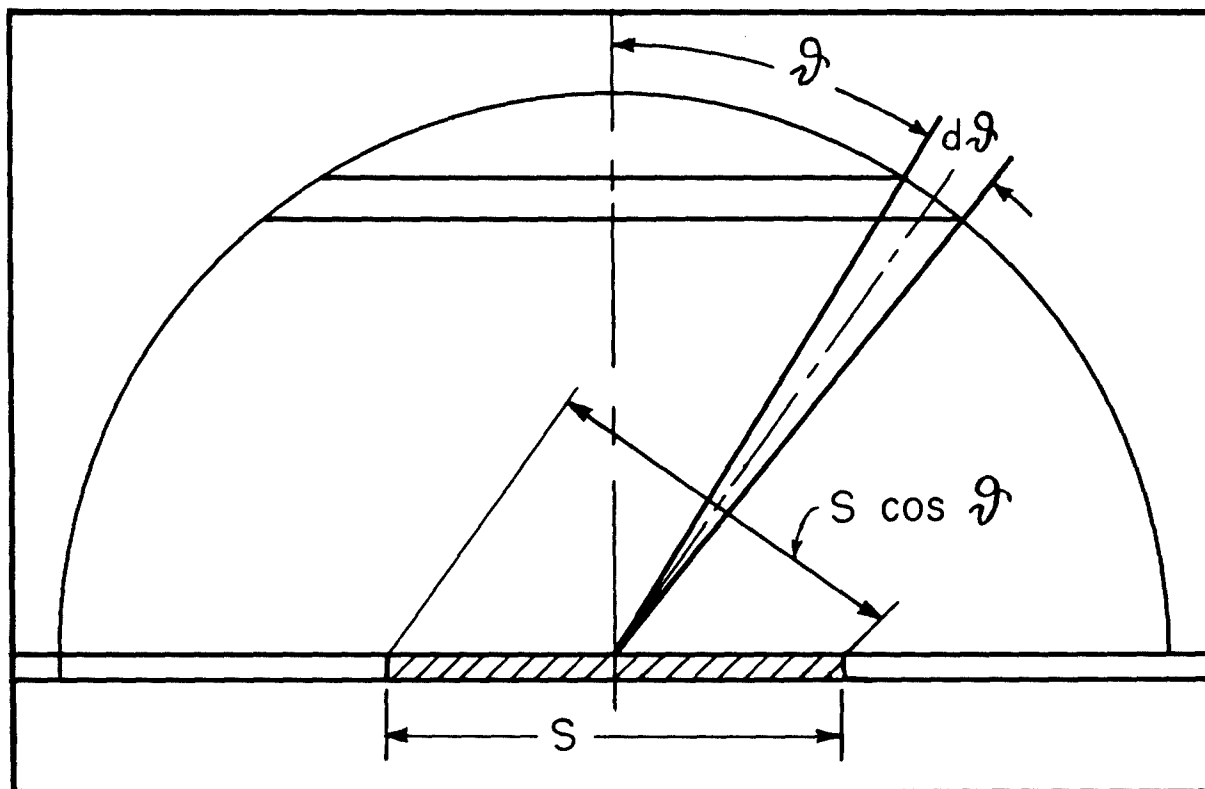
FIGURE 11.2.4

An area S subtends an area S cos ϑ to a plane
sound wave incident at an angle ϑ .

are more sound transmitting than heavy ones; and if it is necessary to save weight, it will always be difficult to have a high TL. However, there may be cases where heavy constructions having special defects are worse than other lighter constructions.

To a rough approximation, the mean TL may be calculated from the formula

$$(TL)_m = 14 \log G + 24 \qquad (11.2.23)$$

where G is the surface weight in lb/sq ft. Table11.2.1 shows the surface weights of some common building materials.

A further empirical fact is that the TL generally increases with frequency f. This may be derived from the mass law observation on the basis of similarity. If a heavier wall is better, then for a given material, the thicker wall is also better. But in a sound field, all thicknesses must be compared with the sound wavelength; therefore, we have to expect a dependence on the ratio h/λ or on the product hf if we replace λ by c/f. This general rule also holds when, as sometimes happens, an increase of frequency results in a decrease of TL. In these cases, an increase in thickness also results in a decrease of TL.*

To explain these general dependences on weight and frequency, the simplest assumption we can make is that the wall behaves like a mass. This means that we have to consider the transmission impedance as a mass reactance

$$Z_\tau = j\omega m \qquad (11.2.24)$$

where m is the surface mass and ω the angular frequency. Putting this into Eq. (11.2.20) we find

$$\tau = 1/[1 + (\frac{\omega m \cos \vartheta}{2 \rho c})^2]. \qquad (11.2.25)$$

---

* See Beranek, Leo L., Phys. Soc. Acoustics Group Symposium p. 1-6 (1949).

Excluding grazing incidence, we may also derive this result from Rayleigh's more general solution for the transmission through a sheet of non-rigid medium having high specific mass and small compressibility 2.1/. This shows that we do not have to discuss transmission through a wall in terms of its movement of an inert mass and as a result of longitudinal waves excited inside the wall. The first kind of motion is only a special limit of the second.

To compare Eq. (11.2.25) with experimental results found for walls between reverberant rooms, we have to average τ over $\cos^2 \vartheta$ according to Eq. (11.2.22). Doing this, we get

$$\overline{\tau} = (2\rho c/\omega m)^2 \quad \ln [1 + (\omega m/2 \rho c)^2]$$

$$(11.2.26)$$

or*

$$[TL]_{random} = [TL]_0 - 10 \log (0.23 [TL]_0).$$

$$(11.2.27)$$

where $[TL]_0$ is the transmission loss for perpendicular incidence. This result sometimes fits the experimental results quite well because it gives values of TL lower than $[TL]_0$ and also a less rapid increase of TL with surface mass and frequency.

However, this last equation can hardly be regarded as the real interpretation of what happens because plotting τ against $\cos^2 \vartheta$ for high values of $\omega m/2 \rho c$, we get a very sharp peak at grazing incidence where τ becomes one.

---

*   This dependence sometimes is called the random-incidence mass law.

TABLE 11.2.1

SURFACE WEIGHT OF COMMON BUILDING MATERIALS

	lb/sq ft/inch of thickness
Aluminum	14
Brick	10-12
Concrete	
Dense	12
Cinder	8
Cinder Fill	5
Glass	13
Lead	65
Plaster	
Gypsum	5
Lime	10
Plexiglas	6
Sand	
Dry loose	7-8
Dry packed	9-10
Wet	10
Steel	40
Transite	9
Wood	4-5

This dependence always has to be expected when Z_{τ} is independent of the angle of incidence or is nearly independent in the region of grazing incidence. We may call this the "component effect" because it has as its basis the fact that the normal velocity of a wall is only a component of the resultant of the velocities of the source side and the back side. We must realize, however, that the limit $\tau = 1$ for $\vartheta = 90^\circ$ infers an infinite wall and infinite plane waves and, therefore, cannot be realized in practice. Furthermore, we know from wave acoustics that in rooms, sound propagation exactly parallel to a boundary plane can never occur.

Therefore, it seems reasonable to exclude angles for which Eq. (11.2.28) does not hold

$$(Z_{\tau} \cos \vartheta / 2\rho c)^2 >> 1. \tag{11.2.28}$$

By integrating only to a limiting angle ϑ', we find for

$$\frac{1}{\tau}' = \int_{\cos^2 \vartheta'}^{1} (2\rho c/\omega m \cos \vartheta)^2 d(\cos^2 \vartheta) = (2\rho c/\omega m)^2 \ln 1/\cos^2 \vartheta' \tag{11.2.29}$$

corresponding to

$$[TL]_o^{\vartheta'} = [TL]_o - 10 \log \ln 1/\cos^2 \vartheta' \quad . \tag{11.2.30}$$

Now we have the difficulty that the result depends on the choice of the limit angle ϑ'. Taking $\vartheta' = 82.5^\circ$ as a value which guarantees that Eq. (11.2.28) is satisfied for $[TL]_o > 24$ db, we get

$$[TL]_o^{82.5^\circ} = [TL]_o - 6 \text{ db}. \tag{11.2.30a}$$

The same result is obtained if we calculate the TL for an angle $\vartheta = 60^\circ$ only, so we also may write

$$[TL]_{60^\circ} = [TL]_o - 6 \text{ db} \tag{11.2.30b}$$

We call this the "60° - mass law". It involves an essential simplification for it replaces the averaging over all angles of incidence by using a mean angle. In the present case where the τ is monotonically increasing with ϑ, the choice of $\vartheta = 60°$ is reasonable.

It would seem better to choose $\vartheta = 45°$ because this angle is in the middle of the ϑ range and has the highest weighting factor ($\cos 45°$ $\sin 45° = 1/2$). In the present case we get

$$[TL]_{45°} = [TL]_o - 3 = 20 \log G - 20 \log f - 31 \text{ db}$$

$$(11.2.31)$$

which also corresponds to the average τ value if we restrict the ϑ region from 0° to nearly 70°. This "45°-mass law" fits the experimental results for light constructions quite well. By averaging over the frequency region from 100 to 3200 cps (which means replacing f by the geometric mean of 100 and 3200 cps),

$$[TL]_{45,m} = 20 \log G - 24 \text{ db}. \qquad (11.2.32)$$

where the second term agrees with that in the empirically determined Eq. (11.2.23).

For higher values of G, all formulas which we have derived from the assumption of Eq. (11.2.24) gives TL's which are much too high. Therefore, we have to look for other reasons to explain this discrepancy.

3. The Influence of Stiffness. It seems likely that stiffness may be of importance. If we try to move the wall very slowly, we feel its stiffness only as the reaction to the driving force. This stiffness is given by the supporting or damping of the wall at the edges and also will be of importance if a very low frequency sound pressure is driving the wall. However, several authors have observed higher TL's at low frequencies than those corresponding to mass law 2.2,2.3/. Although this problem has not been solved theoretically, it seems probable that such deviations may be accounted

for by stiffness. But cases where stiffness gives an increase in the insulation power must be regarded as exceptions for the present. Usually stiffness is a dis advantage because the reactive forces due to stiffness and those due to mass are not added. However, because of their opposite phases they compensate for each other.

(a) <u>Resonance</u>. There are two kinds of effects where this happens. The first is well-known in acoustics as resonance, and means that the periodicity in time of the driving forces equals the periodicity in time of a free motion, i.e., a motion possible without external forces. If we have a bar of the length ℓ supported at both ends, the resonance is given by the condition

$$\ell = \lambda_B/2 \qquad (11.2.33)$$

where λ_B is the wave length of the bending wave corresponding to the same frequency. Formally we have the same condition for an organ pipe open at both ends or for a tube closed at both ends

$$\ell = \lambda_o/2 \qquad (11.2.34)$$

where λ_o is the wavelength in air. But there is an essential difference between the two cases: in the case of the propagation of the longitudinal waves in a tube, the wave length is inversely proportional to the frequency

$$\lambda_o = c_o/f \qquad (11.2.35)$$

whereas in the case of a bending wave, it is inversely proportional to the square root of the wave length

$$\lambda_B = \sqrt[4]{B/m} \; \sqrt{2\pi/f} \qquad (11.2.36)$$

or, the phase velocity of bending waves is proportional to the square root of frequency

$$c_B = \sqrt[4]{B/m} \; \sqrt{2\pi f}$$

$$(11.2.37)$$

In these equations, B is the bending stiffness. For a rectangular bar with Young's modulus E, height h and the breadth b,

$$B = E b h^3/12 . \qquad (11.2.38)$$

If we substitute $m = \rho bh$ and introduce the velocity for longitudinal waves

$$c_L \doteq \sqrt{E/\rho} , \qquad (11.2.39)$$

we can write instead of Eq. (11.2.36)

$$\lambda_B = \sqrt{1.8\ c_L h/f} . \qquad (11.2.40)$$

In the case of plates, Eqs. (11.2.38), (11.2.39) and (11.2.40) should be modified because of the hindered lateral contraction in one direction. Taking this into account, we have

$$B' = Ebh^3/12(1- \mu^2) \qquad (11.2.38a)$$

$$c_L' = \sqrt{E/\rho\ (1-\mu^2)} \qquad (11.2.39a)$$

$$\lambda_{B'} = \sqrt{1.8\ c_L'h/f} \qquad (11.2.40a)$$

where μ is Poisson's ratio. Since this number is 0.3 in most cases, the differences between these two groups of equations, especially between Eqs. (11.2.40) and (11.2.40a) become so small that we may neglect them and speak simply of B, c_L and λ_B only*. Furthermore, these values may depend much more on the individual variation of samples

---

*   In the available handbook tables of sound velocities, it is not even stated whether the longitudinal velocity in a bar, a plate or an infinite elastic medium is meant.

of the same material for such things as concrete, brick, and timber. For exact studies, it is recommended that c_L be evaluated by measuring the lowest natural frequency f_1 of a bar. Then c_L is given by

$$f_1 = .45 \; c_L h / \lambda^2 \qquad (11.2.41)$$

which follows from Eqs. (11.2.33) and (11.2.40). For rough evaluations, the data in Table 11.2.2 may be used.

TABLE 11.2.2

SOUND VELOCITIES FOR LONGITUDINAL WAVES

Glass	18,000 ft/sec
Steel	17,000 ft/sec
Aluminum	17,000 ft/sec
Timber (fir, lengthwise)	16,000 ft/sec
Concrete	12,000 - 15,000 ft/sec
Bricks with mortar	8,000 - 15,000 ft/sec
Plywood	10,000 ft/sec
Asphalt	7,000 ft/sec
Porous Concrete	4,000 ft/sec
Air (20°C)	1,130 ft/sec

FIGURE 11.2.5

The bending wavelength λ as a function of frequency f (in kc/sec) for plates of thickness h (in inches). These curves apply to steel and aluminum, for which $c_L = 17,000$ ft/sec.

STEEL, ALUMINUM
$C_L = 17000$ FT / SEC

h = 1 IN.
½
¼
⅛
1/16
1/32

λ (IN FEET) $\longleftarrow$

$f \longrightarrow$ kc/SEC

CONCRETE
c_L = 12000 FT/SEC

LIMIT OF VALIDITY

h = 16 IN.

8

4

2

1

λ (IN FEET)

$f \longrightarrow$ kc/SEC
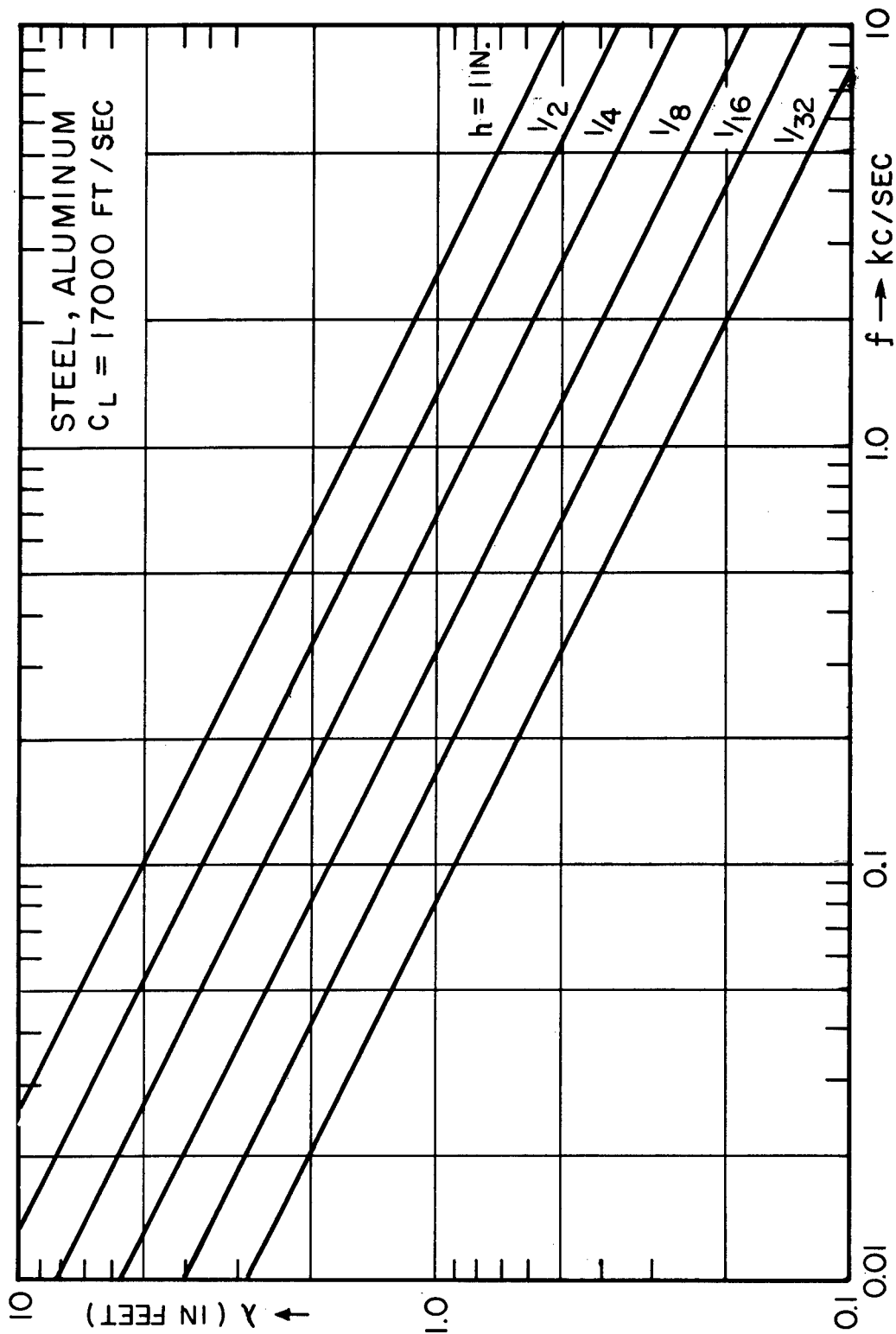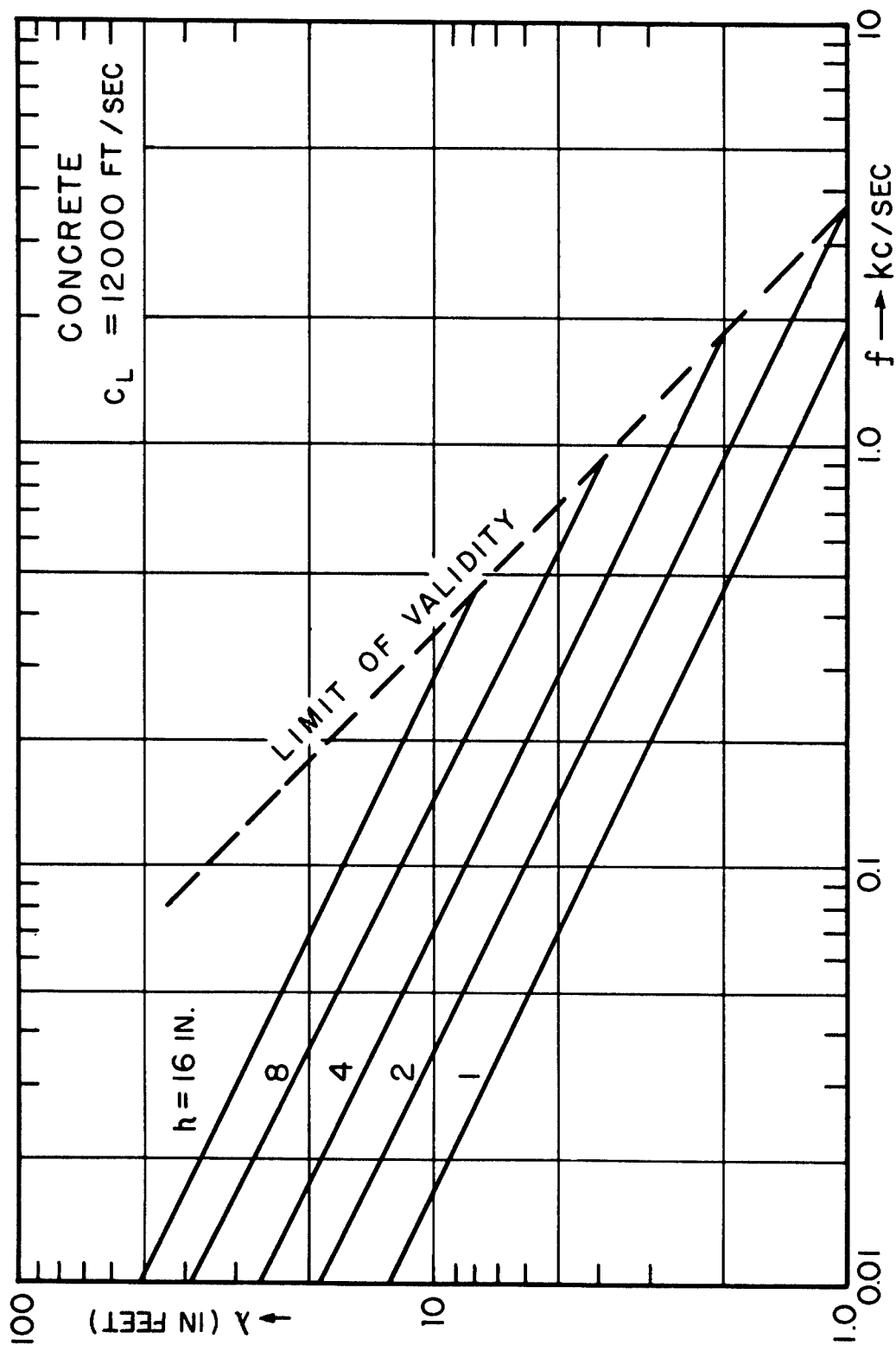
Furthermore, Figs. 11.2.5-11.2.7 contain graphs for the dependence of length of a bending wave on frequency for plates of different thicknesses for steel and aluminum, concrete and plywood. From these graphs we also may find the natural frequency of a rectangular bar supported at the ends or a plate supported on an opposite pair of edges if we remember that the wavelength is the double of the length .

For the case of plates of length ℓ_x and breadth ℓ_y, usually the four edges are supported. Then Eq. (11.2.33) must be changed to read

$$\lambda_B = 2/\sqrt{(1/\ell_x)^2 + (1/\ell_y)^2} .$$

$$(11.2.42)$$

From Fig. 11.2.8, the value λ_B may be found for plates of lengths and breadths between 0.2 and 20 feet. The lowest natural frequency may be found either from this and the graphs in Figs. 11.2.5-11.2.7 or by using directly the formula

$$f_{11} = 0.45\ c_L\ h\ [(1/\ell_x)^2 + (1/\ell_y)^2] .$$

$$(11.2.43)$$

FIGURE 11.2.6

The bending wavelength λ as a function of frequency f (in kc/sec) for plates of thickness h (in inches). These curves apply to concrete, for which c_L = 12,000 ft/sec.
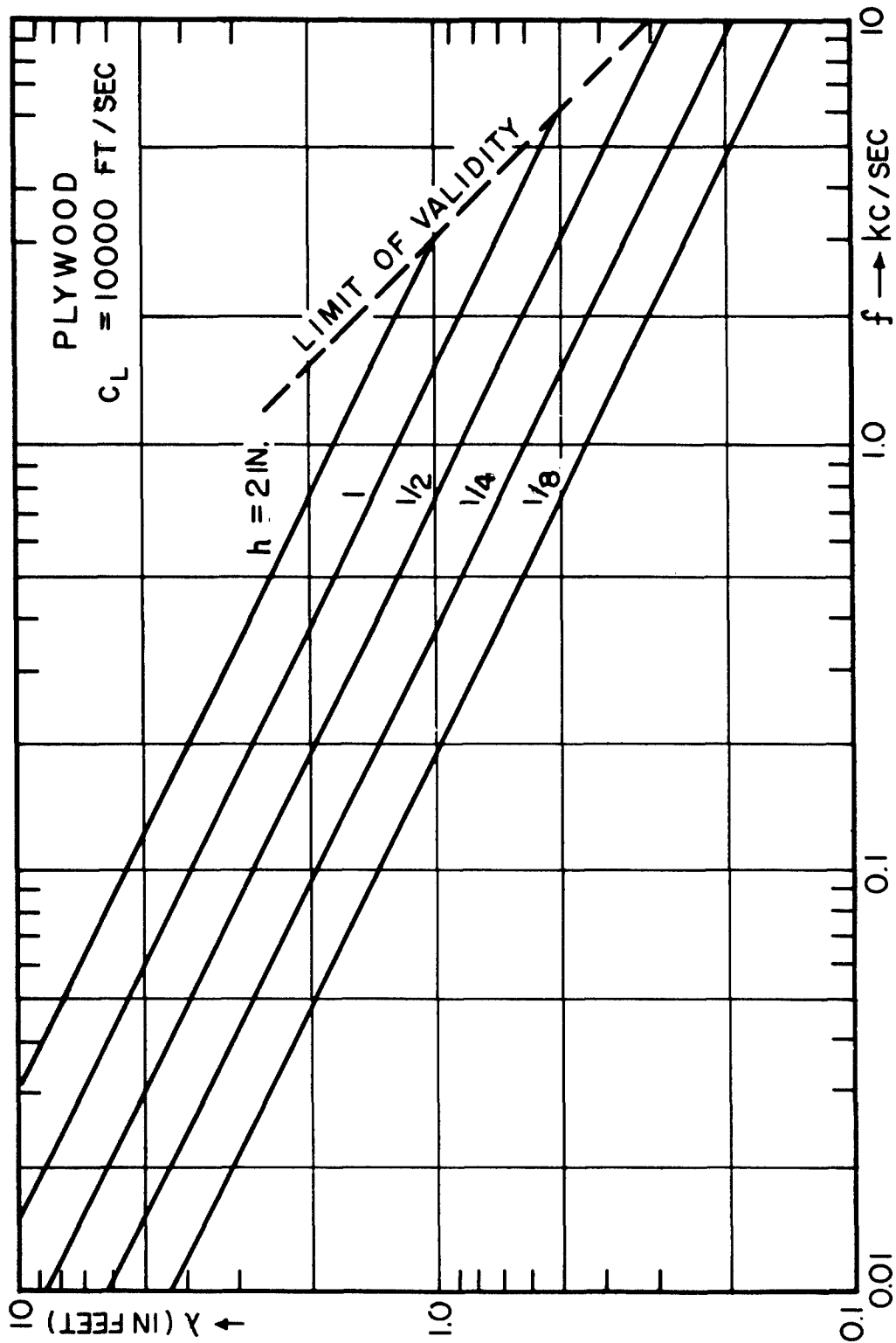
Let us look at two examples: for a steel plate of dimensions ℓ_x = 6 ft, ℓ_y = 3 ft and h = 1/8 in. (which may occur in machinehoods), we find with c_L = 17,000 ft/sec, a frequency below the region of audibility and far below the region of 100-3200 cps. But if we take a common concrete wall of 4 in. thickness with ℓ_x = 72 ft and ℓ_y = 8 ft, assuming c_L = 12,000 ft/sec, we find a frequency of 40 cps. Certainly walls and plates are seldom only supported at the edges which means that only the transverse motion is hindered but not the slope at the boundary. If we assume that the slope at the boundary is also hindered, that the plate is really clamped, we have to expect natural frequency tones more than an octave higher. However, clamping actually occurs very seldom. Usually, the boundary conditions correspond more to supporting than to clamping. Then the lowest natural frequencies are in the low frequency range and an octave below this natural frequency we may say the stiffness alone controls the transmissivity of the wall.

On the other hand, we cannot conclude that above this lowest natural frequency the wall is mass controlled. This would be the case if only this lowest type of natural mode existed. But since a plate is a two-dimensional continuum, we have to consider a doubly infinite number of natural frequencies given by

$$f_{n,m} = 0.45\ c_L h\ [n/\ell_x)^2 + (m/\ell_y)^2]$$

(11.2.44)

FIGURE 11.2.7

The bending wavelength λ as a function of frequency f (in kc/sec) for plates of thickness h (in inches). These curves apply to plywood, for which c_L = 10,000 ft/sec.
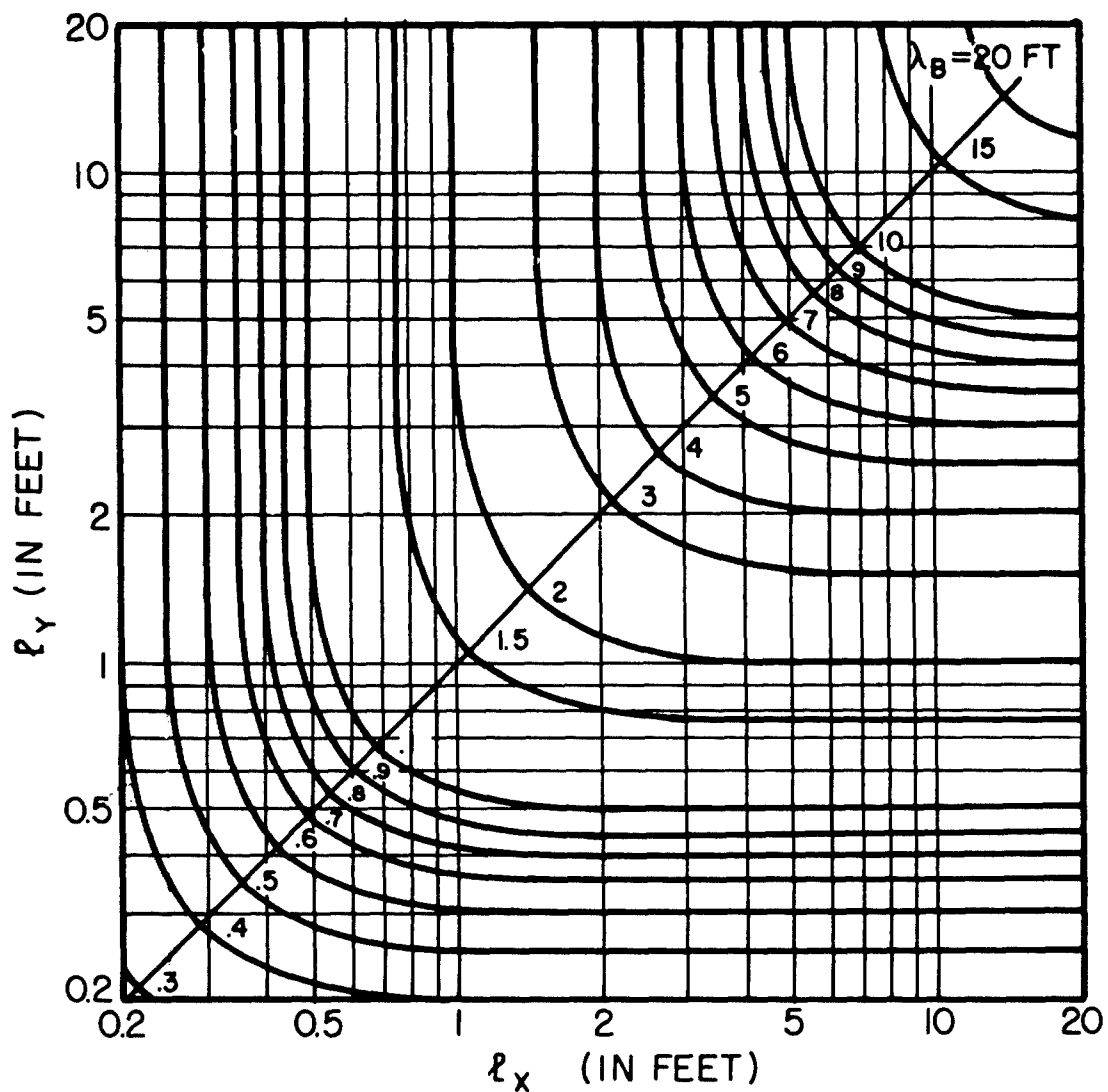
FIGURE 11.2.8

The bending wavelength λ_B for various values of ℓ_x and ℓ_y, (in feet), the sides of a plate supported at the edges.

DIRECTION OF
BENDING WAVE

REFLECTED

TRANSMITTED

INCIDENT

θ

$\frac{\lambda}{\sin\theta}$

$\frac{\lambda}{2\sin\theta}$

VIBRATING PANEL
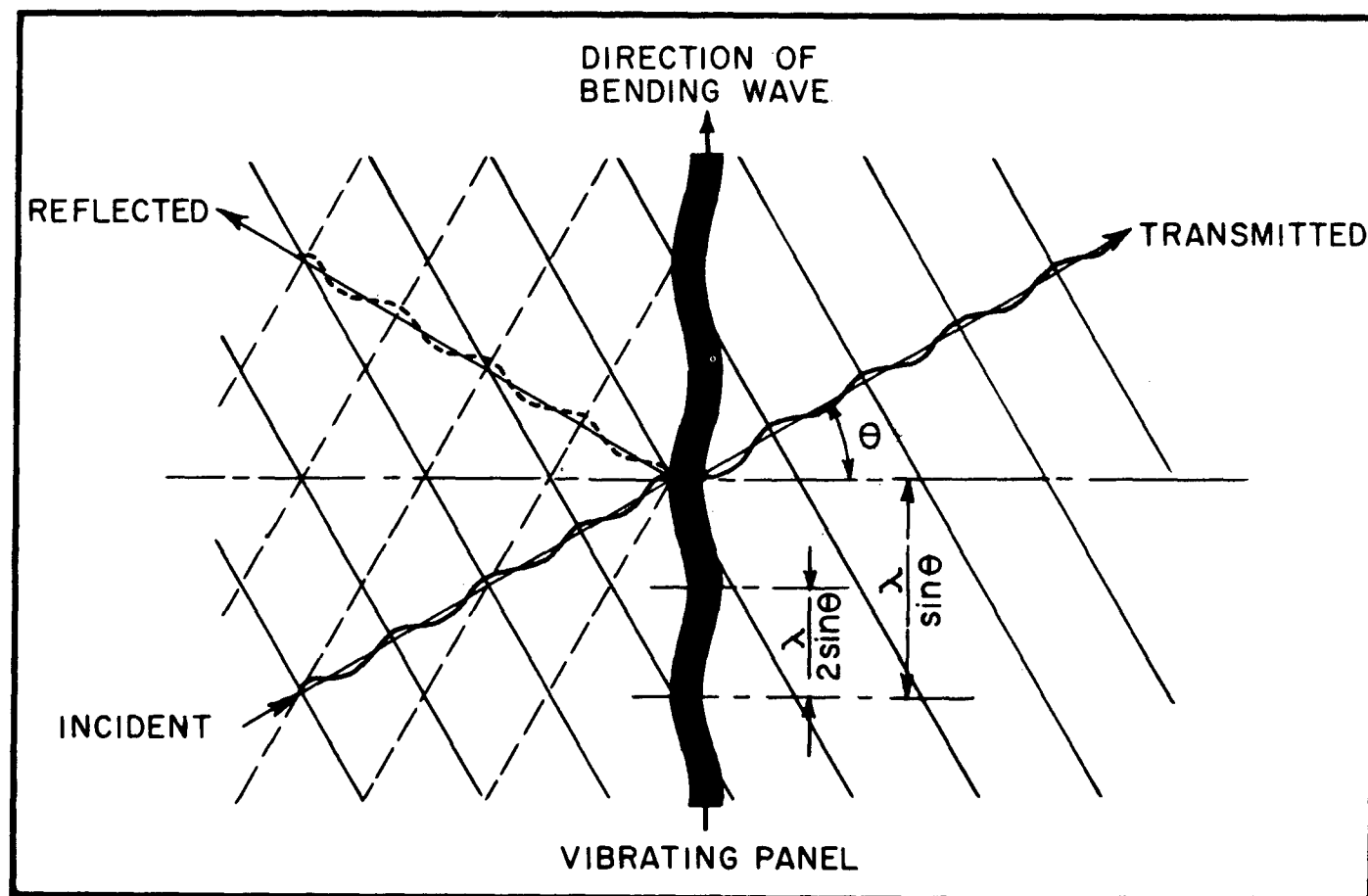
FIGURE 11.2.9

Sketch showing how the coincidence effect operates
when a sound wave in air, whose wavelength is λ
impinges on a plate at the angle θ . When $\lambda/\sin\theta$
is equal to the wavelength of a bending wave in the
plate, the TL becomes quite small.

and so we would have to expect the occurrence of resonances in higher frequency regions too. Indeed, for very undamped systems like a bell, this is the case.

However, if there are energy losses either in the plate or at the boundaries, we know by experience, or on the basis of an asymptotic law derived by Schoch 3.4/, that the higher natural modes have only a small influence. Then a plate on which a sound wave impinges perpendicularly acts like an inert mass the higher the frequency of sound is compared to the lowest natural frequency of the plate.

Summarizing, stiffness is desirable only if the lowest natural frequency is above the frequency region in which we are interested. This condition is usually difficult to fulfill. Thus, we must make the natural frequencies of walls as low as possible. This means we should construct walls of small stiffness but heavy mass.

(b) <u>Trace Matching (Coincidence Effect)</u>. The same rule as above applies because of another effect, where inertia and stiffness also work against one another and which seems to be of greater importance since it may happen in the middle of our frequency region. If a plane sound wave impinges on a wall at oblique incidence then the pressure is working with opposite phases in the distance of half the "trace-wavelength" $\lambda_o/2 \sin \nu$. So the plate is forced to be deformed with the same periodicity as shown in Fig. 11.2.9. For any observer moving with the trace velocity $c_o/\sin \nu$ along the plate, the deformation appears the same as we get if the plate is periodically supported at distances of $\lambda_o/2 \sin \nu$. If this periodicity in space of the driving forces agrees with what the plate would present without forces, i.e., if

$$\lambda_o/\sin \nu = \lambda_B , \qquad (11.2.45)$$

we have to expect total transmissivity just as in the case of resonance. Now by putting this into Eqs. (11.2.36) and (11.2.40), we find that this "coincidence" or, as we may say more precisely, this "trace matching", happens for special combinations of frequency and angles of incidence given by

$$f = (c_o^2/2\pi \sin^2 \nu) \sqrt{m/B} \qquad (11.2.46)$$

and
$$f = 0.56\ c_o^2/c_L h\ \sin^2 \vartheta \qquad (11.2.46a)$$

Furthermore, since sin varies between zero and one, we may find these "trace matchings" only above a critical frequency given by

$$f_c = (c_o^2/2\pi)\ \sqrt{m/B} \qquad (11.2.47)$$

or

$$f_c = 56\ c_o^2/c_L h \qquad (11.2.47a)$$

In Fig. 11.2.10 these frequencies are plotted as a function of the thickness for different materials. The region where trace matching is possible is to the right of these lines. We see that it is possible over the whole frequency range for thick walls and that it is impossible only in thin plates.

The question arises as to how this statement can be in agreement with the general dependence on surface weight found empirically. To discuss this problem more quantitatively, we will again consider the transmission impedance which can be defined for a wall of infinite length on which an infinite plane sound wave is incident. In this case we get 2.5/

$$Z_\tau = j\omega m - jB\ \sin^2 \vartheta\ \omega^3/c_o^4 \qquad (11.2.48)$$

$$= j\ 2\pi\ fm\ (1 - f^2\ \sin^4 \vartheta/f_c^2) \qquad (11.2.48a)$$

The first term gives the inertia reactance and is predominant below the frequency of trace matching. The second term gives the reactance of the bending stiffness; this term increases with the angle of incidence, being zero at perpendicular incidence, and is proportional to the third power of the frequency. From simple resonance phenomena we are accustomed to a stiffness reactance inversely proportional to the frequency. But this is still the case here. The f^3 dependence is overcompensated by the fact that the stiffness of a beam supported at its ends is inversely proportional to the fourth power of the length of the beam and this length is given by $c_o/2f\ \sin \vartheta$; hence $B \sim 1/L^4 \sim 1/f^4$.
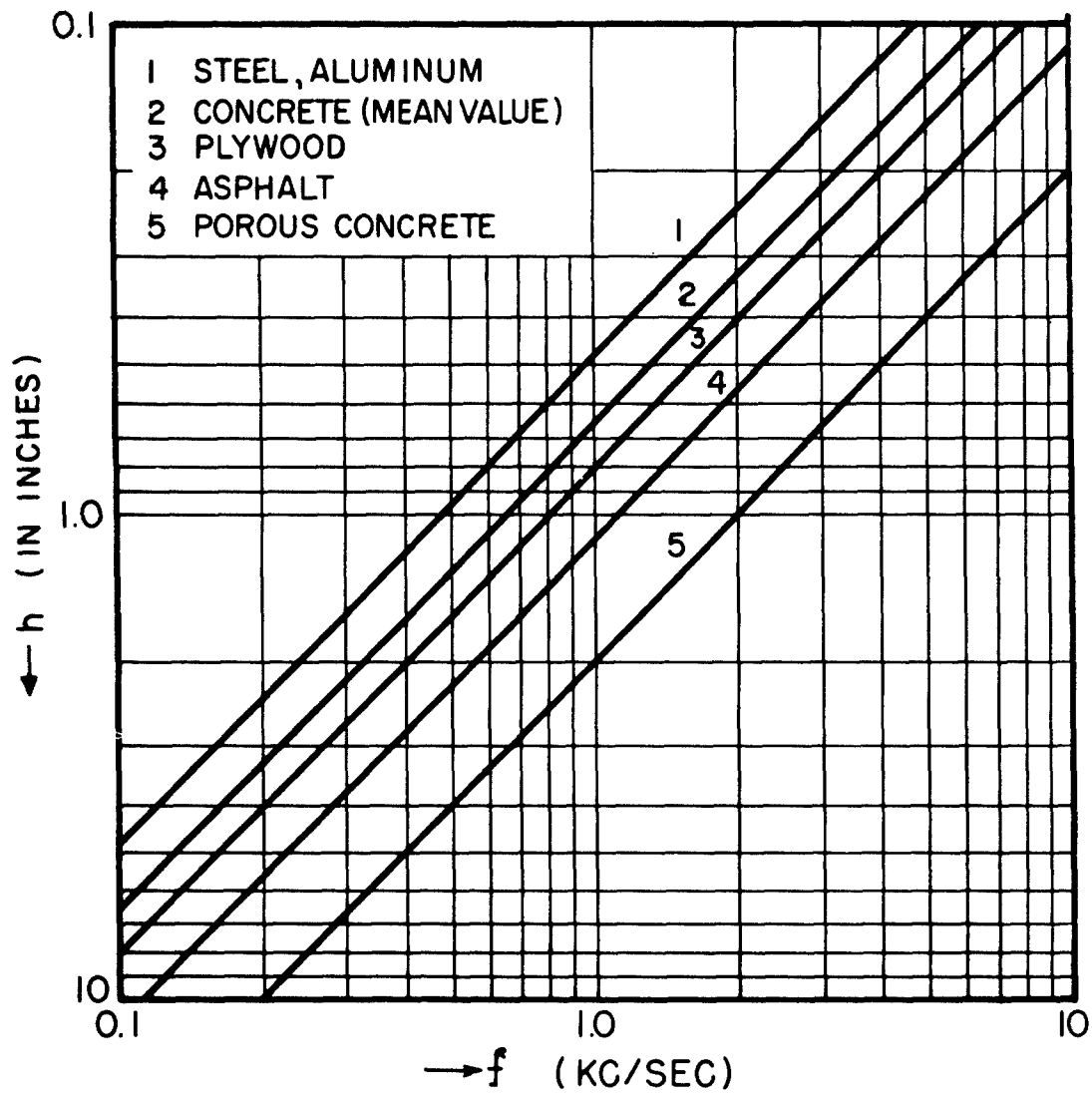
From Eq. (11.2.48a) we get for the TL

$$[TL]_{\vartheta} = 10 \log [1 + (\pi f m \cos \vartheta / \rho c_o)^2 (1-f^2 \sin^4 \vartheta / f_c)^2].$$

$$(11.2.49)$$

In Fig. 11.2.11, a map is given showing contours of equal TL over a [$\log f - \cos 2 \vartheta$] plane. Dark regions indicate good sound insulation; light regions, poor sound insulation. For $\vartheta = 0^o$ we have a monotonic increase of TL corresponding to the 0° mass law. There is, in general, a decrease from bottom to top due to the component effect. The trace matching effect cuts a deep valley beginning at the point (f_c, 0) and curving asymptotically to the ($\cos 2 \vartheta = 1$) line. At the left of this valley the wall is mass controlled while at the right it is stiffness controlled.

Since for a given material and a homogeneous wall, stiffness also increases with thickness with the third power, we see that the heavier wall insulates better also in the region where stiffness predominates. Since the specific material constant, i.e., the longitudinal sound velocity c_L, only varies between 10,000 and 18,000 ft/sec for most materials in which we are interested, it has been very difficult to decide if the empirical dependence on weight means a dependence on mass only or if stiffness is a factor too. From Figs. 11.2.10 and 11.2.11 we conclude that in most cases of walls in buildings, stiffness must be predominant except at perpendicular or near perpendicular incidence. The special values for

---

FIGURE 11.2.10

The critical frequency f_c plotted as a function of the plate thickness h (in inches) for which the coincidence effect is possible. At this frequency, the TL is quite small.

which Fig. 11.2.11 has been calculated corresponds to a plywood panel of 0.8 in. thickness. But the type of dependence may be regarded as general.

For comparison with measurements and also for most of the practical applications, we are interested in the average value for a statistical distribution of angles of incidence. This requires putting Eq. (11.2.48a) into Eq. (11.2.20) and then integrating over $\sin^2 \vartheta$ corresponding to Eq. (11.2.22a). This integration has been carried out omitting only a small region above $f = f_c$. The results are given in Fig. 11.2.12 using the dimensionless parameters

$$\xi = f/f_c \qquad (11.2.50)$$

$$\alpha_c = \pi f_c m/\rho c_o \qquad (11.2.51)$$

The last parameter determines the TL for the critical frequency and perpendicular incidence

$$[TL]_{oc} = 10 \log (1 + \alpha_c^2) \simeq 20 \log \alpha_c$$

$$(11.2.52)$$

The results are shown in Fig. 11.2.12 and can be used to give a general idea of what can be expected for very large, undamped walls. The experimental results never show such a pronounced valley just above f_c. This may be easily understood if we plot τ as a function of

---

FIGURE 11.2.11

Contours of equal TL on a $\cos^2 \vartheta$ - frequency plane. The "valley" at the right is a result of the coincidence effect.
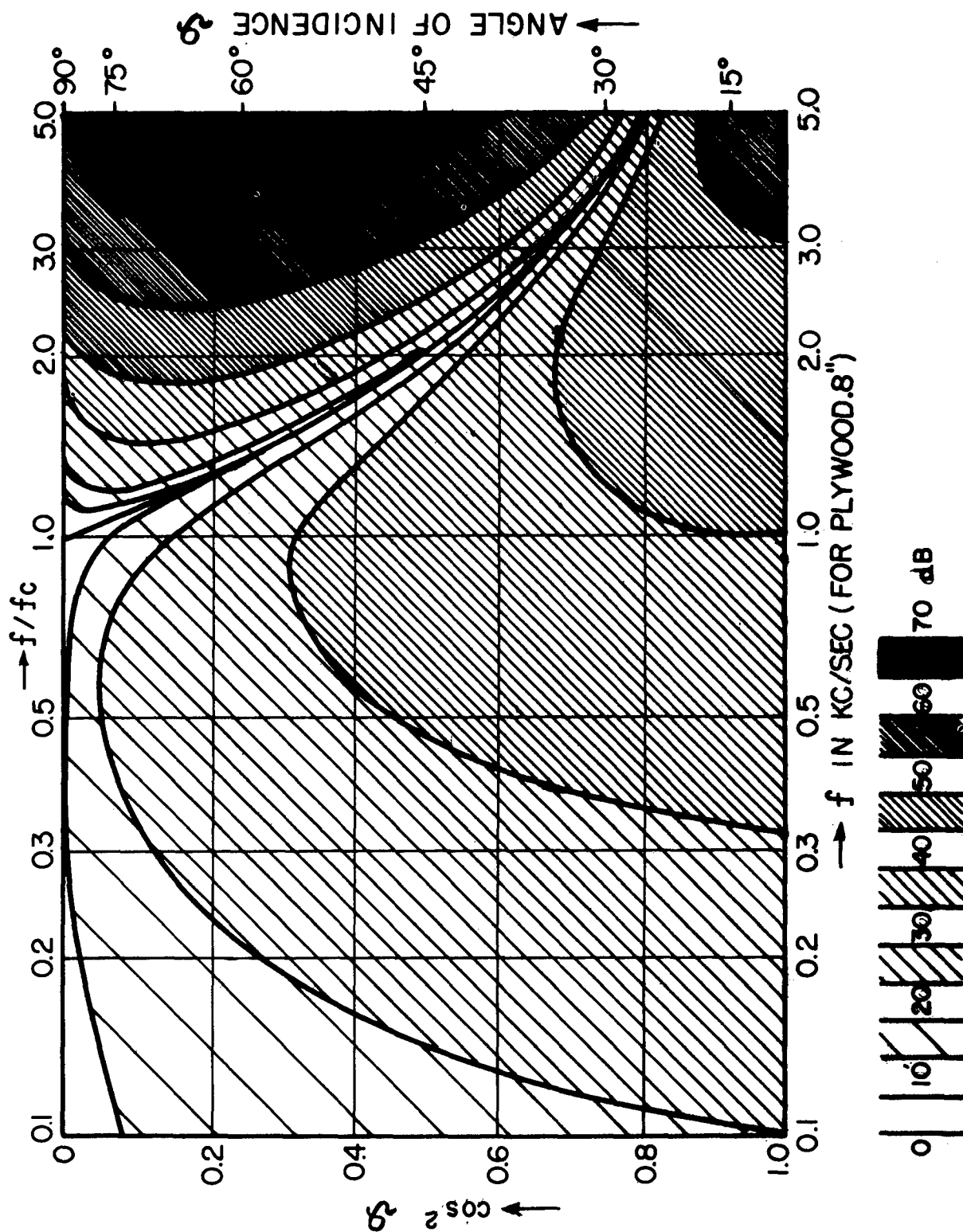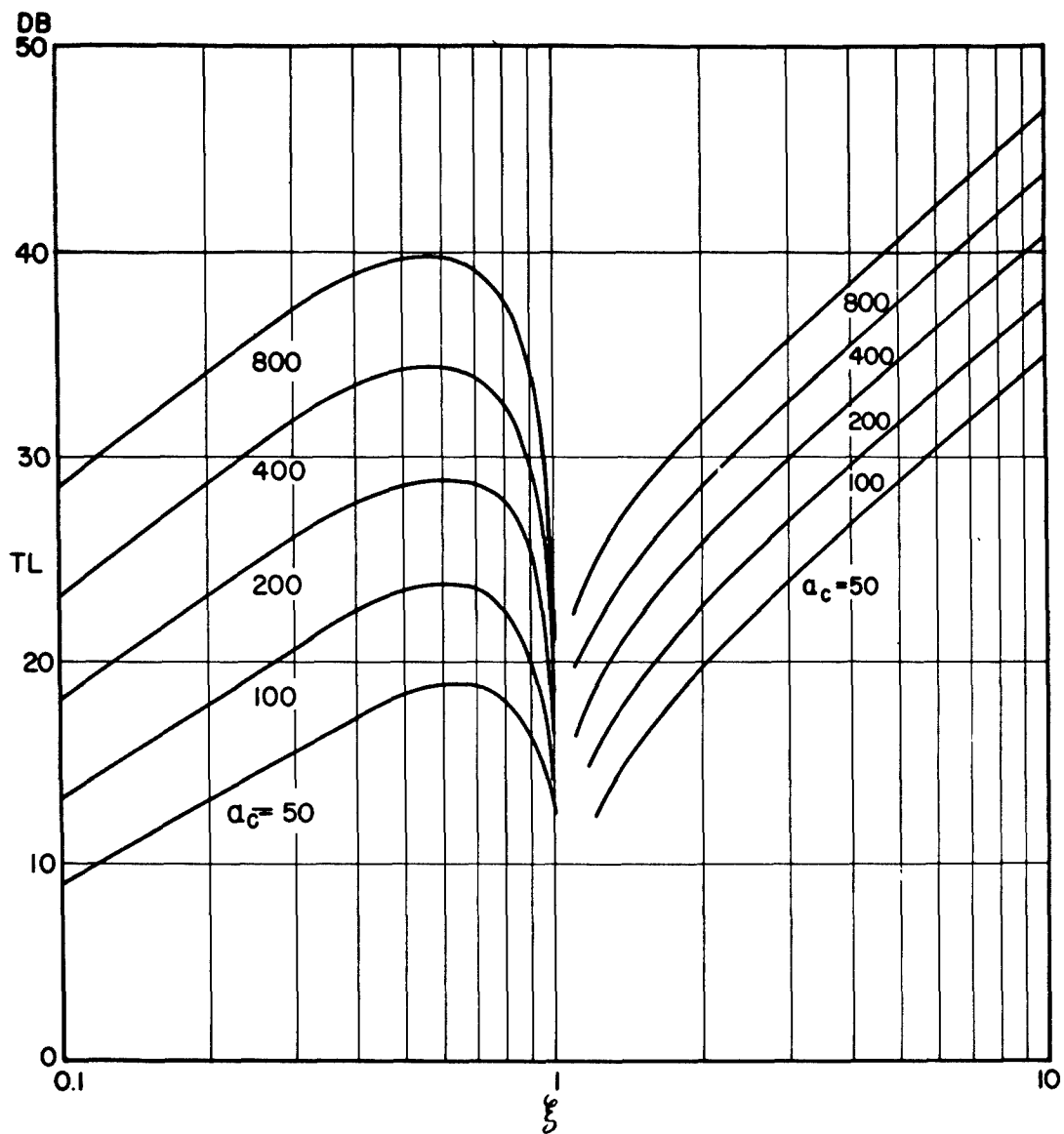
FIGURE 11.2.12

TL vs. the frequency parameter $\xi = f/f_c$, for various values of $\alpha_c = \pi f_c m / \rho c_o$.

$\sin^2 \vartheta$ and see that this curve again has a sharp peak at the angle of trace matching. We may write the expression for τ as

$$\tau = 1/[1 + (\epsilon/\delta)^2] \qquad (11.2.53)$$

where ϵ is the relative variation of the abscissa with

$$\sin^2 \vartheta_o = 1/\xi \qquad (11.2.54)$$

$$\epsilon = \sin^2 \vartheta - 1/\xi \qquad (11.2.55)$$

and 2δ is the bandwidth, which in the present case is

$$\delta = 1/[2 \, \alpha_c \xi^2 \sqrt{1 - 1/\xi}]. \qquad (11.2.56)$$

It is not important that the dependence on ϵ given by Eq. (11.2.53) only holds for a small region because the integration we have to execute gives

$$\overline{\tau} = \int_{-\epsilon_1}^{\epsilon_2} \frac{d\epsilon}{1 + \epsilon^2/\delta^2} = \delta[\tan^{-1}\epsilon_2/\delta + \tan^{-1}\epsilon_1/\delta]$$

$$(11.2.57)$$

or with sufficient accuracy

$$\overline{\tau} = \pi \delta \qquad (11.2.57a)$$

as long as the limits ϵ_2 and ϵ_1 are greater than 3δ. But these restrictions are possible only for higher frequencies where trace matching no longer occurs at grazing incidence. And in this region we would have to expect

$$[TL] = 10 \log (2 \, \alpha_c \xi^2 \sqrt{1 - 1/\xi} \, /\pi) \qquad (11.2.58)$$

$$\simeq (1/2) \, [TL]_{oc} + 20 \log (f/f_c) - 2. \qquad (11.2.58a)$$
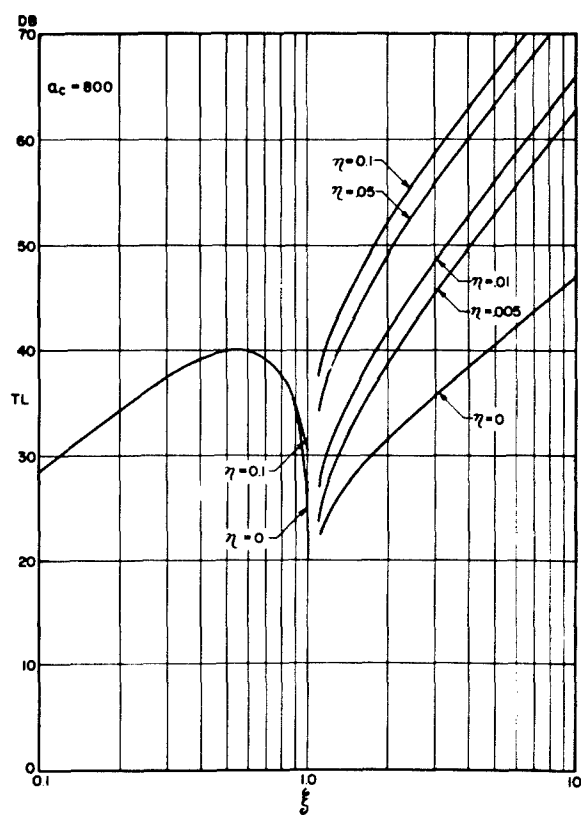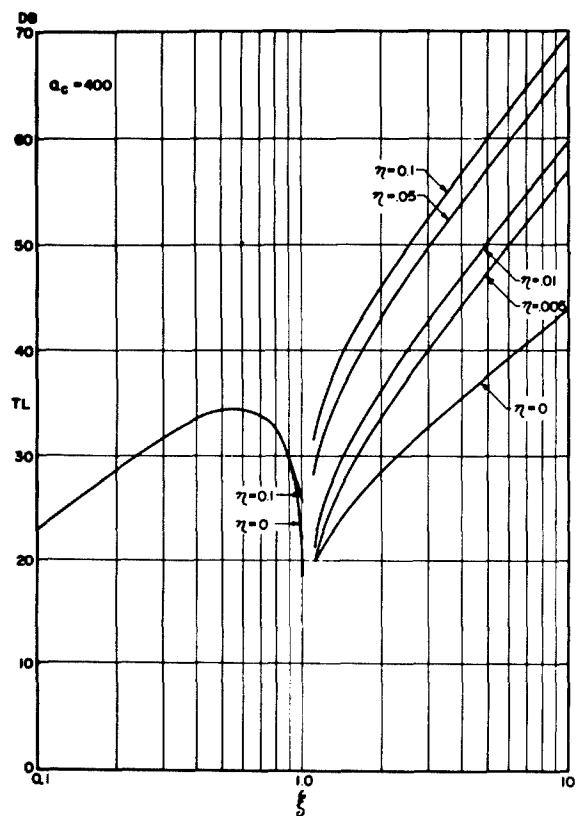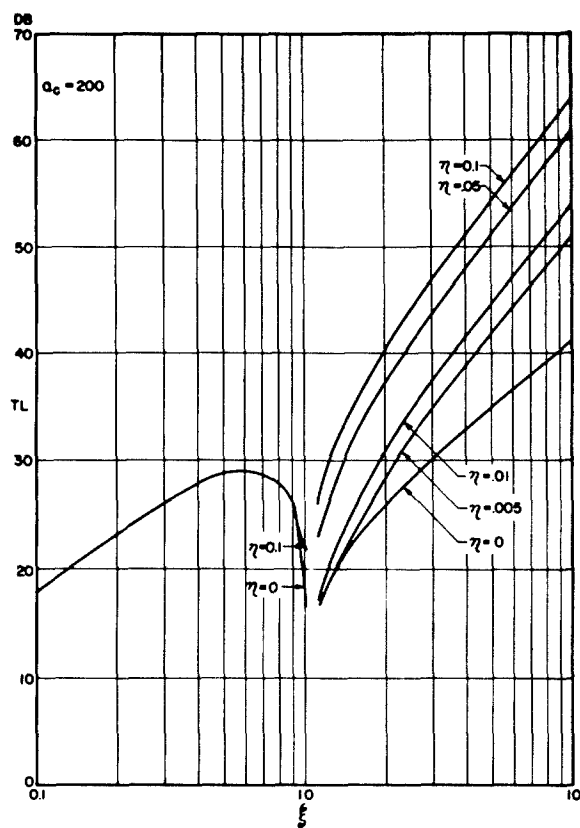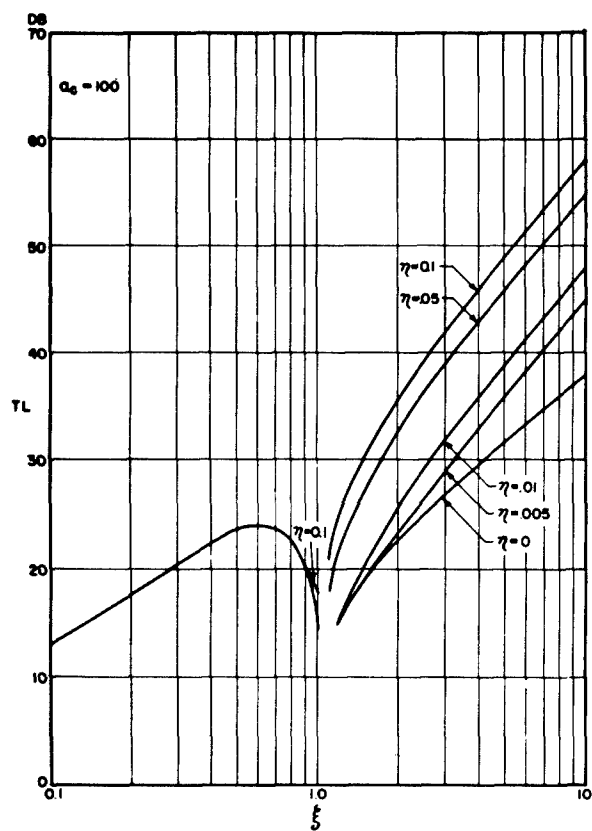
It seems plausible that such sudden changes of transmissivity with the angle of incidence will not really occur and the assumption that under the conditions of trace matching total transmissivity will be reached must be violated; the conditions for trace matching must be also violated if we take into account the finite length of the wall or any kind of losses either in the wall itself or at its edges.

We can treat the inner losses by introducing a complex Young's modulus instead of the usual real modulus E

$$\hat{E} = E(1 + i\,\eta) \qquad\qquad (11.2.59)$$

where η, the loss factor, characterizes the phase shift between strain and stress and from experiment may be regarded as independent of frequency.

With this complex modulus the transmission impedance becomes a complex quantity also, given by

$$Z_\tau = \eta B\omega^3\ \sin^4\vartheta/c_o^4 + j[\omega m - B\omega^3\ \sin^4\vartheta/c_o^4].$$

$$(11.2.60)$$

Putting this into Eqs. (11.2.20) and (11.2.22a), we again may find τ_m and finally TL. The results of this even more troublesome calculation are given in Fig. 11.2.13 for the case of α_c = 100, 200, 400 and 800 corresponding to $[TL]_{oc}$ = 40, 46, 52 and 58 db.

The behavior at high frequencies again may be understood by looking at the neighborhood of the peak only. Here first the peak itself is lowered to the value

$$\tau_{max} = 1/[1 + \eta\alpha_c\ \xi\sqrt{1 - 1/\xi}\ ]^2 . \qquad (11.2.61)$$

FIGURE 11.2.13

TL vs. ξ for various values of α_c when inner losses are introduced into the plate.

If we now write

$$\tau = \tau_{max} / [1 + \epsilon^2 / \delta^2]$$

(11.2.62)

and change δ to

$$\delta \simeq (1 + \eta \alpha_c \xi \sqrt{1 - 1/\xi}) / (2 \alpha_c \xi^2 \, 1 - 1/\xi)$$

(11.2.63)

we get for high frequencies

$$\overline{\tau} = \pi \, \delta \, \tau_{max} = \pi / [2 \alpha_c \xi^2 \sqrt{1 - 1/\xi} + 2 \eta \alpha_c^2 (\xi^3 - \xi^2)]$$

(11.2.64)

or

$$[TL] = 10 \log [2 \alpha \xi^2 \sqrt{1 - 1/\xi} \, (1 + \eta \alpha_c \xi \sqrt{1 - 1/\xi}) / \pi]$$

(11.2.65)

For $\eta = 0$ this is identical to Eq. (11.2.58); for $\eta \alpha_c \xi \sqrt{1 - 1/\xi} > 4$, Eq. (11.2.65) becomes

$$[TL] = [TL]_{oc} + 30 \log(f/f_c) - 10 \log f/(f_c - f) - 10 \log (1/\eta) - 2$$

(11.2.65a)

For a rough evaluation, the third term may be neglected. Equation (11.2.65) also vanishes asymptotically but the first order theory of bending waves which have been used is valid only as long as $\lambda_B > 6h$. This will be the case if $\xi = 3.24 \, c_L \, h/c_0 \lambda_B < 0.54 \, c_L/c_0$; for concrete where $c_L = 12,000$ ft/sec, this means $\xi < 5.2$.

The most essential fact which may be seen from Fig. 11.2.13 is that the insulation power increases again in the region sufficiently far above f_c. One of the physical reasons for this behavior may easily be understood by looking at the contours of Fig. 11.2.11. There the

"valley of trace matching" becomes smaller and smaller.
This is connected with the fact that the "peaks" at both
sides become higher and higher but the latter alone would
be of less importance because the tops scarcely influence
the result. In the case of inner losses, the bottom of
the valley increases in the region of higher frequencies.
This general behavior is in agreement with experimental
results, but the valley in the neighborhood of f_c is not
as deep and the slope above f_c is not as large as would
be expected. Also the influence of damping, which should
be very high, has not yet been confirmed. It seems that
the energy losses at the edges and the finite length of
the wall are of more importance. This finite length has
to be compared with the wavelength of bending waves at
the critical frequency, which means the wavelength in air
also. This may be the reason why pronounced trace match-
ing effects never have been found with thick, heavy walls,
e.g. brick walls, where the critical frequency is below
100 cps. Here the wavelength at 11 ft is of the same
order of magnitude as the length and breadth of the wall.

Generally speaking, we may avoid the trace matching
effects by either use of very thick and stiff walls or by
use of walls which have small stiffness, but not too
small a mass. For homogeneous plates this is a question
of thickness. For example, we may say that walls of
porous concrete of thickness from 1 in. to 3 in. are
dangerous since the critical frequency is in the middle audio
range. Also for wooden plates of common thicknesses the
critical frequencies are in the region of interest.
Fig. 11.2.14 shows the measured TL for a plate of about
5/8 in. thickness. By cutting grooves in the panel, that
is, by decreasing the stiffness without remarkably alter-
ing the mass, it was possible to increase the critical
frequency above the region of interest and so to improve
the insulation 2.6/.

The decreasing of the stiffness not only increases
the critical frequency, it also decreases the lowest
natural frequency, which is a further advantage. As may
be derived by comparing the formulas for the lowest
natural frequency for a bar or a plate only supported
at two opposite edges

$$f_1 = (\pi/2\ell^2)\sqrt{B/m} \qquad (11.2.66)$$

(following from Eqs. (11.2.33), (11.2.36), and (11.2.47),

$$f_1 \, f_c = (c_o/2 \, \ell)^2 \qquad (11.2.67)$$

This is the square of the natural frequency of an open organ pipe of the length ℓ . Equation (11.2.62) may also be used to evaluate f_c experimentally by measuring f_1.

Another possibility for evaluating f_c is by measuring the static sag ζ_{max} due to its weight of a bar or plate of length ℓ supported at the ends. This is proportional to the surface mass and inversely proportional to the bending stiffness

$$\zeta_{max} = 5 \, mg \, \ell^4/384 B \qquad (11.2.68)$$

where g is the acceleration of gravity. Combining this with Eq. (11.2.47), we find

$$f_c = 385 \, c_o^2 \, \zeta_{max}/10\pi \, \ell^2 \, g$$

$$(11.2.69)$$

or since c_o and g are given constants

$$f_c = 90000 \sqrt{\zeta_{max}}/\ell^2 \qquad (11.2.70)$$

where ζ_{max} is given in inches and ℓ in feet. This equation is of special interest because it shows that a plate supported at 6 ft intervals should have a sag of at least 2.5 in. if the critical frequency shall be above 4000 cps. Certainly such plates could never be loaded. But in all cases where plates which are not too heavy are to be installed for noise abatement only, this rule should be observed as far as possible.
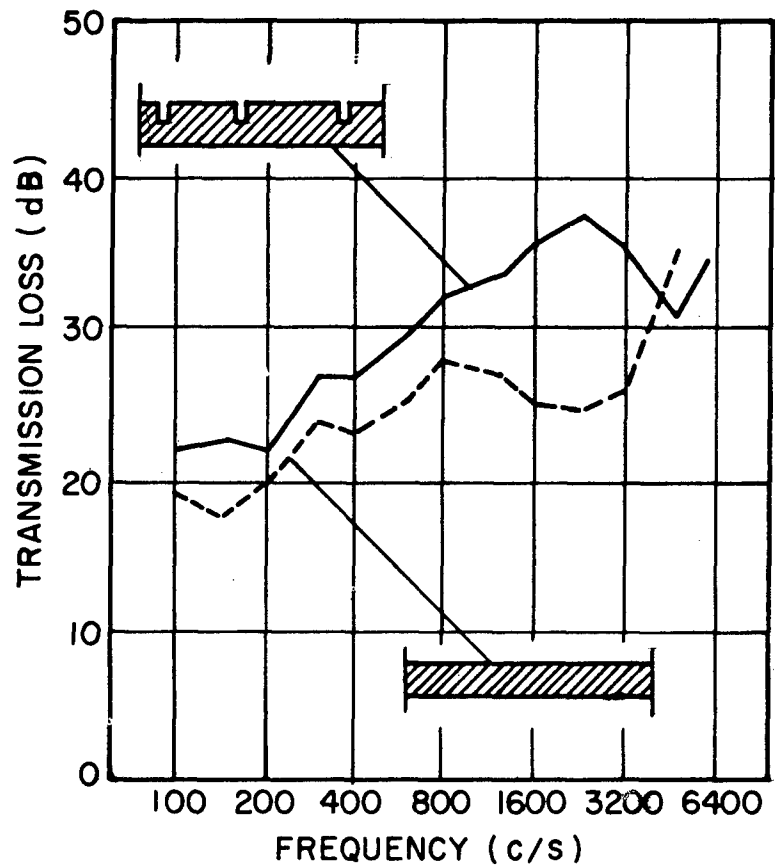
FIGURE 11.2.14

TL vs. frequency for a single panel and for the same
panel when the stiffness was decreased by cutting
grooves into one side of the panel.

Double Walls. Improvement by a Second Rigid Partition.

To attack the problem of double walls, first we may treat the case as one where a rigid partition is present. For example, the rigid partition may have been constructed for structural reasons but was found to be poor with respect to sound insulation qualities. From the results derived for a single plane wall we may conclude that we would have to increase the weight of the wall. But even if it would be possible to double the weight of the wall, we would gain only about 4 db for the mean TL according to Eq. (11.2.23). In practice, we are able to add only about a fifth of the original weight and so as long as the second wall is fixed rigidly to the first, we can obtain at most a 1 db improvement.

But we may gain an appreciable improvement, at least for higher frequencies, if this additional partition is separated by an air space of several inches. It is plausible that such a fourfold change of medium results in better insulation than the twofold change in the case of a single wall. However, there are exceptions where we do not improve the sound insulation, but rather decrease the sound insulation over that of the original wall.

In general, we have to expect that the resulting transmission coefficient now will depend on the transmission impedances of both walls, Z_1 and Z_2, and on the distance d between the walls. Generalizing a very elegant representation given by London 2.7/, we may write instead of Eq. (11.2.20)

$$\frac{1}{\tau} = \left| 1 + \frac{Z_{\tau 1} + Z_{\tau 2}}{2\,\rho_o c_o} \cos \vartheta + \frac{Z_{\tau 1}\,Z_{\tau 2}\,\cos^2 \vartheta}{4\,\rho_o^2\,c_o^2} (1 - e^{-2j\omega d\,\cos \vartheta/c}) \right|^2.$$

(11.2.71)

First we may see that the third term vanishes for d = 0. In this case we get Eq. (11.2.20) where both impedances are simply added. If both impedances are mass reactances, the wall behaves like a single wall of mass $(m_1 + m_2)$. If both impedances are bending stiffness reactances, they are added also. But in this case, two plates of the same material with thicknesses h_1 and h_2, do not behave as one plate of the thickness $(h_1 + h_2)$ because the bending stiffness is proportional to the cube of thickness; here the possibility of tangential motion of one plate against the other decreases the stiffness in the ratio

$$(h_1 + h_2)^3/(h_1^3 + h_2^3) .$$

Since we are interested only in very large values of $Z_{\tau 1}$ and $Z_{\tau 2}$, the product $Z_{\tau 1} Z_{\tau 2}$ is always a large quantity. Therefore, a small value of ωd is sufficient to make the third term equal to the second. We may expand the expression in brackets in the third term for small ωd and obtain

$$1 - e^{-2j\omega d \cos \vartheta/c} = 2j(\omega d \cos \vartheta/c) + 2(\omega d \cos \vartheta/c)^2 .$$

Now considering $Z_{\tau 1}$ and $Z_{\tau 2}$ to be pure reactances, we may split up Eq. (11.2.71) into real and imaginary parts

$$1/\tau = (1 + \frac{Z_{\tau 1} Z_{\tau 2} \cos^4 \vartheta}{2 \rho^2 c^4} \omega^2 d^2)^2 + (\frac{(Z_{\tau 1} + Z_{\tau 2}) \cos \vartheta}{2\rho c}$$

$$+ \frac{Z_{\tau 1} Z_{\tau 2} \cos^3 \vartheta \cdot \omega d}{2 \rho^2 c^2})^2 \qquad (11.2.71a)$$

Now if $Z_{\tau 2}$ is a mass reactance and $Z_{\tau 1} >> Z_{\tau 2}$, the second term vanishes at a frequency given by

$$\omega_0 = \sqrt{\rho c^2/m_2 d \cos^2 \vartheta} \qquad (11.2.72)$$

For $\vartheta = 0$, this frequency corresponds to the free oscillation of a mass m_2 combined with the resilience of the air space $\rho c^2/d$. Furthermore, it can be derived that the resilient reactance of such an air space is increased by the ratio $1/\cos \vartheta$ if the sound impinges at an oblique angle and lateral motion in the air space is not hindered.

But if lateral motion in the air space is hindered, which always may be assumed when some absorbing material is put into the air space, we have to set $\cos \vartheta = 1$ in Eq. (11.2.72), regardless of the angle of incidence. Furthermore, if we express m_2 by the surface weight G_2 in lb/sq ft and the thickness d in inches, we find

$$f_0 = 170/ \sqrt{G_2 d} \qquad . \qquad (11.2.72a)$$

If both reactances can be assumed to be pure mass
reactances and the surface weight of the first wall G_1
is not much greater than G_2, we have to substitute for
G_2 the "resultant surface weight"

$$G_{res} = G_1 G_2/(G_1 + G_2) \quad . \qquad (11.2.72b)$$

In this case, both masses oscillate out of phase with
the ratio of the amplitudes of oscillation inversely
proportional to the ratio of the weights. At this "zero
mode" frequency of the double wall, the transmission loss
is very small; for two equal mass reactances the TL may
be zero. In the neighborhood of this frequency, the
double wall is worse than a single wall even of the weight
of the heavier partition only. Thus the second partition
has not improved the sound insulation.

The first step in calculating a double wall construc-
tion is to make the product of $G_2 d$ or $G_{res} d$ so large that
f_0 is below the region in which we are interested. In
most practical cases, it will be sufficient to choose
$f_0 < 54$ cps; this means that we have to make

$$G_2 d > 10 \text{ lb in./sq ft} \quad . \qquad (11.2.73)$$

The only way to save weight is to enlarge the distance d,
and even this holds only if d is not too large, as we
will see later.

One octave above f_0, the second term in Eq. (11.2.71a),
is very much greater than the first. Comparing the cor-
responding TL with that given by a wall of $Z_{\tau 1}$ only, we
find that the improvement of transmission loss is

$$\Delta \text{ [TL]} = 20 \log (\omega^2 dm_2 \cos \vartheta/\rho c^2) = 40 \log (\omega/\omega_0) \quad .$$

$$(11.2.74)$$

If the lateral motion in the air space is hindered, we
may replace ω_0 by ω_{00}; the improvement of TL becomes then

$$\Delta \text{ [TL]} = 40 \log (f/f_{00}) \quad . \qquad (11.2.74a)$$

This very simple formula allows a rough evaluation of the
slope of TL vs frequency in the region of f/f_{00} from one

to two and sometimes to even three octaves above f_{oo}. But then the slope of TL, which would be 18 db/octave if both walls follow the mass law, decreases. One of the reasons may be seen from Eq. (11.2.71). The expression $(1-e^{-2j\omega d} \cos \nu/c)$ only increases with frequency for small ωd, but it is never greater than 2. This highest value occurs at

$$f_{(2n + 1), \nu} = (2n + 1) \frac{c}{4d \cos \nu}$$

(11.2.75)

or when lateral motion in the air space is hindered, at

$$f_{(2n + 1), 0} = (2n + 1) \, c/4d \qquad (11.2.75a)$$

The corresponding highest values of the improvement in TL are given by

$$\Delta [TL] = 20 \log (\omega m_2/\rho_o c) \cos \nu. \qquad (11.2.76)$$

This improvement is 6 db higher than the TL we would expect from the second wall alone. The straight lines given by Eqs. (11.2.74a) and (11.2.76), the latter calculated for $\nu = 45°$, may be used as upper limits for the improvement by a second partition.

But we have to expect that between the frequencies of maximum transmission loss, given by Eq. (11.2.75), there are always frequencies at which the transmission loss is very small, or even zero for two identical partitions. For $Z_{\tau 1} >> \omega m_2$, these frequencies are given by

$$f_n = nc(1 + \rho d/\pi^2 n^2 m_2)/2d \cos \nu \qquad (11.2.77)$$

or approximately

$$f_n = nc/2d \cos \nu. \qquad (11.2.77a)$$

The difference between Eqs. (11.2.77) and (11.2.77a) is
of interest only if the minimum transmission coefficient
must be calculated. Equation (11.2.77a) is true when
the sound pressure in the air space at the opposite points
of the walls is either in phase or 180° out of phase.
For $\nu = 0$, the condition becomes

$$f_n = nc/2d \qquad (11.2.77b)$$

which is the well known formula for the eigenfrequencies
of one dimensional sound motion between parallel rigid
walls. Therefore we may call the f_n the resonance fre-
quencies of the air space and f_0 the resonance frequency
of the double wall.

   With increasing separation of the two partitions,
the lowest of these resonance frequencies decreases.
This is the reason why increasing this distance may not
always be helpful. If, for example, we want to avoid
the case where f_1 becomes smaller than about 1000 cps,
we should keep

$$d \angle 7 \text{ in.} \qquad (11.2.78)$$

   Again Eq. (11.2.77b) has to be used instead of
Eq. (11.2.77a) if the lateral coupling in the air space
is hindered. If this is done by a porous material, the
difference between minima and maxima of TL in this
frequency region will decrease.

Influence of Absorbing Material in the Air Space.

   As has been shown by London, in most cases we would
not expect any improvement in sound insulation by an
additional partition without introducing any absorption.
The reason is that for each frequency above f_{no}, $(n + 1)$
angles of incidence exist for which total transmission
occurs. By averaging over all angles, the sound trans-
mission in the neighborhood of these angles predominates
and results in an average transmission coefficient that
is higher than that for the single wall. This may be
substantiated in a manner similar to that shown for the
problem of transmissivity in the case of trace matching.
As in that case, it may be shown that the results for
the average transmission coefficient are influenced
strongly by any kind of energy losses.

To get agreement between the experimental data obtained with reverberant rooms and theoretical calculations, London introduced external friction terms in the impedances of the partition walls which he assumed to be inversely proportional to cos ϑ. There is no physical evidence for such resistance terms and, therefore, the physical properties of walls offer no data for the evaluation of these resistances.

Another possible way to introduce energy losses is by means of a complex Young's modulus, as was done in the case of trace matching effects. But here also an adequate value of the loss factor can only be found by experiment and must be assigned a much higher value than the loss factor corresponding to the material alone.

The only kind of energy losses which we are able to calculate from measurable physical data are those which occur when the space between double walls is filled with porous material. The theory of those materials has been developed to such a degree (see Sec. 12.1) that sufficient agreement between theory and experiment has been achieved. We are interested only in porous materials that do not make an elastic connection between the walls by virtue of their skeleton. Under this assumption, we need only two quantities to characterize the porous material. The first is the propagation coefficient for propagation perpendicular to the walls inside the porous material, which is assumed to be a complex quantity

$$\hat{k}_x = k_x - j\, g_x \; . \tag{11.2.79}$$

The second is the characteristic impedance of the porous material, which is defined by the ratio of sound pressure to the component of the velocity perpendicular to the walls for a propagating wave

$$\hat{Z}_x = p/v_x \quad . \tag{11.2.80}$$

This also is a complex quantity. With these definitions, we find for the transmission coefficient

$$\Upsilon = \left| [1+(Z_1+Z_2)\cos\vartheta/2\rho c]\cosh(j\hat{k}_x d)+[(Z_1+Z_2)/2\hat{Z}_x+Z_x\cos\vartheta/2\rho c \right.$$

$$\left. + \rho c/2\hat{Z}_x \cos\vartheta + Z_1 Z_2 \cos\vartheta/2\hat{Z}_x\rho c]\sinh(j\hat{k}_x d) \right|^{-2}$$

$$(11.2.81)$$

Fortunately for most practical applications the last term predominates so that we may simplify the cumbersome expression in Eq. (11.2.81) to

$$\Upsilon = \left| \frac{2\hat{Z}_x\,\rho c}{Z_1\,Z_2\,\cos\vartheta}\,\sinh(j\,\hat{k}_x d) \right|^2$$

$$(11.2.81a)$$

and write for the transmission loss of the whole construction

$$[TL] = \left| 20\log\frac{Z_1\,Z_2\,\cos\vartheta}{2\hat{Z}_x\,\rho c}\,\sinh(j\,\hat{k}_x d) \right|$$

$$= 20\log\left|\frac{Z_1\,\cos\vartheta}{2\rho c}\right| + 20\log\left|\frac{Z_2}{\hat{Z}_x}\,\sinh(j\,\hat{k}_x d)\right|.$$

$$(11.2.82)$$

Finally, we get for the improvement of the transmission loss given by the second partition and the air space filled with absorbing material

$$[TL] = 20\log\left|\frac{Z_2\,\sinh(j\,\hat{k}_x d)}{\hat{Z}_x}\right|$$

$$(11.2.83)$$

To simplify the theory, it seems reasonable for the present problem to neglect the small vibrations of the fibers. These vibrations are of importance at low frequencies only. Then we may write

$$\hat{k}_x = \omega \left[(\mathcal{X} - \sin^2 \vartheta) - jr\,\sigma/\omega\,\rho\right]^{1/2} /c$$

<div align="right">(11.2.84)</div>

and

$$\hat{z}_x = \frac{[\mathcal{X} - jr\ /\omega\,\rho]\ \rho c/\sigma}{[(\mathcal{X} - \sin^2 \vartheta) - jr\,\sigma/\omega\rho]^{1/2}}$$

<div align="right">(11.2.85)</div>

Here σ is the porosity, i.e. the ratio of air volume inside the porous material to its total volume, for which a mean value of 0.8 may be used. Nor will taking $\sigma = 1$ for simplicity change the results seriously. More important is the structure factor $\mathcal{X}$ which may vary between 1 and 10, or even 25. For fiberglas blankets, the lower limit is usually appropriate. But the most important quantity for characterizing a porous material is its specific flow resistance r. This can be measured with a steady state flow driven by a fixed pressure difference across a sample of the material.

If

$$rd > \rho c,$$

<div align="right">(11.2.86)</div>

which is easy to fulfill, we may show from Eqs. (11.2.78), (11.2.84) and (11.2.85) that at the lower frequencies where sinh $(j\,k_x d)$ may be replaced by $(j\,k_x d)$, the improvement is given by the simple relation of Eq. (11.2.74a) for all angles of incidence.

At high frequencies, we may replace sinh $(j\,\hat{k}_x d)$ by $(1/2)\,e^{g_x d}$, which means neglecting some fluctuations about this value. Then we get for the improvement in TL

$$\Delta\,[TL] = 20 \log\,(z_2/2\hat{z}_x) + 8.7\,g_x d \quad .$$

<div align="right">(11.2.87)</div>

In the limit of sufficiently high frequencies, we get for $\sigma = 1$ and $\chi = 1$ from Eqs. (11.2.79), (11.2.84)

$$\Delta \, [\mathrm{TL}] = 20 \, \log \, (z_2 \cos \vartheta / 2\rho c) + 4.3 \, (\mathrm{rd}/\rho c).$$

(11.2.88)

The first term of the above equation corresponds to the transmission loss which would be expected if only the second partition were present. If this partition behaves like an inert mass, we find that

$$\Delta \, [\mathrm{TL}] = 20 \, \log \, (\omega m_2 \cos \vartheta / 2\rho c) + 4.3 \, (\mathrm{rd}/\rho c)$$

(11.2.88a)

The presence of damping material in the space between the walls causes an addition to the transmission losses over those of the single walls. Furthermore, the second term takes into account that even in the short distance between both walls, the propagating sound wave is damped. From this point of view, it seems advantageous to make use of materials with high flow resistance. But there may be restrictions because materials with high flow resistance will introduce higher stiffness at low frequencies and so increase the resonance frequency f_{oo}.

A general experimental evaluation of Eqs. (11.2.83), (11.2.84) and (11.2.85) has not been made as yet, not only because the corresponding calculations would be very cumbersome, but also because the results probably would give much higher values of TL than are actually achieved in practice. The reason for this disagreement between theory and practice is that the sound not only passes through the air space from the first wall to the second wall but also through the rigid bridges found at either the edges or at common studs of the wall. The present aim of research in this field is to decrease those influences either by using special types of bridges for which calculations can be made (see Sec. 11.3) or by using flexible panels whose critical frequencies are as high as possible 2.8/.

References

2.1 Rayleigh, Lord, Theory of Sound Vol. II Sec. 271.

2.2 London, A., J. Res. Nat. Bur. Stand. 42 604 (1949).

   London, A., J. Acoust. Soc. Am. 22 270 (1950).

2.3 Peutz, V.M.A., Acustica 4 281 (1954).

2.4 Schoch, A., Akust. Z. 2 113 (1937).

2.5 Cremer, L. Akust. Z. 7 81 (1942).

2.6 Cremer, L., and A. Eisenberg, Bauplanung u. Bautechnik 2 235 (1948).

2.7 London, A., J. Acoust. Soc. Am. 22 270 (1950).

2.8 Goesele, K., Acustica 4 (1954) report of Congress in Delft.

11.3 Insulation of Impact Sound

Excitation of Impact Sound. In the discussion of
the insulation of airborne sound in the previous section,
we had to deal with structure-borne sound problems be-
cause every airborne sound will be transformed into
structure-borne sound if it impinges on a structural ele-
ment. But structure-borne sound may also be excited
directly. This is the case, for example, if any vibrating
apparatus is mounted on a wall. Also, a very common type
of direct excitation of structure-borne sound is the impact
of rigid bodies against a rod or a plate.

The chief difference between the excitation by air
sound pressures and by forces transferred by rigid bodies
is a difference in the extent of the area over which the
driving force is applied. In the last case, we may regard
this area as being concentrated at a point. Therefore,
we are interested in knowing the reaction of the driven
continuum to a "point source". In other words we are
interested in the mechanical point impedance, i.e., the
ratio of an alternating driving force to the resultant
alternating velocity.

For a rod infinite in one direction and set in
longitudinal vibrations at the free end, this mechanical
impedance is

$$Z_L = A \sqrt{\rho E} = m\, c_L \ . \qquad (11.3.1)$$

Here A is the area of the cross section, ρ the density,
E Young's modulus of the material, m the mass per unit
length and c_L the velocity of longitudinal waves in the
medium composing the bar. In this case, the input imped-
ance, which also is equal to the characteristic impedance
of a progressive longitudinal wave in the rod, is real
and, therefore, independent of frequency.

But if the force is acting transversely at the free
end of the infinite rod, the impedance becomes complex,
it being given by

$$Z_B = \sqrt[4]{m^3 B}\ \sqrt{j\omega/2} = (1 + j)\, m c_B/2 \qquad (11.3.2)$$

where B is the stiffness against bending and c_B the phase velocity of bending waves; see Eqs. (11.2.37 and (11.2.38). The input impedance Z_B is complex because in addition to a progressive bending wave a quasi-stationary motion which dies away exponentially with increasing distance from the source is excited. The general differential equation for bending waves in a rod

$$B \frac{d^4 v}{dx^4} = m\omega^2 v \qquad (11.3.3)$$

is of the fourth order. This equation allows wave motions,

$$v = \exp(\pm 1\ k_B x) \qquad (11.3.4a)$$

as well as motion of the quasi-stationary type,

$$v = \exp(\pm k_B x) \qquad (11.3.4b)$$

where

$$k_B = \frac{2\pi}{\lambda_B} = \sqrt[4]{\frac{m\omega^2}{B}} \qquad (11.3.5)$$

(See Eq. (11.2.36)). Usually both types of motions are needed to fulfill the boundary conditions for the force F, moment of bending M, transverse velocity v and angular velocity ω. A further consequence of the complex character of this impedance is its dependence on frequency, which is included in the dependence of the phase velocity of bending waves on frequency.

If the transverse force is acting at any point on a rod that is infinite in both directions, the impedance has the same character but four times the magnitude. In this case

$$Z_B = 2(1 + j)\ m\ c_B \ . \qquad (11.3.6)$$

The most important point impedance is that of an infinite plate driven by a transverse force. Since here also bending vibrations are excited, a complex impedance

as in Eqs. (11.3.5) and (11.3.6) would be expected. In addition, the problem is more complicated due to its two dimensional character. Fortunately both complications compensate for each other in the case of the point impedance. In this case it is real and independent of frequency and is given by

$$Z = 8 \sqrt{mB} \qquad (11.3.7)$$

where m is the surface mass density in, say, gm/cm^2. For a homogeneous plate of thickness h, this formula may be written

$$Z = 2.3 \, c_L \rho \, h^2 \, . \qquad (11.3.7a)$$

Fig. 11.3.1 gives the values of Z_B as a function of the thickness for homogeneous plates of steel, aluminum, concrete, asphalt and plywood. For the last three kinds of material, the values are mean values. The straight lines are drawn between the limits of thicknesses which are of practical interest. It may be remarked that the values for Z vary over the very large range from 10^2 to 10^6 kg/sec.

For large, thin, damped plates, the values given by Eq. (11.3.7) are in fairly good agreement with measurements 3.1, 3.2, 3.3/. For thicker "plates" such as walls and ceilings, important deviations must be expected 3.2, 3.3/. For this reason the line for concrete walls in Fig. 11.3.1 is dotted and shows only the order of magnitude. For comparison with measurements, the assumptions of the Eqs. (11.3.7) and (11.3.7a) must be considered. First, the plate is assumed to be infinite or at least large compared to the bending wave length. This fixes the limit of validity for low frequencies where the eigenfrequencies are well separated. Here we have to expect large deviations because of resonance phenomena. On the other hand, the simple theory of bending only holds as long as the bending wave length is at least six times greater than the thickness. This fixes the limit of validity for high frequencies. These limits have been given in Fig. 11.2.5. For the present problem this limit may be lowered further because of the point-concentration of the force. For thicker plates, one must always take into account the local elasticity which diminishes the motion of the plate from that of the driving point.
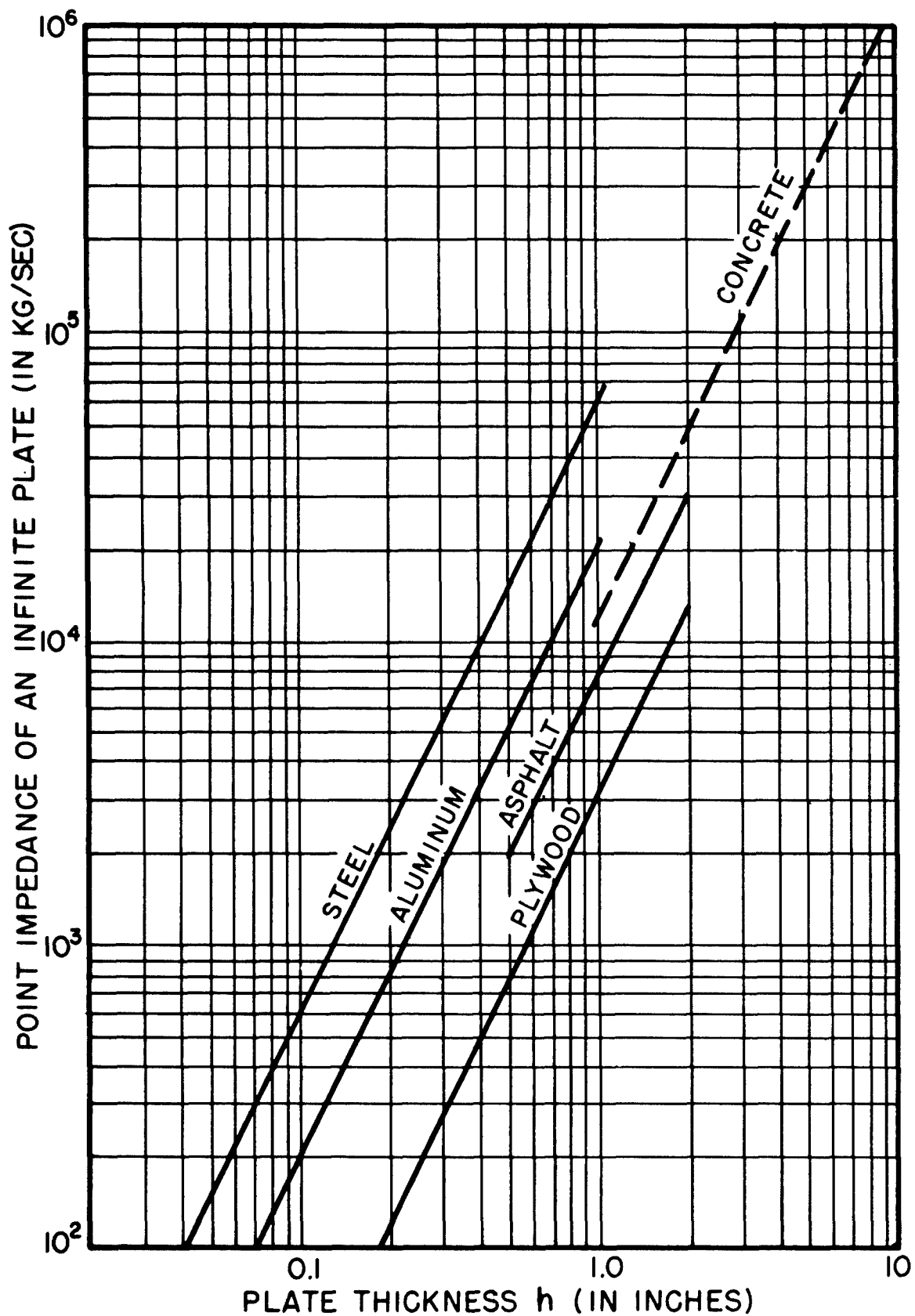
FIGURE 11.3.1

Point impedance of an infinite plate driven at one point,
in kg/sec, as a function of the plate thickness h in in.

Finally, for all frequencies it is important that the plate be homogeneous. However, in many practical cases this assumption is not valid. For example, sometimes a plaster sheet is not in good contact with the wall to which it is attached. In such cases, especially if the construction is obviously inhomogeneous, it may be necessary to measure the impedance. Often it will be sufficient to know the absolute value of the impedance. This can be measured by exciting the plate with an electrodynamic sound source, with the moving coil fixed directly to the wall or ceiling. The magnet system should be connected to the wall only by means of a resilient element. Then the same force (given by the magnetic field and the electric current) acts on the mass reactance of the coil in series with the plate impedance and on the mass reactance of the magnet system. If now the same pick-up is used to measure first the velocity v_1 (or acceleration) of the plate and then that of the magnet system v_2 we get

$$v_2/v_1 = (j \, \omega m_0 + Z)/j\omega m \qquad (11.3.8)$$

where M is the mass of the magnet system and m_0 the mass of the moving coil.

From this we find for the absolute value of Z

$$Z = \omega m \left| v_2/v_1 \right| , \qquad (11.3.8a)$$

or if $Z >> \omega m_0$,

$$Z = [(\omega m)^2 \left| v_2/v_1 \right|^2 - (\omega m_0)^2]^{1/2}$$

$$(11.3.8b)$$

assuming that Z is real. In other cases, the phase angle between v_1 and v_2 must also be measured. One must be sure that the magnet system behaves as a rigid body 3.3/. If it does not, the force must be obtained from the current in the coil and the absolute value of the velocity must be measured 3.2/.

The Spectrum of Impact Sound. The knowledge of the
mechanical impedance has several advantages. For example,
we may estimate whether or not a load will change the
vibration of the body under test. We can calculate the
velocity which may be obtained using a sound source of
known force and known internal impedance. Also, the case
of impact sound may be treated using the mechanical point
impedance.

When a rigid body of the mass m_0 strikes a rod or
plate with the velocity u_0, we get the same result as if
a force impulse $(m_0 u_0)$ works on the mass reactance $j\omega m$
and the impedance of the rod or plate Z in series, pro-
vided that the latter increases less rapidly with fre-
quency than ωm_0. In this case, the mass reactance $j\omega m_0$
may be regarded as the internal impedance of the source.
Since the frequency components of the force impulse are
all equal, namely $m_0 u_0 / \pi$, we find for the corresponding
components of the velocity of the plate

$$u_\omega = m_0 u_0 / \pi (j\omega m_0 + Z) \quad ; \quad (11.3.9)$$

if $Z >> \omega m_0$

$$u_\omega \simeq m_0 u_0 / \pi Z \qquad (11.3.9a)$$

For thin, large and fairly well-damped plates, we
may take for Z the values given by Eq. (11.3.7) or
Fig. 11.3.1. In these cases, the mass reactance is greater
than the wall impedance in the audio frequency region.
The heavier the mass m_0 and, therefore, the lower the "cut-
off" frequency given by the increasing mass reactance in
series with Z, the hollower the impact sounds. Also,
this is in agreement with our experience that an impact
sounds hollower, the thinner, lighter and more flexible
the plate is.

For thick walls, Eq. (11.3.9) is no longer valid
because of the local elasticity around the point of impact.
However, if we take into account a resilience K which for
simplicity is assumed to be linearly dependent on ampli-
tude between the striking mass and the impedance of the
wall calculated according to Eq. (11.3.7), the velocity

in which we are interested is no longer the velocity u of the mass m_0, but the velocity of the plate v outside the local resilient region. As may be derived easily from the schematic given in Fig. 11.3.2, the spectrum for this velocity is given by

$$v_\omega = \frac{m_0 \, u_0}{\pi \, [\, j \, \omega \, m_0 + Z \, (1 - \omega^2 m_0 / K) \,]} \, .$$

<div align="right">(11.3.10)</div>
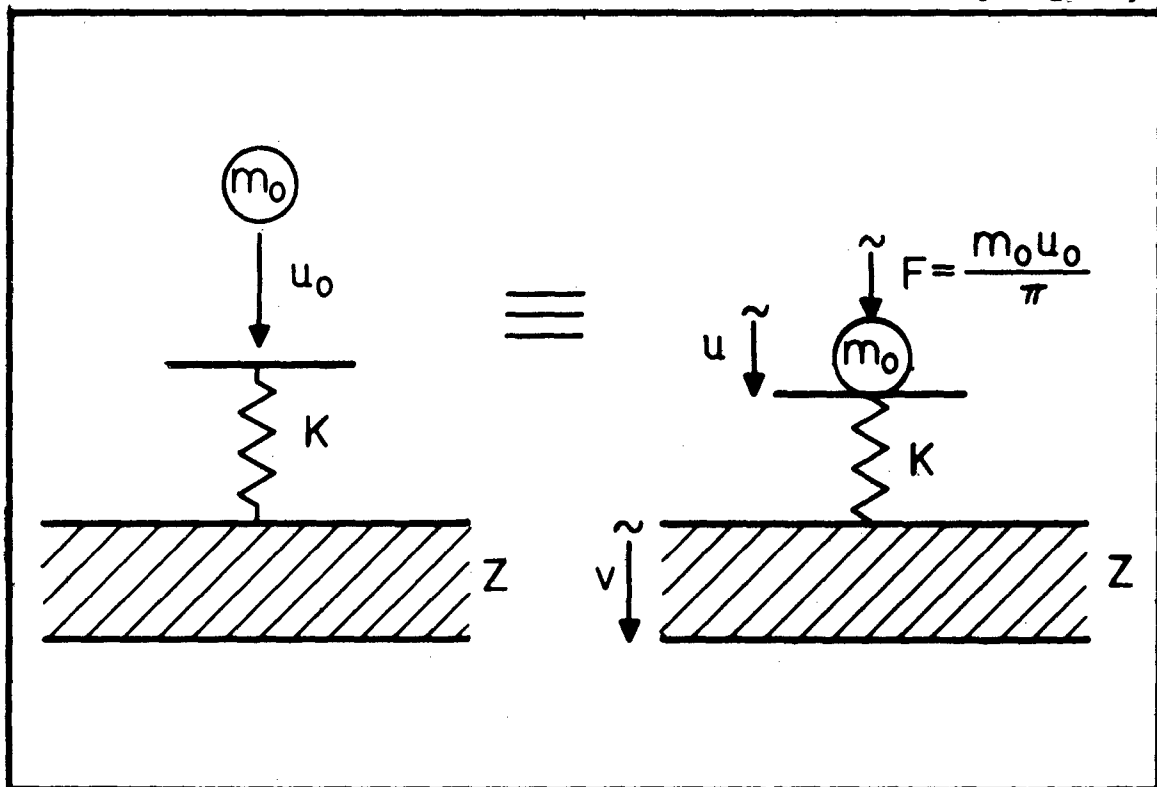
FIGURE 11.3.2

Mechanical schematic diagram for the impact of a mass m_0 with velocity u_0 on an infinite plate with local resilience represented by the spring K.

In Fig. 11.3.3 the spectrum of v_ω is plotted for fixed values of m_0 and Z and different values of K. Since energy losses are neglected, the lack of high frequency components results in an emphasis of the lower frequency components.

For comparison with measurements, it should be noted that Eq. (11.3.10) assumes constant bandwidth. When using octave band filters or third-octave filters, the measured results must be reduced to equal bandwidth, i.e., the measured amplitudes must be multiplied by $\omega^{-1/2}$.

In the routine technique of impact sound measurements in buildings, instead of v the mean sound pressure in the receiving room is measured. In this case the radiation power of the wall or ceiling, which depends on the ratio of the frequency to the critical frequency (see Eq. 11.2.47) and the absorption power of the receiving room, enter into the results.

Improvement With a Resilient Layer. In the last section we have introduced an unavoidable resilience K between the striking mass m and the plate characterized by Z. However, as we know from common experience with thick rugs, such an elastic layer is simple and effective as a remedy for impact noise.

The improvement of such a covering may be expressed by the difference of the sound pressure levels in the receiving room measured with and without the covering. Since the absorption power and the radiating power of the ceiling is not altered, the "improvement" may also be expressed by the ratio of the corresponding velocities of the ceiling or wall at the place of impact

$$\Delta L = 20 \log \left(v_1/v_2 \right) \quad . \qquad (11.3.11)$$

For not too high frequencies, we can use Eq. (11.3.9a) that

$$\mu = v_1 = m_0 u_0/\pi Z$$
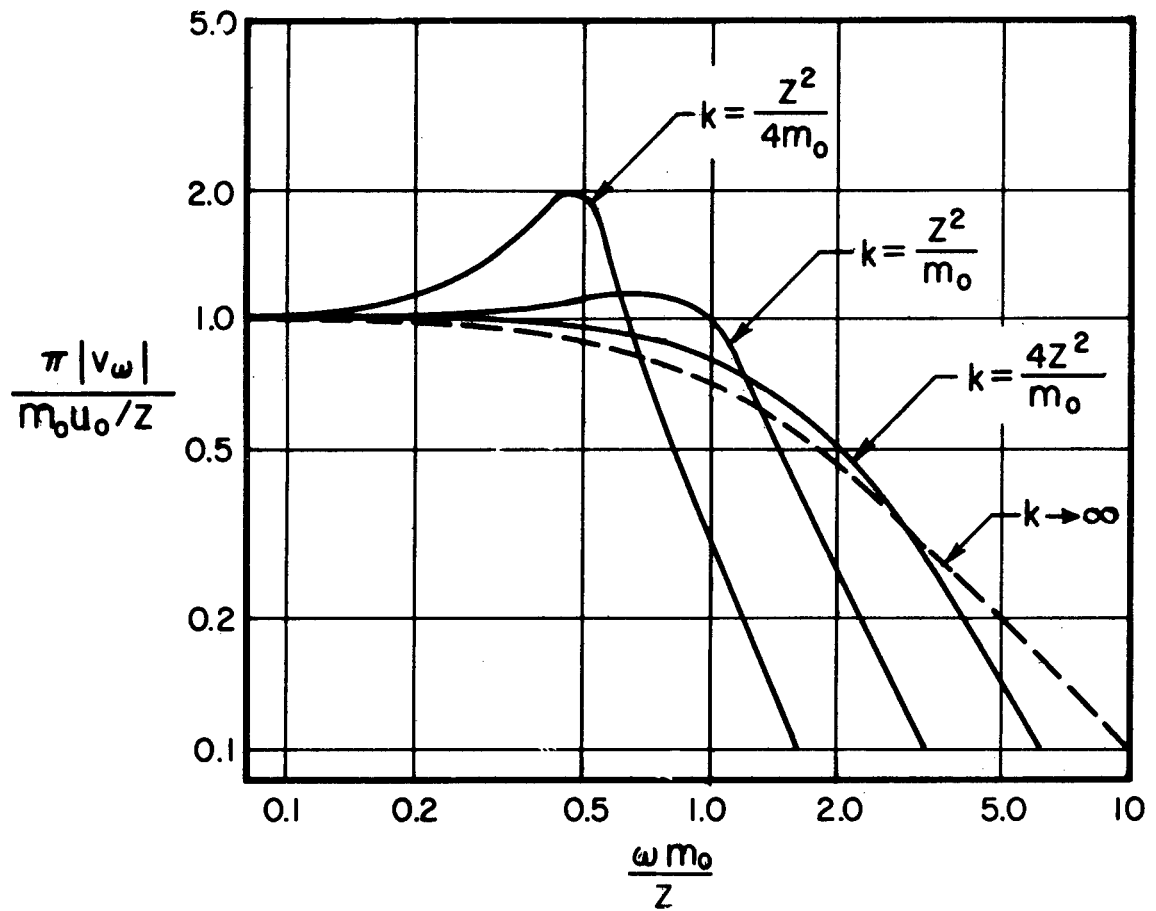
FIGURE 11.3.3

The spectrum shape of the impact-induced vibration when a mass m_o strikes a plate whose point impedance is Z.

and for not too low frequencies we get for the covered ceiling from Eq. (11.3.10)

$$v_2 = - \frac{m_o u_o}{\pi Z} \frac{K}{m_o \omega^2}$$

so that we find

$$\Delta L = 40 \log (\omega/\omega') = 40 \log (f/f') \qquad (11.3.12)$$

where

$$f' = \frac{1}{2\pi} \sqrt{\frac{K}{m_o}} \qquad (11.3.13)$$

is the eigenfrequency of the system consisting of the striking mass m_o and the stiffness K of the elastic layer. This stiffness is not only given by the properties of the layer, but also depends on the compressed area, or in other words, the form of the striking body. Furthermore, in most cases the area changes during the impact. Therefore, the linear resilience which has been assumed can be regarded only as a simple model. From this model we see that the improvement depends not only on the kind of covering but also on the striking body, especially on its mass m_o. As may be seen from Eqs. (11.3.12) and (11.3.13), the improvement increases with ω.

The standardized European test technique for impact sound control uses a falling mass of 500 gm (1.15 lb). Compared to a person walking, this mass seems to be too small to represent step noise 3.4/. However, step noise is not the only kind of impact noise. In the case of light switches, for example, the striking masses are much smaller, but the noise is still annoying.

It may be noticed that the improvement is independent of the impedance of the ceiling provided that it is sufficiently large and provided the local elasticity may be neglected. This is in agreement with measurements 3.5/.

Improvement by a Floating Floor. Ideal Conditions.

It is not always possible to cover a ceiling with only a resilient layer. In addition, a durable finish is needed. Covering the resilient layer with a rigid plate not only protects the layer, but it also has an acoustic advantage. We speak of a "floating floor" if the layer is highly resilient and the plate is stiff enough to bear the load of furniture and persons without too great a deformation.

In this case the improvement may be calculated. The formula is similar to Eq. (11.3.12) 3.6/

$$\Delta L = 40 \log (f/f_1) \quad . \qquad (11.3.14)$$

But now the reference frequency is the eigenfrequency of the system consisting of the surface mass unit area of the floating floor m_1 and the stiffness K_1 per unit area of the elastic layer. Thus,

$$f_1 = \frac{1}{2\pi} \sqrt{\frac{K_1}{m_1}} \quad . \qquad (11.3.15)$$

Here the quantity K_1 is well-defined. It consists of two parts, K_1' and $\bar{K}_1''$ where

$$K_1 = K_1' + K_1'' \quad . \qquad (11.3.16)$$

K_1' is the stiffness of the fibers of the layer which holds the floor at the distance d from the ceiling

$$K_1' = E_1/d \qquad (11.3.17)$$

and K_1'' is the stiffness of the air enclosed between the floating floor and the ceiling

$$K_1'' = \rho_0 c^2 / \sigma d. \qquad (11.3.18)$$

Here σ is the porosity of the fiber blanket and may be assumed to be nearly one. The elastic modulus E_1 may be evaluated by measuring the eigenfrequency of a given mass on a small portion of the blanket 3.7/. In this case the resilience of the air may be neglected since the air can escape laterally. But for an area of floating floor which is large compared to the wavelength of the sound frequencies, the air under the floor must be compressed. Generally it is of no acoustic advantage to make the blanket more resilient than the air but it would be a disadvantage from the structural viewpoint.

If we assume $K_1 \simeq K_1' = \rho_0 c^2/d$, f_1 becomes equal to f_o, defined by Eq. (11.2.71a), i.e.

$$f_1 = 170/\sqrt{G_1 d} \qquad (11.3.19)$$

where G_1 is the surface weight density of the floating floor in lb/sq ft and d is the distance between the floating floor and the ceiling. This distance has to be measured for the finished floor. It may be measured with a part of the blanket loaded by about 40 lb/sq ft, corresponding to the weight of floor and furniture.

It may be remarked that the improvement of the floating floor with respect to impact sound is the same as the improvement with respect to airborne sound which was given by Eq. (11.2.74). But it may be mentioned that the derivations of both formulae and the physical basis are quite different. In one respect, however, we may make further use of this analogy. For the airborne sound problems, we mentioned that for a wave at oblique incidence, lateral motion in the air space is excited and results in a higher stiffness. However, with a fiberglas blanket in the air space, this motion is hindered and the stiffness for waves of perpendicular incidence is obtained for all angles of incidence. From this analogy, we can see that in the case of impact sound also, the flow resistance of the blanket is effective in preventing lateral motion of the air. Hence an air space without a blanket has a higher stiffness, thus gives a smoother improvement.

From Eq. (11.3.14), it is seen that the improvement of a floating floor is independent of the type of ceiling. This is also in agreement with measurements taken 3.5/.

Furthermore, the improvement is independent of the striking mass. However, this statement holds only as far as the point impedance of the floating floor Z_1 may be considered as being large compared to the reactance of the falling mass (ωm_0). For thin rigid coverings and high frequencies, we have to add to Eq. (11.3.14) a second term to obtain for the improvement of the floating floor

$$\Delta L = 40 \log (f/f_1) + 10 \log [1 + (2\pi f m_0/Z_1)^2] \quad .$$

$$(11.3.20)$$

As in the case of the improvement of airborne sound insulation by a separated, second partition wall, Eqs.(11.3.14) and (11.3.20) are valid only if they give values which are not too high. However, the equations are useful for design because the frequency region where they are valid is the most important region.

There are several reasons for the deviation of experimental results from Eq. (11.3.14). First, this formula is derived on the assumption of an infinite ceiling and a floating floor. Since the floating floor is carefully separated from the side walls, there is total reflection of bending waves at the sides. These reflecting waves will also contribute to the mean sound pressure in the receiving room. Furthermore, it seems that the tangential motion in the elastic layer cannot be prevented at higher frequencies. But the most usual and dangerous deviation happens if there are rigid connections between the floating floor and the ceiling, which may be called "sound-bridges."

Improvement by a Floating Floor. With Sound-Bridges. We now will consider the improvement of isolation by a floating floor and how it can be decreased if point "sound bridges" are present 3.8/. Such more or less rigid bridges may not only occur as an error during the construction of a floating floor, they may also be a result of the construction, as for example when the floor is laid on rubber mountings. In all these cases there are two ways for the sound energy to pass from floor to ceiling. The

first is that over the air space inside the fiberglas blanket which is considered in Eq. (11.3.20). The second is the path through the bridges. At high frequencies, the internal impedance of the source $(j\omega m_0)$ has to be considered for both ways. Therefore, the second term of Eq. (11.3.20) remains unchanged.

Generally the expression for the improvement (actually a deterioration by the bridges) may be written as

$$\Delta L = -10 \log \left[(f_1/f)^4 + \sum_{i=1}^{n} \left| \frac{\prod (k_1 \, r_i) \, z_2}{z_{12} + \Lambda_{12} \, z_1} \right|^2 \right]$$

$$+ \ 10 \log [1 + (2\pi \, fm_0/z_1)^2] \quad .$$

$$(11.3.21)$$

Here r_i is the distance between the place of impact and the ith of the n bridges and k_1 is the propagation parameter for a bending wave in the floating floor, which in general is a complex quantity given by

$$k_1 = 2 \ (1 - in/4)/\lambda_1 \qquad (11.3.22)$$

Here λ_1 is the length of the bending wave and n loss factor which has been introduced in Eq. (11.2.59) but which also may be defined by the measured attenuation per wave length.

The function $\prod(k_1 r)$ gives the ratio of the transverse velocity of the floor at a distance r which would be present without the bridge to the velocity of the floor at the point of impact,

$$\prod (k_1 r) = v(r)/v(0) \quad . \qquad (11.3.23)$$

Therefore, in all cases we have

$$\Pi(0) = 1 \quad . \tag{11.3.23a}$$

For an infinite floating floor without damping, Π would increase as $k_1 r$ increases

$$\Pi(k_1 r) = \sqrt{2/\pi \, k_1 r} \; \exp - j(k_1 r - \pi/4)$$

or

$$|\Pi|^2 = 2/\pi \, k_1 r \quad . \tag{11.3.23b}$$

But the assumption of an infinite size is not as valid in the case of the floating floor as it is in the case of the ceiling. The floating floor is carefully separated from the wall so that the reflection of bending waves is total. The energy losses only occur during the propagation. If these losses are high, as in asphalt floors, we may neglect the reflections and set

$$|\Pi|^2 = (2/\pi \, k_1 r) \, \exp(-\eta k_1 r/2) \quad . \tag{11.3.23c}$$

If the loss factor is small, however, many reflections must be taken into account. The resultant velocity will be given by a statistical superposition of all the reflected waves. In this case $|\Pi|^2$ becomes

$$|\Pi|^2 = 4 \, c_{L1} \, h_1/S\omega \, \eta \, \sqrt{3} \tag{11.3.23d}$$

where S is the surface area of the floating floor, c_{L1} is the velocity of propagation for longitudinal waves and h_1 the thickness of the floor.

The velocity at the distance r_1, given by $\Pi v(0)$, has to be distinguished from the velocity v_1 which occurs if a bridge is present, according to the formula

$$v_1 = \Pi v(0) - F_1/Z_1 \quad . \tag{11.3.24}$$
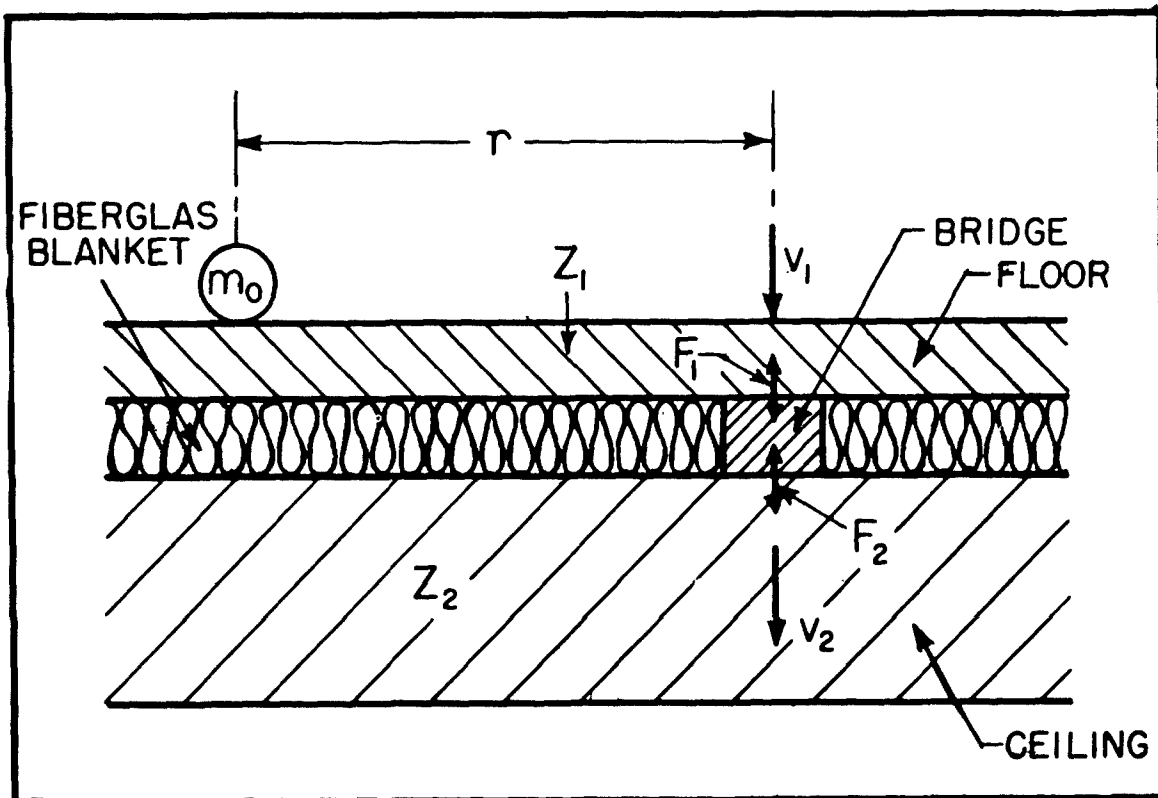
FIGURE 11.3.4

Sketch of a floating floor separated by a
fiberglas blanket and a sound bridge from
the ceiling below. The various quantities
used in the analysis are shown in the figure.

Here Z is the point impedance of the floating floor, Z_2
that of the ceiling and F_1 is the transverse force acting
between the floor and the bridge. See Fig. 11.3.4.

The quantity in which we are interested is the
velocity v_2 at the foot of the bridge. This is related
to v_1 and F_1 by

$$Z_{12} = F_1/v_2 \qquad\qquad (11.3.25)$$

$$\Lambda_{12} = v_1/v_2 \quad . \qquad\qquad (11.3.26)$$

The first of these coefficients has the dimension of an impedance and is, therefore, characterized by the letter Z. Since the second is a pure number, a Greek letter has been chosen. The double subscripts 12 indicate the coupling between quantities before and after the bridge.

For a short, prismatic bridge of the length l, cross sectional area A, density ρ and Young's modulus E we find

$$Z_{12} = Z_2 + j \omega l A \rho \qquad (11.3.25a)$$

$$\Lambda_{12} = 1 + j \omega l Z_2/AE \; . \qquad (11.3.26a)$$

Then the denominator of the second term of Eq. (11.3.2) becomes

$$Z_{12} + \Lambda_{12} Z_1 = (Z_1 + Z_2) + j \omega l (A\rho + \frac{Z_1 Z_2}{AE}) \; .$$

$$(11.3.27)$$

The details of the bridge appear only in this second term, which increases with frequency. We wish to make this term as large as possible. This means that we have to avoid the minimum value for the term in the brackets that occurs when the characteristic impedance of the bridge equals the geometric mean of the point impedances of floor and ceiling. That is, when

$$A \sqrt{E\rho} = \sqrt{Z_1 Z_2} \; . \qquad (11.3.28)$$

This case is of importance for double wall constructions consisting of equal panels, where Eq. (11.3.28) becomes

$$A \sqrt{E\rho} = A\rho \, c_L = Z_1 \; . \qquad (11.3.28a)$$

There it is easy to see that the sound energy from one wall will be transmitted to the other most easily if the

characteristic impedance of the bridge $A\rho\ c_L$ matches the point impedances of the plates Z_1. Avoiding this matching does not necessarily mean that the bridge should be as resilient as possible. If the bridge connects two thin wooden panels of the thickness h, a wooden bridge of cross sectional area A given by

$$A = 2.3\ h^2 \qquad\qquad (11.3.28b)$$

would just give the perfect impedance match, as may be derived by comparison of Eqs. (11.3.28a) and (11.3.7). It is better to mismatch Z_1 and Z_2 as far as possible. So for example, Meyer found experimentally that with wooden panels, heavy iron bridges gave the best sound insulation $\underline{3.9}/$.

In the case of floating floors, Z_2 is so large that mismatching occurs only with very resilient bridges. This means that we may neglect ρA in Eq. (11.3.27) and thus have the quantity AE as small as possible. In this case, Eq. (11.3.21) becomes

$$\Delta L = -10\ \log\left[(f_1/f)^4 + \sum\left| \frac{\prod Z_2}{(Z_1+Z_2) + j\omega\ Z_1 Z_2/AE} \right|^2 \right]$$

$$+ 10\ \log\ [1 + (2\pi\ fm_b/Z_1)^2]\ . \qquad (11.3.29)$$

The more resilient the bridge becomes, the more the length becomes comparable to the wave length of longitudinal waves in the bridge and the formulas, Eqs. (11.3.25a) and (11.3.26a), have to be replaced by the corresponding transmission line equations.

Also we are interested in bridge constructions which at present cannot be calculated at all. In these cases we have to measure Z_{12} and Λ_{12}. Usually Z_{12} can be neglected compared to $\Lambda_{12}\ Z_1$, so that it is sufficient to measure Λ_{12}. This can be done easily by comparing v_1 and v_2 with the same device and with any kind of exciting force. But it should be remarked that Λ_{12} is

defined in connection with a special ceiling Z_2 only. In this case Eq. (11.3.21) may be written

$$\Delta L = -10 \log \left[(f_1/f)^4 + \sum \left| \pi z_2 / \Lambda_{12} \, z_1 \right|^2 \right]$$

$$+ 10 \log [1 + (2\pi \, f m_o / z_1)^2] \quad . \quad\quad (11.3.30)$$

Impact sound, as well as structure-borne sound in general, not only excites one wall, but propagates through the structure. Such vibrations are propagated with relative ease and are not usually hindered by bends or changes in cross sectional area of the structural member; but they may be interrupted by vibration breaks consisting of elastic layers. For a discussion of these matters, see the work of Cremer 3.10, 3.11/.

References

3.1 Cremer, L., Tekn. Tidskr. <u>80</u> 393 (1950)

3.2 Elling, W., Acustica <u>4</u> 396 (1954)

3.3 Heckl, M., Acustica <u>4</u> (1954) (to be published)

3.4 Gosele, K., Gesundheitsingenieur <u>70</u> 66 (1949)

3.5 Gosele, K., Gesundheitsingenieur <u>72</u>, (1951)

3.6 Cremer, L., Acustica <u>2</u> 762 (1952)

3.7 Gosele, K., and W. Bach (to be published)

3.8 Cremer, L., Acustica <u>4</u> 273 (1954)

3.9 Meyer, E., Akust. Z. <u>2</u> 74 (1932)

3.10 Cremer, L., Acustica <u>3</u> 317-335 (1953)

3.11 Cremer, L., "Propagation of Structure-Borne
     Sound" Sponsored Research in Germany,
     Report #1, Series B Dept. of Scientific
     and Industrial Research

11.5 Transmission of Sound Through Cylindrical Pipes

The discussion of Sec. 11.2 of the transmission of sound through walls is valid for curved plates if the radius of curvature is large compared with the sound wavelengths in both the air and the plate. But we have to add a third term to the transmission impedance (see the discussion on single walls in Sec. 11.2 for a concept of transmission impedance) if the radius of curvature becomes comparable with either of these wavelengths. This added term is larger than the first two when the radius of curvature is small compared with the wavelength, as is the case in cylindrical pipes with small diameters at low frequencies. Here the sound pressure inside the pipe is uniform over the cross-section. The constant pressure inside tends to enlarge the diameter and gives rise to elastic restoring forces on account of this tension. Then the transmission impedance is a resilient reactance equal to

$$Z_\tau = \frac{1}{j\omega}\frac{Eh}{a^2} \qquad . \qquad (11.5.1)$$

Here a is the radius of the pipe and h the thickness of its wall, E is Young's modulus and $\omega = 2\pi$ x frequency; we always assume that $h \ll a$.

In the ideal case that the pressure inside the pipe is constant along the pipe, Young's modulus would have to be divided by $(1-\mu^2)$ as in Eq. (11.2.38a). In this case, axial contraction is hindered. But in practice axial contraction is always possible; if the pipe is short, the edges can move; or if the pipe is longer than the wavelength of sound in air, the radial expansions and contractions of the diameter involve the necessary axial motion. In practical cases, the difference between E and $E/1-\mu^2$ is too small to be considered in practical calculations.

It is easy to show that the tension term given by Eq. (11.5.1) is much greater than the inertia term. The sum of both may be written

$$Z_\tau = \frac{1}{j\omega}\frac{Eh}{a^2} + j\omega m = \frac{Eh}{j\omega a^2}\left[1 - \left(\frac{\omega}{\omega_o}\right)^2\right] \qquad . \qquad (11.5.2)$$

Here

$$\omega_0 = c_L/a \quad \text{or} \quad f_0 = c_L/2\pi a \quad . \tag{11.5.3}$$

This is the angular frequency ω_0 or the frequency of the zero order mode of a ring of diameter 2a. The corresponding motion of the pipe is mostly radial with only small axial motion. Since this frequency is a characteristic quantity for the behavior of the pipe, we may relate all frequencies to it by introducing the dimensionless frequency parameter ν given by

$$\nu = f/f_0 \quad . \tag{11.5.4}$$

For small ν, the tension term is $1/\nu^2$ times greater than the mass term, this means that we expect the "transmission loss" to be $40 \log 1/\nu$ higher than that given by the mass law for normal incidence.

For a steel pipe of 4 in. diameter, the zero mode frequency would be about 16,000 cps. Assuming a thickness of about 1/8 in., the "mass law for normal incidence" would give at 1000 cps, TL = 46 db; but to this has to be added 48 db (40 log 1/2), so that the theoretical value of the TL would be 96 db. Furthermore, we have to realize that according to Eq. (11.2.9a) the radiating surface of such a pipe is always small compared with the absorption power of the receiving room. Let us assume that the pipe has a length of 8 ft; its surface will be about 8 sq ft whereas the absorption power of even a small room may be 80 sq ft. According to the discussion in Sec. 11.2, this means that 10 db has to be added in order to get the pressure level difference*. Finally, we must remember that the radiation power of a pipe is not proportional to its surface area if the perimeter becomes smaller than a wavelength. Taking everything into account, the calculated pressure level differences are so high that at 1000 cps, a sound pressure of 100 db inside the pipe would not be heard outside and at lower frequencies even much higher pressures inside

---

*   Although Eq. (11.2.9a) was derived under the assumption of a large source room with statistically distributed sound waves it can be proved that it is also valid for a source room small compared to the wavelength.

would not be audible outside. The amount by which the TL
of small pipes exceeds the mass law has not been studied
experimentally. But there is no doubt that practical
observations do not correspond to these sample calculations.
One of the reasons may be that the pipe is always fixed
to a wall with the possibility of transferring sound energy
to the walls which may then radiate it. Also, even if the
diameter is small compared to the wavelength, small asym-
metries will excite other modes with higher amplitudes.
If we now treat the case of a large cylindrical shell, we
will see that these other modes may offer much smaller
transmission impedances.

When the diameter 2a is large, the zero-mode frequency
will be in the middle audio range. For instance, for an
aluminum shell 7 ft in diameter, corresponding to an air-
plane structure, this frequency would be 770 cps. At this
frequency, the perimeter equals the length of longitudinal
waves in the shell. Since the corresponding velocity of
propagation c_L is about 15 times greater than the sound
velocity in air c_o, we have 15 wavelengths of airborne
sound along the perimeter and we may say that in this re-
gion the radius a is large in comparison to the wavelength.
Then the behavior of the shell will be similar to that of
a plane wall. Therefore, we have to add a term repre-
senting stiffness against bending as in Eq. (11.2.48);
this would change Eq. (11.5.2) to

$$Z_T = j\omega m - j(Eh/\omega a^2) - j(B\omega^3/c_o^4) \sin^4 \vartheta$$

$$= j2\pi fm [1 - (f_o/f)^2 - (f/f_c)^2 \sin^4 \vartheta] .$$

$$(11.5.5)$$

Thus, the critical frequency f_c, defined by Eq. (11.2.47)
appears as a second characteristic frequency for the shell;
in terms of

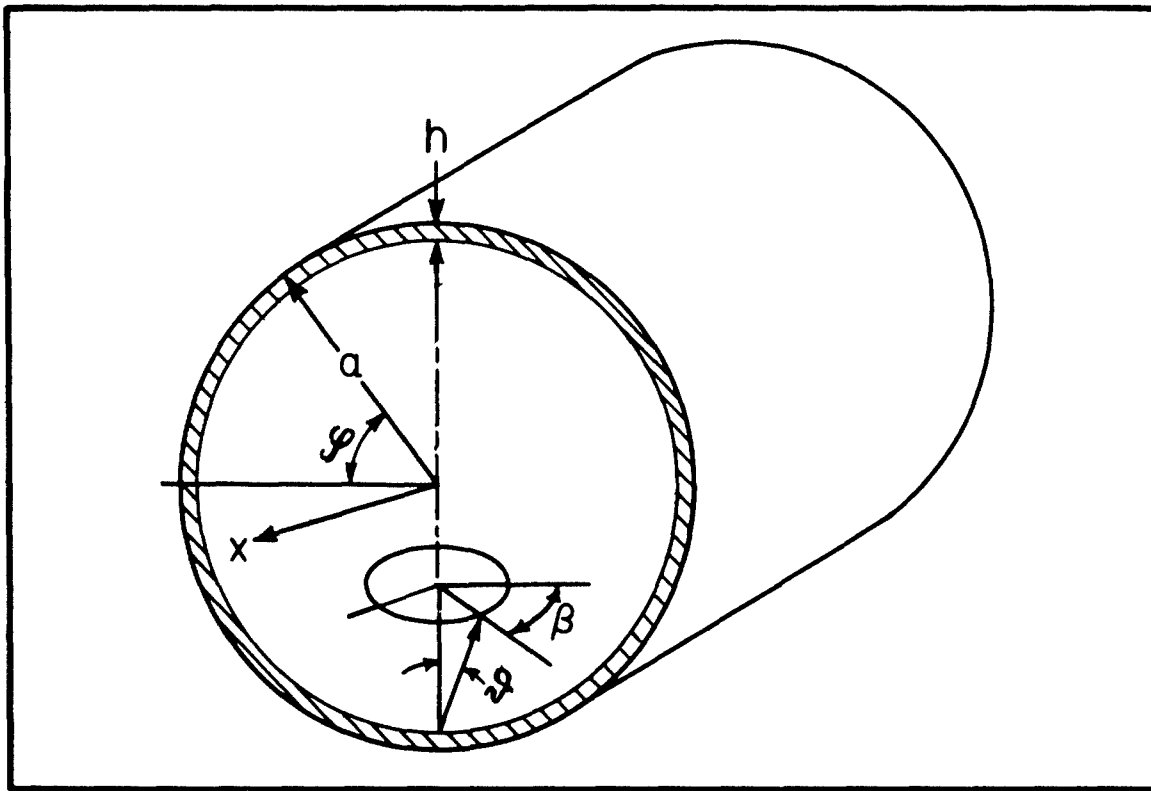$$\nu_c = f_c/f_o = \sqrt{12} (c_o^2 a/c_L^2 h) \qquad (11.5.6)$$

FIGURE 11.5.1

Coordinate system used in the analysis of the
transmission of sound through a cylindrical
shell.

---

appears as a new parameter. For the example of a 7 ft
aluminum shell, we get $\nu_c = 2$ if h is 0.2 in. and $\nu_c = 0.5$
for h = 0.8 in. The angle ϑ is the angle between the
perpendicular to the shell, i.e., the radial direction,
and the direction of the incident wave as shown in
Fig. 11.5.1. But now we have to consider another angle, β,
which determines whether the propagation for $\vartheta = 90^\circ$ in-
volves an axial or a longitudinal motion. For the first
case, β is 90° while in the second, $\beta = 0^\circ$.

It is simple to demonstrate that the second term
in Eq. (11.5.5) must depend on this angle. If we curve a piece
of paper into a cylindrical shape, we see that it is very

easy to bend the cylinder in a direction corresponding to $\beta = 0°$, but that it is very difficult to bend it in any plane containing the line $\beta = 90°$. Omitting only a small region of nearly perpendicular incidence given by $\sin^2 \vartheta < 8(1 + \mu)(c_0/c_L)^2$, we can include this dependence by multiplying the tension term of Eq. (11.5.5) by $\sin^4$ to give

$$Z_\tau = j\omega m - j \frac{Eh}{\omega a^2} \sin^4 \beta - j \frac{B\omega^3}{c_o^4} \sin^4 \vartheta$$

$$= j \, 2\pi f m \left[1 - \frac{\sin^4 \beta}{\nu^2} - (\nu/\nu_c)^2 \sin^4 \vartheta \right].$$

(11.5.7)

Again we are especially interested in the conditions of vanishing impedance. We may plot the corresponding (ϑ, ν) lines (contours of equal TL) with β as parameter on a $(\log \nu, \sin^2 \vartheta)$ plane as was done in Fig. 11.2.9. The results are given in Figs. 11.5.2 and 11.5.3 for $\nu_c = 2$ and $\nu_c = 1/2$ respectively. For $\sin^2 \beta \sin^2 \vartheta \ll \nu_c/2$ and, therefore, for $\nu_c \gg 2$, two different types of trace matching appear. (In Fig. 11.5.2 this is the case except for the curve $\beta = 90°$ in the region $\sin^2 \vartheta > 0.8$). One is the trace matching for bending waves already discussed in the case of plane walls. This is independent of β and is given by Eq. (11.2.46) with new parameters given by

$$\nu = \nu_c/\sin^2 \vartheta \; . \qquad\qquad (11.5.8)$$

This situation occurs only above $\nu = \nu_c$ or $f = f_c$.

The second type is a trace matching for tensional waves. Here the two first terms of Eq. (11.5.7) are equal. This is independent of ϑ but dependent on β by the relation

$$\nu = \sin^2 \beta \; . \qquad\qquad (11.5.9)$$

This occurs only below $\nu = 1$ or $f = f_o$.

For a given direction of the incident sound, we may say that the sound insulation of the shell is stiffness-controlled below $\nu = \sin^2 \beta$, that it is mass-controlled in the region $\sin^2 \beta < \nu < \nu_c / \sin^2 \vartheta$ and that it is again stiffness-controlled above $\nu_c / \sin^2 \vartheta$.

If $\nu_c < 2$, as may be the case for thicker shells, the two kinds of trace matching cannot be separated further and the lines for $Z_\tau = 0$ continually pass over from the one limiting case to the other (see Fig. 11.5.3 except $\beta = 15^\circ$). Here for special values of ϑ and β given by $\sin^2 \vartheta \sin^2 \beta > \nu_c/2$, the wall is always stiffness-controlled; at low frequencies it is controlled by the stiffness for tension and at high frequencies by the stiffness for bending.

For a given direction of the incident sound we may also calculate the transmission coefficient τ by putting Eq. (11.5.7) into Eq. (11.2.20). Here Eq. (11.2.20) has to be considered as an approximation because it was derived for plane waves whereas here we have cylindrical waves in the radial direction. But the difference is important only at low frequencies. Also, here the region of grazing incidence must be excluded. But for all other cases we may write

$$[\text{TL}]_{\vartheta, \beta} = 10 \log \left[1 + \left(\frac{\pi f m \cos \vartheta}{f_o c_o} \right)^2 \left(1 - \frac{f_o^2 \sin^4 \beta}{f^2} - \frac{f^2 \sin^4 \vartheta}{f_c^2} \right)^2 \right]$$

(11.5.10)

There is seldom a preference for special angles of incidence. In practice we have mostly a distribution of sound over various angles of incidence. Then the result for a given frequency region essentially depends on whether or not an angle for trace matching appears. If it does, most of the transmitted sound energy is due to this special direction. Furthermore, the result will depend on the damping of the shell and also on the size of the shell. In the case of a plane plate, all this happens above f_c only. Here, for a curved shell, it also happens at frequencies below f_o with the result that the TL will be much lower than the mass law would predict. The proper value will depend on the maximum transmission coefficient and on the bandwidth as in Eq. (11.2.64).
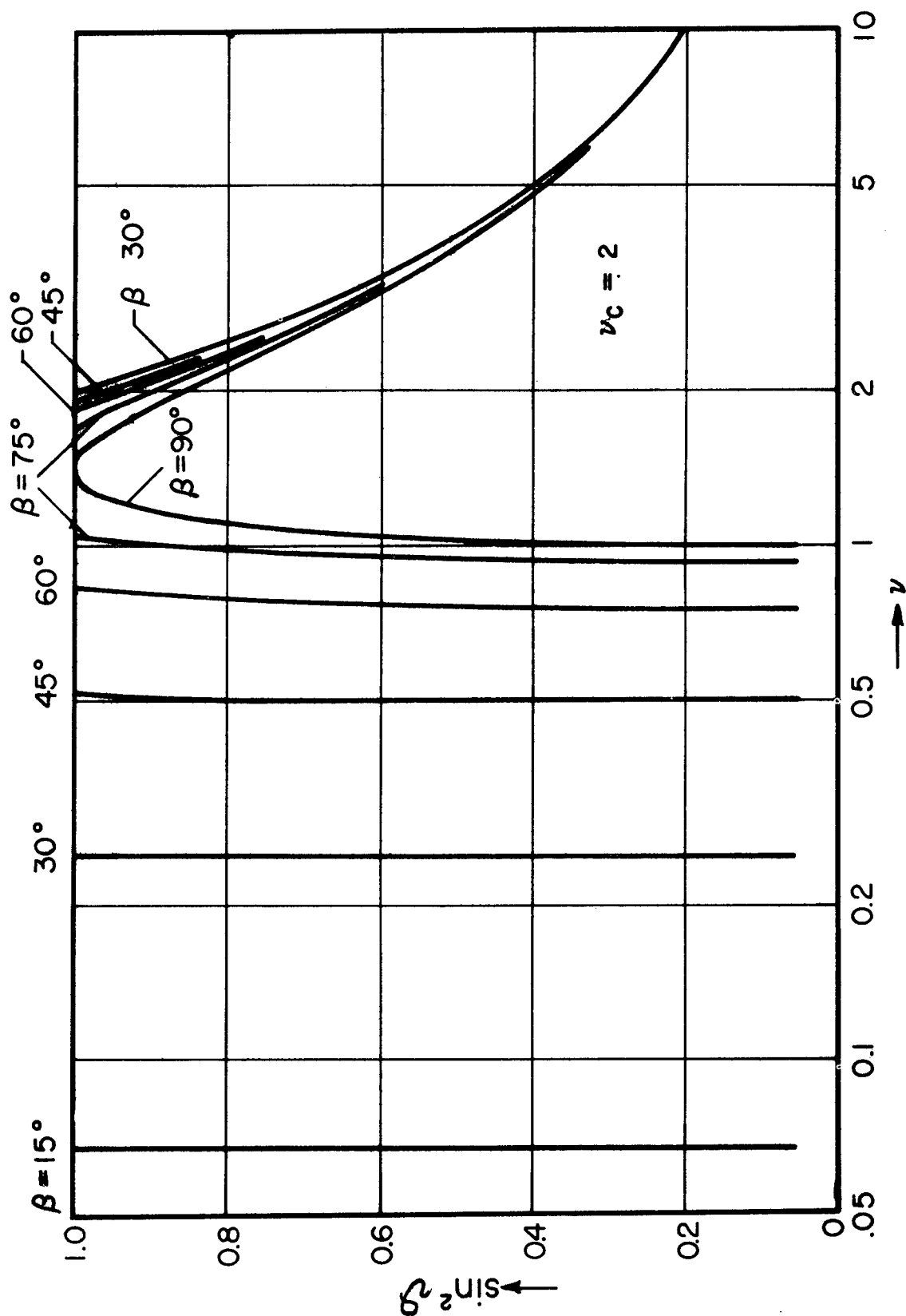
FIGURE 11.5.2

Contours of equal TL for various values of the frequency parameter $\nu = f/f_o$, $\sin^2 \vartheta$ and $\nu_c = f_c/f_1 = 2$.

When averaging over the various angles of incidence, we have again to take into account the fact that a portion of the wall S will intersect only the area S cos ϑ of the wave front, whereas with respect to β no such weighting factor appears. Also with respect to the probability of a special direction, all β will have the same probability. Therefore, no special weighting factor is required but if it can be assumed that the sound inside will be distributed over all directions equally the region between ϑ and $d\vartheta$ has to be multiplied by $\sin\vartheta$. But in the case of a cylindrical enclosure, two further aspects render the problem more difficult. First, not all combinations of ϑ and β appear inside a given cylinder. It is easy to understand that in the tangential direction around the perimeter, the periodicity must be a proper fraction of the perimeter. A second, not so simple condition, holds in the radial direction. From both it can be derived that in the above-mentioned case of a cylindrical shell of 7 ft diameter, at 500 cps there exist only 17 different pairs of angles ϑ and β. Furthermore, these angles are not equally distributed over all the possible directions. This is a consequence of the well-known fact that each curved wall results in focusing of the sound. If the sound source is located in the center we will get perpendicular incidence for $\beta = 0$, i.e., $\vartheta = 0^\circ$ only. If the source is located near the perimeter, the incidence will be grazing. It can be seen geometrically and may be proved more rigorously by the wave theory that a really tangential sound propagation, i.e., $\vartheta = 90^\circ$ for $\beta = 0^\circ$ is possible only in the limit of infinitely high frequencies. On the other hand, the focusing qualities of a cylinder will be destroyed if there are deviations from the ideal geometric form and especially if there are any kind of obstacles inside. Therefore, it is hazardous to base extensive calculations on the angular distribution of sound in a perfect cylinder. To the same degree of approximation, we may assume a uniform distribution of angles of incidence as in the case of a plane wall.

If we assume a statistically uniform distribution of angles of incidence, the average is given by

$$\tau_{random} = \frac{2}{\pi} \int_0^{\pi/2} \int_0^1 \tau \, d(\sin^2\vartheta) \, d\beta \, . \qquad (11.5.11)$$

For $\nu_c > 2$, i.e., for thin walls and a pipe of large diameter, above the critical frequency τ becomes independent of β and the results are the same as in the case of the plane wall. Therefore, we may use the Eqs. (11.2.58) and (11.2.65) in this region or Figs. 11.2.10 and 11.2.11.

In the mid-region $1 < \nu < \nu_c$ we can expect the mass law to hold if the frequency region is sufficiently broad.

For $\nu < 1$ we may calculate the mean transmission coefficient with respect to β in the same way as we did for the case of bending wave trace matching. In regard to ϑ, it may be reasonable to choose the mean value of $\vartheta = 45°$. Then we get for $\nu < 0.8$

$$[TL]_{45,\ random} = 10 \log \left(\frac{a_c}{\nu_c}\right) + 5 \log (\nu - \nu^2) + 1.5$$

$$(11.5.12)$$

where a_c is the value given by Eq. (11.2.51). Therefore, the first term which corresponds to the 0° mass law at the zero mode frequency represents one half the transmission loss. Thus we see that the transmission loss will be, in general, smaller than would be calculated using the mass law. Furthermore, we see that the frequency response is rather flat. In Fig. 11.5.4, $[TL]_{45,\ random}$ is plotted against frequency for the region $0.05 < \nu < 0.8$ for different values of a_c/ν_c. As in Fig. 11.2.10, the practical value of these curves is doubtful since even a small amount of damping will change the results.

Introducing energy losses by means of a loss factor as defined in Eq. (11.2.59), we have to add to Eq. (11.5.9) a further term

$$[TL]_{45,\ random} = 10 \log (a_c/\nu_c) + 5 \log (\nu - \nu^2) + 1.5$$

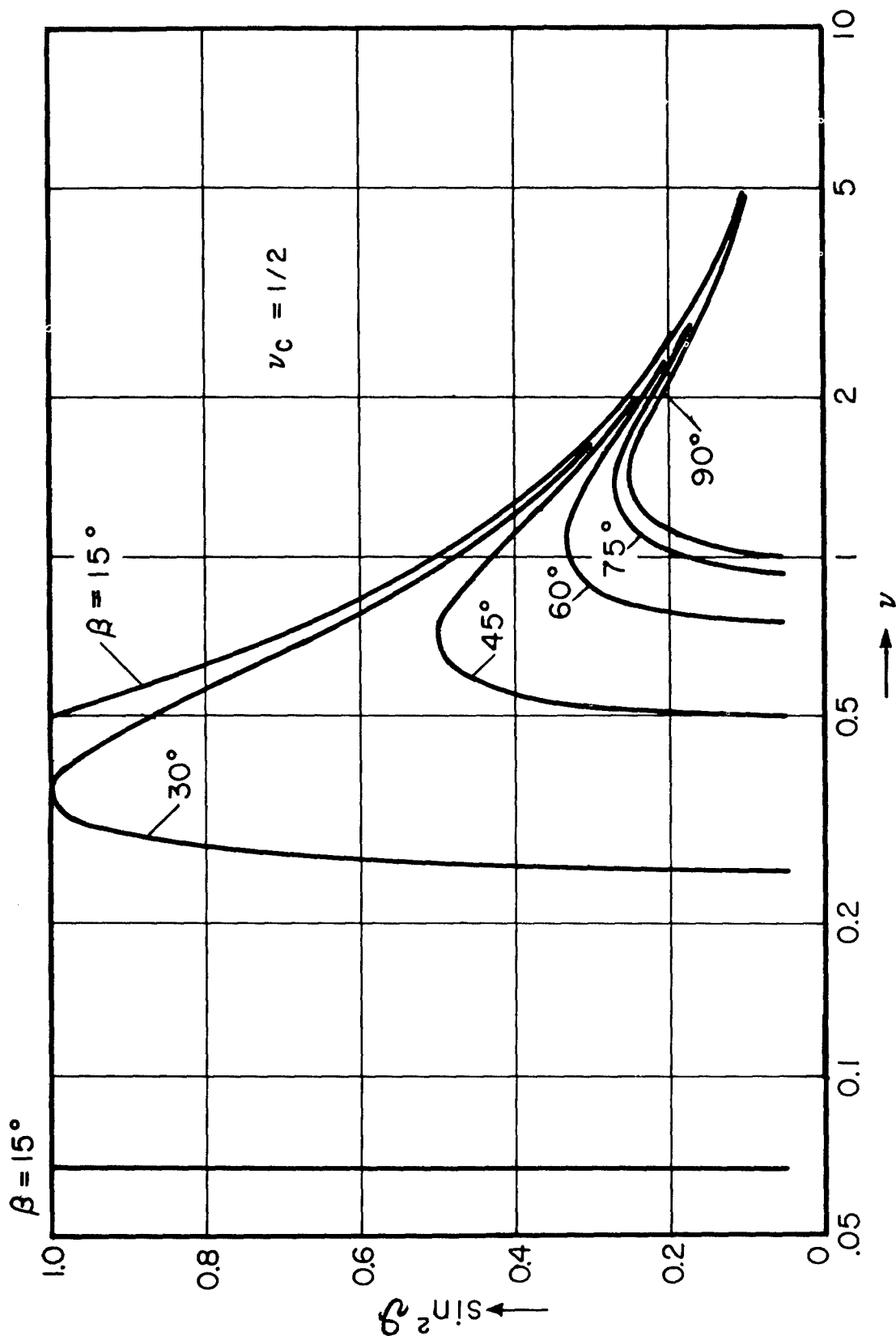$$+ 10 \log (1 + 0.71 \eta\, a_c\, \nu/\nu_c)$$

$$(11.5.13)$$

FIGURE 11.5.3

Contours of equal TL for various values of the frequency parameter $\nu = f/f_o$, $\sin^2\vartheta$ and $\nu_c = f_c/f_o = 1/2$.
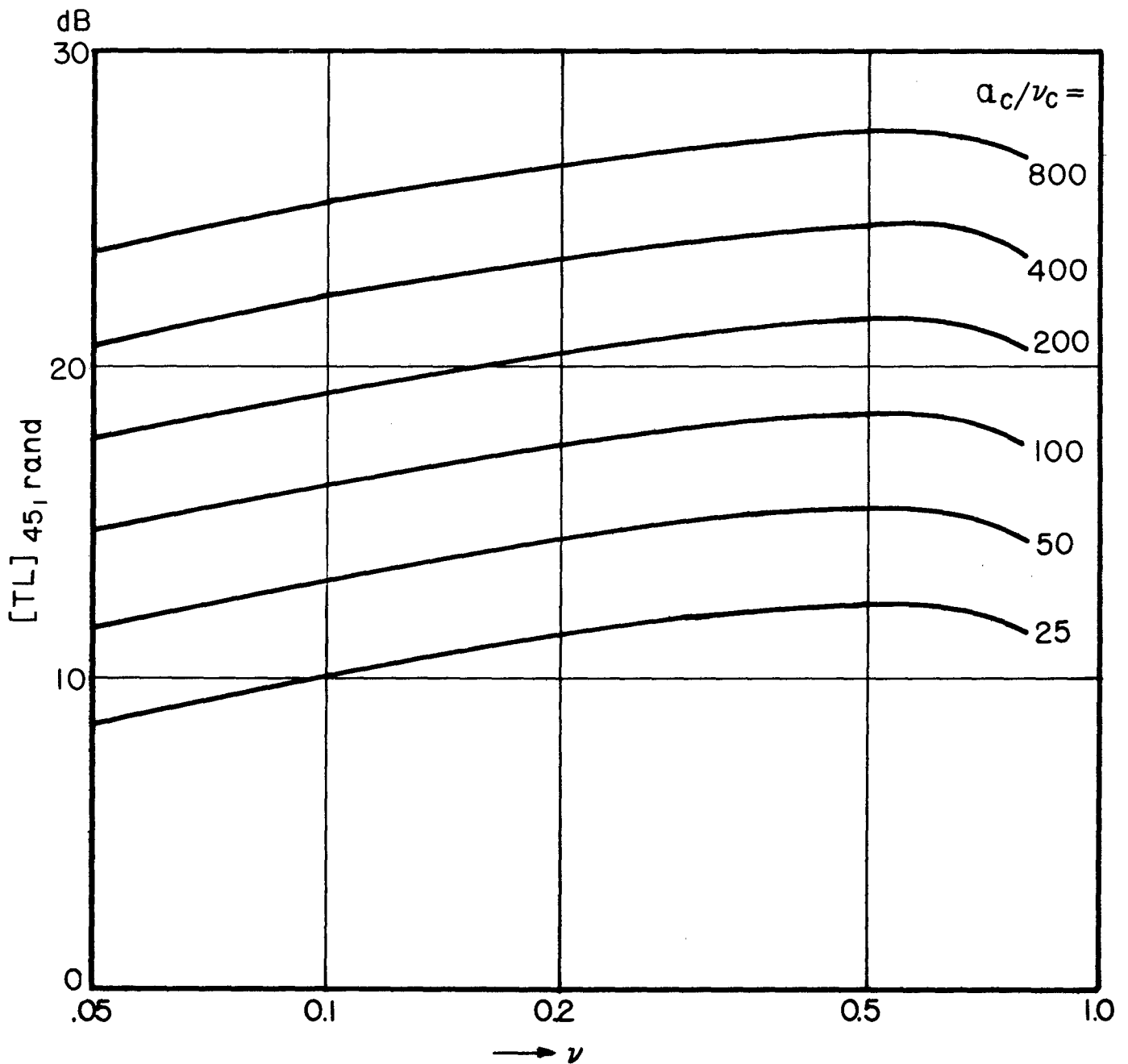
WADC TR 52-204   156

dB

$a_c/\nu_c =$

800

400

200

100

50

25

$[TL]_{45,\,rand}$

ν

FIGURE 11.5.4

The TL through a cylindrical shell for a random distribution of
angles of incidence ϕ and $\vartheta = 45°$ as a function of the frequency
parameter $\nu = f/f_o$. Several curves are plotted for various
values of the parameter α_c/ν_c.

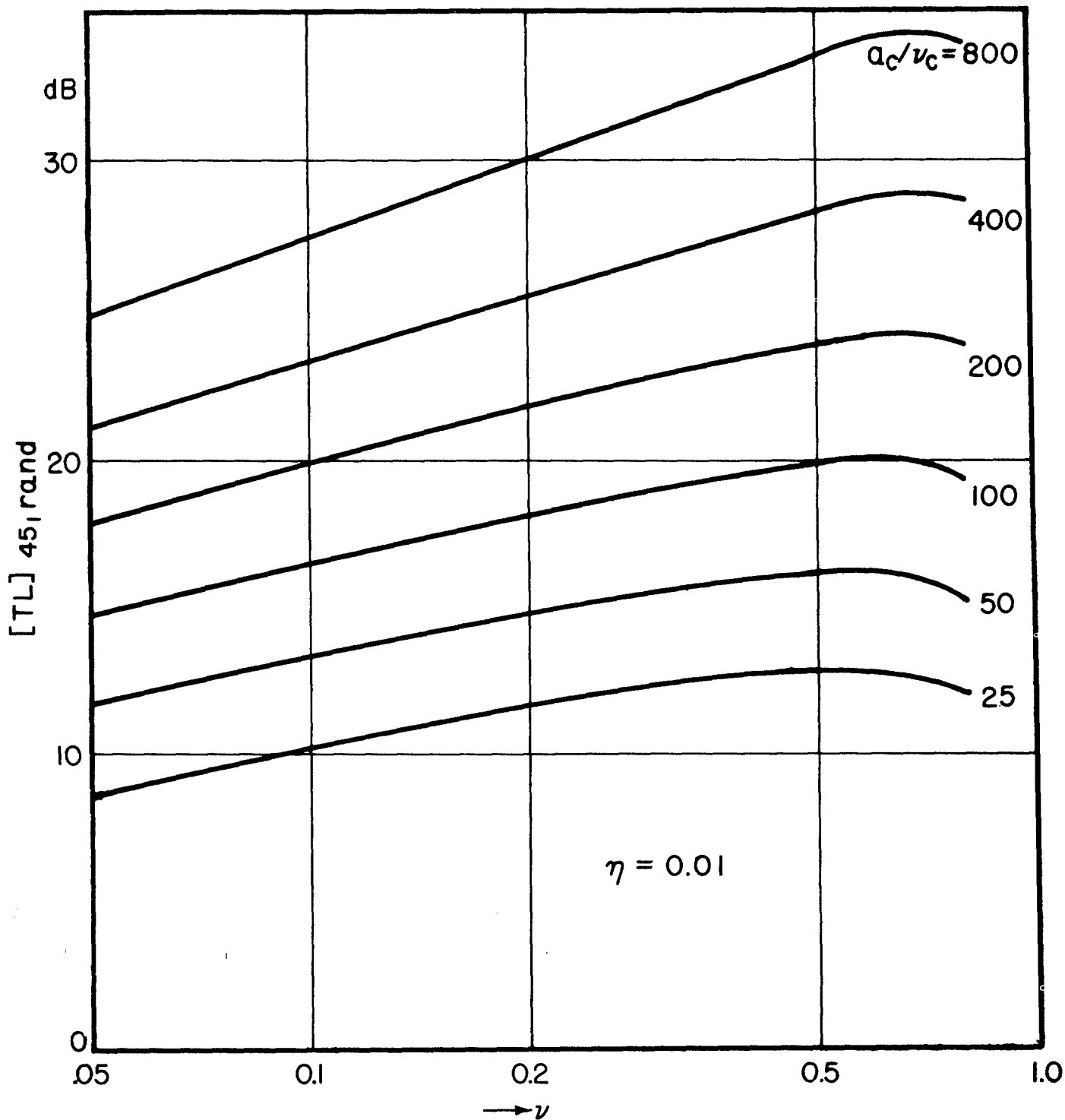**FIGURE 11.5.5**

The TL through a cylindrical shell for a random distribution of angles of incidence β and $\vartheta = 45^o$ for the case of a loss factor $\eta = 0.01$. This latter value represents a common situation, even when no damping is specifically introduced. The abscissa is the frequency parameter $\nu = f/f_o$ and the TL is given for various values of the parameter α_c / ν_c.

In Fig. 11.5.5, the corresponding values of TL are plotted as a function of ν for various values of a_c/ν_c as in Fig. 11.5.4 and for a loss factor of $\eta = 0.01$ (which may be assumed in most practical cases, even if there is no special material used for damping). For small a_c/ν_c, this amount of damping does not essentially alter the results shown in Fig. 11.5.4. For high values of $a_c\nu/\nu_c$, generally if $0.71 \quad \eta \, a_c\nu/\nu_c > 4$, we may approximate Eq. (11.5.13) by

$$[TL]_{45,random} = 20 \log \left(\frac{a_c}{\nu_c}\right) + 5 \log (\nu^3 - \nu^4) + 10 \log \eta$$

$$(11.5.14)$$

Here we see that doubling the loss factor increases the TL by 3 db. Therefore, it would be advantageous to increase the loss factor of a shell for both high and low frequencies.

12.1 Specification of Sound Absorptive Properties

In connection with certain problems in the control of airborne sound, and in the special problems of sound in rooms, the acoustical designer has to deal with the properties of sound absorbing materials. It is necessary, therefore, to describe briefly the physical principles of absorbing materials, the manner in which the physical properties and the sound absorbing properties are measured, and in a general way, some of the applications of the data which describe the materials.

In this limited discussion, it is possible to describe the significance of several of the concepts only in a qualitative way. The reader who desires a fuller knowledge of any of the topics touched on in this section should consult more extensive discussions which have been published 1.1, 1.2, 1.3, 1.4/.

The Several "Coefficients" for an Acoustical Material. The energy-absorbing ability of an acoustical material at a given frequency is most commonly specified by an "absorption coefficient". The widespread use of such a quantity suggests that this single measure is sufficient to indicate the performance of the material in all situations. However, this is not true. Detailed acoustical theory shows that the specific acoustic impedance has much wider applicability in describing the material. This quantity, in general a complex number, varies with frequency and may vary with the angle of incidence of the sound. Under special conditions some real number (a "coefficient") may describe the behavior of the material. Actually there are several different coefficients, each useful in special circumstances as a measure of energy absorption. Each is derivable from the specific acoustic impedance. Since the complex specific acoustic impedance contains two parts, it cannot, in general, be calculated from any single value of any of the coefficients.

Before discussing the energy-absorption coefficients, it will be helpful to review the behavior of a simple oscillator. A "simple oscillator" may be a mechanical system equivalent to a mass, a spring, and a damping element, an analogous simple electrical circuit or a confined volume of

air in which one of the natural sinusoidal acoustical vibra-
tions has been excited. In any case, elementary theory shows
that the energy of vibration of the simple oscillator decays
exponentially with time when the system is in free vibration
(no external driving force). Thus, if the instantaneous
energy of vibration is W, and if the initial energy of vibra-
tion is W_o, the energy at any time t follows the equation:

$$W = W_o\ e^{-2kt},\qquad (12.1.1)$$

where k is the damping constant. By differentiation of
this relation, the definition of the damping constant is ob-
tained in the form:

$$k = -\frac{1}{2}\ \frac{dW/dt}{W}\qquad (12.1.2)$$

Ordinarily a sound source in an enclosure excites
more than one mode of acoustical vibration. When a sound
source is turned off, each mode which has been excited acts
as a simple oscillator at its natural frequency. In general
each mode has a different decay rate, but it is found that
in a rectangular enclosure there exist three groups of modes,
within each of which the damping is roughly the same for all
modes. The mode groups are designated as axial, tangential,
and oblique. It will be seen later that these designations
refer to the extent to which the wave motion of a particular
mode involves tangential or oblique incidence on the various
walls.

The detailed wave theory shows that the damping rates
of the various modes can be related to quantities called
wall coefficients. The wall coefficients depend upon the
size and shape of the enclosure, the distribution of the
absorbing material, and the mode of vibration which is ex-
cited, but in certain cases the special forms of the wall
coefficients can be regarded as intrinsic properties of the
absorbing material.

The normal wall coefficient of a surface, αp, is
defined as eight times the real part of the admittance ratio
(impedance and admittance are discussed later in this section).
This quantity measures, for a wall which is not highly absorb-
ing, the damping of waves which meet the wall at normal or
oblique incidence.

The grazing wall coefficient α_t, is a measure of the amount by which a wall in a chamber of regular shape contributes to the damping of an acoustical vibration consisting of wave motion "parallel" to that wall. For a relatively nonabsorbent wall, however, there exists in place of the grazing coefficient a supplementary wall coefficient, which in the case of a rectangular enclosure, depends upon the properties of the opposite wall. These coefficients can be computed from the acoustic impedance. When both walls of a pair are not highly absorbing, both the grazing coefficient and the supplementary coefficient are nearly equal to $\alpha_p/2$. (See Ref. 1.1 for a discussion of limits of validity of these several coefficients.)

The wall coefficients above are related to the damping of the energy of an acoustical mode of vibration in an enclosure. Another set of coefficients, which will now be described, has to do with the fraction of incident power which is absorbed when a free sound wave in space strikes an absorbing surface. There is no general relation between these absorption coefficients and the wall coefficients given above, but it will be shown that under special conditions the absorption coefficients are related to the rate at which the total energy of a group of modes of vibration in an enclosure decays with time. This leads to the very restricted reverberation theory of elementary acoustics, and to the ordinary procedure of characterizing an acoustical material by an absorption coefficient as measured in a "reverberation chamber".

The basic quantity in the absorption of a single wave at a wall is the free-wave absorption coefficient, $\alpha(\theta)$ This coefficient is simply the fraction of the power in the wave, incident at an angle θ, which is absorbed by the wall. The notation indicates that the free-wave absorption coefficient is a function of the angle of incidence, θ. The concept of absorption as a function of angle of incidence (the angle between the normal to the absorbing surface and a line perpendicular to the wavefront striking the surface) is valid in practice for angles as great as $80°$. However, the concept of a free-wave absorption coefficient breaks down for larger angles of incidence, because of distortion of the wave by the absorbing boundary*.

---

* The case of $\theta = 90°$ is meaningless in any case, because a wave cannot travel absolutely parallel to a surface having absorption; the wave fronts are curved by continuous flow of energy into the surface. For this reason, quotation marks were used above in statements concerning waves traveling "parallel" to a wall.

The free-wave absorption coefficient can be obtained by a
direct measurement of the amplitudes of incident and re-
flected waves, or by techniques which depend upon the effect
of an absorbing sample at the end of a tube in which "stand-
ing waves" are set up.

The normal free-wave absorption coefficient, denoted
by α_0, is the value of the free-wave absorption coefficient
in the special case of normal incidence ($\theta = 0^\circ$). Therefore,
α_0 is the fraction of incident power which is absorbed
when a free plane wave is normally incident on the absorbing
surface.

Finally, when the power incident on the absorbing
surface is carried by an infinite number of plane waves uni-
formly distributed through all possible angles. The fraction
of the power which is absorbed is defined as the statistical
absorption coefficient α_{stat}. For reasons which will be
given, this coefficient is sometimes called the Sabine absorp-
tion coefficient, and at high frequencies this coefficient
is closely equal to the chamber absorption coefficient
ordinarily reported by the manufacturers of acoustical absorb-
ing materials. The statistical absorption coefficient is
simply a suitably averaged value of the free-wave absorption
coefficient, which may be defined by the equation:

$$\alpha_{stat} = 2\int_0^\pi \alpha(\theta)\ \cos\theta\ \sin\theta\ d\theta. \qquad (12.1.3)$$

Relation of the Statistical Coefficient to Reverberation.
W. C. Sabine, in the earliest systematic work on sound waves
in rooms, suggested on the basis of a series of experiments
that the total sound energy decays exponentially in the "rever-
beration" which occurs after the sound source is turned off 1.5/
The damping constant of the exponential decay is proportional
to the average "sound absorption coefficient" of the walls.
A mathematical analysis shows that the sound absorption
coefficient which is important in reverberation is identical
with the statistical coefficient defined above, if certain
very special conditions are realized. These conditions are,

1. Only a small fraction of the total energy is lost
in the time required for sound to travel the greatest dimen-
sion of the enclosure.

2.   The sound energy in the room is <u>diffuse</u>, so that for each wall, all directions of incidence are equally likely during the reverberation process.

3.   The energy density in the enclosure is substantially uniform, so that the transfer of energy to the walls may be considered a continuous process of absorption of a random group of free waves.

If these conditions are realized, it is readily shown that the rate of loss of sound energy is proportional to the average value, for all the wall surfaces of the statistical absorption coefficient or the <u>Sabine absorption coefficient</u>. The equation for the decay of the total sound energy is

$$W = W_o \, e^{-\frac{c \, \bar{\alpha} \, St}{4V}} \qquad\qquad (12.1.4)$$

where S is the total wall area, V is the volume of the enclosure, c is the speed of sound, and $\bar{\alpha}$ is the Sabine absorption coefficient averaged over all walls according to the relation

$$\bar{\alpha} S = (\alpha_1 S_1 + \alpha_2 S_2 + \alpha_3 S_3 + \dots\dots). \qquad (12.1.5)$$

Here S_1, S_2, S_3 . . . are areas in which the statistical absorption coefficient has uniform values α_1, α_2, α_3, . . . The quantity $\bar{\alpha} S$ is called the total absorption, and is in units of <u>Sabins</u> when its dimensions are sq ft. That is, one Sabin equals the absorption of one sq ft of perfectly absorbing surface, under the special assumptions of the Sabine picture.

By comparison of Eq. (12.1.4) with (12.1.1), the decay process can be described by an effective damping constant

$$K = c \, \bar{\alpha} \, S/8V. \qquad\qquad (12.1.6)$$

This is not really the damping constant for any single oscillator; the detailed wave theory shows that this damping constant is only an average of slightly differing values for all the individual modes of vibration, even when the very special assumptions behind Eq. (12.1.4) are justified.

WADC TR 52-204   165

The customary way of stating the result of the simple reverberation theory is in terms of the reverberation time T, which is defined as the time required for the total sound energy to decrease to 10^{-6} (one millionth) of its original value. In units of feet and seconds, the reverberation time formula as obtained from Eq. (12.1.4) is

$$T = 0.049 \ V/\bar{\alpha} S. \qquad (12.1.7)$$

A somewhat different form of the reverberation formula, due to C. F. Eyring, has proved to be more satisfactory than (12.1.4) in cases where $\bar{\alpha}$ is larger than one tenth. The conditions assumed in Eyring's derivation are the same three already stated, except that now the sound energy is imagined to exist in discrete wave trains. The energy in a wave train remains constant as the train travels a mean path $4V/S$ between reflections, and decreases discontinuously at each reflection. Since a fraction $(1 - \bar{\alpha})$ of the energy is reflected in each encounter and the average time between reflections is $4V/cS$, the intensity at a time t is proportional to $(1 - \bar{\alpha}) \ Sct/4V$. This relation can be written in the form of an exponential function as in Eq. (12.1.1), or the result can be written as a reverberation time formula as shown in Eq. (12.1.8) with units of feet and seconds.

$$T = 0.049 \ V/[-S \ \ln(1 - \bar{\alpha})] \qquad (12.1.8)$$

The average absorption coefficient is defined, as before, by (12.1.5). Equation (12.1.8), although sometimes seriously in error when the absorption coefficient varies greatly between different wall areas, is the basis for most practical calculations for sound decay in rooms. Equations (12.1.7) and (12.1.8) give essentially identical results when $\bar{\alpha}$ is less than 0.1.

Reverberation Chamber Measurement of Absorption Coefficient. Equation (12.1.7) or (12.1.8)* is commonly used to derive values of the absorption coefficient from the experimentally measured reverberation time in a specially designed

---

* The two equations give the same result for the values of $\bar{\alpha}$ ordinarily used in these measurements.

room known as a reverberation chamber. Typically, a rever-
beration chamber is an enclosure of 10,000 to 20,000 cu ft
volume and with walls of very small absorption so that the
reverberation time is long (preferably greater than 10 sec
when no absorbent sample is present). Measurements of the
reverberation time with and without a sample of absorbing
material in the chamber give sufficient data to determine
both the effective absorption due to the walls and the en-
closed air, and that absorption due specifically to the
sample. Since the finite patch of absorbing material which
is used as a sample has more absorption per unit area than
would a complete wall covering (because of diffraction effects),
suitable empirical corrections are used to derive effective
values of the absorption coefficient for a large area. Fur-
ther references to the measurement method are given in Ref.1.2.

The absorption coefficient derived from these measure-
ments is, by definition, the chamber absorption coefficient.
Details of the testing procedure must be stated in order to
specify a chamber coefficient completely. Various artifices
are used in reverberation chambers to produce random direc-
tions of sound travel (i.e., a diffuse sound field), with the
aim of producing conditions which will allow the chamber co-
efficient to be identified with the statistical absorption
coefficient. It is impossible, however, to obtain a diffuse
sound field in the required sense unless the smallest chamber
dimension is many times a wavelength. For this reason it
appears that the chamber coefficients which are commonly
reported are a close approximation to the statistical coeffi-
cient only for frequencies of 2,000 cps and higher. The
chamber coefficient at lower frequencies becomes more nearly
equal to the normal wall coefficient, α_p, which governs the
decay of most of the acoustic modes of vibration in a room
where the largest dimension is only a few times the wave-
length.

It appears that the departure from diffuse conditions
in the reverberation chamber at the lower frequencies is
responsible for a disagreement between calculated and measured
values of the low-frequency reverberation time for large
auditoria or other enclosures of several hundred thousand cu
ft volume, when the chamber coefficient is used for calcula-
tions by means of Eq. (12.1.8). The sound field in a large
auditorium or other large room of irregular shape approaches
the diffuse condition at all audio frequencies. The observed
reverberation time is longer than that calculated on the basis

of the chamber coefficient. This is because the chamber coefficient approaches α_p at low frequencies, and α_p is generally larger than the quantity α_{stat} which should be used in Eq. (12.1.8) for diffuse sound fields.

Table 12.1.1 shows a comparison of the statistical coefficient and the chamber coefficient for one particular absorbing material. The effects just mentioned are apparent. The statistical coefficient was calculated from acoustic impedance data. The chamber coefficient is the result of measurements of the same sort as those reported by the Acoustical Materials Association 1.6/. This organization publishes sound absorption data for commercial materials, as measured by a carefully standardized reverberation chamber technique. The large discrepancy at 512 cps is found in other data comparisons and is probably a systematic effect in the chamber measurements.

TABLE 12.1.1

COMPARISON OF STATISTICAL ABSORPTION

COEFFICIENTS AND AMA CHAMBER COEFFICIENTS
(material: 10.5 lb/ft^3 PF Fiberglas, 4"
thick, hard backing)

Frequency cps	Statistical Coefficient α_{stat}	AMA Chamber Coefficient
128	0.53	0.66
256	0.69	0.69
512	0.78	0.99
1024	0.82	0.88
2048	0.90	0.90
4096	0.93	0.93

Comparison of Statistical Coefficient and Wall Coefficients. The statistical absorption coefficient applies to problems of sound absorption only where a diffuse sound field exists. In this special case Eqs. (12.1.7) or (12.1.8) may be used to compute the reverberation time. These equations infer that the absorption coefficient of the acoustical material at a given frequency is independent of the shape of the room, of the position of the material, and of the sound source in the room.

The detailed theory of wave acoustics, which has been worked out for enclosures of simple shape, shows that in general the acoustical damping produced by absorbing material in a room depends upon the material, the shape of the room, the position of the material in the room, and which modes of acoustical vibration in the enclosure are excited by the sound source. The Sabine assumptions represent only a special limiting case, which can be approached when the enclosure (or the arrangement of absorbing patches within the enclosure) is irregular, and when the wavelength is very small compared to the shortest dimension of the enclosure. Also, the general wave theory indicates that, because the damping constants differ for the various groups of vibrational modes, the decay of the total acoustical energy in the enclosure is not a single exponential function, and the reverberation phenomenon cannot be described adequately by a single reverberation time except under the special Sabine conditions.

The distinction between the two approaches may be illustrated for the case of a rectangular enclosure. Let the dimensions of the enclosure along the x, y, and z axes be L_x, L_y, and L_z. According to wave theory, the frequencies of free acoustical vibration of the enclosure are given approximately by

$$f(n_x, n_y, n_z) = (c/2) \sqrt{(n_x/L_x)^2 \ (n_y/L_y)^2 \ (n_z/L_z)^2}$$

$$(12.1.9)$$

where each n may be equal to any integer (including zero). The value of n_x is equal to the number of pressure maxima between the walls $x = 0$ and $x = L_x$ in the wave pattern of the vibration; for $n_x = 0$, the pressure is nearly uniform in the x direction. The other n's have corresponding interpretations.

Oblique waves correspond to the case of none of the n's equal to zero. Tangential waves correspond to one n equal to zero; for example, for $n_x = 0$, the wave motion is tangential (grazing) with respect to the x walls (the walls at $x = 0$, $x = L_x$). Axial waves correspond to two n's equal to zero; for example, for $n_x = 0$, $n_y = 0$, the wave motion is grazing with respect to both x and y walls.

The damping of any one vibration in the rectangular enclosure, according to wave theory, is computed by using in Eq. (12.1.6), in place of the Sabine absorption αS, the room absorption factor, a_N, defined by Eq. (12.1.10). It is assumed that each wall has uniform acoustical properties.

$$a_N = L_y L_z (\alpha_{x1} + \alpha_{x2}) + L_x L_z (\alpha_{y1} + \alpha_{y2}) + L_x L_y (\alpha_{z1} + \alpha_{z2})$$

$$(12.1.10)$$

The α's are the wall coefficients. Subscripts x1, x2 refer to the walls at $x = 0$ and $x = L_x$ respectively, and so forth. While considerable calculation may be required to find the α's from acoustic impedance data for the walls, simple approximations hold when the walls are "hard".* For a room with hard walls, each α for a wall where the wave motion is obliquely incident is approximately equal to the normal wall coefficient α_p, and each α for a wall subject to grazing incidence is equal to the grazing wall coefficient, which in this case is approximately $\alpha_p/2$.

For a numerical example, consider an enclosure having dimensions L_x, L_y, L_z equal respectively to 10,15, and 20 ft, with a freely decaying acoustical vibration in the mode $n_x = 0$, $n_y = 1$, $n_z = 1$. According to Eq.(12.1.9), the frequency of this vibration is approximately 46 cps (using c = 1100 ft/sec).

----

* A "hard" wall is one for which the specific impedance ratio is greater than twice the length of the room in wavelengths, measured perpendicular to that wall; all ordinary acoustical tiles on massive backings may be considered hard below 200 cps in rooms not larger than 20' in any direction.

Let the normal absorption coefficient for each wall be 0.05 at this frequency. The α's in Eq. (12.1.10) are then each equal to 0.05 except that grazing incidence occurs on both of the 10 x 15 ft walls, and the α value for each of these is therefore 0.025. The room absorption factor a_N from Eq. (12.1.10) is 50 ft^2. This value can be used in place of $\bar{\alpha}$ S in Eq. (12.1.6) to obtain the damping constant. The value of the Sabine quantity of $\bar{\alpha}$ S is 65 ft^2; hence appreciably greater damping would be realized under the Sabine conditions than for the case considered here, in which the (0,1,1) mode is excited. The discrepancy is more severe if only the 15 x 20 ft ceiling is absorptive; then a_N is 7.5 ft^2 and $\bar{\alpha}$ S (the Sabine factor) is 15 ft^2. In the hard wall approximation, there is no disagreement between the wave theory and the diffuse-room reverberation formula for oblique modes. Thus, in practice the oblique modes decay most rapidly, at roughly the rate given by the Sabine relation, and leave the axial and tangential vibrations dying out at slower rates. This effect is especially pronounced when all the absorbing material is on one surface.

When the hard-wall approximation is not introduced, the complete wave theory indicates further effects of the position of the material and the nature of the excited modes upon the damping. For example, the effects of opposite walls are not necessarily additive. The presence of a soft wall may result in a concentration of the acoustical energy in the end of the room near that wall. This in turn increases the effectiveness of the soft wall as a sound absorber, so that the normal wall coefficient for a soft wall may be greater than unity.

The Specific Acoustic Impedance and Related Quantities. A measure of the acoustical properties of a surface which has more general application than any of the "coefficients" is the normal specific acoustic impedance. This quantity is defined by the relation

$$z = r + jx = p/v, \qquad (12.1.11)$$

where p is the acoustic pressure at the surface, and v is the resulting velocity component normal to the surface of air particles just in front of the surface. Ordinarily p is in dynes/cm^2 and v in cm/sec. The resulting unit for z is called a rayl. The acoustic pressure is the sum of the instantaneous pressure produced by an incident acoustic wave and of the

instantaneous pressure of any reflected wave which
may be set up.

The normal specific acoustic impedance is independent
of the angle of incidence of the sound if there is no effec-
tive wave propagation behind the surface in a direction
parallel to the surface. This requirement means that such
wave motion must be highly attenuated or have a velocity
much smaller than the velocity of sound in air; this is the
condition of "local reaction" discussed in Sec. 12.2. It
has also been shown experimentally that z is practically
independent of the incident angle for materials representa-
tive of commercial acoustic tiles 1.7/.

The impedance is usually a complex number. The complex
representation, which has meaning only for sinusoidal signals,
has the same significance as that used in alternating current
theory. Thus, the real part of z is the ratio to v of the
component of p which is in phase with v, while the imaginary
part of z is the ratio to v of the portion of p which is 90°
out of phase with v. The real and imaginary parts of z, r
and x, are respectively the normal specific acoustic resis-
tance and the normal specific acoustic reactance. The adjec-
tive "normal" will be omitted except where there is a possi-
bility of confusion with some impedance not concerned with
the normal component of particle velocity.

The specific acoustic impedance for a perfect absorber
of plane waves (or for an infinite body of air, which is
effectively a perfect absorber) is ρc, where ρ is the density
of air (Fig. 3.1) and c is the speed of sound. It is often
convenient to express z in units of ρc. The dimensionless
quantity obtained in this way is called the specific acoustic
impedance ratio denoted by

$$\zeta = \frac{z}{\rho c} \equiv \theta + j \chi .$$

The reciprocal of the specific acoustic impedance is
the specific acoustic admittance, y. The reciprocal of the
specific acoustic impedance ratio is the specific acoustic
admittance ratio, $\eta \equiv 1/\zeta \equiv \mu + jk$. The quantity μ is the
specific acoustic conductance ratio, and k is the specific
acoustic susceptance ratio.

Several methods for the measurement of the specific acoustic impedance are described in the literature 1.2/. All the methods have to do, in a general way, with measuring various aspects of the system of incident and reflected waves which is set up when an acoustic wave is incident on the test surface, either in open space or in an enclosure. Ordinarily acoustic impedance measurements are made on samples not larger than one sq ft; usually the samples are much smaller, particularly if measurements in a standing-wave tube are to be made to several thousand cps.

Because of the limitations on sample size, an averaging problem arises in connection with materials having large-scale variations in structure. Also, with small samples it is difficult to reproduce any kind of backing other than that of an effectively rigid wall. In the techniques most commonly used, the sample is cut to fit snugly within the end of a containing tube. It has been shown that materials having a very light skeleton (not heavier than about 2 lb/ft3) must be treated with great caution in tube mountings, because the clamping effect of the walls hinders the ordinarily appreciable motion of the skeleton in response to the sound wave and seriously changes the impedance. When the above difficulties are not important, impedance measurements can be made with laboratory apparatus to within 3 per cent on acoustic tiles and blankets. The angle of incidence is 0° in most impedance measurements.

Relation Between Impedance and Absorption Coefficients. For surfaces which can be characterized by a normal impedance independent of angle of incidence (this includes ordinary acoustical tiles and blankets with hard backing), the relation between impedance and free-wave absorption coefficient is simple. This relation can be derived by setting up expressions for incident and reflected waves, and imposing the condition that the phase and amplitude relations between the waves shall be such that the relation between total pressure at the surface and the normal particle velocity is just that corresponding to the specific acoustic impedance. It is then possible to compute the difference of intensity of the incident and reflected waves, and to obtain the absorption coefficient, which is the fractional loss of intensity. In this way, it is found that the free-wave absorption coefficient, where the angle of incidence as measured from the normal is θ,

$$\alpha(\theta) = \frac{4\mu \cos \theta}{k^2 + (\mu + \cos \theta)^2} , \qquad\qquad (12.1.12)$$

where μ and k are the real and imaginary parts of the specific acoustic admittance ratio. For a wall having an acoustic impedance several times ρc, so that $|\mu + jk| \ll 1$, it follows from this relation that the normal free-wave absorption coefficient ($\theta = 0^\circ$) is simply equal to 4μ.

The method for computing the statistical (Sabine) absorption coefficient from $\alpha(\theta)$ has been shown in Eq. (12.1.3). When the indicated averaging process is applied to (12.1.12), it is found that the statistical coefficient is given by:

$$\alpha_{stat} = 8\mu \left\{ 1 - \mu \ln[1 + \frac{2\mu + 1}{|\eta|^2}] + [\frac{\mu^2 - k^2}{k}] \tan^{-1}[\frac{k}{|\eta|^2 + \mu}] \right\}$$

This relation is derived for the case in which η is independent of angle of incidence. Figure 12.1.1 is derived from this equation but it reads in terms of impedance rather than admittance. When values of the real and imaginary parts of the specific impedance ratio are available, this chart gives the statistical coefficient directly. Note that a surface must have a resistive impedance of almost 1.6 ρc to give a statistical absorption coefficient of 0.951, which is the largest possible value, whereas the impedance must be ρc to give the normal free-wave coefficient, (0°), its largest possible value (unity). This difference represents an averaged effect of the variation of $\alpha(\theta)$ with angle of incidence.

FIGURE 12.1.1

The statistical absorption coefficient, α_{stat} in terms of the real and imaginary parts of the normal specific acoustic impedance ratio . It is assumed that the normal impedance is independent of angle of incidence.

$$X/\rho c$$

$$R/\rho c$$
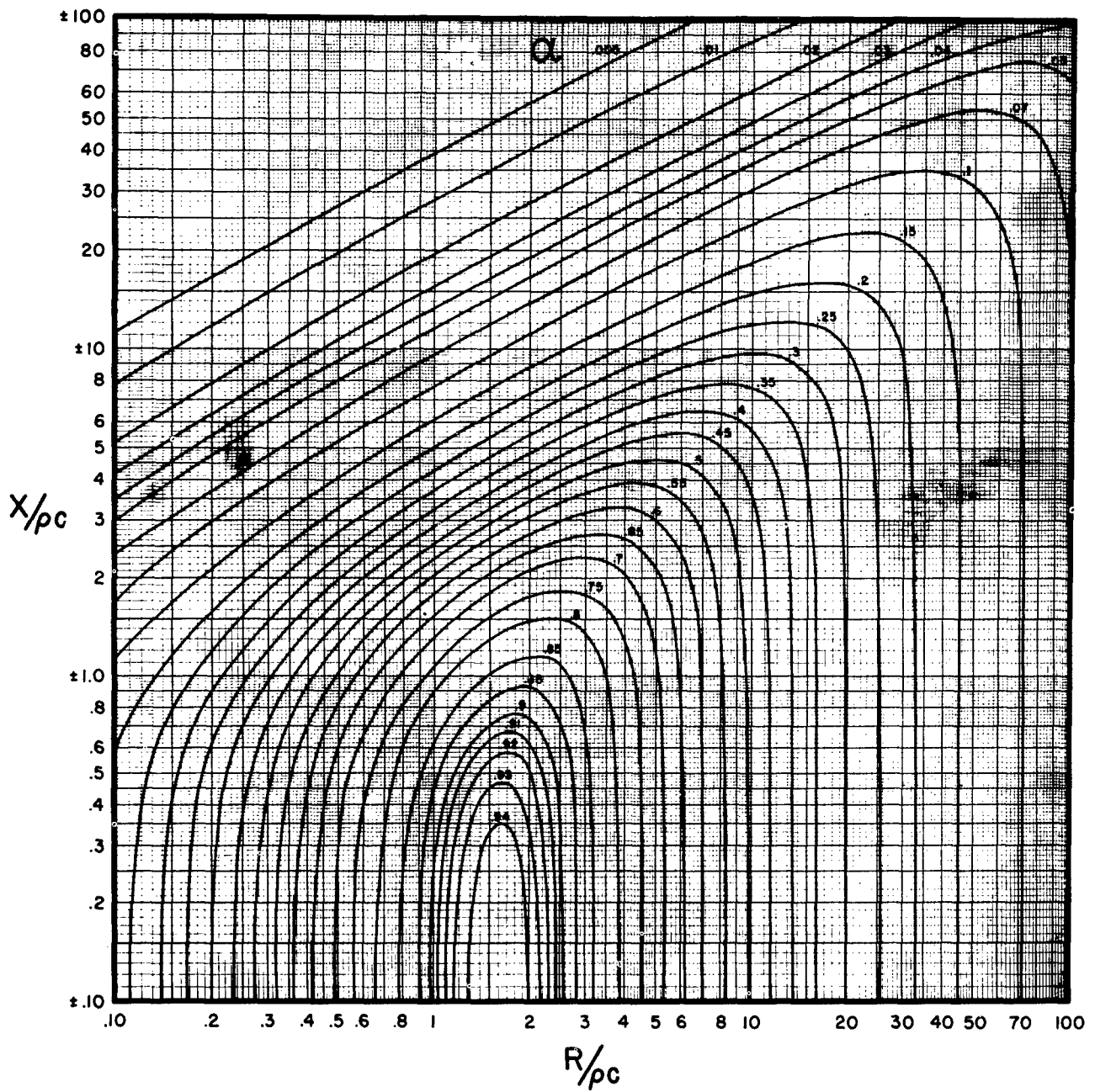
<u>Behavior of Acoustical Materials in Terms of Their</u>
<u>Physical Structure</u>. While the normal specific impedance
is a quantity of wider applicability than any of the coeffi-
cients, the physical structure parameters of the material
sometimes have even wider applicability than the specific
impedance. For materials whose acoustic behavior is readily
subject to analysis, a knowledge of several structural
parameters permits the calculation of the impedance for any
thickness of material, subject to a variety of backing condi-
tions, and for any angle of incidence, even when the
impedance varies with angle. Since the structure parameters
can be measured simply, we can determine the acoustical
behavior of a material with a minimum of experimental effort.
Moreover, working from the basic physical properties of
material sometimes makes it possible to derive much more
useful design equations or charts, showing the complete
frequency behavior of a sound-reducing structure in terms
of a few simple quantities. An example of this is found in
Sec. 12.2, in the discussion of a duct lined with a porous
material.

Considerable published material is available for the
calculation of acoustical properties from structural con-
stants <u>1.1, 1.2, 1.3, 1.8, 1.9</u>/ The present discussion will
be restricted to the simple case of an isotropic porous
material with a rigid skeleton and mounted on a rigid backing.
It will appear that the important parameters are the porosity
(the fraction of the total volume which is occupied by air),
the structure factor (related to the increased effective
inertia of air which is accelerated in small passages), and
the flow resistance.

The porosity can be obtained from an experiment which
involves finding the apparent compressibility of the air
in the sample. Because the solid is virtually imcompressible,
the specimen acts like a volume of air in which the modulus
of compression is $1/h$ times the true compressional modulus
of air, where h is the porosity. For practical materials,
h is at least 0.7 and is usually not less than 0.9. The
flow resistance of a sample is obtained by direct measure-
ment of the pressure drop across the sample when air is
forced at a known, steady rate through a slab of known area
and thickness. The result is usually reduced to the specific
flow resistance (r_f) (rayls per cm thickness). This is
numerically equal to the pressure drop associated with an
air flow of one cm3/sec through a sample of area one sq cm

and thickness one cm (sometimes specific flow resistance
is reported in rayls per inch of thickness). The structure
factor, the exact definition of which can be obtained from
Eq. (12.1.15), must be found from an experimental measure-
ment of impedance or of propagation constant in the material.
This does not discourage the use of this approach because
(1) the structure factor ordinarily does not vary rapidly
with frequency, so that extensive measurements are unneces-
sary; (2) it is not necessary to know the structure factor
in order to compute the impedance of a rigidly backed layer
which is thin compared to a wavelength.

The theory of the absorbing layer gives the surface
impedance in terms of the propagation constant, the char-
acteristic impedance for waves traveling in the layer, and
the thickness. The case of perpendicular incidence will be
considered here, since it is an experimental fact that the
result is substantially independent of angle for most porous
layers. Suppose that a sinusoidal pressure variation at the
surface of the porous layer sets up plane waves in the layer,
traveling normally to the surface. The pressure in the wave
entering the material is proportional to $\exp(-jk_1 x)$, where
distance is measured from the surface into the layer, and
k_1 is the propagation constant which is to be found. The
layer thickness is t. At the backing $(x = t)$ a reflected
wave is set up. The ratio of the pressure in the reflected
wave to that in the incident wave, at $x = t$, is defined as
$\exp(2\psi)$. Then the reflected wave must have pressure pro-
portional to $\exp(2\psi + jk_1 x - j2k_1 t)$. It is desired to
find the specific surface impedance, which is the ratio of
pressure to particle velocity at $x = 0$. The total pressure
at $x = 0$ is proportional to $1 + \exp(2\psi - j2k_1 t)$. The
particle velocity at the surface due to either wave is equal
to the pressure divided by Z_1, which is the characteristic
impedance of the layer material (analogous to the quantity
ρc for open air). Since the waves are oppositely directed,
the particle velocities must be subtracted, and the total
surface particle velocity is proportional to $[1 - \exp
(2\psi - j2k_1 t)]/Z_1$. Dividing the pressure by the particle
velocity gives for the surface specific impedance

$$z = Z_1 \coth(jk_1 t - \psi) \qquad (12.1.14)$$

The value of ψ depends upon the reflectivity of the backing. For a rigid backing, complete reflection occurs with no pressure phase shift, so that ψ is zero and the specific surface impedance is

$$z = Z_1 \coth (jk_1 t) \; . \qquad (12.1.14a)$$

(Rigidly backed layer)

If the layer is thin enough that $k_1 t << 1$,

$$z \simeq - j(Z_1/k_1 t) \left[1 + \frac{j}{3} (k_1 t)^2\right] \; . \qquad (12.1.14b)$$

(Rigidly backed layer thin compared
to wavelength)

The negative of the imaginary part of k_1 is the attenuation constant $1/8.69$) times the attenuation in db per unit distance) for wave motion in the layer. For $-\text{Im}(k_1) > 1/t$, a condition which will be realized at high frequencies, the total attenuation is sufficiently large that the effect of the reflected wave may be neglected. Roughly speaking, this condition occurs when the thickness of a practical porous material is greater than $\lambda/4$. For this case, the surface impedance is

$$z \simeq Z_1 \qquad (12.1.14c)$$

(Thick layer, any backing)

The propagation constant and the characteristic impedance will now be related to the structure parameters of the porous layer. It is assumed that motion of the skeleton can be neglected, which in practice seems to require porous materials having a density of 6 lb/ft^3 or more. A sinusoidal wave in the layer with pressure proportional to $\exp (j\omega t - jk_1 x)$ is assumed. The volume velocity* per unit area, which at the surface is equal to the ordinary particle velocity in the outside air, is v_1. The negative of the pressure gradient is $jk_1 p$. A portion of the pressure drop in a thin volume element, as described by this quantity, is associated with

---

* The volume velocity is the rate of volume flow (e.g., cm^3/sec).

the acceleration $j\omega v_1$ of the volume flow in the element, and another portion with overcoming the frictional resistance to air flow, as indicated in Eq. (12.1.15).

$$jk_1 p = jm\rho\omega v_1 + r_f v_1 \quad . \qquad (12.1.15)$$

Note that this equation effectively defines the structure factor, m. The rate of change of volume is related to the rate of pressure change by the effective modulus of compression of the gas. The adiabatic modulus of free air is ρc^2, but on account of the solid content present, the effective modulus is $\rho c^2/h$ in the adiabatic case, or $\rho c^2/h$ in the event that the compression is isothermal. Here γ is the ratio of the specific heat at constant pressure to the specific heat at constant volume, which for air is equal to 1.40. Thus:

$$jk_1 \rho c^2 v_1/h \ (\gamma) = j\omega p \quad . \qquad (12.1.16)$$

(γ to be omitted for the adiabatic case)

Combining Eqs. (12.1.15) and (12.1.16) gives for the propagation constant,

$$k_1 = k\sqrt{h(m - j\,r_f/\rho\omega)\ (\gamma)} \qquad (12.1.17)$$

(γ to be omitted for the adiabatic case)

where k denotes the propagation constant for open air, equal to ω/c. To obtain the characteristic impedance, which is the ratio of pressure to volume velocity in a plane wave, Eq. (12.1.16) may be used. This gives $Z_1 = k_1 \rho c^2/(\gamma)h\omega$, or:

$$Z_1 = \rho c \sqrt{(m - jr_f/\rho\omega)/h\ (\gamma)} \qquad (12.1.18)$$

(γ to be omitted for the adiabatic case).

The specific acoustic impedance of the rigidly backed layer can now be calculated by going back to Eqs. (12.1.14), and the statistical absorption coefficient can be calculated from the impedance. Where the layer is thin compared to the wavelength, so that Eq. (12.1.14b) applies, a particularly simple result is obtained. The surface specific impedance then is:

$$z - \frac{1}{3} r_f t - j \frac{\rho c^2}{(\gamma)\omega th} \qquad (12.1.19)$$

(γ to be omitted for adiabatic case)

Thus, the thin layer behaves like a resistance added to the reactance of a stiffness element, the latter representing simply the stiffness of air in the layer. The equation agrees reasonably with the experimental behavior of mineral wool or glass wool tiles under the isothermal assumption, whereas conditions are more nearly adiabatic, even at the low frequencies, in materials having larger pores. Further applications of the theory are made in Sec. 12.2 in the discussion of lined ducts.

The theory is considerably more complicated when the skeleton cannot be considered rigid. Beranek 1.8/, however, has developed computation charts for a "soft blanket" in which the skeleton rigidity can be neglected completely. Certain special cases where the skeleton has finite rigidity are described by Zwikker and Kosten 1.3/.

Perforated Facings for Acoustical Materials. By suitable selection of a perforated facing for an absorbing material, the designer can either insure that the facing does not materially alter the performance of the material, or bring about a greatly increased sound absorption in a selected frequency range, sometimes at the expense of absorption at other frequencies. Two cases which have appeared in the literature will be reviewed. In the first case, the perforated facing lies directly against an acoustical material which is described only in terms of a normal impedance, independent of angle 1.10/. In the second case, the perforated facing is separated from a rigid backing by an air layer, and the absorbing material, which is described only in terms of its flow resistance is either a thin cloth in contact with the facing, or a highly porous substance 1.11/. It is necessary to consider separately the effect of an air space with cellular partitioning and the effect of an unpartitioned space, since the latter arrangement makes the impedance dependent on angle of incidence.

For the first case, in which the facing lies directly against a layer of given angle-independent impedance, the symbols below are used:

$R_B + jX_B$ normal specific acoustic impedance of
                                   absorbing layer

n   number of holes per sq ft

d   diameter of hole in inches

t   thickness of facing in inches

σ weight of perforated facing in lb/ft^2

f   frequency in cps

Where the holes are non-circular with area S per hole, the results will apply approximately if d is taken to be $\sqrt{4S/\pi}$. Application of the theory to slit perforations will also be described. The analysis considers only the effects of adding to the impedance of the acoustical material the mass-like reactance of the facing. The mass-like facing reactance is a combined effect of the surface mass (which is counted only if the facing is a flexible material) and the air mass in the holes. The air mass is computed by relations which are valid only if the wavelength of the incident sound is greater than the hole circumference, and also if the spacing of the holes is not less than two hole diameters. These considerations require

$$d < 4000/f$$
$$d < 6/\sqrt{n} \ .$$

Since the flow resistance of the holes is neglected, the following condition must also be observed:

$$d < 0.01 \ t \sqrt{f}/nd^2$$

This condition insures that the hole resistance is less than $0.2\rho c$, so that its effect is negligible under ordinary conditions.

The moving mass of air associated with a hole of radius a in a plate of thickness b is 1.11/:

$$M_h \simeq \rho \ (\pi a^2 b + 16 \ a^3/3), \qquad\qquad (12.1.20)$$

where ρ is the density of air. The specific reactance of one hole is $M_h \ \omega/\pi a^2$, and multiplying by the ratio of total

facing area to hole area gives the specific reactance for the facing as a whole, which is $M_h \, \omega/n(\pi a^2)^2$. The additional specific reactance $M\omega$, where M is mass per unit area in the case of flexible facing material, is in parallel with the previous reactance. Finally, in the engineering units originally defined, the specific impedance ratio of the facing is:

$$\xi_f = j \, \frac{X_f}{\rho c} \simeq j(0.072)M \, f$$

$$M = \frac{k}{1 + \frac{K}{\sigma}}$$

$$K = (1 + 1.18 \, t/d)/nd$$

$$(12.1.21)$$

These equations are represented in the left upper, right upper, and right center sections of the design chart in Fig. 12.1.2 which is taken from Ref. (1.10). For a further discussion of the charts and equations, see Ref. (1.10). The lower two sections of the chart give the normal wall coefficient α_p and the statistical absorption coefficient α_{stat} for the structure as a whole, when the values R_B and X_B for the absorbing layer are known. The chart for the normal wall coefficient is obtained from the relation

$$\alpha_p = 8 \gamma = 8(R/\rho c/[(R/\rho c)^2 + (X/\rho c)^2],$$

while the chart for the statistical absorption coefficient is obtained from Eq. (12.1.13). The left center section

FIGURE 12.1.2

Design chart for perforated facings, to give transmission loss for isolated facing, or to give statistical absorption coefficient when facing is used with an acoustical material of known impedance. Ref. (1.10).

$\sigma = .01 \quad .02 \ .03 \ .05 \ .07 \ .1 \quad .2 \ .3 \ .5 \ .7 \ 1 \ 2 \ 3 \ 5 \ 10$

(K)

n = number of holes/sq.ft.
d = diameter of holes
t = thickness of facing } inches

σ = weight of facing material
(K) = effective mass of holes
(M) = effective mass of perforated facing } lb./sq.ft.

nd

(M)

TL–DB

TL = Transmission loss through panel with ρc backing impedance

TL

ν = frequency
$\dfrac{X}{\rho c}$ = reactance of perforated facing

$\dfrac{X}{\rho c}$

$\dfrac{R_B}{\rho c} + j\dfrac{X_B}{\rho c}$ = Impedance of backing material

STATISTICAL ABSORPTION COEFFICIENT

$R_B/\rho c$

NORMAL COEFFICIENT

$\dfrac{X_T}{\rho c}$

$\alpha_p = .60$

$R_B/\rho c$

Frequency cycles per second

Statistical Absorption Coefficient (α_{stat})

shows in addition the transmission loss for the perforated facing alone, on the basis of ρc impedances on both sides. The transmission loss chart represents the mass law discussed in Chap. 11.

The use of Fig. 12.1.2 is as follows: Given a facing specified by n, d, t, and σ, enter upper left graph with nd on the abscissa, move up to specified value of t/d, move right (crossing K value) to specified value of σ, move down (crossing M value) to desired frequency, move left to read $X/\rho c$ (facing reactance).

To obtain transmission loss read left from $X/\rho c$ to heavy line marked TL, and find value on upper scale of (left center) section of chart.

To obtain absorptivity read left from $X/\rho c$ to curve for given value of $X_B/\rho c$, move down, crossing $X_T/\rho c$ which is total reactance of facing and backing material, to (one of the two) heavy slant lines and read on right scale of (left lower) section the total reactance magnitude $|X_T|/\rho c$ of facing and backing; move left or right to given value of $R_B/\rho c$ as marked along lower scales and read α_{stat} (left lower section or α_p (right lower section) from curves.

The charts of Fig. 12.1.2 also apply approximately in the case where the perforations consist of a series of long narrow slots, each slot of width d inches, and the on-center spacing of the slots equal to s inches. To use the charts in this case, replace nd by 183/s.

An example of the effects of the perforated facing is shown by the calculations plotted in Fig. 12.1.3, where several different facings as listed in Table 12.1.2 have been used. The assumed impedance characteristic for the

FIGURE 12.1.3

Computed statistical absorption coefficient versus frequency, for the various facings of Table 12.1.2 used with an acoustical material having the impedance characteristic of Fig. 12.1.4.

absorbing layer is shown in Fig. 12.1.4. The impedance is selected to be representative of experimental data for one-inch blankets on rigid backing. The resonance effect indicated by the calculations is closely observed experimentally, but the observed absorption does not always fall off as rapidly on the high frequency side of the resonance as the calculations predict. This disagreement has been attributed to the existence of a small amount of wave propagation within the material, parallel to the backing. This greatly increases the high-frequency absorption. The experimental high-frequency value of α_{stat} is of the order of several tenths.

In general, a facing having a specific reactance ratio $X/\rho c$ of less than 0.5 will have little effect on the absorption of common acoustical materials. On the other hand, if $X/\rho c$ exceeds 20, the absorption will generally be reduced to less than 10 per cent, except in unusual cases where the stiffness reactance of the acoustical material may cancel the large facing reactance at a particular frequency.

The second perforated facing analysis, 1.10/ where only the flow resistance of the acoustical material is specified, will now be described. At first, we assume that the acoustical material is a cloth applied to the facing; a modification when the space between the perforated facing and the rigid wall is completely filled with mineral or glass wool will be given later. The symbols are defined below. While the analysis involves dimensionless variables, the design charts are for an air layer thickness in centimeters.

L   air layer thickness, from perforated facing to the rigid wall, cm

r_o radius of hole in facing, cm

FIGURE 12.1.4

Normal specific impedance characteristic used in calculating the results of Fig. 12.1.3 for perforated facings. The characteristic is typical for a one-inch homogeneous, porous tile (e.g., rigid glass wool or rock wool sheet).

R/ρc

X/ρc

Frequency cycles/second
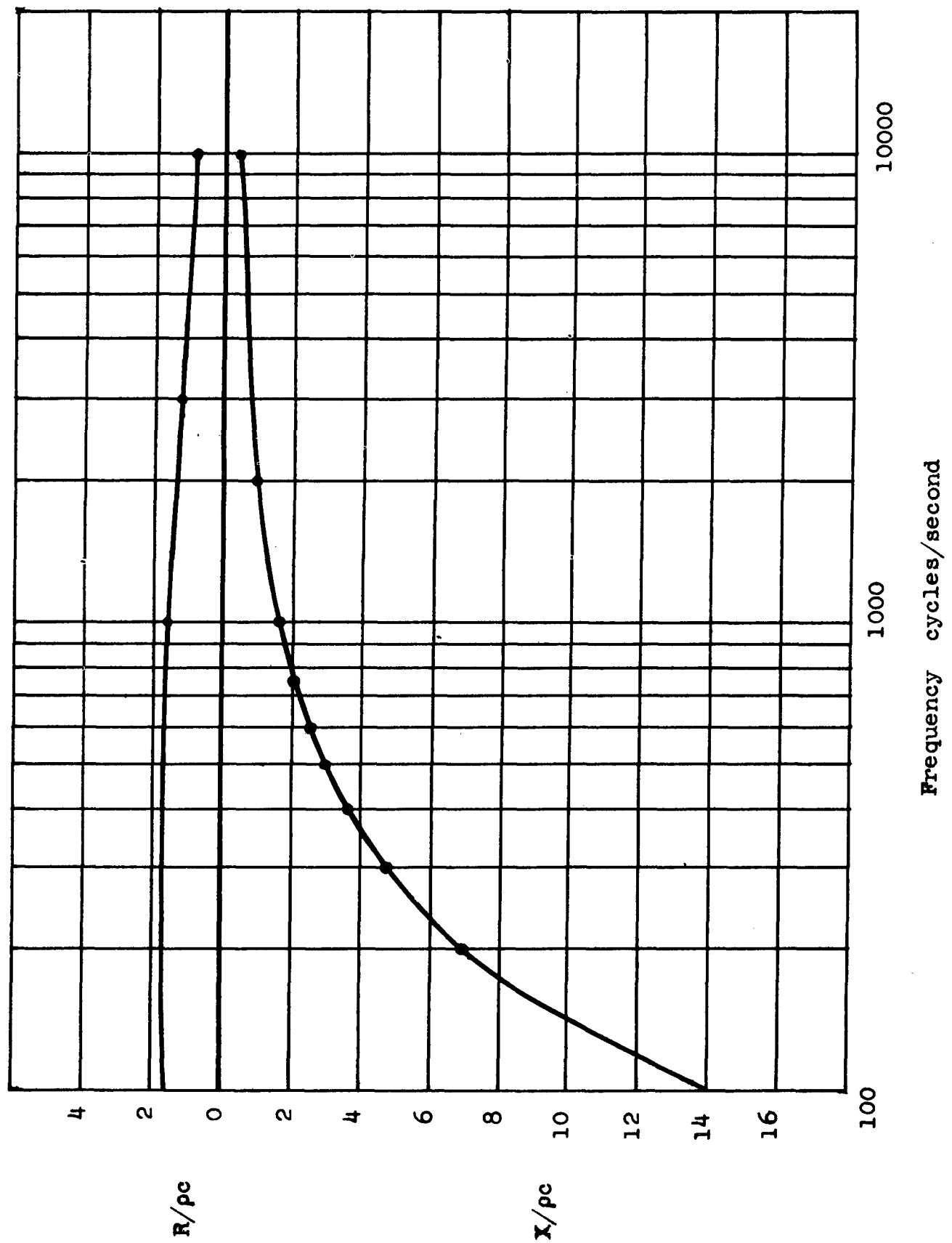
TABLE 12.1.2

PERFORATED FACING DATA USED TO COMPUTE THE ABSORPTION CHARAC-
TERISTICS IN FIG. 12.1.2 REFERENCE 1.10

Fac- ing	n holes per sq'	d hole diameter inches	t facing thickness inches	σ surface density lb/ft^2	% open area	M total effective density lb/ft^2
A	9	5/8	3/16	1.5	1.92	0.22
B	36	5/8	3/16	1.5	7.65	0.06
C	144	5/16	3/16	1.5	7.65	0.038
D	576	5/32	3/16	1.5	7.65	0.027
E	4608	0.068	0.0179	0.75	11.67	0.0046

ν	frequency of incident sound, cps
ν_o	resonance frequency in cps for normal incidence
c	speed of sound in air
$k_o = 2\pi\,\nu_o/c$	propagation constant for air at frequency ν_o
p	fraction of area which is open
$r\ell$	total flow resistance in rayls of material attached to facing. The specific flow resistance of the material (unit thickness) is r, and the effective thickness of the material is ℓ .
$\alpha_{av} = \alpha_{stat}$	statistical absorption coefficient
γ	the ratio of the frequency ν to the resonance frequency ν_o
$\theta = r\ell/p\rho c$	

The analysis assumes that the facing is rigid. The specific impedance due to the perforations is obtained on the basis of the effective air mass from Eq. (12.1.20). The added specific impedance due to the flow resistance of the cloth is $r\ell/p$*. The specific impedance due to the air layer of depth L is $-j\rho c \cot(k_0 L)$, as may be shown from Eq. (12.1.14a), if the air layer is partitioned into cells or if the incoming wave is at normal incidence. A more complicated relation is necessary for oblique incidence on a nonpartitioned layer. The total specific impedance of the layer is the sum of the three contributions (air mass reactance, cloth flow resistance, air layer impedance).

Resonances occur at those frequencies where the reactance of the air layer is just sufficiently negative to compensate for the hole reactance. Large absorption may occur at these resonances if the resistive component of the impedance is properly chosen. The statistical absorption coefficient is computed by use of Eqs. (12.1.12) and (12.1.3). In the case of the unpartitioned air layer, the relations are sufficiently complicated to require numerical integration.

The results of the analysis outlined above are given as the statistical absorption coefficient vs a frequency parameter, in Fig. 12.1.5, (for the partitioned air layer) and Fig. 12.1.6, (for the unpartitioned case). An auxiliary chart, Fig. 12.1.7, is required to compute the lowest normal incidence resonance frequency, corresponding to $\gamma = 1$. This provides numerical values for the dimensionless frequency scale used on the preceeding absorption coefficient charts.

---

* The open area factor p is used here because the air flow is confined to the parts of the cloth which are behind perforations. For a cloth much thicker than the hole diameter, the flow would spread out sufficiently that the factor p should be omitted.

A method for using the charts is the following: The designer selects from one of the charts in Fig. 12.1.5 or Fig. 12.1.6 an absorption-frequency characteristic which will be acceptable, and decides upon the frequency in cps, ν_0, at which the normal incidence resonance is to be established. Fig. 12.1.5 or 12.1.6 shows the values of Θ and k_0L which must be used to obtain the desired characteristic. In Fig. 12.1.7, the set of lines sloping upward to the right is then used to obtain the required value of L, in centimeters, from the known values of ν_0 and k_0L. The set of curves sloping upward to the left then indicates a relationship which must be realized between t/r_0 and r_0/pL. Successive trials may be necessary to discover an available facing which will give the required relation, or it may prove that it is necessary to start with an available facing panel, and to select a somewhat different frequency characteristic which can be realized with this. The working method is illustrated by the numerical example which follows.

Suppose that it is desired to obtain the absorption characteristic (with unpartitioned air backing) given by $\Theta = 4$, $k_0L = 1.0$, in Fig. 12.1.5 with the frequency ν_0 corresponding to 300 cps. Suppose also that the available perforated facings are those in Table 12.1.2. From Fig.12.1.7 it is found that the air layer depth, L, must be 18 cm, to make ν_0 equal to 300 cps with k_0L equal to 1.0. It is now possible to calculate values of r_0/pL for the various facings, as tabulated in Table 12.1.3. Then, as also shown in the tabulation, the required value of t/r_0 for each facing is found from Fig. 12.1.7. The required t/r_0 values are compared with the values actually found in each facing. The facing B is selected, since its value of t/r_0 is sufficiently close to the desired value to place both ν_0 and k_0L within a few per cent of the original design values. If none of the available facings had given this agreement, it would have been necessary to select a new design curve with new values of Θ and k_0L.

FIGURE 12.1.5

Statistical absorption coefficient, as a function of frequency parameter ν/ν_0, for perforated facings with unpartitioned air backing of depth L, and material of known flow resistance. Lowest frequency of normal-incidence resonance is ν_0. Θ is equal to flow resistance in rayls, divided by pc; k_0 is equal to $2\pi\,\nu_0/c$ 1.11/
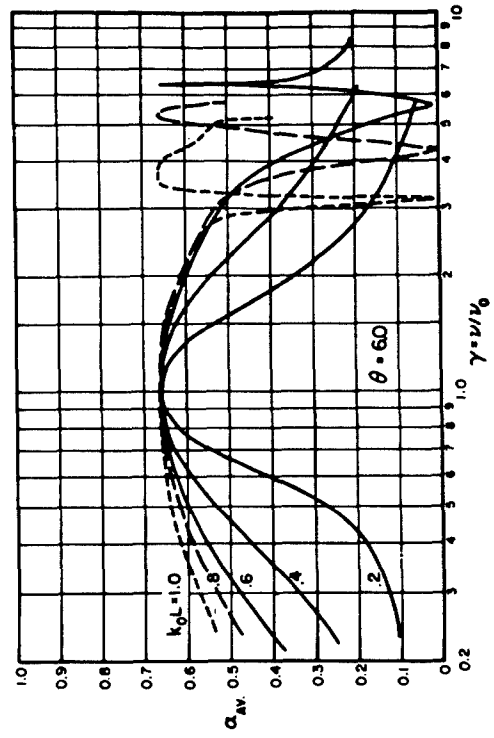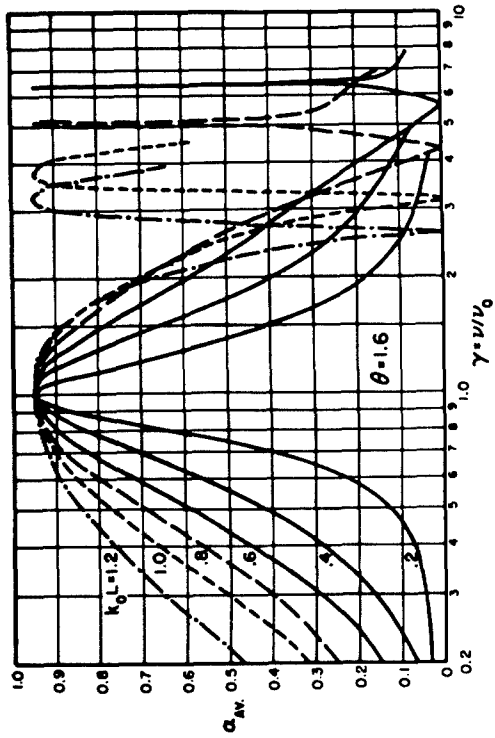
192
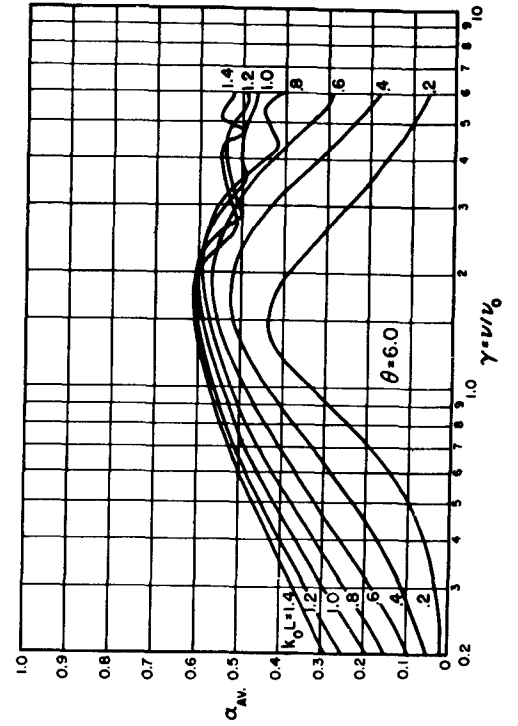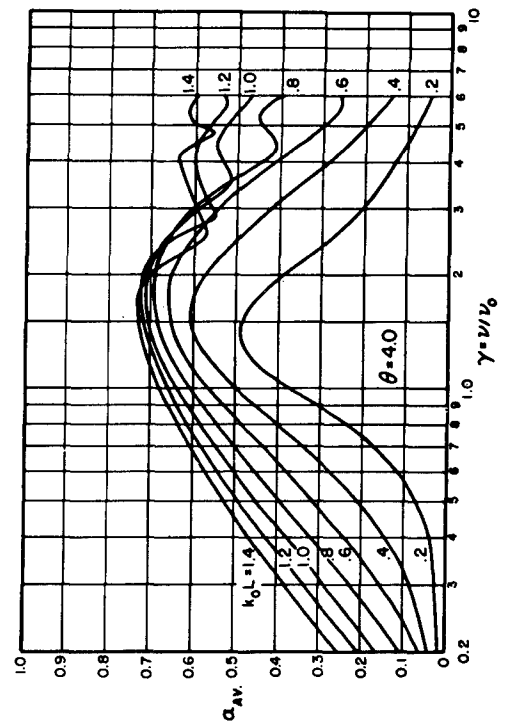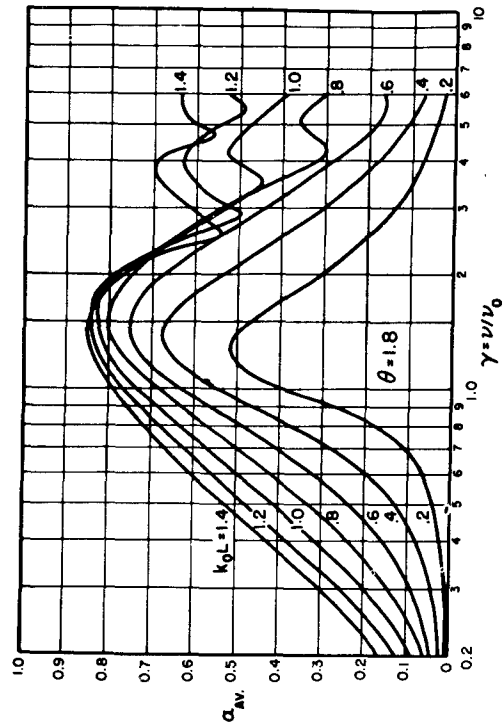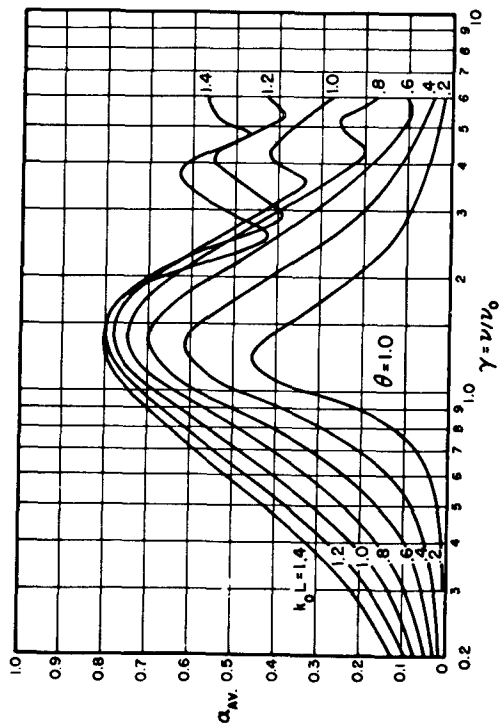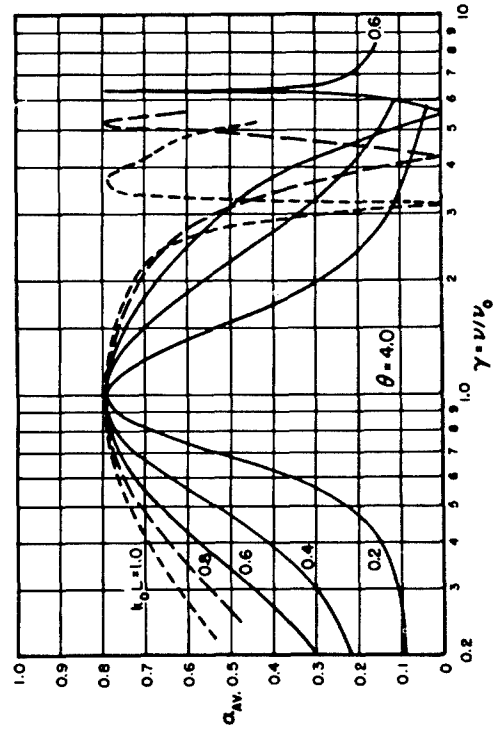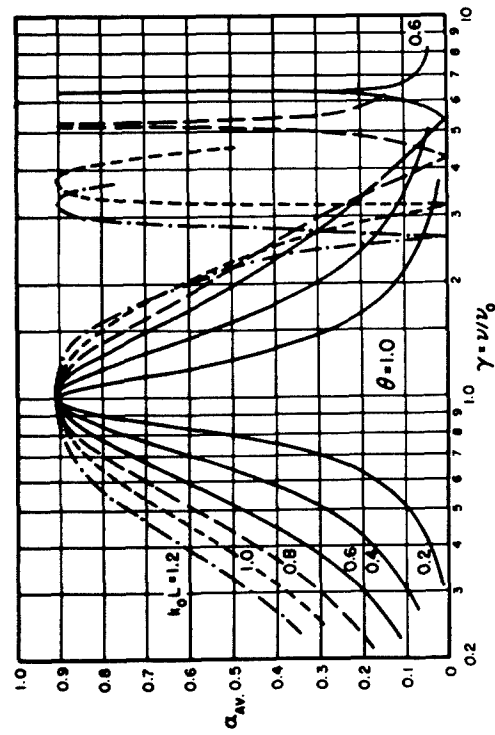
TABLE 12.1.3

CALCULATIONS OF PERFORATED FACING CHARACTERISTICS

Facing (from Table 12.1.2	A	B	C	D	E
Hole Radius r_o, cm	0.397	0.397	0.198	0.0993	0.0864
t/r_o	0.6	0.6	1.2	2.4	5.26
Fraction Open Area p	0.0192	0.0765	0.0765	0.0765	0.117
r_o/pL for L = 18 cm	1.15	0.288	0.144	0.0721	0.0411
Required t/r_o from Fig. 12.1.7	0	0.7	3	5	- - -

Figure 12.1.6

Statistical absorption coefficient, as a function of frequency parameter ν/ν_o, for perforated facings with partitioned air backing of depth L and material of known flow resistance. Lowest frequency of normal-incidence resonance is ν_o. θ is equal to flow resistance in rayls, divided by ρc. k_o is equal to $2\pi \nu_o/c$. Ref. (1.11).
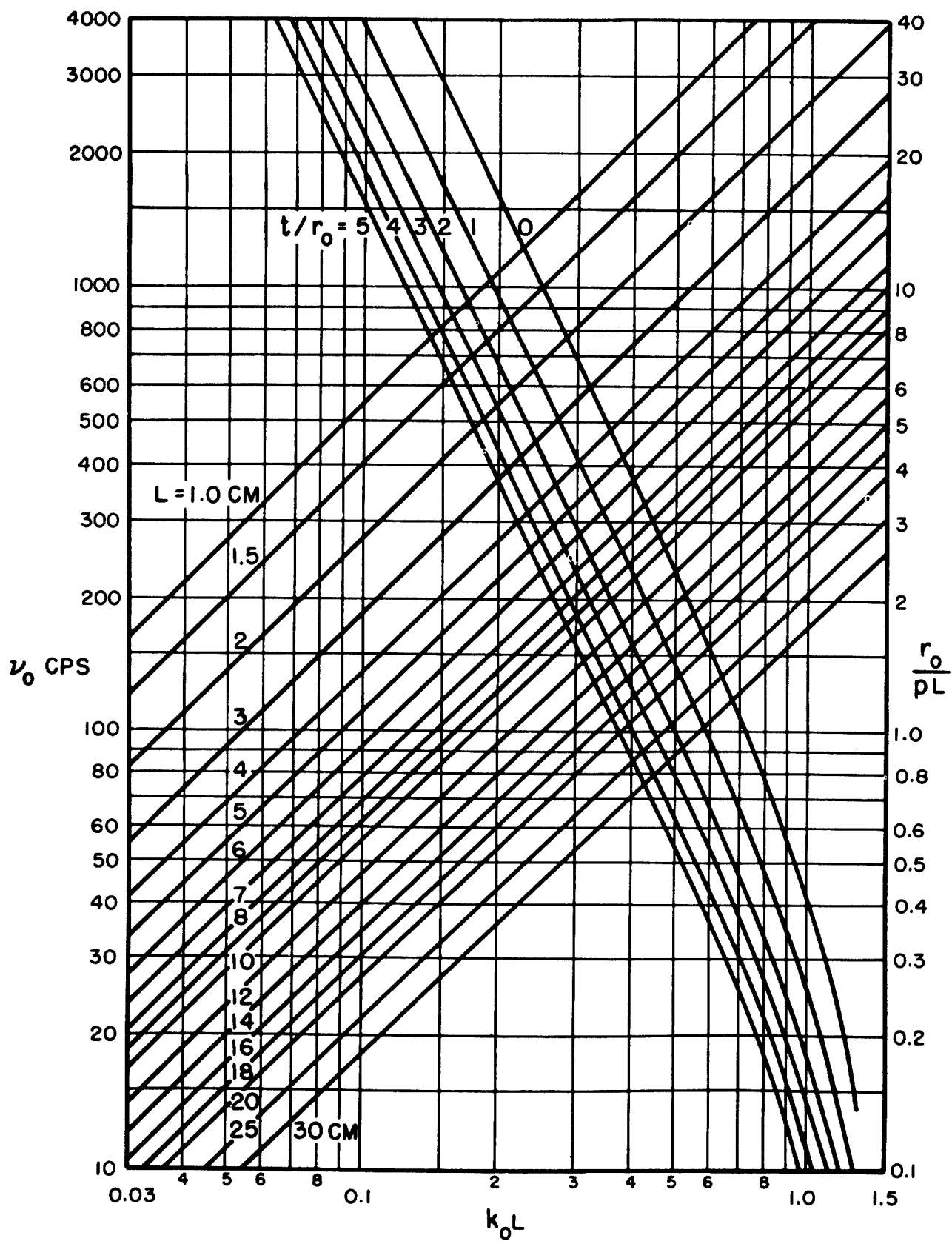
Since $\Theta = 4$, the specific acoustic resistance $(r\ell/p)$ must be $4\rho c$, or about 165 rayls. If a thin cloth is used immediately against the facing as in Fig. 12.1.8a, its flow resistance $r\ell$ must be $p(4\rho c) = 0.0765\ (4\rho c)$ or about 12.5 rayls. If a blanket is used as in Fig. 12.1.8b, where the blanket thickness is several times the hole diameter, it may be assumed that the flow spreads out over the whole area, and the flow resistance $r\ell$ must be simply $\Theta\ (\rho c)$, or 165 rayls. This is also true if the cloth or blanket is spaced from the facing by one or more hole diameters, as in Fig. 12.1.8c, but still completely contained within a distance $L/4$ of the facing. If the air cavity is completely filled with a porous material as in Fig. 12.1.8d, the total flow resistance $r\ell$ must be $3\Theta\ (\rho c)$. The last relation is accurate only for a partitioned backing, however. Intermediate cases are more complicated.

Generally, the value of Θ should be not less than 1.8 for the unpartitioned backing, and not less than 1.6 for the partitioned backing. These values give the highest absorption maxima. Smaller Θ values give smaller absorption at all frequencies than do the optimum values. Values of Θ larger than 1.8 and 1.6 give broadened maxima with somewhat increased absorption at frequencies far from the peak, but with decreased absorption at the peak.

The unpartitioned air backing gives a greater high-frequency statistical absorption coefficient than does the partitioned backing. When the backing is unpartitioned, there is always at least one angle of incidence for which the absorber is resonant at any given frequency. Practical

---

FIGURE 12.1.7

Design chart for perforated facing with air backing, which may be used in connection with Figs. 12.1.5 and 12.1.6. The family of curves sloping upward to the right determines the air backing depth L to place the lowest normal-incidence resonance at frequency $\mathcal{V}_o$ when $k_o L$ has been chosen. The family of curves sloping upward to the left determines the necessary relation between t/r_o and r_o/pL when $k_o L$ has been chosen. Facing thickness, t; hole diameter, r_o; fractional open area, p. Ref. (1.11).
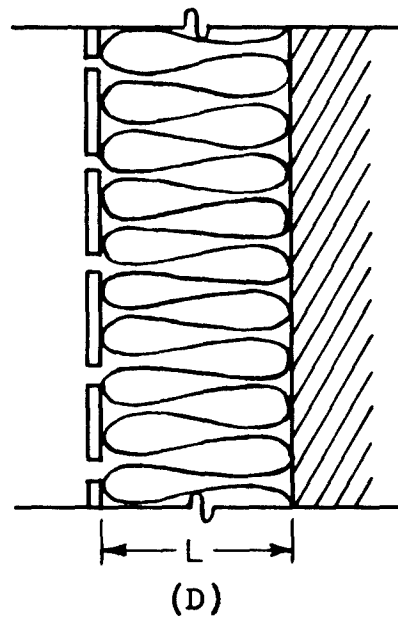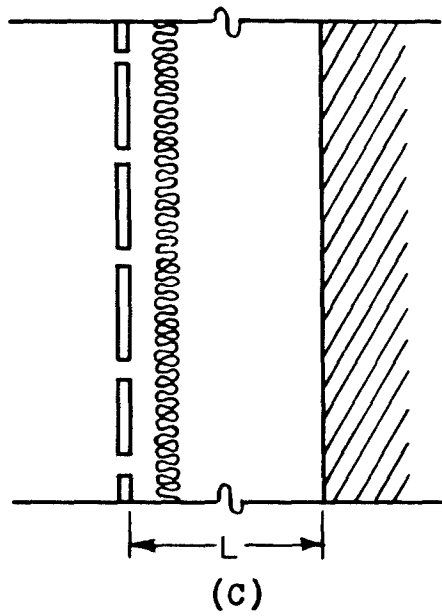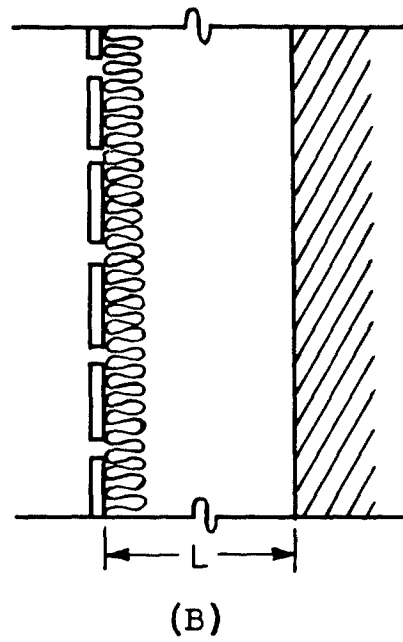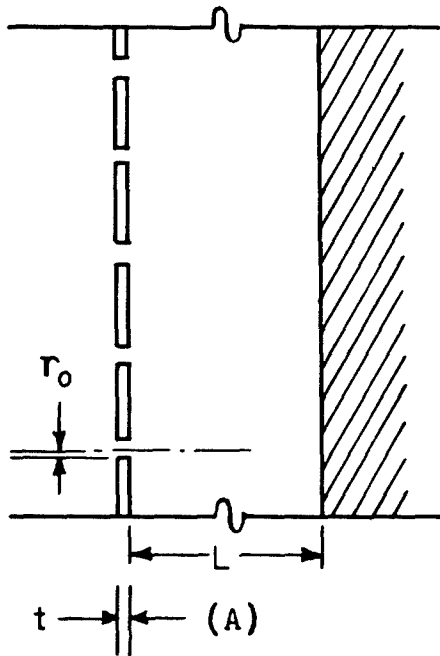
measurements with partitioned backing show performance which is intermediate between the partitioned and non-partitioned predictions at very high frequencies; as the wavelength becomes smaller than the width of the cells formed by partitioning, the performance approaches that expected for no partitions. At and below the frequency of maximum absorption, the absorption is increased by the presence of partitions.

The method of calculation applies with reasonable accuracy if the facing is perforated by long narrow slots rather than by circular holes. The calculations should be based on an equivalent hole radius equal to half the slot width.

Flow Resistance Data for Acoustical Materials.
Figure 12.1.9 summarizes measured values of specific flow resistance for several porous materials as a function of volume density in lb/ft^3. Individual samples may vary by some 20 per cent from the nominal values.

It has been found 1.13/ that the flow resistance of loose sand can be expressed approximately by the equation

$$r = 19/d^{1.3}$$

(12.1.22)

FIGURE 12.1.8

Illustrations of special cases for which the effective flow resistance r' in the expression $\Theta = r'/\rho c$ is easily computed in the perforated facing analysis. Case A, cloth adjacent to facing, cloth thickness much less than hole diameter, use r' equal to $r\ell/p$, where $r\ell$ is flow resistance of cloth in rayls and p is fractional open area of facing. Case D, blanket with thickness greater than hole diameter is adjacent to facing, but located entirely in left-hand quarter of backing space, use $r' = r\ell$, flow resistance of blanket in rayls. Case C, cloth or blanket spaced from facing by at least one hole diameter, but within left-hand quarter of backing space, use $r' = r\ell$, flow resistance in rayls. Case D, entire space filled, use r' equal to one-third of blanket flow resistance in rayls.

Specific Flow Resistance R/T rayls/in.

Volume Density lb/ft^3
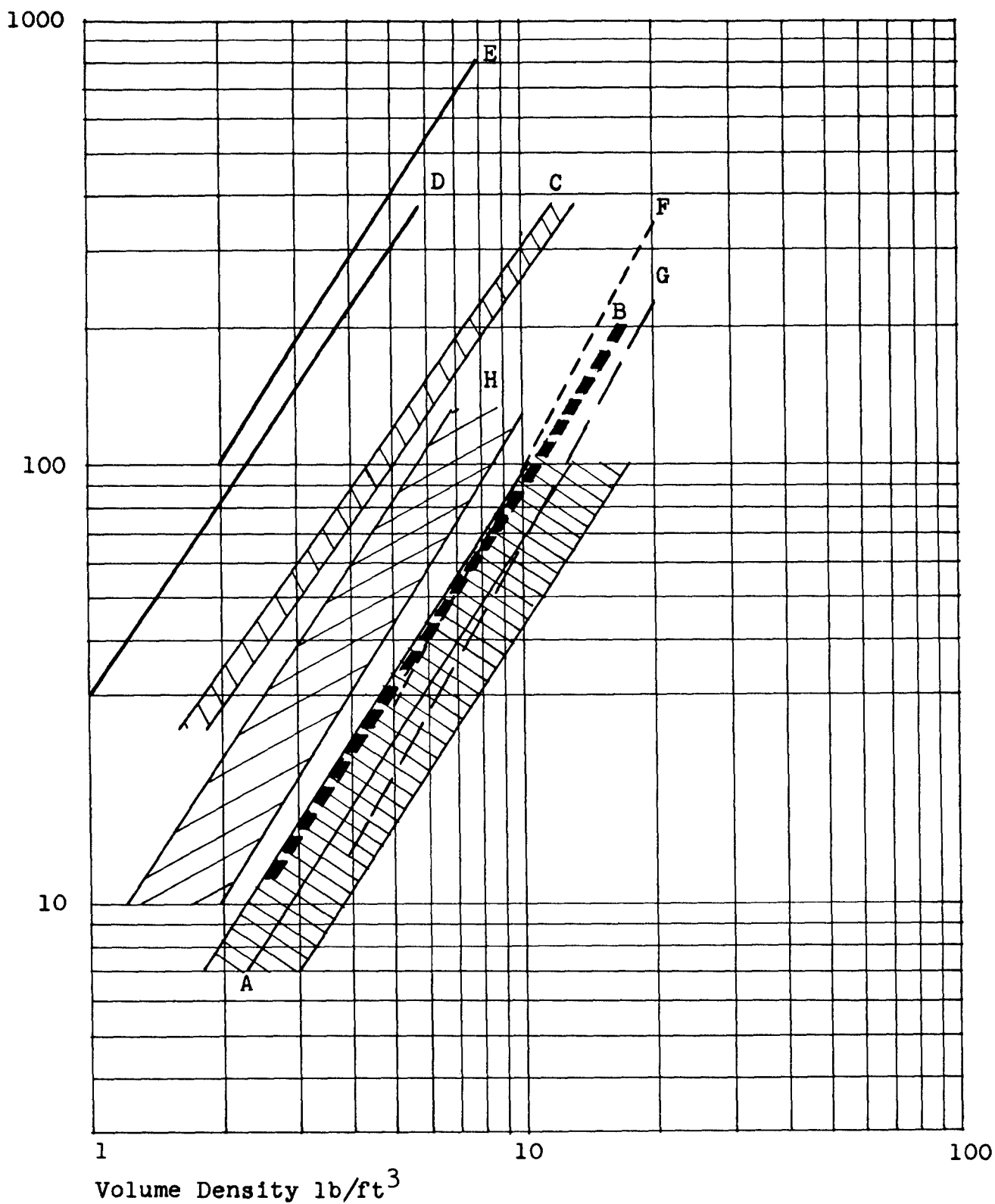
where r is the specific flow resistance in rayls/cm and d is the average particle diameter in mm. This result applies where the particle size is reasonably uniform so that an average diameter can be given. The flow resistance in rayls for a number of cloths and screens is given in Table 12.1.4.

Porosity values for several materials are given in Table 12.1.5. The porosity of fibrous blankets of the materials given, but having a different density may be estimated by means of the principle that (1 - porosity) is proportional to the density.

The structure factor m has been evaluated in a few cases. A value of 2.7 for a structure consisting of many wire screens in close contact for the case of perpendicular incidence has been reported. However, considerable variation with frequency was observed. 1.9/. The computed value of m is 3.0 for a structure which contains long narrow passages oriented at random angles, 1.3/. The experimental value for loose sand is 4.3, 1.13/. Generally, m appears to be about 1.5 for blankets of porosity 0.95 or more, 1.9/.

Propagation Constant. Illustrative propagation data for two weights of Fiberglas, based on measurements 1.14/ in the range 50-1000 cps, are summarized in Table 12.1.6. The propagation constant is the quantity k_1 corresponding to the expression exp $(-jk_1x)$ for the phase and amplitude behavior of a plane wave. Expressions for the phase velocity and the attenuation are given separately in the table. Measurements of the propagation constant for a rock wool (J-M Stonefelt, Type M) 1.9/ and for loose sand, 1.13/ have also been published.

FIGURE 12.1.9

Specific flow resistance (rayls/inch) for various glass and mineral wools, as a function of volume density. A, PF (board) Fiberglas (the material meant by reference to "PF" Fiberglas unless a specific style is stated); B, TWF white wool Fiberglas; C, PF 450 Fiberglas; D, Aerocor Fiberglas; E, J-M Thermoflex; F, B-H rock wool, Style #1, with wire facing; G, B-H rock wool, Style 2; H, J-M #305 mineral wool.

TABLE 12.1.4

FLOW RESISTANCE OF CLOTHS AND SCREENS

WIRE MESH

Number of Wires per Linear Inch	Wire Diameter cm	Flow Resistance rayls
30	0.033	0.567
50	0.022	0.588
100	0.0115	0.910
120	0.0092	1.35
200	0.0057	2.46
30	0.0305	0.111
45	0.0203	0.174
85	0.0101	0.430
210	0.005	0.980

CLOTHS

Manufacturers Designation	Finish	Flow Resistance rayls	Peak SPL for $\sqrt{2}$ Increase of Flow Resistance	Thickness per inch	Weight oz/yd^2	Construction ends x picks per inch
63	none	1.3	---	0.013	9.6	16 x 14
82	none	40	134	0.014	14.5	60 x 56
84	none	22	120	0.028	24.6	42 x 36
120	none	30	118	0.004	3.2	60 x 58
126	none	4.5	108	0.0065	5.4	34 x 32
138	none	220	> 130	0.007	6.7	64 x 60
138	none	220	> 130	---	---	64 x 60
181	none	38	130	0.0085	8.9	57 x 54
1032	none	0.50	---	---	---	---
1044	114	3.6	106	0.022	19.2	14 x 14
1544	114	1.9	---	0.022	17.7	14 x 14
1550-24	none	4.2	108	---	---	24 x 32
2 oz matte	114	22	130	---	18	---

TABLE 12.1.5

POROSITY VALUES

Material	Porosity	Source (Ref.No)
Celotex QT Duct Liners	0.90	1.8
J-M Permacoustic	0.875	1.8
Fiberglas, 9 lb/ft^3 PF	0.965	1.14
Fiberglas, 4.25 lb/ft^3 TWF	0.985	1.14
J-M Sanacoustic Pad	0.94	1.8
J-M Stonefelt Type M Refined Rock Wool 2.7 lb/ft^3	0.97	1.9
USG Quietone	0.93	1.8
USG Perfatone Pad	0.96	1.8
Kapok	0.99	1.8
Sand, Nearly uniform particle size packed	0.36	--
Sand, nearly uniform particle size loose	0.41 av	1.13

Specific Acoustic Impedance Data. Specific impedance data for a number of acoustical materials are shown in Figs. 12.1.10-14. While the data are in all cases obtained under normal incidence in a standing-wave impedance tube, usually of 3" in diameter, the normal impedance may be assumed practically independent of angle of incidence for the materials which are considered. In some cases, the measured impedance-frequency curves are supplemented by curves which are calculated by assigning suitable physical constants to the material. Calculations are made by the procedures of Ref. 1.9; for rigid tiles (materials more dense than

TABLE 12.1.6

PROPAGATION CONSTANTS FOR FIBERGLAS BLANKETS

	4.25 lb/ft^3 TWF	9 lb/ft^3 PF (hard)
Propagation Constant, cm^{-1}	$10^{-3}(2.67\ f^{0.66}-3.90\ f^{0.48})$	$10^{-3}(1.96 f^{0.74}-5.0\ f^{0.48}$
Phase Velocity, cm/sec	$2.35 \times 10^3\ f^{0.34}$	$3.20 \times 10^3\ f^{0.26}$
Attenuation, db/cm	$0.034\ f^{0.48}$	$0.43\ f^{0.48}$

f is frequency
   in cps

---

6 lb/ft^3), the procedure is equivalent to using Eqs.(12.1.14)
and (12.1.17) or, if the layer is also thin compared to the
wavelength, to using Eq. (12.1.19). Reasonable agreement
between calculated and measured values is obtained, but the
calculations are restricted to homogeneous materials. It
will be observed that the impedance function for other
materials (e.g., Celotex C-4, a perforated material) shows
additional complexity; particularly in the reactance behavior.
No rigorous method for calculating the impedance has been
advanced in these cases.

Statistical Absorption Coefficients. The statistical
absorption coefficient is shown as a function of frequency,
for several acoustical materials, in Fig. 12.1.15. The data
are obtained by calculation from the specific impedance
curves in the preceding figures.

Normal Absorption Coefficient Data. Fig. 12.1.16 shows
the normal absorption coefficient, as a function of frequency,
for several "soft blankets" of Fiberglas. The information
was obtained by measurements in a standing-wave impedance tube.

<u>Chamber Absorption Coefficients</u>. Figs. 12.1.17-19 show the absorption coefficients as a function of frequency for perforated acoustical tiles of thickness 1, 1/2 and 1/4 in. In each chart individual curves show the behavior of material of given thickness on standard mountings 1, 2 and 7 as defined by the Acoustical Materials Association. The charts are constructed from averages of the AMA chamber absorption coefficients for perforated tiles of the various manufacturers. The data for the different tiles are sufficiently close together to justify the use of these average charts for most engineering purposes. Detailed information for individual products is available in Ref. 1.6.

Average values of the <u>noise reduction coefficient</u> are also shown for each mounting condition and for each tile thickness. The noise reduction coefficient is defined as the average of the chamber absorption coefficients at 256, 512, 1024 and 2048 cps, given to the nearest 5 per cent. (The average values given here are not rounded to the nearest 5 per cent).

The mounting conditions are defined as follows:

<u>Mounting 1</u>.

   Sample cemented to plaster board.
   Considered equivalent to cementing to
   plaster or concrete ceiling.

<u>Mounting 2</u>.

   Sample nailed to 1 in. x 3 in. wood
   furring, ordinarily 12 in. on centers.

<u>Mounting 7</u>.

   Sample mechanically mounted (spaced
   from ceiling).

Frequency cycles/second
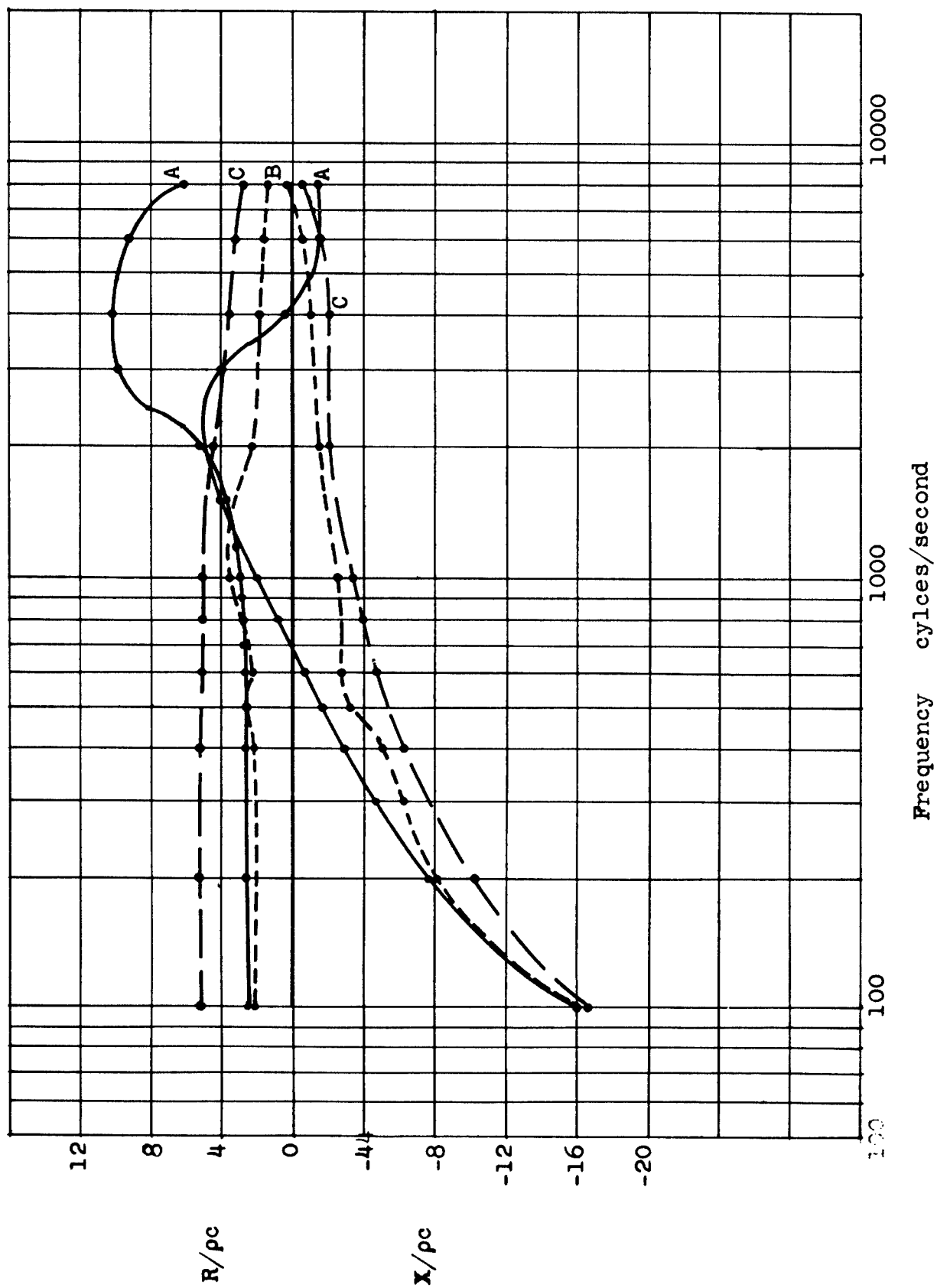
FIGURE 12.1.10

Measured specific acoustic impedance for: A, Celotex C-4 (1.25 in.); B, Johns-Manville Sanacoustic pad (1 in.); C, Johns-Manville Airacoustic (1 in.). From Ref. 1.7.
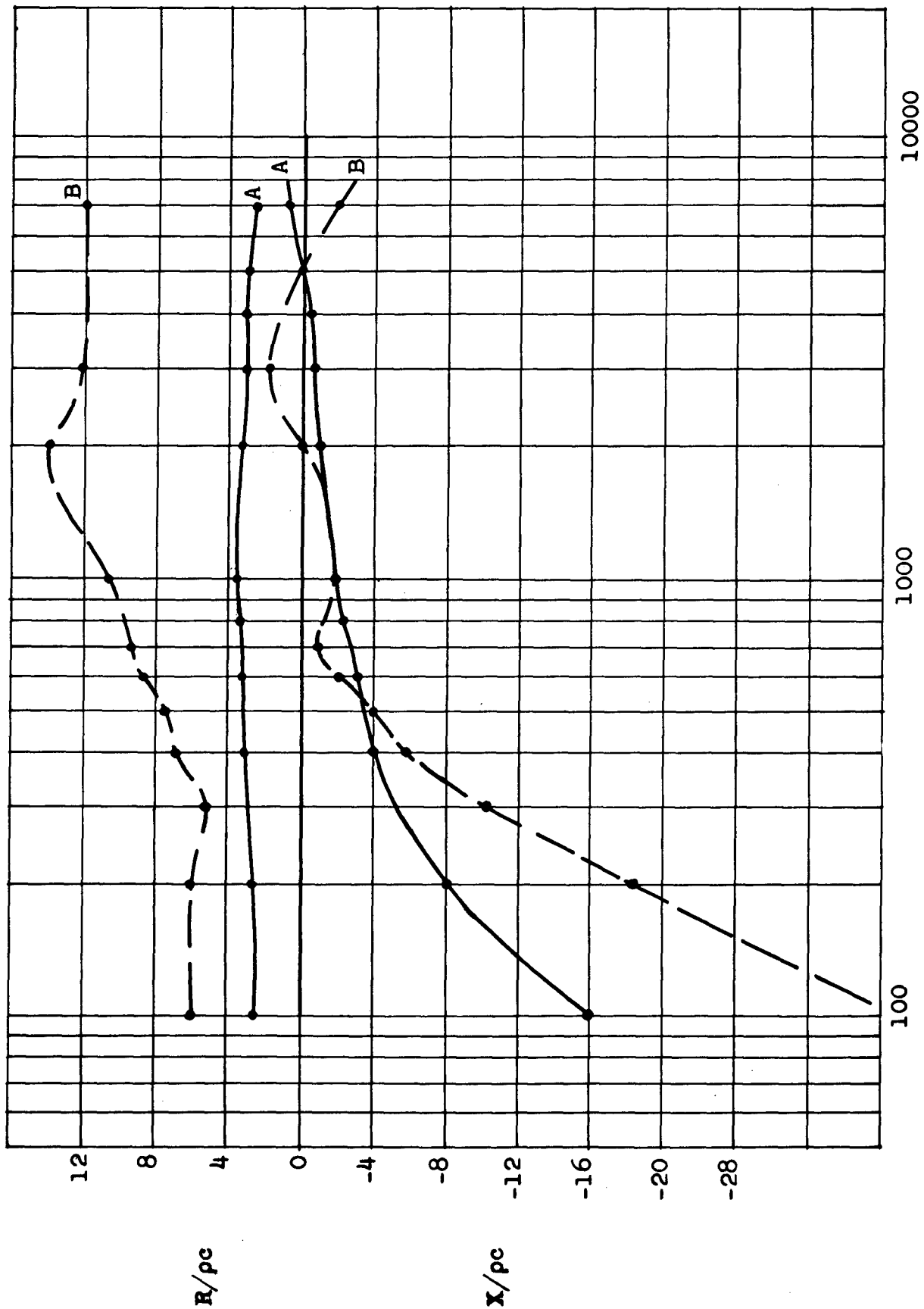
Measured specific acoustic impedance for: A, U.S. Gypsum Quietone (Auditone perforated)(1"); B, Armstrong Cor-koustic (1.5"). From Ref. 1.6.

FIGURE 12.1.11

Frequency cycles/second

FREQUENCY – CYCLES PER SECOND
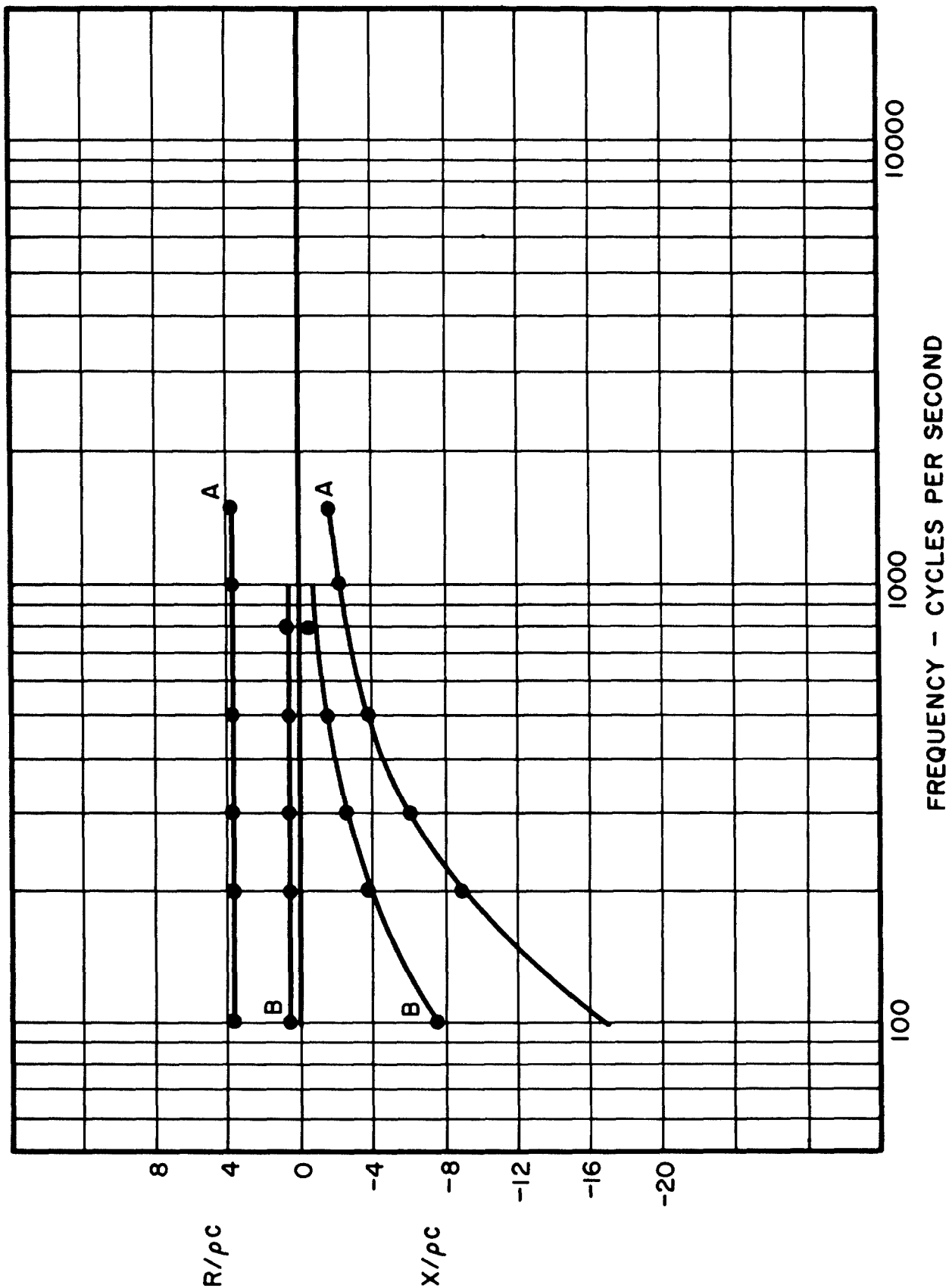
FIGURE 12.1.12

Measured (points) and computed (solid curves) specific acoustic impedance for: A, Celotex Ductliner (1"); B, Kapok (1"). From Ref. 1.7.
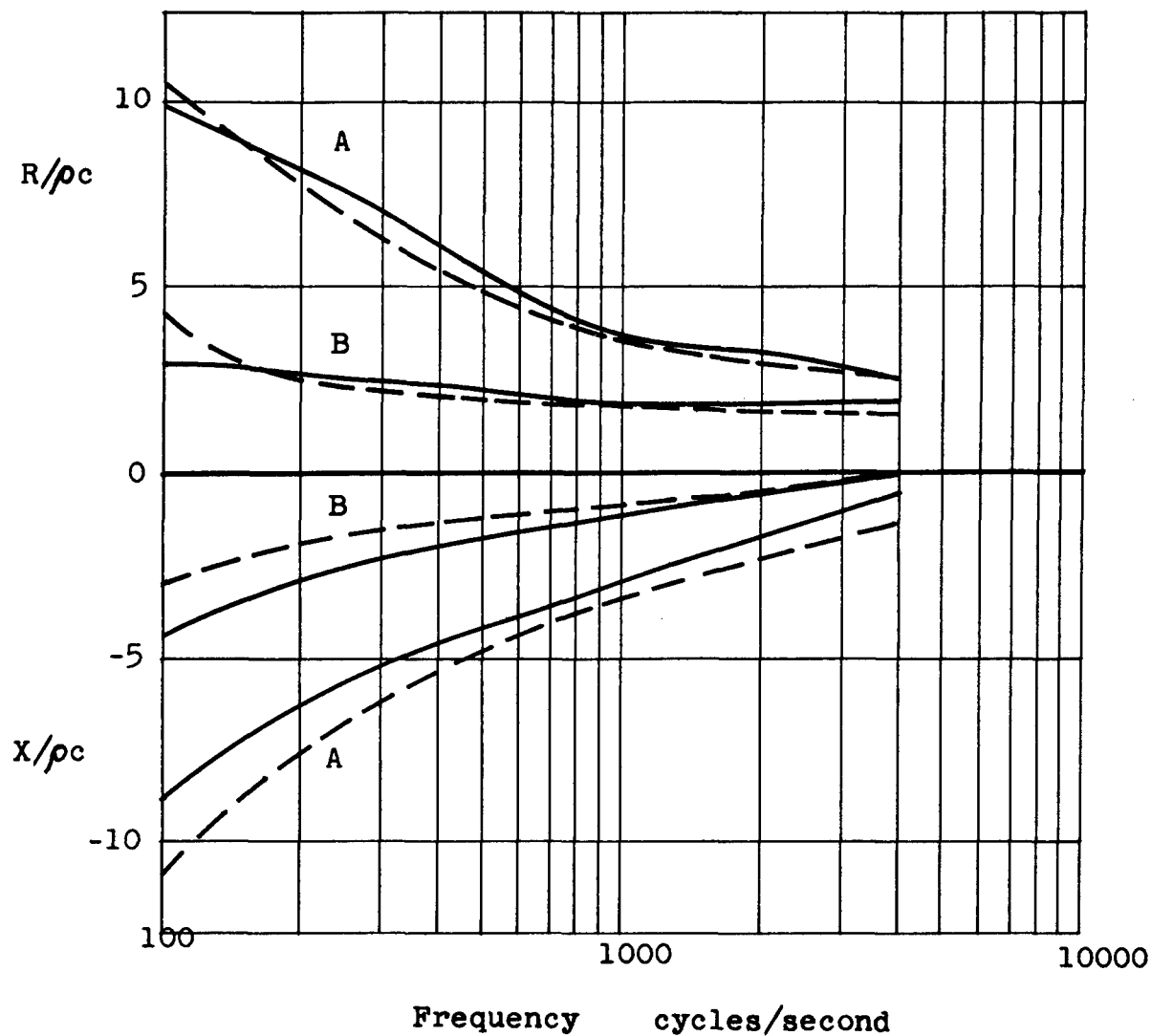
FIGURE 12.1.13

Measured (solid curves) and computed (broken curves) specific acoustic impedance for: A, Baldwin-Hill Monoblock 4" layer); B, 105 lb/ft^3 PF Fiberglas (4" layer).
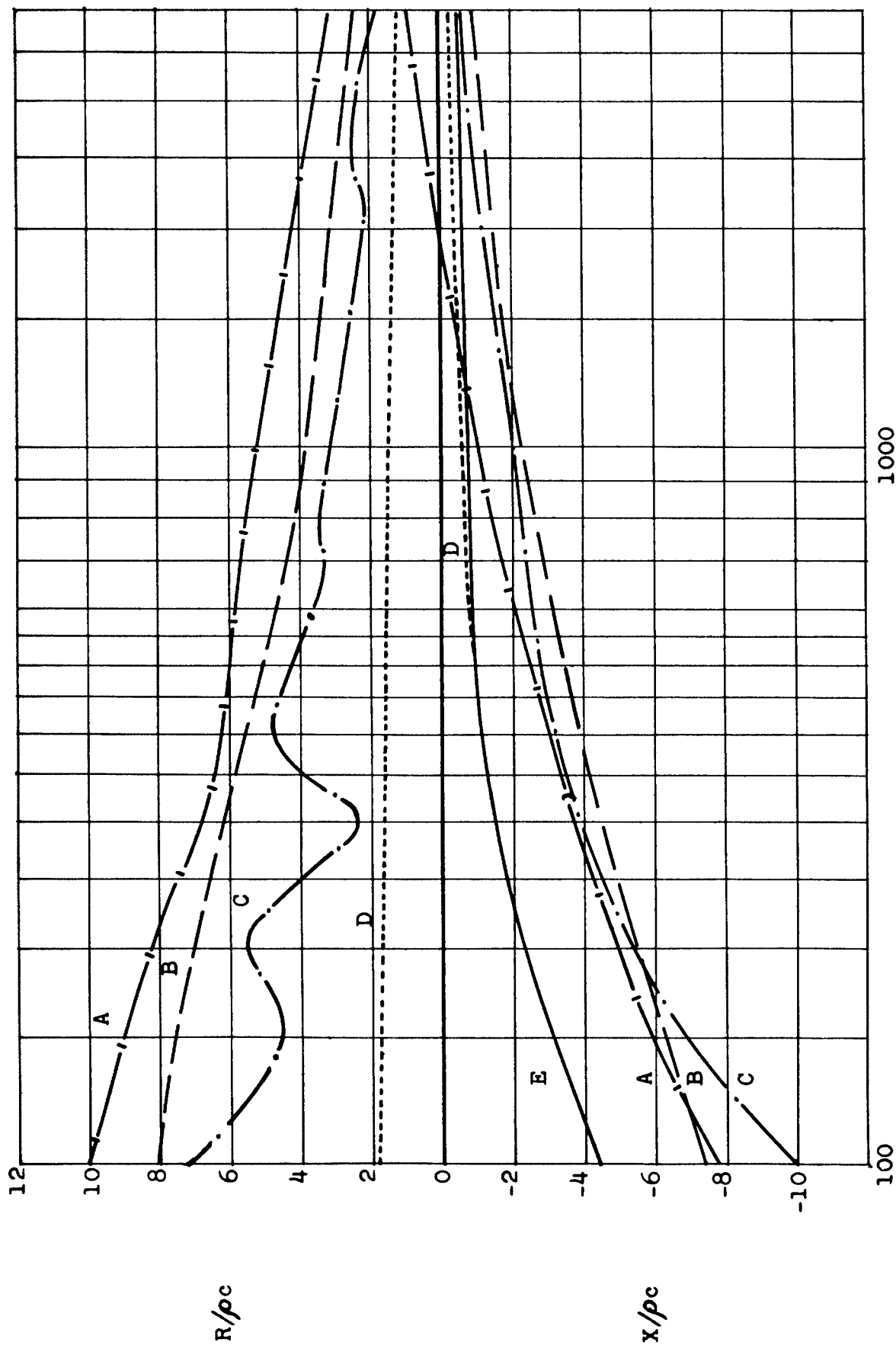
Frequency   cycles/second

FIGURE 12.1.14

Measured specific acoustic impedance (4" layers) for: A, Baldwin-Hill Soundliner; B, B-H Koldboard; C, B-H rock wool, Style No. 2; D, B-H rock wool, Style No. 1 (with wire facing).
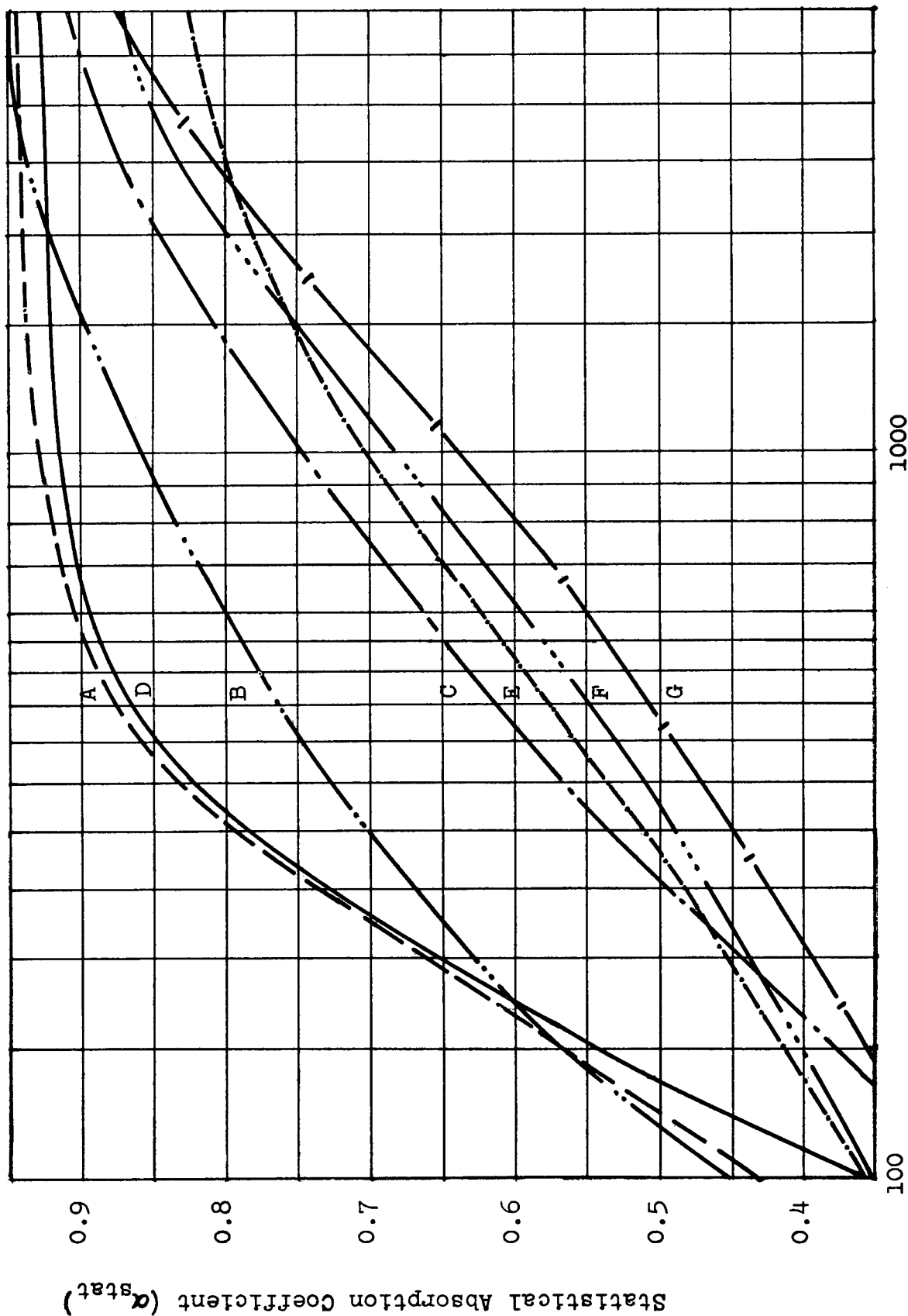
Statistical absorption coefficient, computed from acoustic impedance data on 4" layers, for: A, 6 lb/ft^3 PF Fiberglas; B, 10.5 lb/ft^3 PF Fiberglas; C Baldwin-Hill rock wool, Style No. 1 (with wire facing); D, B-H rock wool, Style No. 2; E, B-H Soundliner; F, B-H Koldboard; G, B-H Monoblock.
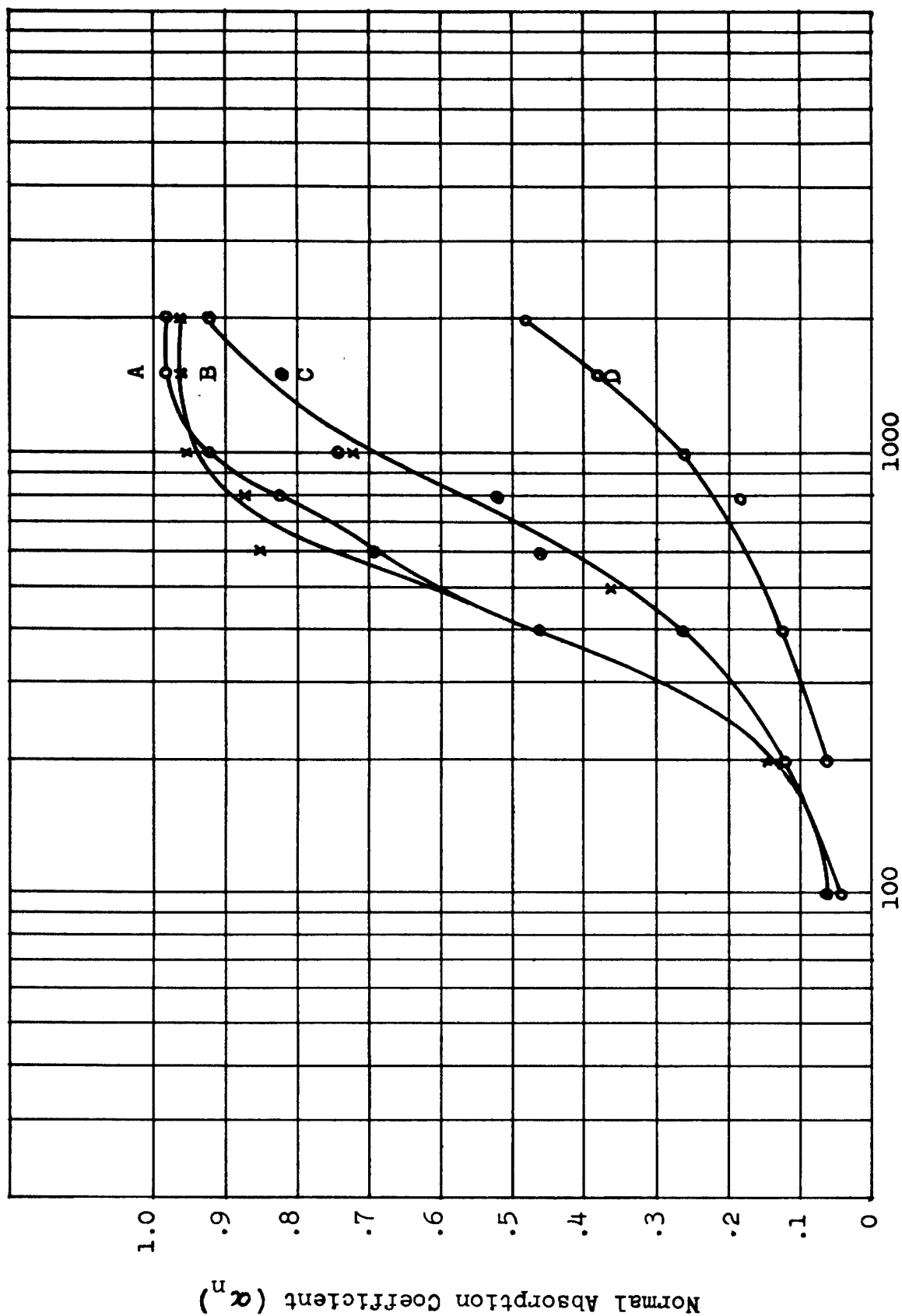
FIGURE 12.1.15

Frequency cycles/second

FIGURE 12.1.16

Normal absorption coefficient as obtained by impedance tube measurements. A, 2" FB-2 heat-treated Aerocor Fiber-glas, 1 lb/ft³; B, 2" Aerocor Fiberglas, 1 lb/ft³; C, 2" TWF Fiberglas, 3 lb/ft³; D 1" TWF Fiberglas 3 lb/ft³.
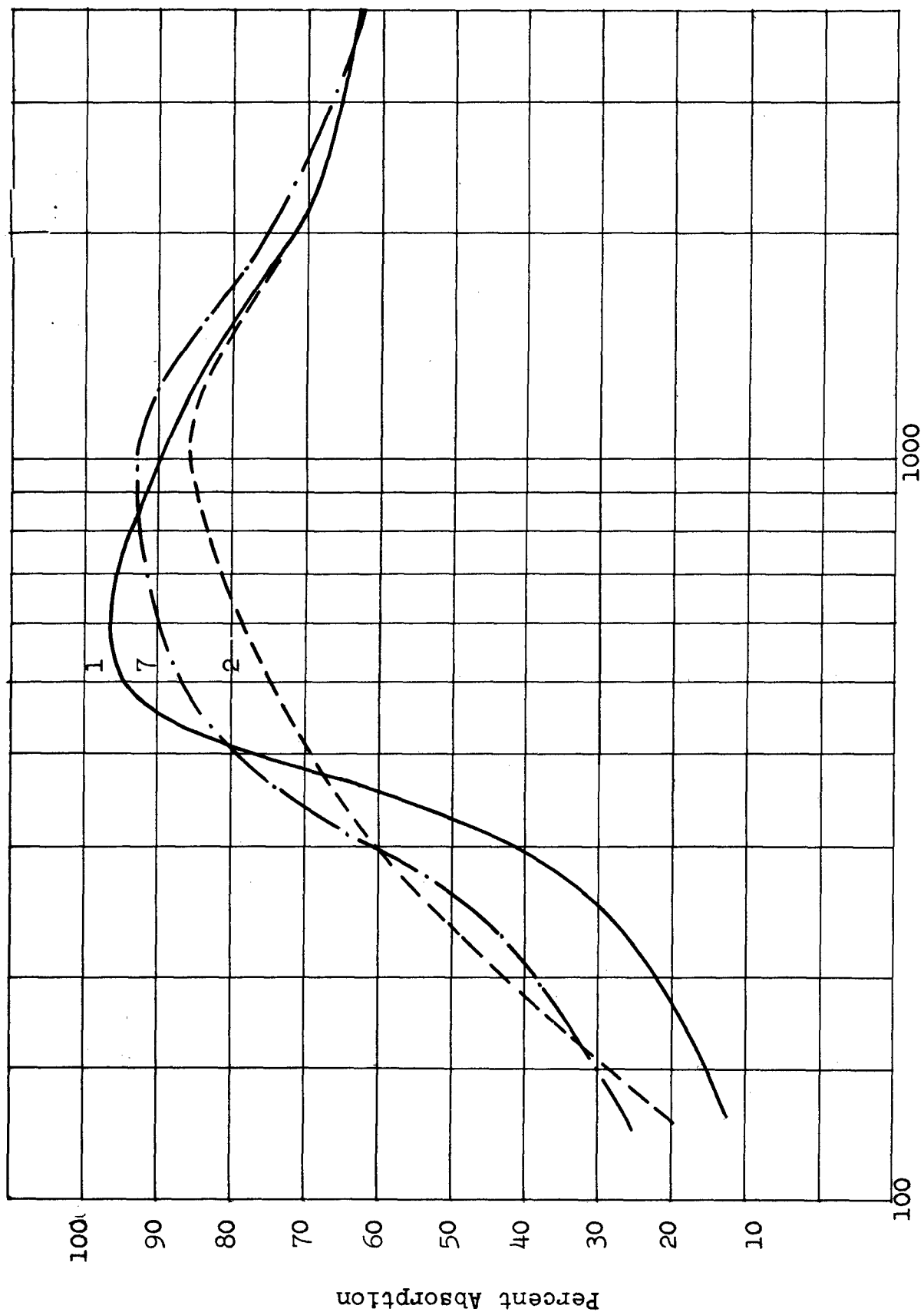
Frequency cycles/second

FIGURE 12.1.17

Average AMA chamber absorption coefficients and noise reduction coefficients for one-inch perforated tiles on standard mountings 1, 2, and 7.

Frequency cycles/second
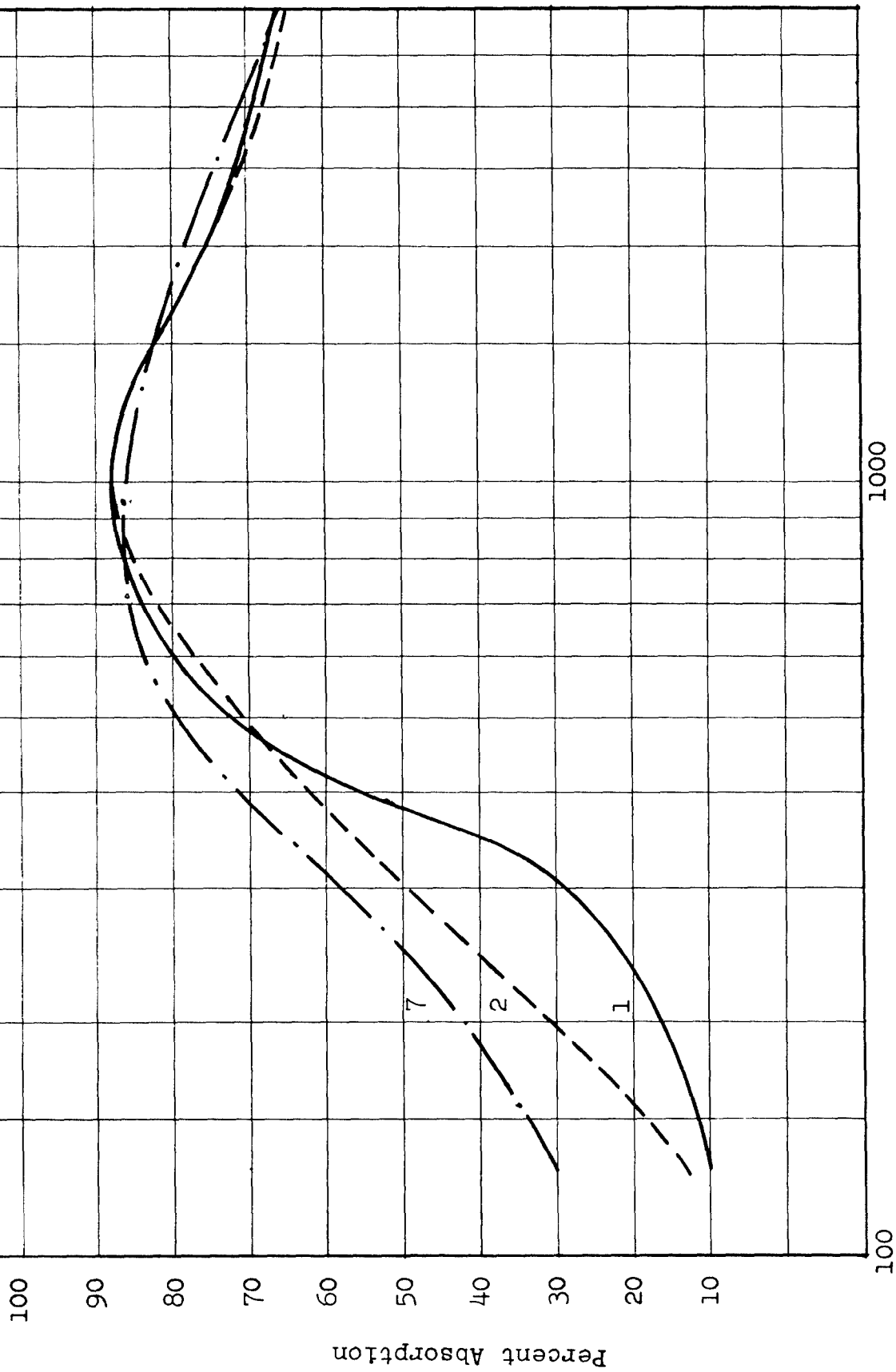
FIGURE 12.1.18

Average AMA chamber absorption coefficients and noise reduction coefficients for 3/4-inch perforated tiles on standard mountings 1, 2, and 7.

Percent Absorption

100

1000

100

90

80

70

60

50

40

30

20

10

7

2

1
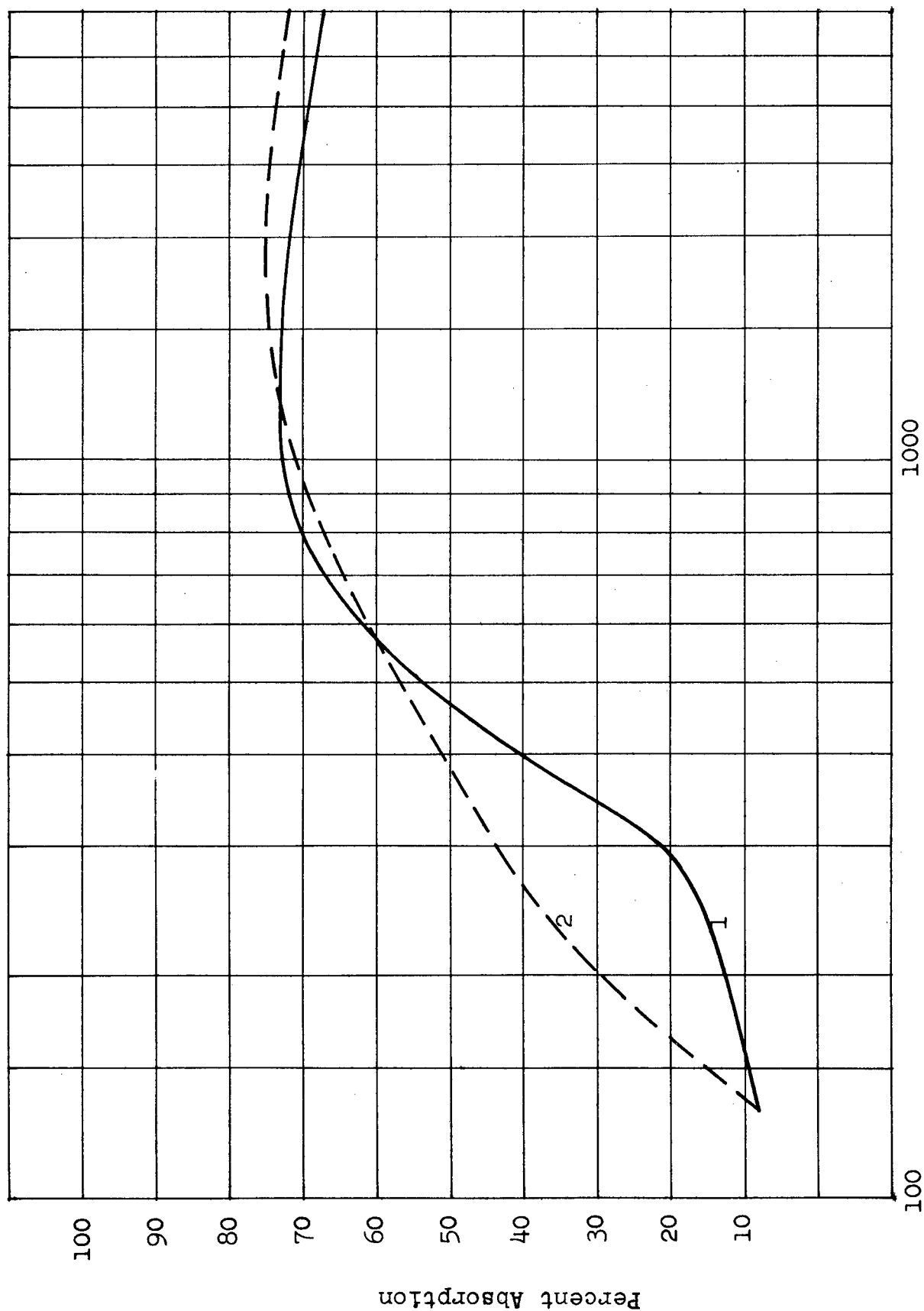
Frequency cycles/second

FIGURE 12.1.19

Average AMA chamber absorption coefficients and noise reduction coefficients for 1/2 -inch perforated tiles on standard mountings 1 and 2.

References:

(1.1) Morse, P.M., and Bolt, R. H., "Sound Waves in Rooms," Rev. Mod. Phys. 16, 69-150 (1944).

(1.2) Beranek, L. L., Acoustic Measurements, J. Wiley and Sons (1949).

(1.3) Zwikker, C. and Kosten, C. W., Sound Absorbing Materials, Elsevier Publishing Co., Inc. (1949).

(1.4) Knudsen, V. O. and Harris, C. M., Acoustical Designing in Architecture, J. Wiley and Sons (1950) Chaps. 6-8 and App.1.

(1.5) Sabine, W. C. Collected Papers on Acoustics Harvard University Press (1927).

(1.6) Acoustical Materials Association, Bulletin XIII, Sound Absorption Coefficients of Architectural Acoustical Materials, Acous. Mats. Assn., 59 E. 55th St., New York (1951).

(1.7) Beranek, L. L., "Acoustic Impedance of Commercial Materials and the Performance of Rectangular Rooms with One Treated Surface," J. Acous. Soc. Am 12, 14-23 (1940).

(1.8) Beranek, L. L., "Acoustic Impedance of Porous Materials," J. Acous. Soc. Am 13, 248-260 (1942).

(1.9) Beranek, L. L., "Acoustical Properties of Homogeneous, Isotropic Rigid Tiles and Flexible Blankets," J. Acous. Soc. Am 19, 556-568 (1947).

(1.10) Bolt, R. H., "On the Design of Perforated Facings for Acoustic Materials," J. Acous. Soc. Am., 19 917-921 (1947).

(1.11) Ingard, U., and Bolt, R. H., "Absorption Characteristics of Acoustic Material with Perforated Facings," J. Acous. Soc. Am., 23, 533-540 (1951).

(1.12)   Morse, P.M., <u>Vibration and Sound</u>, McGraw-Hill
Book Co., Inc. New York (1952), pp. 247-278.

(1.13)   Ferrero, M. A. and Sacerdote, G. G., "Parameters
of Sound Propagation in Granular Absorbent
Materials," Acustica <u>1</u>, 137-142 (1951).

(1.14)   Esmail-Begui, Z. and Naylor, T. K., "Measurement
of the Propagation of Sound in Fiberglas," J. Acous.
Soc. Am. <u>25</u>, 87-91 (1953).

12.2 Lined Ducts

A lined duct consists of a set of walls, usually assumed to be acoustically rigid and impervious, covered with an absorbent material which surrounds a channel or space of uniform section. This is shown in Fig. 12.2.1. The absorbent lining is usually a porous acoustical material, but it may also include a facing and an air layer. The passage is the central open section through which air can flow. The important dimensions for design discussions are the lining thickness, the width or widths of the passage (measured between lining surfaces,) and the total length. In the case of a circular duct, the diameter of the open section will be considered the effective passage width.
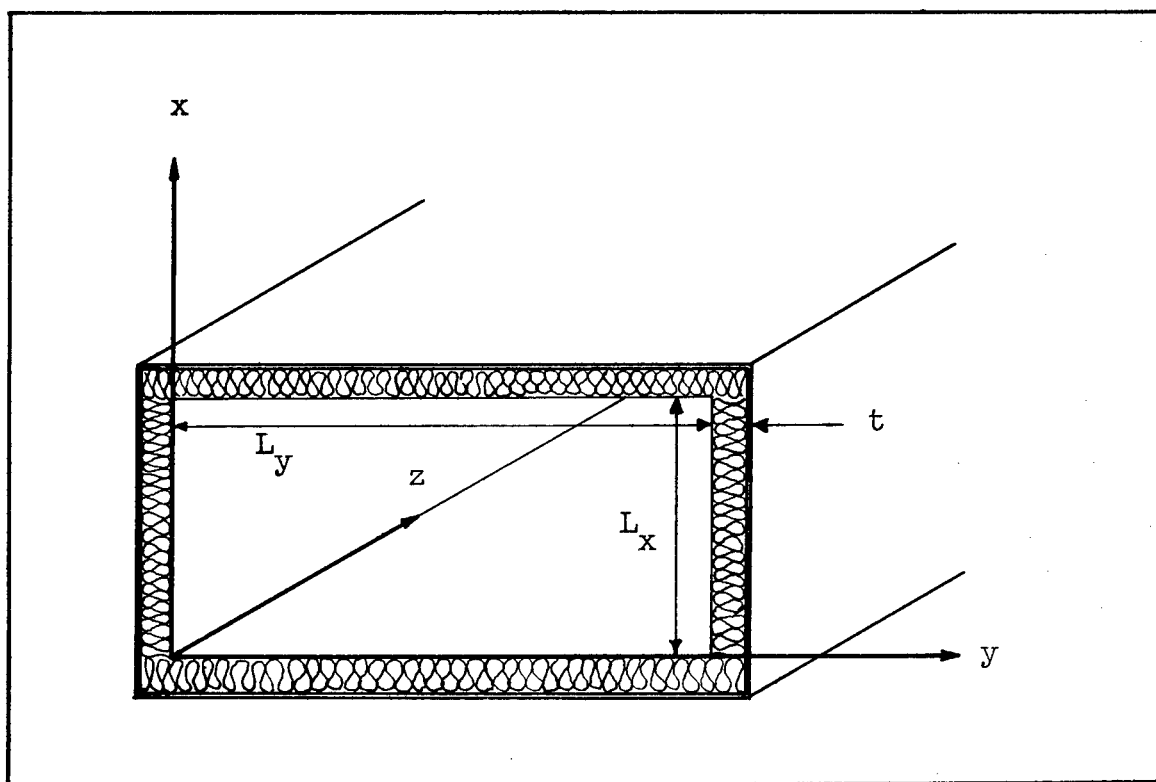
FIGURE 12.2.1

Sketch showing geometry of rectangular lined duct, and coordinates used in analysis.

A lined duct is usually designed to have an attenuation-frequency characteristic possessing a broad maximum. The frequency of the maximum is governed both by the passage dimensions and by the properties of the lining. In most practical cases, the condition of maximum attenuation is realized when the wavelength of sound is of the order of the smaller passage width. The frequency of maximum attenuation can be lowered somewhat by increasing the lining thickness. For this reason, the lining sometimes consists of a layer of porous material (e.g., mineral wool or glass fiber blanket) which is separated by an air space from the enclosure wall. This arrangement economically increases the effective depth of the lining for a given amount of acoustical material.

Qualitative Discussion of Attenuation in Ducts. The acoustic attenuation of a lined duct is the result of conversion of acoustical energy into heat in the absorbing layer. This energy absorption is most readily discussed for the case in which the lining reacts locally with the sound wave. Local reaction means that there is no important transmission of waves within or behind the absorbing material, in the direction parallel to the duct axis. Such wave transmission may materially reduce the attenuation of sound in the duct; therefore, in all applications to be discussed, it is assumed that local reaction approximation is valid. In order to prevent longitudinal wave motion in an air space behind the lining, it is necessary to insert rigid partitions which are perpendicular to the duct axis. Successive partitions should be spaced by about one tenth of the wavelength at which maximum attenuation is obtained. When the lining extends to the wall without an air space, lateral partitioning is usually unnecessary because of the large attenuation of sound in the lining material.

The duct lining may be characterized by its normal specific acoustic impedance, which is the ratio of acoustic pressure to particle velocity normal to the surface. For the case of local reaction, the normal specific acoustic impedance is independent of the angle of incidence and hence is the same for all directions which the incident wave in the duct may have with respect to the lining.

The normal impedance of the lining usually contains a resistive term, so that there is a component of the normal

particle velocity at the lining surface which is in phase
with the pressure. Thus, power is delivered to the lining
at a rate proportional to the product of acoustic pressure
and the in-phase particle velocity. Physically, this
power is transformed into heat due to both viscous friction
within the lining and compression by the acoustic wave of
the gas contained within the lining.

The simplest analysis of duct action is obtained if
it is assumed that the acoustic pressure is uniform across
the open portion of the duct. It is then an easy matter
to compute the effects of air flow into the lining, and to
find the attenuation of sound in the duct.

The uniform-pressure assumption is always reasonable
(though not rigorous) for the special case in which the
wavelength of sound is greater than the narrowest passage
width, and at the same time the absorption coefficient of
the lining is much less than unity. For this reason, simple,
approximate attenuation formulas obtained from the uniform
pressure treatment are almost always satisfactory in prac
tice for frequencies well below the attenuation peak for
a given duct. Moreover, if the lining has a relatively high
impedance, such simple formulas are valid for frequencies
closely approaching the peak. Since it can be shown that
the low-frequency formulas can be expressed in terms of
the absorption coefficient of the lining, it is not neces-
sary to know the specific acoustic impedance of the lining
for this approximate analysis.

Unfortunately, serious errors may be made by injudi-
cious application of the approximate results obtained with
the uniform plane-wave assumption. If the frequency is
sufficiently high to allow the formation of cross-modes in
the duct, or if the lining has very large absorption, the
acoustic pressure near the lining will be appreciably less
than that at the axis of the duct; in this case the result-
ing attenuation will be less than that computed on the
plane wave assumption.

It is possible to solve the acoustic wave equation
to determine the propagation of sound waves in a duct of
simple shape for any frequency and for any boundary

impedance. The rigorous solution has been relatively
little used, because the practical work is laborious even
with the aid of computational graphs. It is possible,
however, to derive from the wave solution approximate,
limiting formulas which are much more accurate at relatively
high frequencies than the results of the uniform pressure
approximation. A combination of the approximate formulas
obtained by the two methods leads to simplified charts from
which the designer can very quickly form a rough estimate
of the performance of a given duct. Although these charts
(Figs. 12.2.2-6) must be supplemented for precise work by
experimental data and by more elaborate calculations, the
charts and the analysis leading to them are valuable because
they show in a direct way the operation of several of the
important design parameters.

Calculated attenuation values for a certain frequency
should not be expected to apply to a section of duct having
a length less than the wavelength of sound at that frequency.
While it will be shown that end effects of one type (asso-
ciated with cross modes in the duct) will cause the measured
attenuation to exceed calculated values at high frequencies,
other effects (associated with the impedance change at the
duct ends) often cause a relatively short duct to give less
attenuation than the calculated value.

The behavior of ducts in the frequency range of
maximum attenuation cannot be treated by simple formulas,
for the various approximations fail in this range. A further
difficulty in practice, for frequencies in and above this
range, is that sound can be carried through the duct by
various modes of propagation; not only by the principal,
or axial wave, but by oblique waves which are, in a sense,
reflected back and forth between the duct walls. The

Figure 12.2.2

Approximate design chart for attenuation in rectangular duct
lined on two opposite walls with a porous layer of known flow
resistance. For a given value of the flow resistance parameter
θ, the attenuation curve for low, mid and high frequencies is
given by three line segments, representing respectively Eqs.
(12.2.25), (12.2.26), and (12.2.24). Broken lines show where
the first approximation is extended beyond nominal limit of
validity. Arrow on horizontal axis shows the nominal lower
limit of validity for the second approximation. Entire chart
is for $(t/\ell_x) = 0.2$.
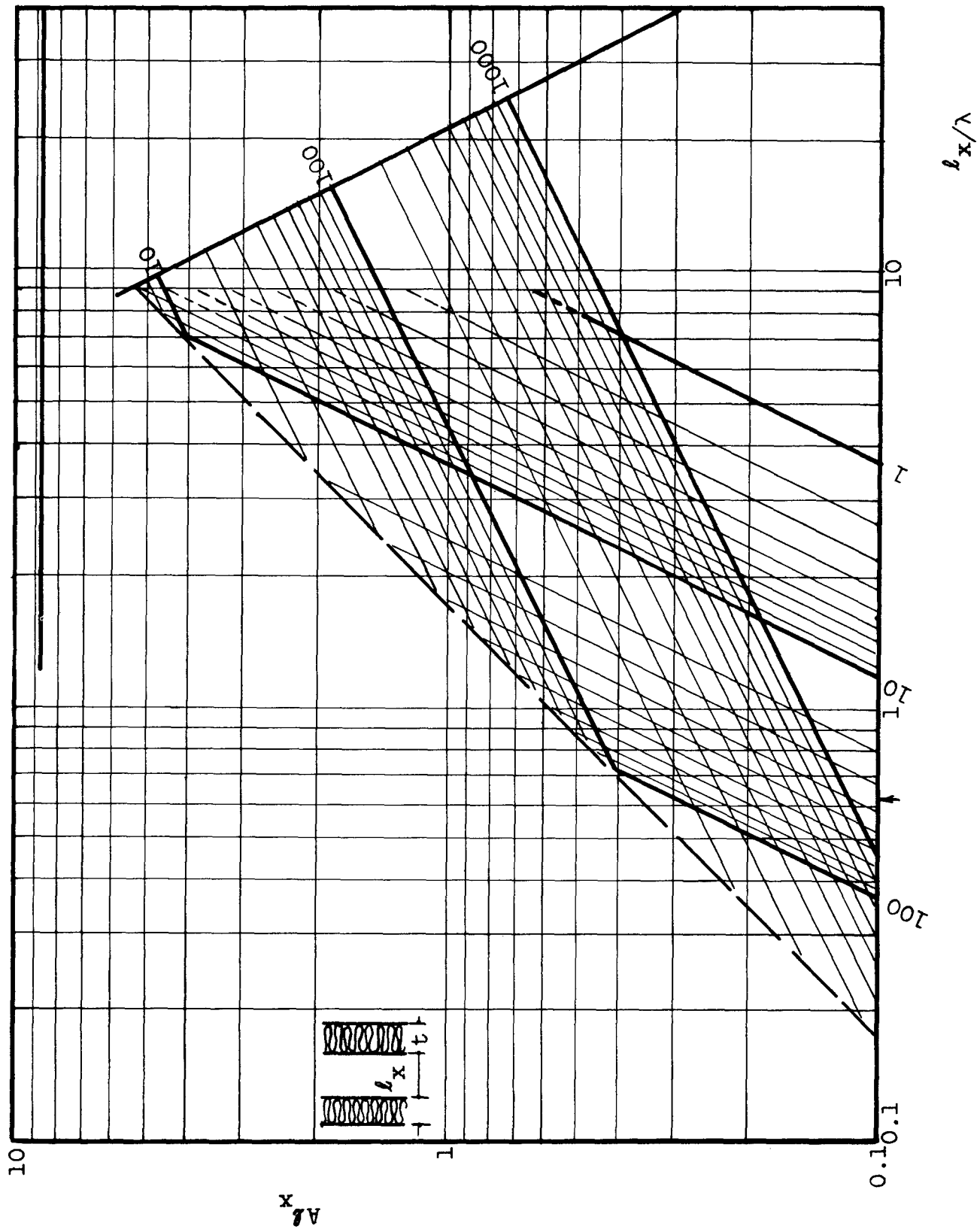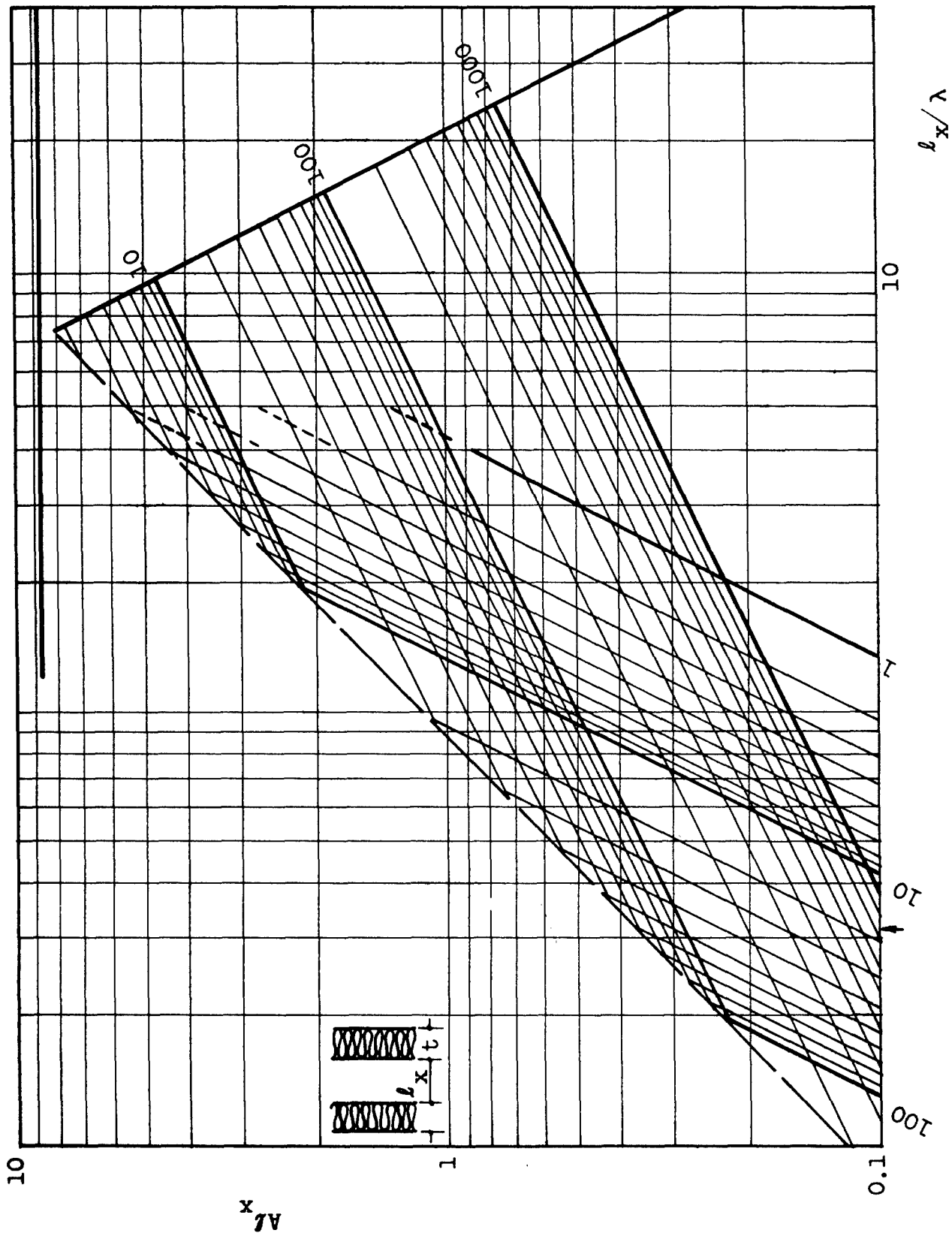
attenuation is greater for the higher modes (oblique waves) than for the principal waves. Thus if a large portion of the acoustical energy is carried in the higher modes, the attenuation will be greater than that predicted by calculation, since calculations are ordinarily made for the principal wave.

In principle, acoustical theory would permit calculation of the distribution of the energy among the various modes of travel, but in practice this calculation is almost never feasible. To make the calculation requires much more detailed information about the acoustical field near the sound source than is ordinarily available. For these reasons, considerable use is made of experimental data for frequencies in or above the range of the attenuation peak.

The remainder of this section contains brief derivations of the simplified attenuation formulas based on both the uniform pressure approximation and the wave-theory treatment; design charts summarizing the results from these approximations and additional charts based on typical experimental data are given.

Quantitative Treatment Under the Uniform Pressure Assumption. The expression for a unidirectional plane wave traveling in the positive x direction contains the space factor $\exp(-jkx)$, where k is the propagation constant and x is the distance coordinate. For sound waves in a lossless

---

Figure 12.2.3

Approximate design chart for attenuation in rectangular duct lined on two opposite walls with a porous layer of known flow resistance. For a given value of the flow resistance parameter θ, the attenuation curve for low, mid and high frequencies is given by three line segments, representing respectively Eqs. (12.2.25), (12.2.26), and (12.2.24). Broken lines show where the first approximation is extended beyond nominal limit of validity. Arrow on horizontal axis shows the nominal lower limit of validity for the second approximation. Entire chart is for $(t/\ell_x) = 0.4$.

tube (or in open air) the propagation constant* is given very closely by:

$$k = \frac{\omega}{c} = \frac{2\pi}{\lambda} = \omega (K \rho)^{1/2} \quad , \qquad (12.2.1)$$

where K is the compressibility of air, ρ is the density, c is the speed of sound in air, and ω is radian frequency. When the rigid boundary of the lossless tube is replaced by a non-rigid boundary, (the duct lining), the moving mass is not changed as far as the wave motion is concerned, but the effective compressibility is changed by the flow of air into the lining. This effect is conveniently expressed in terms of the admittance index of the lining, η , which is equal to the reciprocal of the impedance index. (See Sec. 12.1). The effective compressibility is defined as $K' = (1/p)(dV/V)$, where dV is the change of volume for an initial volume V, under the excess pressure p.

The passage area of the duct will be denoted by A, and the total perimeter by P. If a sinusoidal excess pressure p is applied across a length dx of the duct, the volume of air inflow is that due to the compressibility of the gas in the passage which is pKA dx, plus that due to the flow into the lining, which is $pP \eta$ dx/($- j \omega \rho$ c). If the

---

* The term <u>propagation constant</u> is used in the literature in some cases to denote k and in some cases to denote the complete coefficient of x, which is -jk.

Figure 12.2.4

Approximate design chart for attenuation in rectangular duct lined on two opposite walls with a porous layer of known flow resistance. For a given value of the flow resistance parameter θ, the attenuation curve for low, mid and high frequencies is given by three line segments, representing respectively Eqs. (12.2.25), (12.2.26), and (12.2.24). Broken lines show where the first approximation is extended beyond nominal limit of validity. Arrow on horizontal axis shows the nominal lower limit of validity for the second approximation. Entire chart is for t/λ_x) = 0.6.
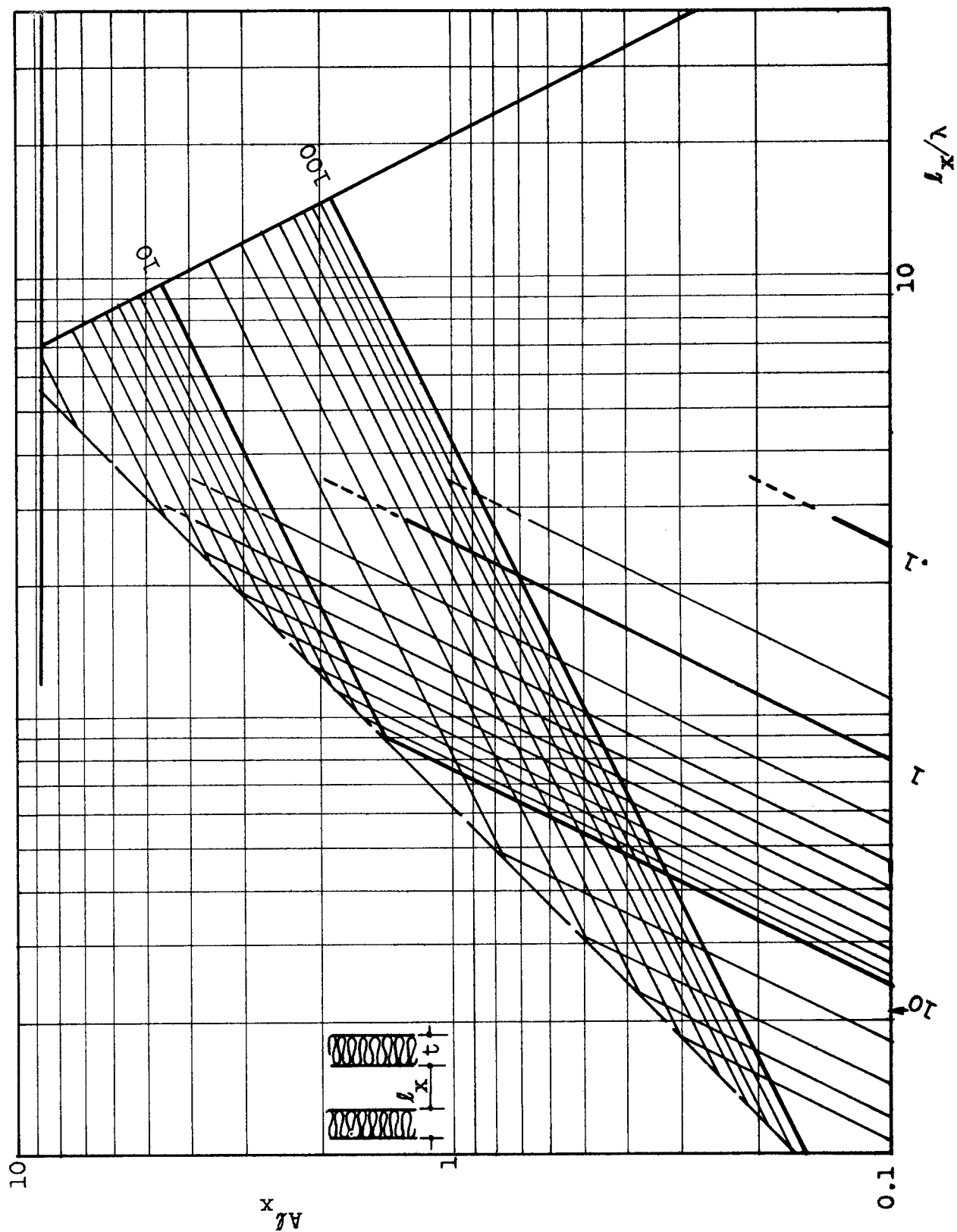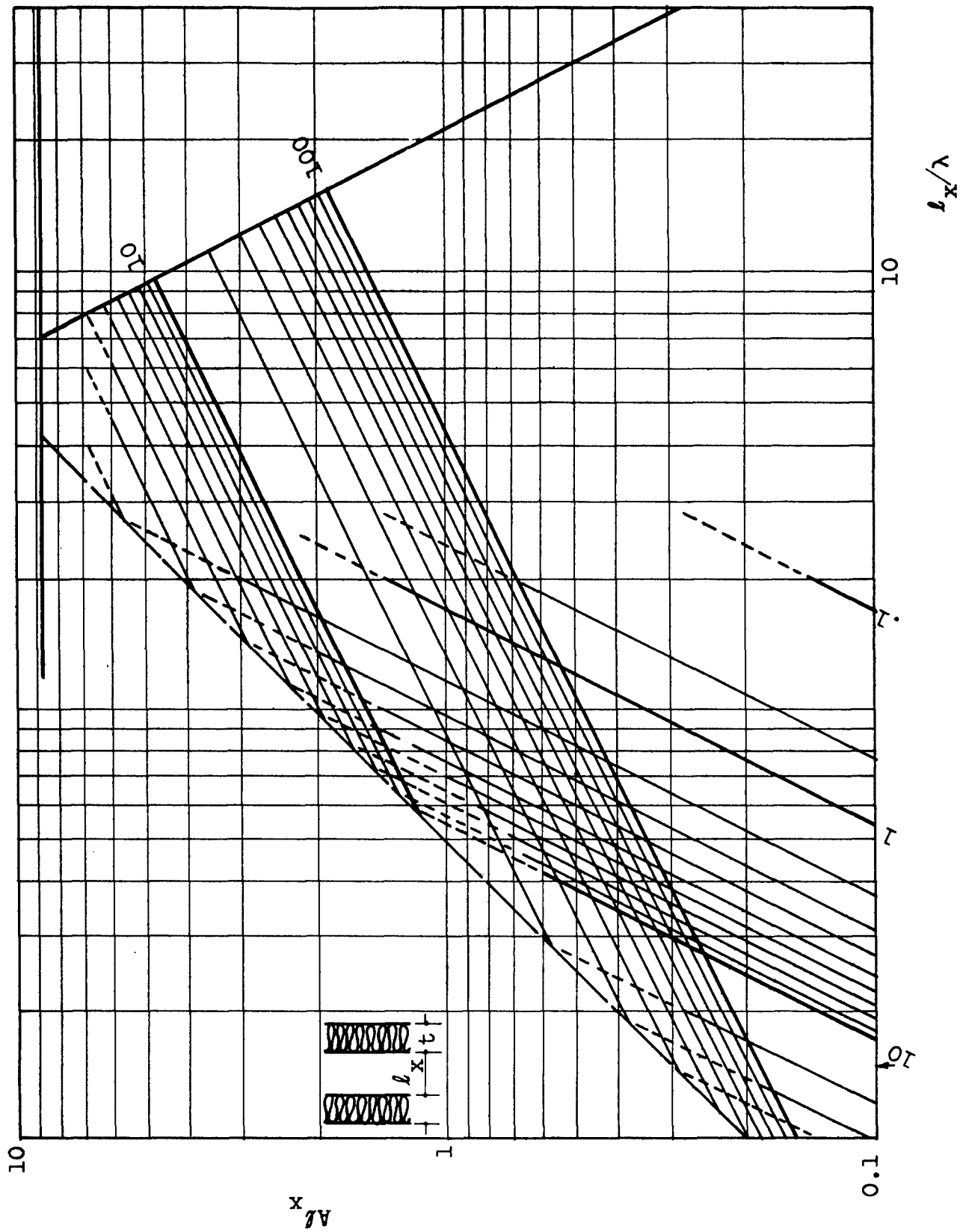
definition of the compressibility is now applied, where the volume of gas in the section is V = Adx, it is found that the effective compressibility is:

$$K' = K + \frac{P\eta}{-j\omega\rho cA} \quad . \quad (12.2.2)$$

The propagation constant for the lined duct is then computed by substituting (12.2.2) into (12.2.1). By standard wave theory, the attenuation constant is equal to the negative of the imaginary part of the propagation constant and the attenuation σ in db per unit length is 8.69 times as great, so that

$$\sigma = -8.69 \, \mathrm{Im}\left(k\sqrt{1 - \frac{\eta}{jkL}}\right). \quad (12.2.3)$$

This is the desired attenuation formula. The quantity L equals the ratio A/P and k is the propagation constant (ω/c) for open air. In case the passage perimeter is not uniformly treated with a single material, the admittance η is given by:

$$\eta = (\eta_1 P_1 + \eta_2 P_2 + \cdots \eta_n P_n)/P \quad (12.2.4)$$

where the length P_1 of the perimeter has the admittance η_1, the length P_2 has the admittance η_2, etc.

Figure 12.2.5

Approximate design chart for attenuation in rectangular duct lined on two opposite walls with a porous layer of known flow resistance. For a given value of the flow resistance parameter Θ, the attenuation curve for low, mid and high frequencies is given by three line segments, representing respectively Eqs. (12.2.25), (12.2.26), and (12.2.24). Broken lines show where the first approximation is extended beyond nominal limit of validity. Arrow on horizontal axis shows the nominal lower limit of validity for the second approximation. Entire chart is for $(t/\ell_x) = 0.8$.

The formula (12.2.3) is a good approximation only for $|\eta| << 1$ (a "hard" wall); otherwise the uniform pressure assumption may be unwarranted. In practice the lining usually has $|\eta| << 1$ for frequencies well below the attenuation maximum. Also, the relation will often be inaccurate for frequencies sufficiently high that the wavelength is less than the narrowest passage width of the duct, for again the pressure is not likely to be uniform.

A further simplification may be made if, in addition to the condition $|\eta| << 1$, the condition $|\eta| >> kL$ is realized*. Then the radical in (12.2.3) may be expanded to give the

---

*   It can be shown for ordinary tiles and blankets that this condition is substantially equivalent to requiring that the lining thickness be much less than L.


Figure 12.2.6

Approximate design chart for attenuation in rectangular duct lined on two opposite walls with a porous layer of known flow resistance. For a given value of the flow resistance parameter θ, the attenuation curve for low, mid and high frequencies is given by three line segments, representing respectively Eqs. (12.2.25), (12.2.26), and (12.2.24). Broken lines show where the first approximation is extended beyond nominal limit of validity. Arrow on horizontal axis shows the nominal lower limit of validity for the second approximation. Entire chart is for $(t/\mathcal{l}_x) = 1.0$.
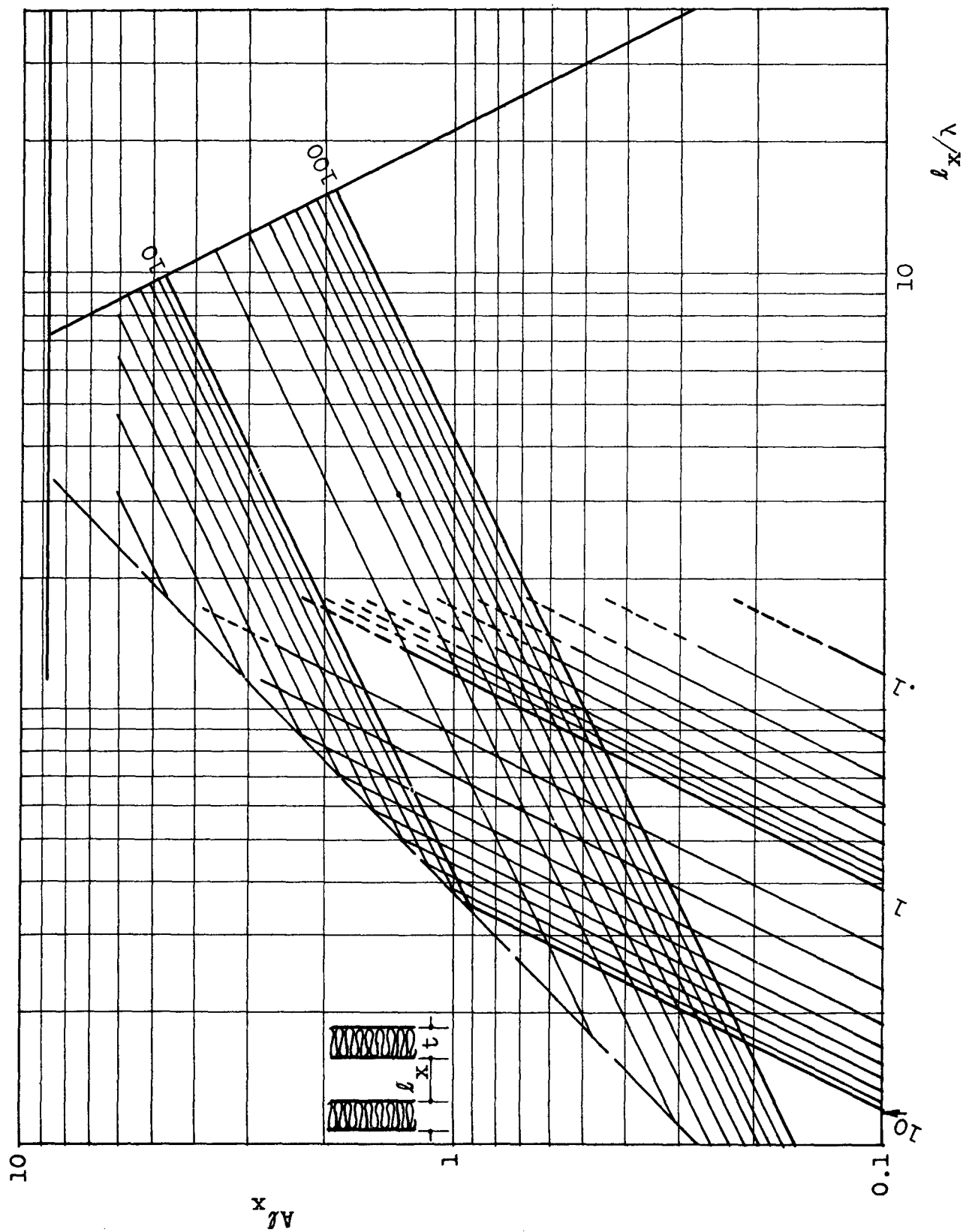
approximate result

$$\sigma L \simeq 4.34\, \mu \text{ db} \qquad (12.2.5)$$

which is a compact expression for the decibel loss in a section of length L. The quantity μ, the conductance ratio, is the real part of η. Another way of writing (12.2.5) is

$$\sigma L \simeq 1.1\, \alpha_\eta \text{ db} \qquad (12.2.6)$$

where α_η is the normal free-wave absorption coefficient of the lining. The expression may be justified by noting that this absorption coefficient is approximately equal to 4μ (Sec. 12.1) provided that $|\eta| << 1$, which is a condition already assumed.

The approximate expressions for duct attenuation which have been given in the literature are generally similar to (12.2.3), (12.2.5) or (12.2.6). These expressions give useful results within their limitations. Equation (12.2.6) is less accurate than the former two relations, and always predicts smaller values of the attenuation than are measured experimentally.

Special attention should be given to an empirical expression, comparable to Eq. (12.2.6), which was used by Sabine 2.1/. In the present notation, it may be written*

$$\sigma L = 1.05\, \bar{\alpha}^{1.4} \qquad (12.2.6a)$$

where α is the chamber absorption coefficient of the lining as ordinarily reported by acoustical materials manufacturers. This relation applies to a duct uniformly lined on all sides. While no theoretical justification for the exponent 1.4 is provided, it appears that this compensates approximately for both the differences between free-wave normal absorption coefficients and chamber coefficients,

---

* The original form is (db/ft) $12.6\, \alpha^{1.4}(P/A)$, where P and A are expressed in inches and square inches respectively.

and for the errors of approximation inherent in a formula of the nature of (12.2.6) as the absorption coefficient increases with increasing frequency. Sabine showed that (12.2.6a) is approximately in agreement with experimental attenuation measurements up to frequencies of 2000 cps for six ducts whose open dimensions were combinations of 9, 12 and 18 inches. These ducts were lined with rigid mineral wool one inch deep. According to Beranek's interpretation 2.2/ of the Sabine experiments, the value of $|\eta|$ did not exceed 0.3; hence it may be considered that (12.2.6a) was verified for $|\eta| << 1$. Beranek further showed that (12.2.6a) was in approximate agreement with rigorous calculations from wave theory, under the stated conditions, and showed that the formula should not be applied if the duct shape is far removed from square. This approximate relation has been widely used in attenuation calculations for ventilating ducts, and is to be recommended when used within its limitations. Practically, it is advisable to restrict application to cases where the long passage-width is not greater than twice the short passage-width.

Special Expressions for Boundary Consisting of a Porous Layer. The relations developed above convey no clear idea of the manner in which the attenuation will vary with frequency in a practical case. The frequency dependence comes about in part through the behavior of the admittance index, η , and this can be stated only when the nature of the lining is specified. In many cases, however, the lining consists of a porous layer; i.e., a homogeneous acoustical blanket or tile. Consequently, it will be helpful to analyze this common case in detail by utilizing available theory for the porous layer (Sec. 12.1). The resulting expressions will enable one to predict the frequency dependence to be expected in certain special cases, even though complete experimental admittance or absorption measurements for the lining are not available. The symbols which will be used in discussing the porous lining are listed below:

m   structure factor

t   layer thickness

h   porosity

ϱ density of air

r   specific flow resistance of the lining material

$$k_1 = k[h(m - jr/\rho\omega)]^{1/2} \text{(Propagation constant in porous lining)}$$

$$Z_1 = c[(m - jr/\rho\omega)/h]^{1/2} \text{(Characteristic impedance of lining material)}$$

$$\theta = rL/\rho c$$

c speed of sound in air

k propagation constant in air

L ratio of passage area to passage perimeter

By the theory of absorbing materials (Sec. 12.1), the admittance of the layer is

$$\eta = (\rho c/Z_1)\tanh(jk_1t). \tag{12.2.7}$$

This expression may be replaced in certain regions of frequency by suitable approximations. First, a low-frequency region may be defined by $|k_1t| \ll 1$. For frequencies in this region, the hyperbolic tangent in Eq. (12.2.7) may be replaced to good accuracy by the first two terms in a series expansion. When this is done, and when the appropriate approximations for k_1 and Z_1 are introduced, (12.2.7) becomes

$$\eta \simeq \frac{1}{3}h^2\theta(kL)^2\left(\frac{t}{L}\right)^3 + jh[kt + \frac{1}{3}mh(kt)^3] . \tag{12.2.8}$$

To obtain the speed of sound in the duct, c', and the attenuation in db per unit length, σ, it is necessary to use the standard relations of wave theory, $c' = \omega/\mathrm{Re}(k')$, and $\sigma = -8.69\,\mathrm{Im}(k')$. With the restriction given below in Eq. (12.2.14), Eqs. (12.2.1) and (12.2.2) can be expanded to give the simple relations

$$c' \simeq c/[1 + \frac{\mathrm{Im}(\eta)}{kL}]^{1/2} \tag{12.2.9}$$

$$\sigma \simeq 4.34\,\mathrm{Re}(\eta)/L[1 + \frac{\mathrm{Im}(\eta)}{kL}]^{1/2}. \tag{12.2.10}$$

Combination of these relations with (12.2.8) gives the following low-frequency equations for the phase velocity of sound, and for the db attenuation in a length L, in a

duct with a porous lining.

$$c' \simeq c/[1 + \frac{ht}{L}]^{1/2} \qquad (12.2.11)$$

$$\sigma L \simeq 1.45 \, h^2 \theta (kL)^2 (\frac{t}{L})^3 / [1 + \frac{ht}{L}]^{1/2} \qquad (12.2.12)$$

The restrictions imposed in deriving these approximate relations are summarized in the two relations:

$$(kL)^2 << \frac{L^2}{m^2 h^2 t^2} - \frac{\theta^2}{m^2} \qquad (12.2.13)$$

$$kL << \frac{3}{\theta} (\frac{L}{t})^3 \frac{1 + \frac{ht}{L}}{h^2} \, . \qquad (12.2.14)$$

The first of these expresses the condition $|k_1 t| << 1$, while the second expresses the condition $Re(\eta)/kL(1 + ht/L) << 1$, which allowed the radical in (12.2.1) to be approximated. In Eq. (12.2.12), θ is the flow resistance parameter $rL/\rho c$, while kL is the frequency parameter.

Another range of approximation for the duct lined with porous material, still under the uniform-pressure assumption, is obtained when the lining may be regarded as a "thick layer." The "thick-layer" condition means that the porous lining is sufficiently thick that any wave motion, entering the lining perpendicularly, will be so highly attenuated after experiencing reflection at the duct wall and then completing a round trip in the lining layer that the energy returned to the surface is negligible. There is not necessarily any frequency range in which the wavelength is short enough for this assumption to be applicable and in which also the uniform pressure assumption is applicable, but in a number of cases of practical interest such a range does exist. The "thick layer" condition, as described above, may be defined in terms of the attenuation constant for

wave motion in the porous material, which is $-\text{Im}(k_1)$; a reasonable definition for the thick-layer condition is $t > 1/-\text{Im}(k_1)$. For porous materials likely to be chosen in practice, this is <u>roughly</u> equivalent to saying that the lining thickness <u>must</u> exceed one-eighth the wavelength of sound in air.

The quantitative significance of the thick-layer condition is that the admittance of the thick layer is closely equal to Z_1^{-1}. The expression for Z_1 has already been given; it is evident that this expression is a radical which can be expanded in one form if the frequency parameter kL is much less that θ/m, and in another form if the reverse holds. The low frequency condition (that is, $kL \ll \theta/m$) will be assumed. The admittance for this condition is approximately

$$\eta \simeq (1 + j) (hkL/2\theta)^{1/2} . \qquad (12.2.15)$$

This value for the admittance is put into Eq. (12.2.3) to give the attenuation. It will be assumed that the frequency and the flow resistance are sufficiently large that $(2kL\theta/h)$ is much greater than unity. Then, approximately, the attenuation in db per length L is given by Eq. (12.2.16).

$$\sigma L \simeq 3.1 (hkL/\theta)^{1/2} . \qquad (12.2.16)$$

The assumptions made in obtaining this relation are:

$$t > \frac{1}{-\text{Im}(k_1)} , \text{ or roughly } t > \lambda/8$$

$$mkL/\theta >> 1$$

$$2kL\theta/h >> 1$$

Uniform pressure across the duct opening.

Although these special conditions are not found over any appreciable range of frequencies in a practical design, Eq. (12.2.16) gives useful information regarding the frequency dependence of the attenuation in a duct with porous

lining. This equation shows that the attenuation is proportional to the square root of the frequency, while in the low frequency range, according to Eq. (12.2.12), the attenuation increases with the square of the frequency.

Finally, in the thick-layer approximation and at sufficiently high frequencies, it is found that Z_1 is approximately equal to $\rho c \sqrt{m/h}$. The criterion for this range is $kL \gg \theta/m$. The attenuation per length L is approximately

$$\sigma L \simeq 4.34 \sqrt{h/m} \quad db. \tag{12.2.17}$$

This limiting formula will almost never apply in practical cases because uniform pressure is not found ordinarily in the frequency range for which it is valid. Its importance is that it seems to represent an upper limit, not normally attainable, for the attenuation in a duct with porous lining.

The uniform-pressure approximation has been discussed in the literature by Bosquet, Sivian, and Willms 2.3,2.4,2.5/.

Quantitative Treatment by Wave Theory. The rigorous treatment of wave propagation in a duct is restricted to ducts whose cross-section is of simple shape. A rectangular section (Fig. 12.2.1) is assumed for the present discussion. The solution to the acoustic wave equation for the rectangular duct may be written, for a sinusoidal wave, as

$$p = X(x) \ Y(y) \ Z(z) \ e^{j\omega t}$$

where

$$X(x) = \cosh(-jk_x x + \psi_x)$$

$$Y(y) = \cosh(jk_y y + \psi_y)$$

$$Z(z) = e^{-jk_z z}. \tag{12.2.18}$$

The propagation constants must obey the relation

$$k_x^2 + k_y^2 + k_z^2 = k^2. \tag{12.2.19}$$

To determine the attenuation, $Im(k_z)$ must be found. Basically, the solution is obtained by finding k_x and k_y, each of which is determined by the frequency and by the impedances on one pair of walls, and then by computing k_z

from (12.2.19). The relation giving k_x, for example, is

$$-jk_x \ell_x = \coth^{-1}\left(\frac{k_x}{k\,\eta_{1x}}\right) + \coth^{-1}\left(\frac{k_x}{k\,\eta_{2x}}\right), \quad (12.2.20)$$

where ℓ_x is the passage width in the x direction, η_{1x} is the admittance of the wall at x = 0, and η_{2x} is the admittance of the wall at x = ℓ_x. A similar relation holds for k_y.

In general there is no simple calculation procedure for solving Eq. (12.2.20). Morse has discussed a graphical method of solution 2.8,2.9/. This method is recommended for accurate work, but it is time-consuming and is sufficiently complicated that it permits little insight into the relationships between the properties of the lining and the acoustical performance of the duct. For low frequencies or for sufficiently high frequencies, approximate formulas may be derived by expanding (12.2.20) in series form, by procedures which have been given by Morse in connection with the problem of sound waves in rooms 2.10/

The low-frequency series approximation for Eq. (12.2.20) gives

$$-(k_x \ell_x)^2 \simeq -jk\,\ell_x(\eta_{1x} + \eta_{2x}). \quad (12.2.21)$$

This is a good approximation if both $|\,k\,\ell_x\,\eta_{1x}\,|$ and $|\,k\,\ell_x\,\eta_{2x}\,|$ are less than unity. The equation in the above form shows the additive effect, at low frequencies, of the treatments on opposite walls. Henceforth, for simplicity, it will be assumed that all of the lining material has the same admittance, so that $\eta_{1x} = \eta_{2x} = \eta$. A similar approximate equation can be derived for the effect of the linings on the walls y = 0 and y = ℓ_y. If the attenuation is then found from Eq. (12.2.19), the result for a square duct is, to the approximations employed, the same as that already obtained at low frequencies with the uniform pressure assumption.

Of more interest, however, is information regarding the attenuation of oblique waves (higher order modes) which can be obtained from the wave theory but which cannot be obtained using the uniform-pressure approximation.

A case involving higher order modes is obtained by letting the dimension ℓ_y be considerably greater than ℓ_x, such

that $\underline{m}$ pressure nodes exist between the floor and ceiling of the duct ($y = 0$ and $y = \ell_y$). For simplicity, the floor and ceiling are considered to be non-absorbing. Then the y-axis wave constant is given by $k_y \ell_y = m\pi$. The attenuation constant, equal to $-\text{Im}(k_z)$, is computed from (12.2.19). The result is

$$\sigma\ell_x = -\text{Im}[(k\ell_x)^2 - (\frac{\ell_x}{\ell_y})^2(m\pi)^2 - j2\eta k\ell_x]^{1/2}. \quad (12.2.22)$$

It is still assumed that $|k\ell_x \eta|$ is less than unity. The term $-(\ell_x/\ell_y)^2 (m\pi)^2$ makes a large contribution to the imaginary part of the expression, and therefore to the attenuation. Thus the attenuation for higher modes ($m > 0$) is in general greater than that for the principal wave. The case treated here (long, narrow opening) is most nearly related to the practical situation found in parallel baffles (Sec. 12.3), but qualitatively the behavior of oblique waves is the same in all duct problems.

Experimentally, when a large part of the energy is carried into the duct in the form of oblique waves, these higher modes have the effect of making the total attenuation exceed the calculated value, which ordinarily refers to the principal wave. There may be a region just inside the source end of the duct where the signal level drops more rapidly with distance than is the case further along in the duct. This first region is the one in which the higher modes are rapidly reduced. It follows that if the duct is relatively short, so that this first region occupies a large fraction of the length, the reported attenuation per unit length may be considerably greater than the principal-wave value. Since there is ordinarily no practical way to calculate how much of the acoustical energy will be carried by the higher modes this effect can only be estimated on the basis of past experience with particular structures and sound sources. The effect is usually significant only for frequencies above that where the attenuation peak for the principal wave occurs.

Other aspects of the low-frequency approximation are discussed in the textbook by Morse 2.9/.

From the wave theory viewpoint, the approximate solution for high frequencies is obtained by finding a series expansion for Eq. (12.2.20) which is valid when $k\ell_x \eta \gg 1$.

If, in addition, the frequency is sufficiently high that $k \ell_x >> (n + 1)\pi$, the resulting expression for the attenuation in a duct with two walls lined is

$$\sigma \ell_x \simeq 17.4 \ (n + 1)^2 \ \pi^2 \ \frac{\text{Re} \ ^1\!/\eta}{(k \ell_x)^2} \quad . \tag{12.2.23}$$

Here $\underline{n}$ is the mode number, equal in this case to the number of pressure nodes between $x = 0$ and $x = \ell_x$. Again, the attenuation for the higher modes exceeds that for the principal wave. Most important, the attenuation is inversely proportional to the square of frequency in this high-frequency range. This is the result of an increasing concentration of acoustical energy in the center of the duct at high frequencies, thus reducing the amount of energy absorbed by the lining.

If the duct is lined with a porous material, it is reasonable to expect that the high-frequency form of the thick-layer impedance approximation will apply in this high frequency range. As was the case in (12.2.17), η may be approximated by $\sqrt{h/m}$, so that the principal-wave attenuation in distance ℓ_x for porous linings on two opposite walls is*

$$\sigma \ell_x \simeq \frac{17.4 \pi^2 \sqrt{m/h}}{(k \ell_x)^2} \quad . \tag{12.2.24}$$

The quantity $\sqrt{m/h}$ is roughly equal to unity for most practical porous linings; thus the attenuation at very high frequencies is nearly independent of the material.

Other discussions of the duct from the standpoint of wave theory have been given by Willms 2.5/, Cremer 2.11/ and Scott 2.12/.

---

*   Scott 2.12/ has shown that the high-frequency limiting expression for the attenuation is proportional to $(k \ell_x)^{-3/2}$ rather than to $(k \ell_x)^2$ in the case where the lining is not locally reacting but is instead a wave-propagating medium. It appears that many practical blankets and tiles are not locally reacting at high frequencies and that the Scott result may therefore apply in a number of cases.

Theoretical Design Charts for Duct with Porous Lining.
Figures 12.2.2 through 12.2.6 are a series of design charts
to permit rapid calculation from the approximate formulas
which have been developed for the principal-wave attenuation
in a duct lined with porous material. These charts are
constructed for the case in which only a single pair of
opposite walls is lined, for this arrangement is often pre-
ferred for economy and simplicity over four wall lining.
The effect of lining four walls instead of two is, roughly,
to double the attenuation if the lining thickness is kept
constant. The principal wave attenuation can be as readily
increased by making the lining thicker on two walls as by
covering all four walls, however, so that there is no dis-
tinct advantage in four-wall lining in many practical cases.

In order to use the charts, it is necessary to know
the dimensions of duct and lining, and the specific flow
resistance of the porous material i.e., the flow resistance,
in rayls, for a sample one centimeter thick. The attenuation
is given in terms of $\sigma \ell_x$, the attenuation in db in a dis-
tance equal to the passage width ℓ_x between the lined walls.
In each case, frequency is read from the horizontal scale
in terms of the parameter $\ell_x/\lambda = f\ell_x/c$. Each chart
refers to a single value of the ratio t/ℓ_x (lining thick-
ness t to passage width ℓ_x). On each chart there are a
number of approximate attenuation-frequency curves; each
curve is for a specified value of the flow resistance para-
meter θ_ℓ (where $\theta_\ell = r\ell_x/\rho c$).

An individual attenuation-frequency curve consists of
three straight-line segments on the logarithmic chart.
These segments represent the three frequency ranges already
studied. The low frequency segment of each curve represents
the relation

$$\sigma \ell_x \simeq \frac{2.9h^2\theta_\ell \ (k\ell_x)^2(t/\ell_x)^3}{[1 + 2ht/\ell_x]^{1/2}}, \quad (12.2.25)$$

which is the form taken by Eq. (12.2.12) when two walls
are lined.* In plotting the curves, the porosity $\underline{h}$ has
been taken as unity.

The middle-frequency segment of each curve is given
by

$$\sigma \ell_x \simeq 6.2 \ (hk\ell_x/\theta_\ell \ )^{1/2}. \qquad\qquad (12.2.26$$

This is obtained from Eq. (12.2.16) for the case of two
walls lined. Again $\underline{h}$ has been taken as unity.

The high-frequency segment is identical for all charts
and is given by Eq. (12.2.24), with $\sqrt{m/h}$ taken as unity.

The use of broken lines indicates where one of the
lower two approximations has been extended beyond the range
of validity. The arrow on the horizontal axis of each chart
indicates approximately the lower limit of validity of the
thick-layer assumption, basic to the middle approximation.
In some cases it is necessary to use this approximation
below the limit indicated by the arrow.

The method of approximation used in these charts does
not give a good quantitative description of the attenuation
peak, but the results at low frequencies ($\ell_x/\lambda < 0.2$) and
at high frequencies ($\ell_x/\lambda > 1.5$) are sufficiently accurate
that the attenuation-frequency function as a whole is fairly
well defined.

Experimental Design Curves for Ducts Lined with Porous
Material. Experimental attenuation data, which have been
obtained for a series of ducts under certain conditions likely
to be encountered in practice, are summarized in the form of
a design chart in Fig. 12.2.7. The experimental chart
covers a more restricted range of conditions than do the pre-
ceding charts. However, the experimentally determined curves

---

*   The discussion up to this point has not been concerned with the
    difference between lining only two opposite walls or all four walls.
    However, if only two walls are lined, L is defined as the passage
    area to the lined perimeter. Therefore, for a square passage area
    of length ℓ_x, using this definition $L = \ell_x{}^2/2\ell_x = \ell_x/2.$

where applicable, will prove more detailed and accurate in the range of peak attenuation than those based on the approximate formulas.

The variables plotted on the chart axes are the same as those for the previous charts - db attenuation in a length ℓ_x as a function of ℓ_x/λ , where ℓ_x is the passage width between the treated pair of walls. Each curve is identified by the proper value of t/ℓ_x. The data for these curves were obtained with structures having the Θ values listed below:

Value of t/ℓ_x	Θ
3	1.5
1	3
0.5	4.5
0.25	6
0.1	7.5

These values correspond to a region in which the shape and height of the attenuation peak are not highly sensitive to changes in flow resistance. Therefore these design curves can be applied over an appreciable range of Θ values. Further experimental data, obtained for the case $(t/\ell_x) = 0.25$, indicate that the peak and high-frequency portions of these curves $(\ell_x/\lambda > 0.3)$ are not seriously affected by varying Θ between half the nominal value and four times that value. At low frequencies the attenuation must be approximately proportional to Θ, as indicated by Eq. (12.2.25) and by the previous charts. A full allowance for this effect of varying the flow resistance should be made for frequencies below $\ell_x/\lambda = 0.1$.

The experimentally determined chart represents conservative values for the attenuation per length ℓ_x in ducts having lengths up to 15 ℓ_x. When the duct is relatively short (length less than $4\ell_x$) the observed attenuation per length ℓ_x in the region of the peak may be about 25 per cent greater than that shown by the chart. This discrepancy represents end effects, including the attenuation of higher modes.

The designer who uses the complete theoretical computation charts will discover that certain critical combinations of the parameters will give attenuation as great as 12 db in a length ℓ_x, 2.8/. Unfortunately, the large attenuation given by these critical combinations is usually confined to a very narrow frequency band, and may also be difficult to obtain because of practical variations in flow resistance of the lining and of dimensions in actual construction. The empirical chart of Fig. 12.2.7 shows broad-band attenuation which can be expected without critical design. Because of the effects of higher modes, the effective attenuation in a practical installation, for frequencies above the peak, may be well above the values indicated by this chart.

The results shown in Fig. 12.2.7 are attenuation per length ℓ_x for a duct having effectively infinite length. The experimental measurements show that the end effects in a finite length of duct are approximately explained if a length ℓ_x is imagined to be added to each end of the duct. Therefore, the attenuation for a duct which has an actual length of 3 ℓ_x for example, should be computed as though the length were 5 ℓ_x.

Under the non-critical conditions represented by Fig. 12.2.7, the indicated attenuation can generally be obtained either with two opposite walls lined as indicated, or, in the case of a duct which is not too far from square (ratio of passage widths less than 2:1), with the same

Figure 12.2.7

Attenuation design chart, derived from a set of experimental measurements, for ducts lined on two opposite walls with porous layer of approximately-known flow resistance. Flow resistance is not critical for the conditions shown and results are substantially unchanged when Θ varies from half the indicated values to four times indicated values. The curves may be applied approximately to ducts lined uniformly on all four sides if per cent open area instead of (t/ℓ_x) is used to specify amount of lining. To allow for end effects, add $2\ell_x$ to the actual length of a duct and compute total attenuation from this corrected length.
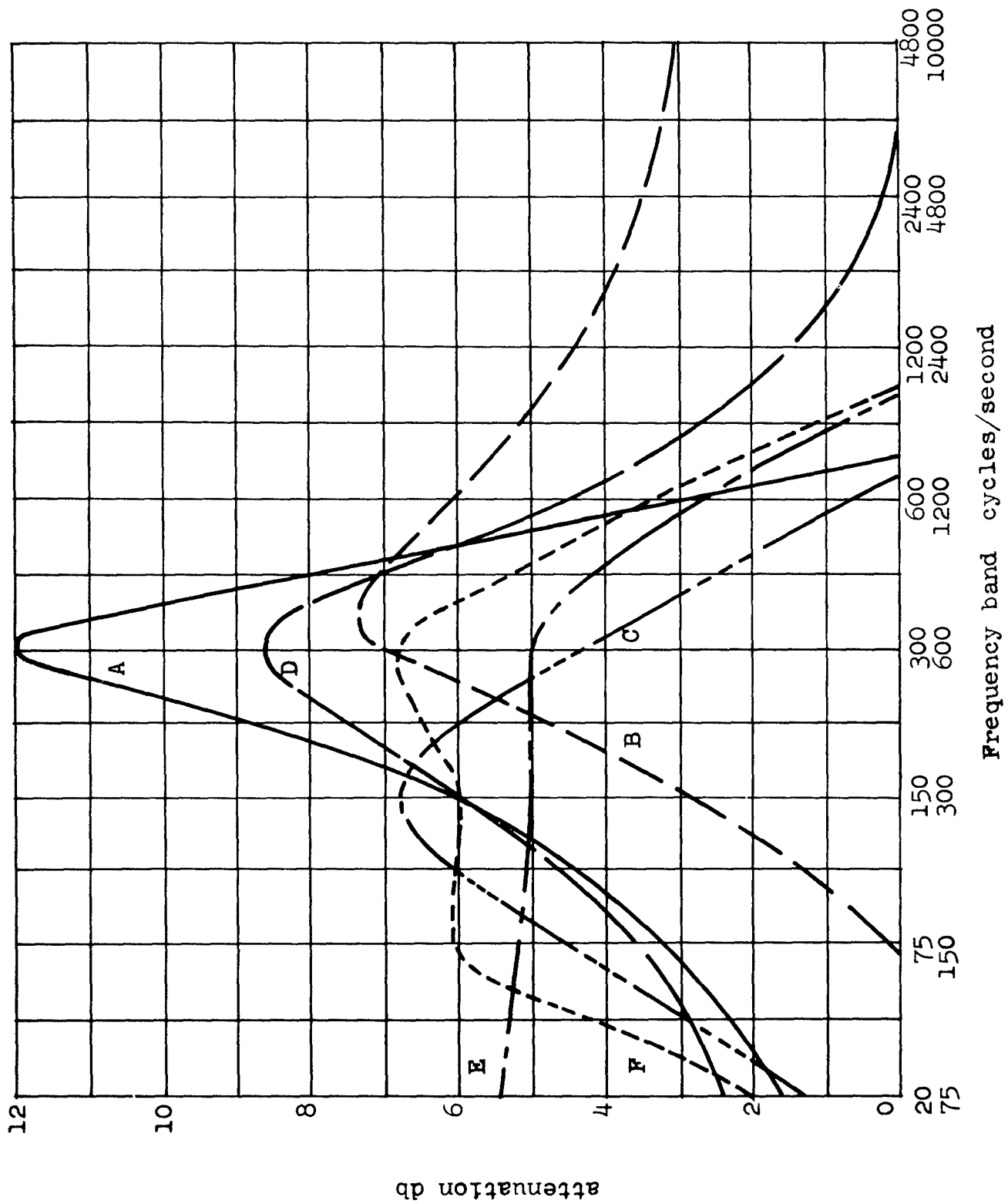
amount of material redistributed to give uniform coverage of all four walls. For this reason, the parameter (t/ℓ_x) can be represented alternatively in terms of per cent of open area, and values of this quantity are indicated beside the curves.

Scaling of Duct Designs. When the designer already has performance data for a duct which is suitable for the intended purpose in all respects except size, the entire design procedure may be replaced by a process of changing the scale of size of the known duct. The proper method for scaling is apparent from the parameters which were used in the design charts. Thus, the attenuation-frequency characteristic, if expressed as $(\sigma \ell_x)$ vs. (ℓ_x/λ), is independent of the physical size of the duct, provided that Θ and (t/ℓ_x) are kept constant as the size is varied. This means that the specific flow resistance of the absorbing material used in the model will be different from that used in the full scale design since $\Theta \sim r L$. When L is decreased, r must be increased by the same factor to keep Θ constant.

When a very costly duct installation is to be designed, it has proved advantageous to perform tests on a model of reduced scale and then to use the principles above to transfer the data to the full-scale case. It is preferable that scaling include length as well as width dimensions, so that a realistic evaluation of end effects will be included. It is also desirable that the sound source used in model tests shall have approximately the relative size, position and directional properties found in the full-scale situation so that the higher modes will be excited in approximately the proper relative amplitudes.

Experimental Results for Specific Installations. Figure 12.2.8 shows experimental attenuation in octave bands for several specific duct installations. Included among these are several designs in which an air space is used behind the lining. Dimensions and design details for the several cases

---

*   Figure 12.2.8

Attenuation as a function of frequency (in octave bands) for the lined duct structures of Table 12.2.1. The vertical scale gives attenuation in decibels for a length of duct equal to the narrower passage width.

are given in Table 12.2.1. The performance data for these designs have proved useful as a basis for scaling.

The performance of structure F illustrates the nature of a disagreement which sometimes occurs between theory and practice. This structure, according to the rigorous wave theory, should have a maximum attenuation of approximately 12 db per width unit of length. The observed attenuation peak has half of this value, and is broader than the computed maximum. This is a case where the theoretical design uses a critical set of values which are not realized because of practical tolerances.

Commercial Mufflers. Prefabricated circular ducts with absorbent linings, usually constructed with heavy steel shells, are available commercially under the generic term "mufflers." Other structures commercially designated as mufflers including resonators as well as absorbent linings, will not be discussed here. The measured attenuation for several commercial mufflers (Maxim and Industrial Sound Control Products) is shown in Fig. 12.2.9. Physical data and dimensions for these mufflers are shown in Table 12.2.2.

Duct with Resonant Lining. The attenuation for a selected band of lower frequencies can be greatly increased by the use of a lining which resonates (has a purely resistive impedance) at the center of that band. This is considered in detail in Sec. 12.7.

Attenuation in Smooth Pipes. Even if the absorbent lining were removed from a duct so that the structure could be considered a smooth pipe, some sound attenuation would remain. This attenuation results from viscous drag of the air at the walls, and from heat loss to the walls. Ordinarily the attenuation resulting from these mechanisms is smaller by orders of magnitude than that in a lined duct and is therefore neglected in duct calculations. Attenuation in smooth pipes is discussed briefly in Sec. 12.15.

Effects of Nonrigid Side Walls. The discussion in this section has assumed that the duct enclosure is formed by

---

Figure 12.2.9

Attenuation as a function of frequency (in octave-bands) for the commercial mufflers of Table 12.2.2.

Frequency band   cycles/second

attenuation for a duct length equal to a duct diameter   db

TABLE 12.2.1

INFORMATION ON DUCTS FOR WHICH ATTENUATION IS GIVEN IN FIG. 12.2.8, MINI-

MUM LENGTHS, 10 FT, MICROPHONE PLACED AT 2 FT INTERVALS FOR ATTENUATION

MEASUREMENTS

Duct	A	B	C	D	E	F
Dimensions of open areas, ft	3.8x12	2.3x30	2.3x30	3x30	10x10	4x4
Number of sides lined	2	2	2	2	4	4
Lining thickness, inches	16	4	6	6	6	2.4
Lining material*	2.5#PF	6#PF	3#PF	3.5#PF	3#PF	5.5#PF
Depth of Air space behind lining, inches	0	0	12	16	24	9.6
Frequency bands for measurement	1/3 octave	octave	octave	octave	pure tone	pure tone
Sound source	Jet engine	Reciprocating engine			pure tone	pure tone

* Linings of PF Fiberglas, figures give density in lb/ft^3.

TABLE 12.2.2

INFORMATION ON COMMERCIAL MUFFLERS FOR WHICH ATTENUATION IS GIVEN IN

FIG. 12.2.9, ALL LENGTHS 15 FT OR GREATER

Muffler	A	B	C	D
Inside diameter, inches	22	36	72	36
Lining thickness, inches	3.5	3.4	5.3	(a) 2 in. (b) 4 in.
Lining material	Copper wool	Copper wool	Copper wool	(a) Monoblock (b) JM-305 PF blanket
Air space behind lining, inches	13	17.5	20	0

(a) layer next to air stream

(b) layer between a and shell

acoustically rigid, impervious walls. This assumption is reasonable for concrete or masonry ducts and usually for metal or wooden ducts with heavy walls. The assumption is not valid for the lower frequencies (several hundred cycles per second and lower), however, in the case of light sheet metal ducts used in ventilation systems. Evidence of the effects of nonrigid walls is found in Sabine's measurements 2.1, 2.2/. Nonrigid walls cause the low-frequency attenuation to exceed calculated values. The amount of this effect cannot be estimated accurately except on the basis of experience with full-scale structures. Furthermore, nonrigid walls radiate sound. In a case where large attenuation is required, side-wall radiation from a light structure may constitute an acoustic leak great enough to negate the attenuation in the duct. The amount of sound transmitted through the duct walls may be estimated using Secs. 11.2 and 11.5.

Summary of Design Methods for Lined Ducts. The tabular summary below shows the applicability of the various design equations and charts which have been presented in this section and will facilitate reference to them. The statements as to restrictions on the uses of the various relations are greatly simplified for compactness in this listing. More accurate statements of the validity conditions have been given in the previous discussion of the individual relations.

The symbols listed and defined below are consistent with the usage in the preceding parts of this section.

λ wavelength of sound in open air

η acoustic admittance ratio of the lining

μ real part of

α chamber absorption coefficient

α_η normal free-wave absorption coefficient

t   thickness of lining

L   passage area divided by passage perimeter

ℓ_x narrowest passage width

A. Design methods for low frequencies - $\lambda > \ell_x$

I. Relations where lining is described by admittance or absorption data

Nature of Data on Lining Material	Use Equation	Further Restrictions
η known	12.2.3	$\lvert\eta\rvert << 1$
μ known	12.2.5	$\lvert\eta\rvert << 1$, and $t << L$
α_η known	12.2.6	$\lvert\eta\rvert << 1$, and $t << L$
α known	12.2.6a	$t << L$ If duct nearly square, results useful for λ as small as one-third of greatest width.

II. Relations where lining is a porous layer of known flow resistance

	12.2.12 or low-frequency segments of Figs. 12.2.2-6	$t < \lambda/10$ and other restrictions; range indicated in Figs. 12.2.2-6
	12.2.16 or middle-frequency segments of Figs 12.2.2-6	$\ell_x < \lambda < 8t$

B. High frequencies - $\ell_x > \lambda$

	12.2.24 or high-frequency segments of Figs. 12.2.2-6	ℓ_x several times λ

C. General theoretical methods - all frequencies - impedance data available for lining. Use method given by Morse 2.8, 2.9/ and discussed by Beranek 2.2/

D. Design from experimentally determined charts - all frequencies - flow resistance of porous lining known very approximately. Use Fig. 12.2.7, where applicable.

E. Design by scaling from specific cases, including instances with air layer behind lining. Flow resistance of materials must be known for scaling. Use scaling principles with Fig. 12.2.8, where these specific designs are applicable.

Note Added in Publication

<u>Simplified Procedure for Duct Calculations by Exact Wave Theory</u>. Cremer 2.13/ has developed charts giving the attenuation coefficient that would be found by solving Eq. (12.2.20) by the rigorous wave theory. While these charts cannot be applied to an arbitrary frequency (except in the frequency ranges far below or above the attenuation peak), they have the advantage of showing in simple form, at certain frequencies, the relation between lining impedance and attenuation. This relation is not apparent in the more general charts of Morse.

The Cremer charts are shown in Figs. 12.2.10-14. The first and last of the series of five charts represent respectively the low-frequency and high-frequency cases corresponding

---

FIGURE 12.2.10

This chart gives $F\beta$ as a function of ϕ and $|\zeta|/F$. F is a frequency parameter equal to $2\ell_x/N\lambda$, ϕ is the phase angle of the normalized impedance ζ and $|\zeta|$ is the magnitude of the normalized impedance; β is the attenuation parameter, defined as $1/2\pi$ times the duct attenuation in nepers per wavelength. This chart is valid for low frequencies.

F = 0

$\beta F = 0,1$

0,2

0,3

0,4

0,6

0,5

$\dfrac{|\xi|}{F}$

$\longrightarrow \varphi°/13,2$

F = 0,25

βF = 0,1

0,2

0,3

0,6

0,5

0,4

$\dfrac{|\zeta|}{F}$

$\longrightarrow \varphi^\circ / 13,2$
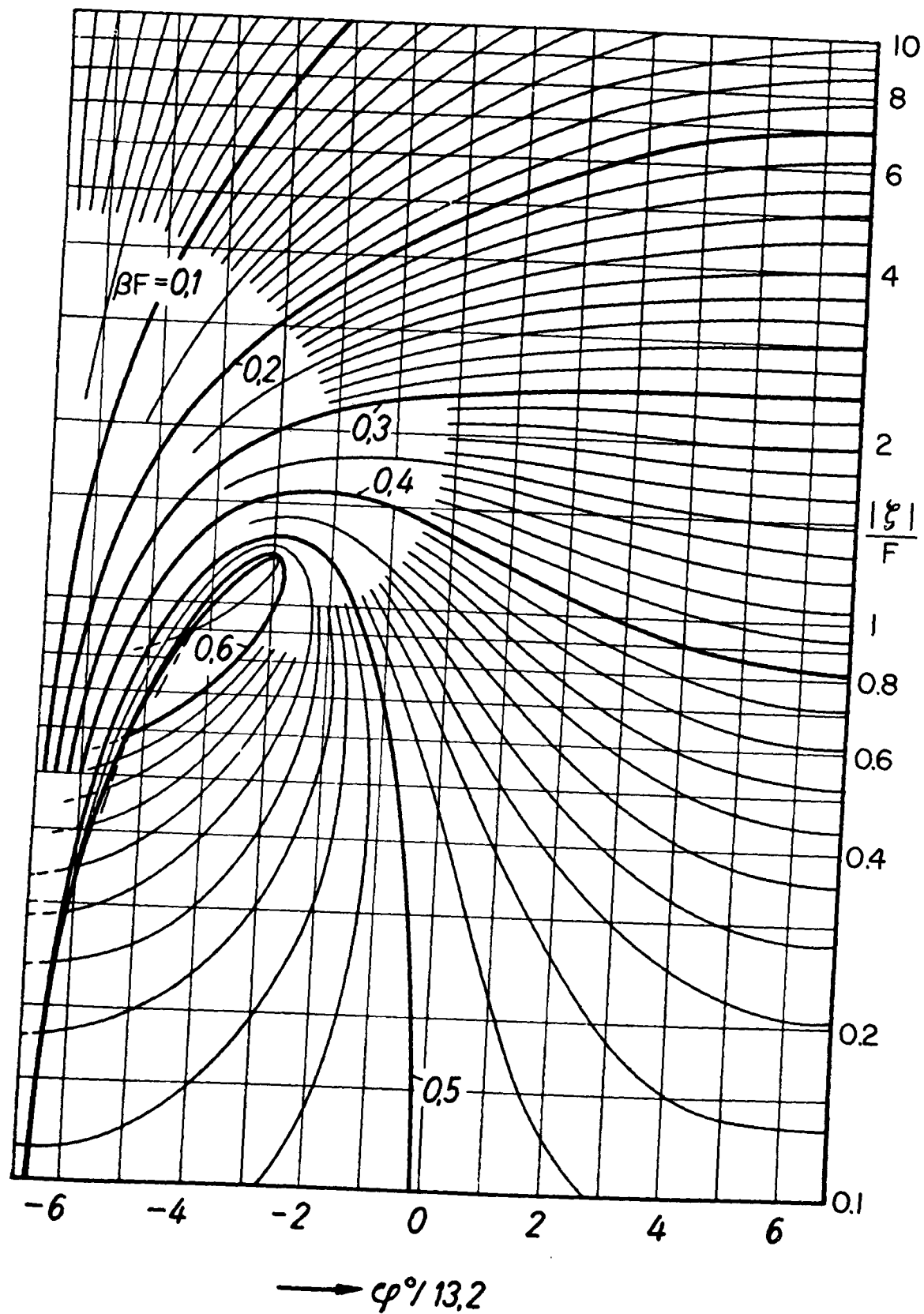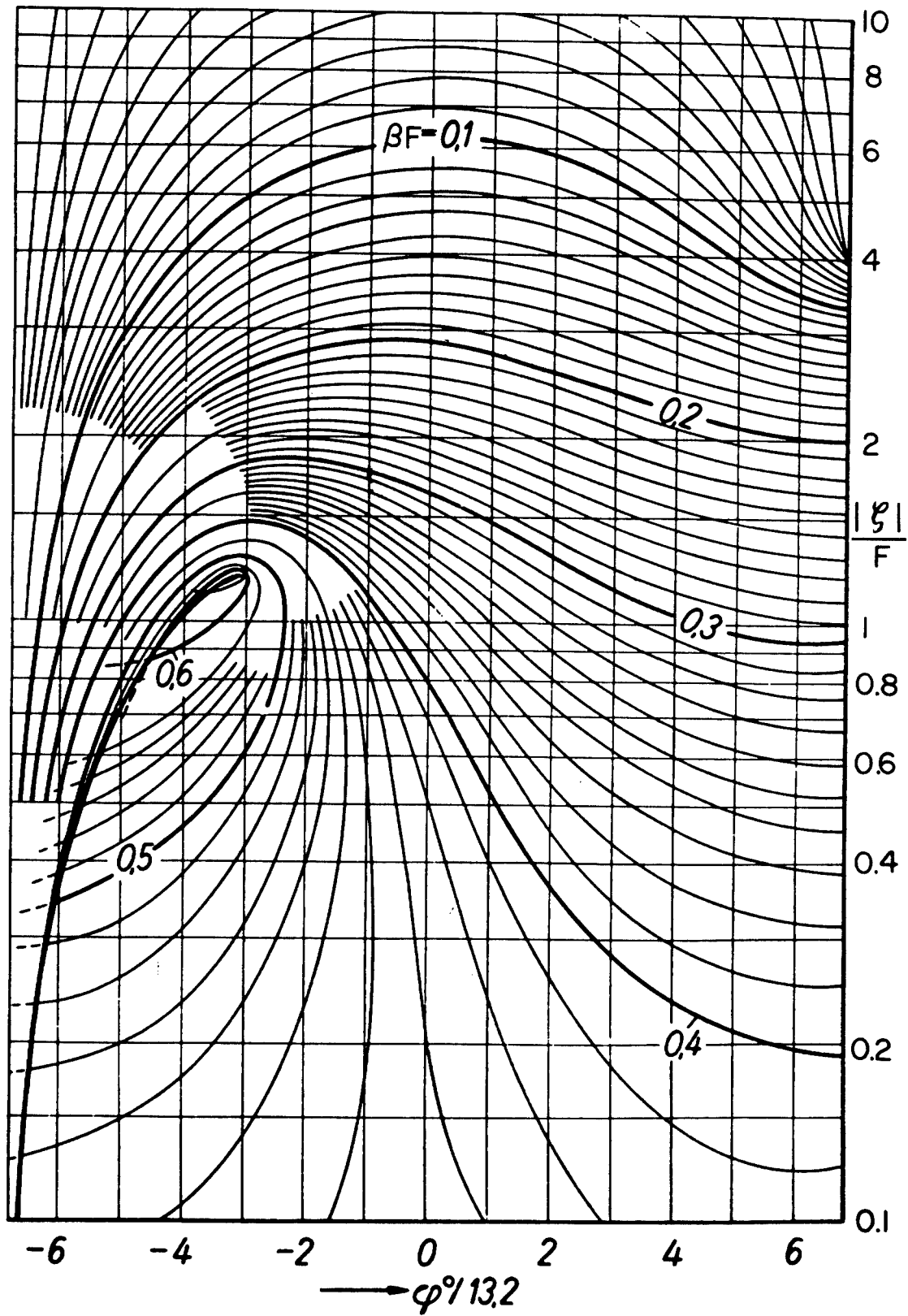
to Eq. (12.2.5) and (12.2.23). The first chart is more
general than Eq. (12.2.5) for low frequencies, however, as
the chart is correct for any lining impedance, whereas the
equation assumes a "hard" lining. In the case of any imped-
ance value which is too large for the chart, the approximate
equation gives sufficient accuracy. In addition to the two
charts for low and high frequencies, there are three charts
that apply when the wavelength of sound bears certain speci-
fied ratios to the passage width. The Cremer charts apply
to a duct with two opposite walls lined, or with one wall
lined. Where the attenuation constants for two different
modes of propagation are nearly the same, the chart value is
for the mode having the lower attenuation, in order that the
attenuation will not be overestimated. The use of the charts
is illustrated below by a numerical example. The symbols,
some of which have been given previously, are defined below.

N number of walls lined (one or two)

F frequency parameter, equal to $2 \ell_x / N \lambda$

ℓ_x passage width normal to lined walls

σ attenuation constant in db per unit length

ζ normal impedance index of lining (reciprocal of η)

$\emptyset$ phase angle of ζ in degrees, positive values
    representing mass-like impedance

β attenuation parameter, equal to $(1/2\pi)$ times attenua-
    tion in nepers per wavelength

Suppose that it is desired to calculate the attenuation,
for various frequencies, for a duct having a passage width of

---

FIGURE 12.2.11

Same as Fig. 12.2.10, but for a frequency parameter $F = 0.25$.

$\ell_x = 34$ cm, lined on two sides. The calculation can be done for low frequencies (say, F < 0.1), for high frequencies (say, for F ≫ 3), and for the frequencies representing F values of 0.25, 0.5, and 1.0. From the definition of F, these values represent frequencies of 250, 500, and 1000 cps in the present example. To proceed further, it is necessary to know the lining impedance for frequencies at which the attenuation is to be found. The values tabulated below will be used for

Frequency, cps	80	250	500	1000	3000
F	0.08	0.25	0.50	1.0	3.0
$|\zeta|$	9.0	3.0	1.5	1.3	1.2
$\emptyset$, degrees	-79	-26	-13	-6.6	+13
$\emptyset/13.2$	-6.0	-2.0	-1.0	-0.5	+1.0
βF	0.0222	0.184	0.212	0.086	
βF^2					0.054
$\sigma\ell_x$ (db in distance ℓ_x)	1.2	10.1	11.6	4.7	1.0

Also shown in the tabulation are the values of the attenuation in the form βF or βF^2 as given by the various charts, and finally the attenuation values reduced to $\sigma\ell_x$ (that is, db in the distance ℓ_x). The relation between βF and $\sigma\ell_x$ is

$$\sigma\ell_x = 27.3 \, NF\beta$$

This relation follows directly from the definitions.

While only one frequency in the range of F ≫ 3 is shown, and only one in the range F ≪ 0.1, calculations can be carried out in these ranges for any number of frequencies for

---

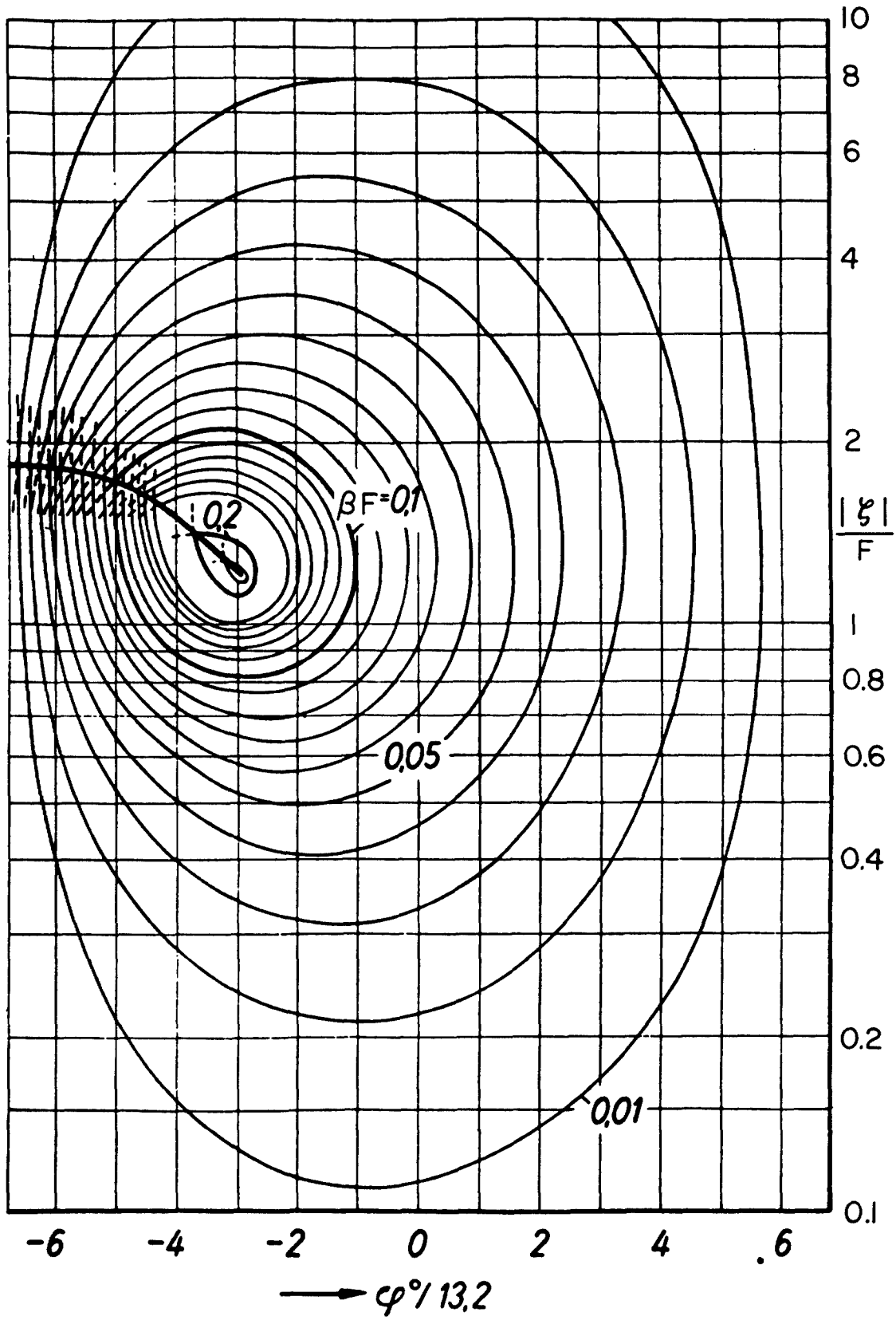**FIGURE 12.2.12**

Same as Fig. 12.2.10, but for a frequency parameter F = 0.5

F = 0,5

$\dfrac{|\xi|}{F}$

$\longrightarrow \varphi°/\,13{,}2$

F = 1

$\frac{|\xi|}{F}$

φ° / 13,2
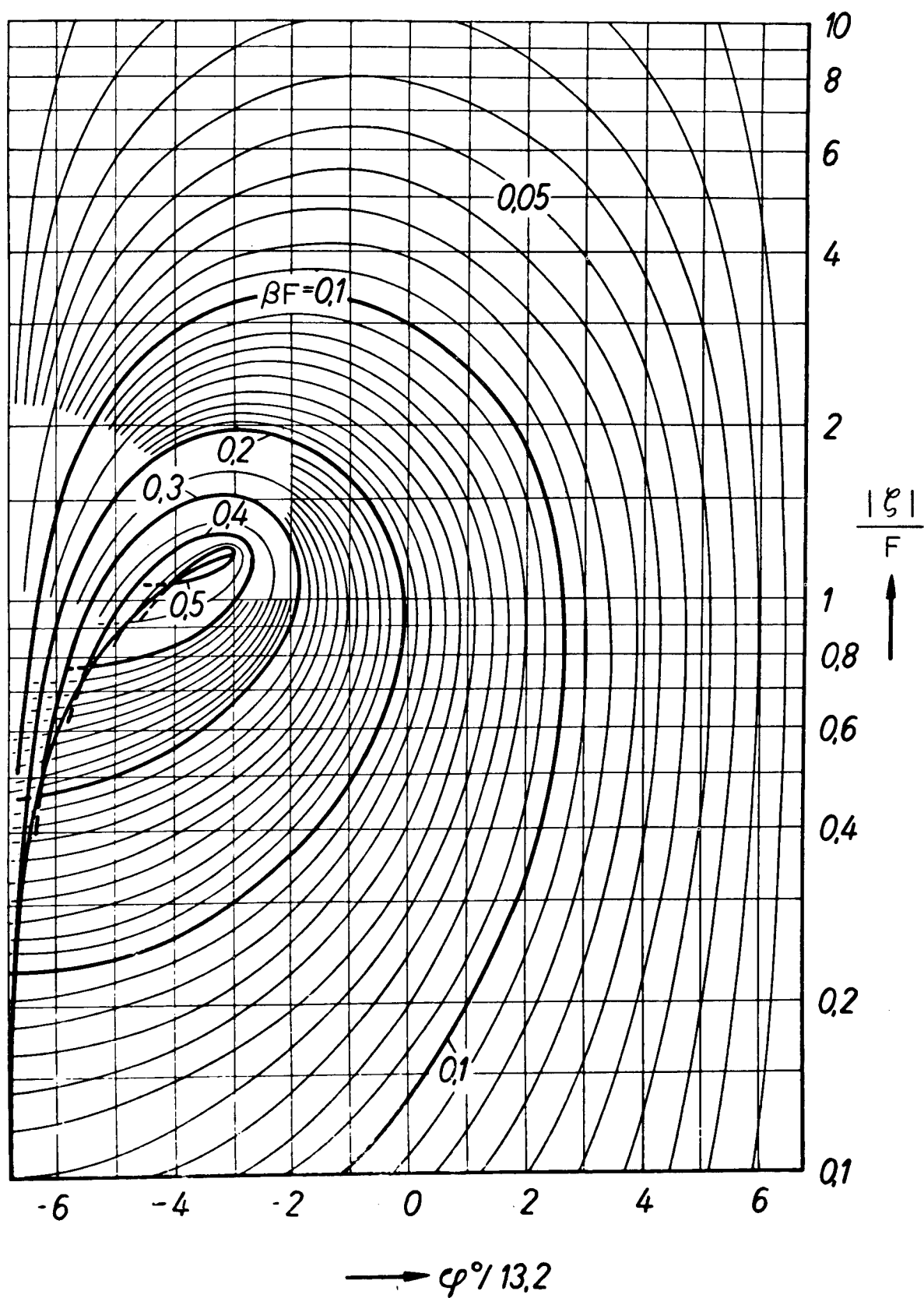
which the lining impedance is known. The results for frequencies near the peak are restricted to the frequencies corresponding to the three intermediate charts.

Use of these charts is to be recommended whenever duct attenuation is to be calculated on the basis of a known lining impedance. While the results do not show in detail the sharp attenuation peak which is shown by careful use of the Morse charts, they do show the peak in sufficient detail for design work dealing with wide-band noise, and in much more detail than the charts in Figs. 12.2.2-6. The latter charts, on the other hand, are simpler to use than the Cremer charts in the special case for which they are intended, where the lining is a porous blanket.

Difficulty in obtaining normal impedance data for the lining will to some extent limit the use of the Cremer charts. Normal impedance data for a few materials are given in Sec. 12.1. Normal impedance for porous blankets may be calculated from Eq. (12.1.14) or, for long wavelengths, from Eq. (12.1.19).

In the Cremer charts, Figs. 12.2.10-14, the values of lining impedance which give greatest attenuation are evidenced by inspection. Cremer 2.13/ gives the following simple formula for the optimum lining impedance index as a function of frequency:

$$\zeta_{optimum} = 1.2\ e^{-0.7i}(2N\ \ell_x/\lambda) \qquad (12.2.27)$$

For a duct having the lining impedance versus frequency characteristic given by this relation, the attenuation if one wall were lined would be 19 db per distance ℓ_x up to F = 0.3; for higher frequencies the attenuation would be $(3.5\ \lambda/\ell_x)$ db. These figures would be doubled if two sides were lined. All actual ducts, in which this ideal impedance behavior cannot be perfectly realized, will have an attenuation versus frequency characteristic which lies below the one given by the preceding values.

FIGURE 12.2.13

Same as Fig. 12.2.10, but for a frequency parameter F = 1

$F = \infty$

$\dfrac{|\xi|}{F}$

$\beta F^2 = 0{,}1$

$0{,}2$

$0{,}05$

$0{,}01$

$\longrightarrow \varphi^\circ / 13{,}2$
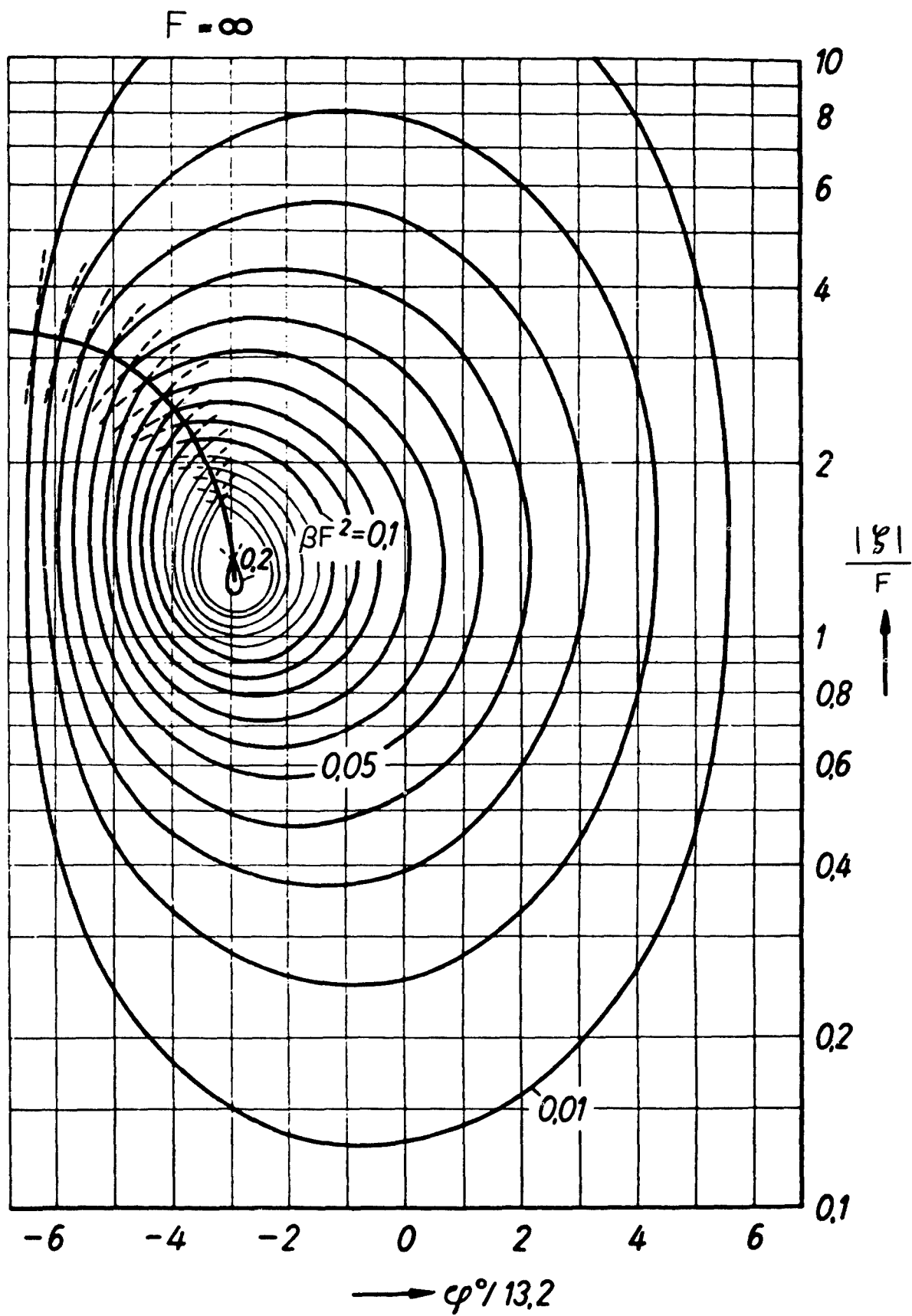
References, Section 12.2

(2.1)   Sabine, Hale J., "The Absorption of Noise in
        Ventilating Ducts." J. Acoust. Soc. Am. 12,
        53 (1940).

(2.2)   Beranek, Leo L., "Sound Absorption in Rectangular
        Ducts." J. Acoust. Soc. Am., 12 228 (1940).

(2.3)   Bosquet, I.P., Bull. Techn. Assoc. Ing. Bruxelles
        31, No. 12 (1935).

(2.4)   Sivian, L. J., "Sound Propagation in Ducts Lined
        with Absorbing Materials," J. Acoust. Soc. Am.
        9 135 (1937).

(2.5)   Willms, W. Akustische Zeits. 6 150 (1941).

(2.6)   Piening, W., Zeits. Ver. Dtsch. Ing. 31 776 (1937).

(2.7)   Parkinson, J. A., Heating and Ventilating, pp 23-
        26 (March 1939). See also Heating Ventilating
        Air Conditioning Guide 1953 (Vol. 31) (Am. Soc.
        Heating and Ventilating Engrs., New York, 1953),
        pp. 898-899; also earlier editions of this guide.

(2.8)   Morse, P. M., "Transmission of Sound Inside Pipes,"
        J. Acoust. Soc. Am. 11 205 (1939).

(2.9)   Morse, P. M., Vibration and Sound, 2nd Ed.
        McGraw-Hill (1948) pp. 368-376.

(2.10) Morse, P. M., "Some Aspects of the Theory of Room
        Acoustics," J. Acoust. Soc. Am., 12 56 (1939).

(2.11) Cremer, L., Akustiche Zeits   5 57 (1940).

(2.12) Scott, R. A., Proc. Phys. Soc. (London) 58 358
        (1946).

(2.13) Cremer, L., "Theory of Airborne Sound Damping
        in Rectangular Ducts with Absorbing Walls and
        Which Have a Very High Damping Constant".
        Acustica 3, 249-263 (1953).

FIGURE 12.2.14

Same as Fig. 12.2.10 but for "high" frequencies.

12.6a The Resonator as a Free-Field Sound Absorber

The use of the resonator to attenuate sound in a duct was considered in Sec. 12.6. Another use, that of absorbing sound in rooms, is considered in the present section. In this application, the behavior of a resonator is best described by giving its sound absorption in sabins, rather than by giving a pressure reduction ratio.

The effect of a resonator in a room, for frequencies near the resonance, is similar to that of a patch of highly efficient sound absorbing material. The reduction of sound pressure in the room is dependent upon the position of the absorbing element, as pointed out in Sec. 12.1. Therefore, the sound absorption of a resonator can be stated only for specified positions in the room. Two idealized cases will be considered, namely, (a) the resonator in open air (free field); (b) the resonator with its opening in a plane wall bounded by open air. The practical situations represented by a resonator near the center of a room, or by a resonator in a room wall, are approximations to these idealized cases.

The properties of a resonator as a sound absorber are summarized briefly in the next paragraph. Following the summary, a brief derivation of the equations for the resonator in free field is given. In the remainder of the section, the roles of the various parameters are considered in detail, and design procedures are developed.

Summary of Properties of the Resonator as a Sound Absorber.

(1) The maximum absorption of a single resonator, in sabins, is approximately $\lambda^2_0/4\pi$ if the resonator is in substantially free air, and is $\lambda^2_0/2\pi$ if the resonator opening is in a large wall, where λ_0 is the wavelength of sound, in feet, at the frequency of resonance.

(2) The minimum Q (corresponding to maximum bandwidth) which can be obtained in a practical resonator having maximum absorption of the amount indicated above is about 25 for a resonator in free air, or about 13 for a resonator having its opening in a wall.

(3) The width of the frequency band in which the absorption is not less than half the value found at resonance is equal to the frequency of resonance divided by Q.

(4) While the bandwidth of the absorption can be varied over wide limits by adjusting the size of the resonator and the resistance material placed in the aperture, the absorption for all frequencies decreases greatly as the bandwidth is increased, so that it is usually not profitable to reduce the Q below the values given in (2) above.

A resonator is, therefore, useful primarily when relatively large sound absorption is required in a narrow frequency band. The resonator has great practical value particularly for frequencies below about 200 cps, where it is often difficult to obtain large absorption by other methods. For example, a resonator (or a group of resonators not too close to one another) can be used effectively to reduce the 120 cps "hum" in a transformer room. A group of resonators tuned to successively larger frequencies is sometimes used to give sound absorption in a wider frequency band.

The Absorption Cross Section. A resonator placed in a progressive plane wave absorbs energy at a rate proportional to the intensity of the wave. The power absorbed by the resonator can be expressed as the power which the undisturbed plane wave would deliver in some effective area, σ_a, perpendicular to the direction of wave travel. The quantity σ_a is the absorption cross section of the resonator; if expressed in square feet, the absorption cross section becomes the absorption in sabins. The absorption cross section at resonance will be denoted by σ_{ao}. (The subscript zero with any quantity will always refer to the resonance condition.)

For purposes of analysis, the resonator is assumed to have the spherical shape shown in Fig. 12.6a.1, where the symbols for the dimensions are also shown. In all practical designs, the resonator is small compared to the wavelength of sound at resonance, λ_o. Therefore, diffraction effects may be neglected, to a first approximation, and the rms acoustic pressure at the opening is equal to P_o, the rms pressure in the incoming plane wave. If the resonator is mounted in a wall, the pressure at the opening becomes $2P_o$, because of reflection at the wall. Both of these situations will be covered by writing the driving pressure as $\langle 2 \rangle P_o$. Throughout this section, a quantity enclosed in broken brackets is understood to apply only when the resonator is mounted in a wall, and is to be replaced by unity if the resonator is in free air.
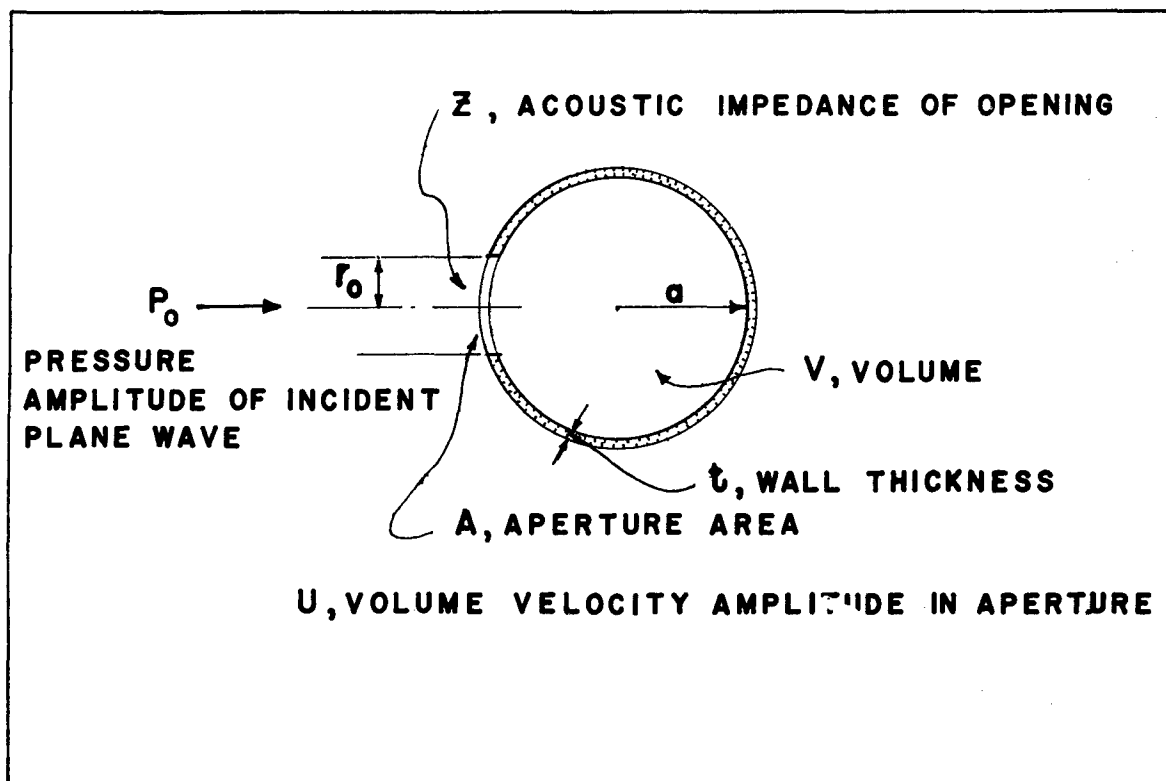
FIGURE 12.6a.1

Sketch of resonator, showing definitions of several quanti-
ties used in the analysis.

Let Z be the acoustic impedance at the resonator open-
ing, and let R be the real part of Z. The aperture resis-
tance R is the sum of two quantities, R_i, the resistance
representing losses within the resonator and at the opening,
and R_r, the resistance associated with re-radiation of sound
by the moving air in the aperture. The volume velocity in
the opening is $\langle 2 \rangle P_0/|Z|$. The power dissipated in the
resonator is R_i times the square of the volume velocity, or
$\langle 4 \rangle P_0^2 R_i/|Z^2|$. By definition of the absorption cross
section, the power absorbed is also equal to $\sigma_a P_0^2/\rho c$, since
$P_0^2/\rho c$ is the intensity of the incident wave. Thus, the
absorption cross section is

$$\sigma_a = \langle 4 \rangle \rho c R_i / |Z^2| . \qquad (12.6a.1)$$

It will be shown how the absorption varies with frequency,
with the physical properties of the resonator, and with
sound pressure.

The maximum absorption of a given resonator occurs at
the resonance frequency f_0, where the resonator impedance Z
is simply equal to $R_i + R_r$. The resonance absorption cross
section is therefore

$$\sigma_{ao} = \frac{\langle 4 \rangle \rho c R_i}{(R_i + R_r)^2}$$

It is assumed that the circumference of the resonator aper-
ture is appreciably less than the wavelength of sound. This
makes it possible to approximate the radiation resistance
by $R_r = \langle 2 \rangle \rho c \pi/\lambda^2$, where λ is the wavelength. The
resonance-frequency absorption cross section then becomes

$$\sigma_{ao} = \frac{\langle 2 \rangle \lambda_0^2}{\pi} \frac{(R_i/R_r)}{(1 + R_i/R_r)^2} \qquad (12.6a.2)$$

This function has a maximum value of $\langle 2 \rangle \lambda_0^2/4\pi$ when
$(R_i/R_r) = 1$. A slight correction to this calculation will
be introduced later.

Variation of the Absorption Cross Section with Frequency.

The acoustic impedance of the aperture can be expressed as

$$Z = R[1 + jQ(\gamma - 1/\gamma)] \qquad (12.6a.3)$$

where

$$\gamma = f/f_o$$

$$Q = 2\pi M f_o/R$$

$$R = R_i + R_r$$

$$M = \text{acoustic mass of air in the resonator opening; see Eq. (12.6a.5).}$$

It follows that, if the relatively slow variation of R with frequency is neglected, the variation of absorption with frequency can be expressed in the form

$$\sigma_a/\sigma_{ao} = [1 + Q^2(\gamma - 1/\gamma)^2]^{-1} \qquad (12.6a.4)$$

The bandwidth, defined as the frequency range within which σ_a is not less than one-half of σ_{ao}, is given by $BW = f_o/Q$. The acoustic mass of the air in the resonator opening is proportional to the "effective" length of the opening, equal to the wall thickness t plus an "end correction" δ. This end correction is proportional to the radius of the aperture and accounts for the fact that some air not directly in the resonator opening moves as if it were in the opening. For a small opening in a large flat plate, the end correction is $\delta' = 1.70 \, r_o = 0.96 \sqrt{A}$, where A is the area of the aperture. The value given for M in Sec. 12.6 is derived on this basis. In many cases δ is somewhat different from δ'; typically, $\beta = \delta/\delta'$ is about 0.9. The acoustic mass may be written as

$$M = \rho \, \frac{t + \delta}{A} = \frac{1.70 \, \rho \, r_o}{A} \left(\beta + 0.59 \, \frac{t}{r_o} \right) \qquad (12.6a.5)$$

Methods for computing β in certain special cases are given at the conclusion of this section. For present purposes, the value $\beta = 0.9$ will be assumed.

The frequency of resonance, f_0, can be computed by the procedure of Sec. 12.6; it may be expressed as:

$$f_0 = 0.666 \, (c/2\pi a) \left[\frac{r_0/a}{\beta + 0.59 \frac{t}{r_0}} \right]^{1/2} \qquad (12.6a.6)$$

Total Aperture Resistance at Resonance. The internal resistance of the resonator is the sum of the frictional resistance due to air flow within the aperture, the resistance due to air flow over the surfaces at the ends of the aperture, and the acoustic resistance due to any cloth or screen which may be placed in the aperture. The values of the first two contributions are approximately 6a.1/

Frictional acoustic
resistance within aperture = $2tR_s/Ar_0$

Frictional acoustic
resistance of end surfaces = $4R_s/A$

$$\text{where } R_s = [\pi\mu\rho f]^{1/2}$$

Here μ and ρ are respectively the viscosity and density of air, as in Sec. 12.6. The acoustic resistance due to the cloth or screen will be described by introducing the parameter

$$\epsilon = 1 + \frac{R'}{4R_s}$$

where R' is the flow resistance in rayls* of the cloth or screen.

---

* The flow resistance R' must not be confused with the other acoustic resistances and impedances. By definition, acoustic impedance is impedance in rayls, divided by aperture area.

The total internal acoustic resistance (that is, the resistance other than that due to radiation) is then expressible as

$$R_i = 4R_s/A \left[\epsilon + 0.5 \frac{t}{r_o} \right] \qquad (12.6a.7)$$

Except for the introduction of a resistance due to a screen or cloth, this is equivalent to Eq. (12.6a) in Sec. 12.6.

The acoustic resistance due to radiation will be expressed by the approximate relation

$$R_r = \langle 2 \rangle \rho c \pi / \lambda^2$$

as already noted. In order to incorporate this resistance in a fashion which is convenient for the final design formulas, it is necessary to define two dimensionless parameters, h and C, as follows:

$$h \equiv \frac{(\beta + 0.59 \frac{t}{r_o})^2}{\epsilon + 0.5 \frac{t}{r_o}} \qquad (12.6a.8)$$

$$C \equiv (k_o a)^{-6} (R_r/R_i) \qquad (12.6a.9)$$

Here k_o denotes $2\pi/\lambda_o$, or $2\pi f_o/c$. The latter parameter is given by

$$C = 0.316 \langle 2 \rangle h\rho c/R_s \quad, \qquad (12.6a.10)$$

as may be shown by combining Eqs. (12.6a,b) through (12.6a.9) Therefore the total resistance $R = R_i + R_r$ can be expressed as

$$R = (4R_s/A)(\epsilon + 0.5 \frac{t}{r_o}) \left[1 + (k_o a)^6 C \right] \qquad (12.6a.11)$$

It is useful to notice that if no cloth or screen is used, ε is equal to unity, and if also $(t/r_o) \ll 1$, then also h is approximately equal to unity.

Resonator Formulas in Terms of Generalized Parameters. The basic resonator formulae, when expressed in terms of the dimensionless parameters $(k_o a) = 2\pi f_o/c$, are suitable as a basis for orderly design work or for the construction of general design charts. The relations below, which give the absorption cross section, the Q, and the reverberation time of the resonator, are particularly useful.

The absorption cross section at resonance is

$$\sigma_{ao} = \frac{\langle 2 \rangle \lambda_o^2}{4\pi} \frac{4(k_o a)^6 CF}{[1 + (k_o a)^6 C]^2} \qquad (12.6a.12)$$

where

$$\left.\begin{array}{ll} F = 1 + \frac{9}{4}(k_o a)^2 & \text{(Resonator in space)} \\[2ex] F = 1 \quad . & \text{(Resonator in wall)} \end{array}\right\} \qquad (12.6a.13)$$

The correction factor F, which is of the order of 1.2 in a practical resonator in space, is obtained by detailed wave-theory analysis of the spherical resonator.

The generalized expression for the Q is obtained by combining the expressions for f_o and M to give

$$2\pi M f_o = 0.240(2\pi f_o) \; \rho/a(k_o a)^2$$

and by combining the expressions for R, f_o , and C to give

$$R = \langle 2 \rangle [0.0793 \; \rho c/a^2 \; (k_o a)^4 C][1 + (k_o a)^6 C]$$

Thus, the Q, which is equal to $2\pi M f_o/R$, is given by

$$Q = \frac{3.03}{\langle 2 \rangle} \frac{(k_o a)^3 C}{1 + (k_o a)^6 C} \qquad (12.6a.14)$$

The reverberation time (the time for the power re-radiated by the resonator to decrease by 60 db after the external signal ceases) is equal to $2.19\ Q/f_o$. Therefore, the reverberation time is

$$T = \frac{6.65}{\langle 2 \rangle} \frac{1}{f_o} \frac{(k_o a)^3 C}{1 + (k_o a)^6 C}$$

Optimum Design Values. When values are assigned to two of the three quantities f_o (frequency of resonance), h (hole parameter), and V (cavity volume), there then exists an optimum value for the remaining parameter such that the resonance absorption cross section σ_{ao} will be as large as possible. For the resonator in space, this maximum possible value of σ_{ao} for any given set of conditions usually lies between $\lambda_o/4\pi$ and $1.5\ (\lambda_o^2/4\pi)$. These limits correspond to values of F between 1.0 and 1.5. The calculation of optimum values where f_o and the hole parameter h have already been chosen will be considered here. The value of h is dependent upon choices of t/r_o and ϵ, the latter quantity being an index of the amount of flow resistance introduced by a cloth or screen. The problem is then one of finding the optimum value of the spherical cavity radius, a_1, for which the absorption cross section is maximum. (The subscript 1 will refer to an optimum value.) The required value of the aperture radius, r_o is also easily found.

Since the frequency is given, the quantity C is a constant. From Eq. (12.6a.12) it is found that the maximum absorption cross section is obtained when $(k_o a_1)^6 C = 1$, or

$$k_o a_1 = \frac{1.08}{(\langle 2 \rangle \rho ch)^{1/6}} [4\pi\mu\rho f_o]^{1/12} \qquad (12.6a.16)$$

When numerical values for room temperature are inserted, the optimum sphere radius is

$$a_1 = 1080 \, f_o^{-11/12} \, h^{-1/6} \text{cm (resonator in space)}$$

$$a_1 = 963 \, f_o^{-11/12} \, h^{-1/6} \text{cm (resonator in wall)}$$

$$(12.6a.17)$$

For a cavity having the optimum radius a_1, the absorption, the Q, and the reverberation time are given by the relations below, where the numerical forms are for room temperature (70°F).

$$\sigma_{al} = (\lambda_o^2/4\pi)F \qquad (12.6a.18)$$

$$Q_1 = 0.85(h\rho c)^{1/2}/[(\pi\mu\rho f_o)^{1/4}\langle\sqrt{2}\rangle] = 189\sqrt{h}/(f_o^{1/4}\langle\sqrt{2}\rangle)$$

$$(12.6a.19)$$

$$T_1 = 1.87(h\rho c)^{1/2}/(\pi\mu\rho)^{1/4}f_o^{5/4}\langle\sqrt{2}\rangle = 415\sqrt{h}/(f_o^{5/4}\langle\sqrt{2}\rangle)$$

$$(12.6a.20)$$

Sometimes, when the optimum value of a has been obtained, it is desirable to be able to calculate directly the change in the above quantities which will result from changing to a non-optimum value for a. For this purpose, the equations can be rewritten in the normalized forms

$$\frac{\sigma_a}{\sigma_{al}} = \frac{4B^6}{(1+B^6)^2} \qquad (12.6a.21)$$

$$\frac{T}{T_1} = \frac{Q}{Q_1} = \frac{2B^3}{1+B^6} \qquad (12.6a.22)$$

where $B = a/a_1$

Almost all calculations necessary to evaluate the optimum resonator design, for given resonance frequency and hole parameter, can be performed using the charts of Figs. 12.6a.2-7. For those calculations which involve β , the value β = 0.9 has been used in constructing the charts. Room temperature values of the air constants have been used, and where the relations for resonator-in-space differ from those for resonator-in-wall, the charts apply to the in-space case. The use of the charts is explained below.

Procedure for Optimum Design Calculation. It is assumed that the resonance frequency and the hole constants (the ratio t/r_o and the flow resistance of the cloth or screen in the aperture) are known, and an optimum design is desired. Alternatively, if the value of the hole parameter h is known, the first step in the calculation is reversed, and possible values of t/r_o and of flow resistance are found which will permit the desired h value to be realized. The calculations may be made in the order shown below.

1. Compute h, from known values of t/r_o and of flow resistance R', from Eq. (12.6a.8) or from Fig. 12.6a.2. The chart assumes β = 0.9.

2. Compute the optimum cavity radius, a_1, from Eq. (12.6a.17) or from Fig. 12.6a.3. (For resonator-in-wall, multiply result from chart by $2^{-1/6}$ = 0.890.)

3. Compute $k_o a_1 = 2\pi f_o a_1/c$, or obtain this quantity from Fig. 12.6a.4.

4. Compute r_o/a (and hence r_o) from Eq. (12.6a.6) or obtain this value from Fig. 12.6a.4. The chart assumes β = 0.9.

5. Compute F from Eq. (12.6a.13).

6. Compute the maximum absorption cross section,
$$\sigma_{a1} = \langle 2 \rangle \ F \ \lambda_o^2/4\pi.$$

7. Compute Q_1 from Eq. (12.6a.19), or from Fig. 12.6a.5. The bandwidth in which the absorption cross section is at least $\sigma_{a1}/2$ is BW = f_o/Q_1. (If the resonator is in wall, multiply result from chart by $1/\sqrt{2}$.).
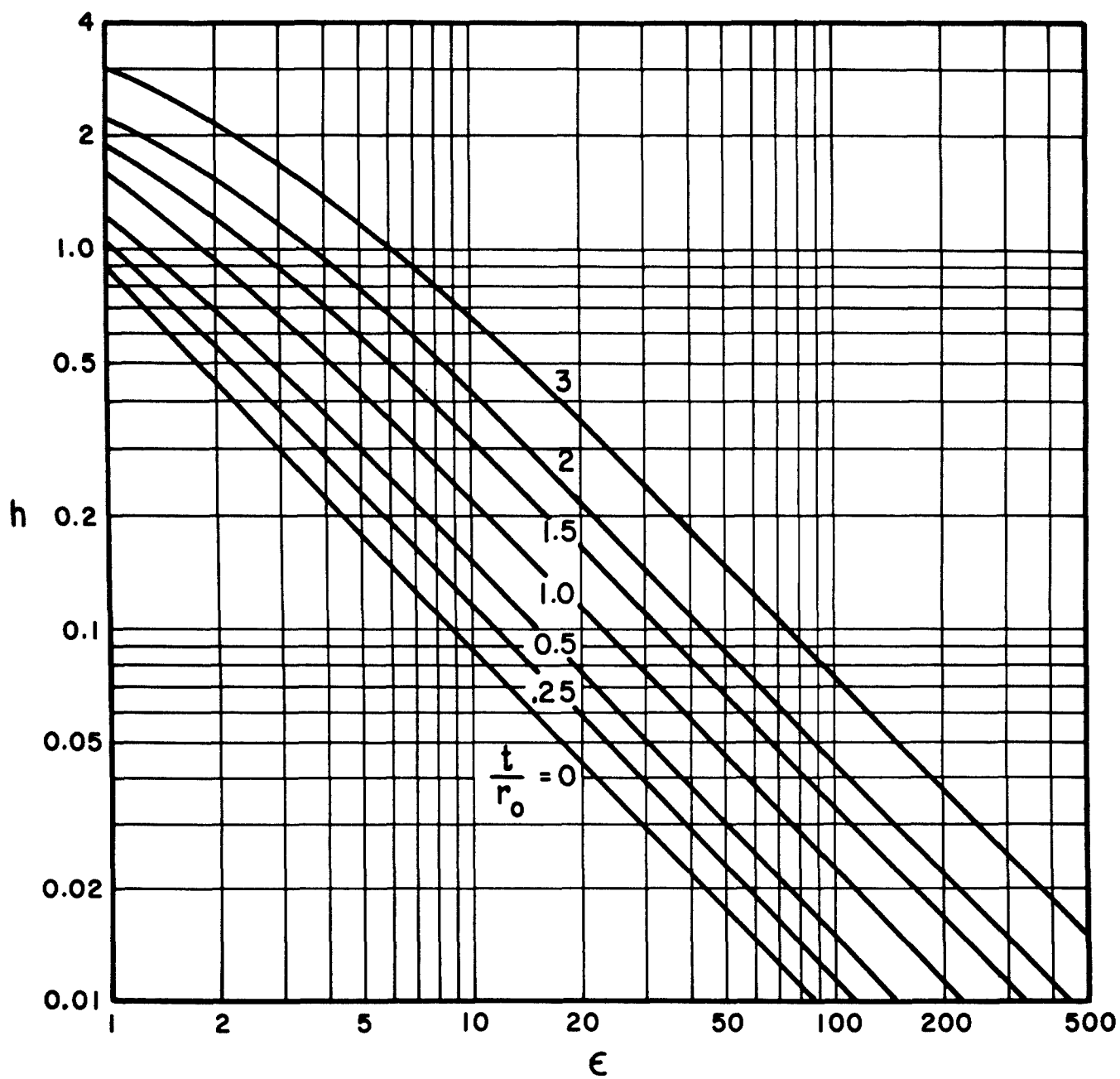
8. If desired, obtain the reverberation time T_1 from Eq.(12.6a.20) or from Fig. 12.6a.6. (If resonator is in wall, multiply result from chart by $1/\sqrt{2}$.)

9. If it is desired finally to explore the effect of changing to a cavity radius a other than the optimum value a_1, consult Eqs. (12.6a.21,22) or Fig. 12.6a.7. (Not valid if resonator operation is in the nonlinear orifice resistance range, see Sec. 12.6 and the later discussion in this section; Eq. (12.6a.31) gives the non-linear resistance.)

Selection of Efficient Design. The calculation procedure outlined above shows how to obtain an optimum set of related values, once the resonance frequency and the hole parameter are specified. Some further consideration must be given to indicate on what basis the designer can make the original choice of the hole parameter h, and to show certain other practical aspects of the design problem.

1. The smaller values of h correspond to resonators having relatively large volume, but relatively low Q and hence relatively large bandwidth. Conversely, the larger values of h correspond to small-volume, high-Q, narrow-band resonators.

2. Small h is obtained by use of a short-neck aperature ($t/r_0 << 1$) in which a cloth or screen has been introduced to increase the resistance ($\epsilon > 1$); larger values of h are obtained with apertures having longer necks, with no added resistance.

3. The basic equations are not applicable unless the radius of the aperture is appreciably less than the radius of the cavity. In practice, it is considered that r_0/a should not exceed 0.3. At any given frequency, this requirement indirectly determines the smallest value of h,

---

FIGURE 12.6a.2

The hole parameter, h, when the flow resistance parameter, ϵ, and the ratio t/r_0 of aperture thickness to radius, are known. The chart represents Eq. (12.6a.8) for the case $\beta = 0.9$. From Ingard 6a.1/.
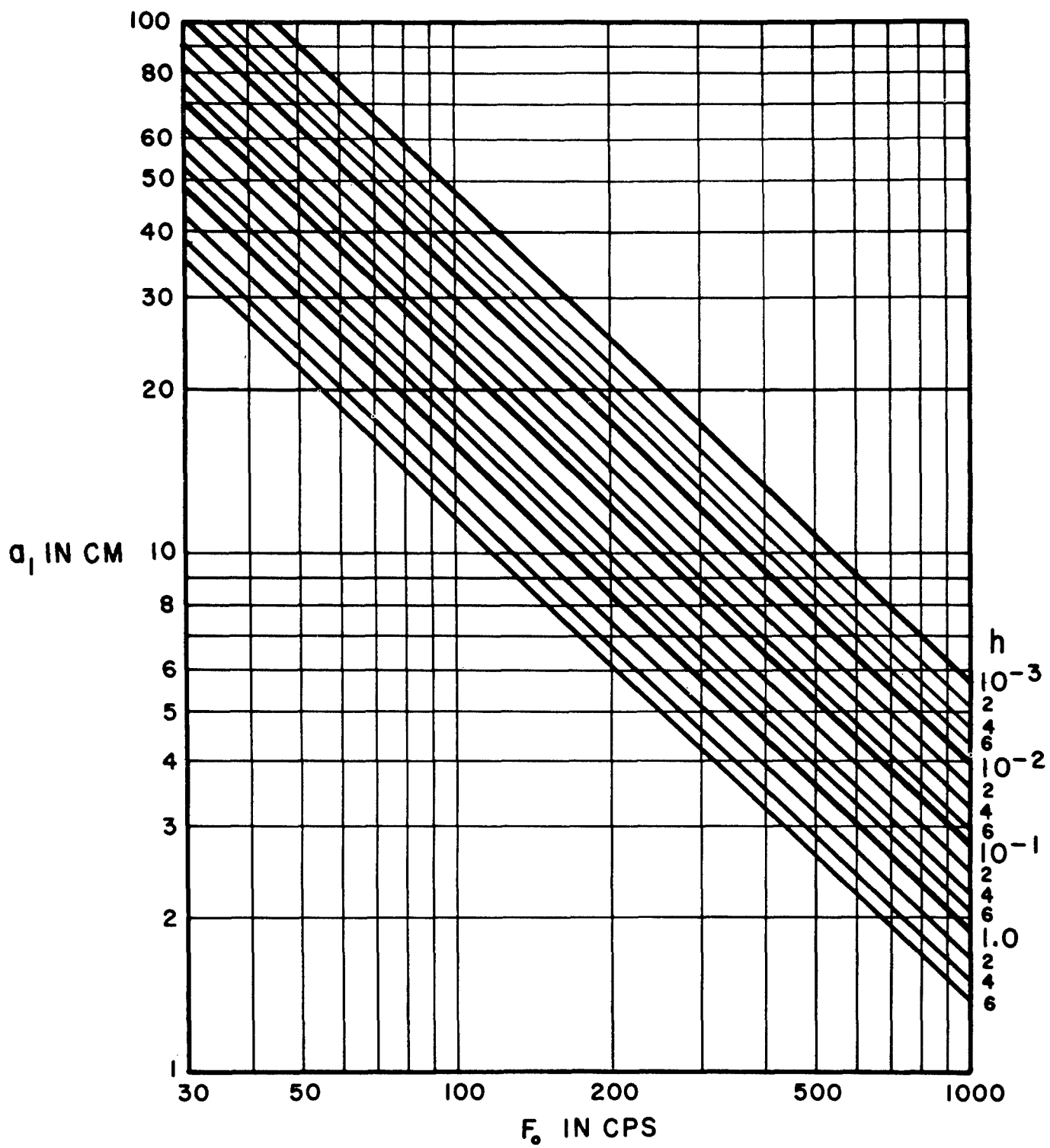
and hence the smallest Q, which can be obtained. This is because r_o/a increases with increasing resonator volume, and hence with decreasing h. (It will be shown that the Q cannot be less than 25 for optimum-design resonators in space, or less than 13 for the wall location, if the restriction on (r_o/a) is observed .

4. From the foregoing considerations, it follows that efficient design (minimum volume used) for a resonator which is to absorb sound of only one frequency is obtained when the aperture (neck) length t is made several times the aperture radius r_o, and no additional resistance is added. This design results in small volume, large Q, and small bandwidth, but the absorption obtained at resonance, with an optimum combination of values, is always $\lambda_o^2/2\pi$ for the resonator in a wall or of the order of $\lambda_o^2/4\pi$ for a resonator in space.

5. The greatest possible absorption in the greatest possible bandwidth, for a single resonator, is obtained by putting $(t/r_o \ll 1$, and choosing the largest allowable volume, which corresponds to $(r_o/a) = 0.3$. Optimum design is then completed by finding the value of h for which the resulting cavity radius a_1 is an optimum value, and selecting a cloth or screen of suitable flow resistance to give a value of ϵ which will result in this selected value of h.

6. The effect of using a cavity radius a other than the value which is optimum for a given f and h is to decrease the absorption σ_{ao} at resonance and to increase the bandwidth, in such a way that the product $\sigma_{ao}(BW)^2$ is constant. Specifically, the relation is

$$\sigma_{ao} (BW)^2 = \langle 4 \rangle 2.8F \sqrt{f_o}/h \qquad (12.6a.23)$$

FIGURE 12.6a.3

The optimum radius, a_1, for a spherical resonator cavity when the frequency of resonance F_o, and the hole parameter h, are given. This is for air at room temperature only. For a resonator in space this chart is the same as Eq. (12.6a.17). Multiply result by 0.890 if resonator opening is in or very near the wall. From Ingard 6a.1/.

where σ_{ao} is in ft^2 (sabins), and BW and f_o are in cps. This relation may be obtained by combining Eqs. (12.6a.12), (12.6a.14), and (12.6a.10). For optimum design, σ_{ao} is equal to σ_{al}, or $F \lambda_o^2/4\pi$, and for other designs σ_{ao} is less than that value.

7.   From Eq. (12.7a.23) or from the basic equations, it follows that the optimum design (the design which maximizes absorption for a given h) represents the maximum possible Q for a given h.

8.   By further interpretation of Eq. (12.6a.23), it is found that a departure from the optimum design, for a given h, reduces the absorption not only at resonance but at all frequencies, even though the Q is decreased. For this reason, it is preferable to use optimum combinations of values except in unusual circumstances where a low Q is absolutely necessary and greatly reduced absorption can be accepted (or in cases where nonlinear effects necessitate a reduced Q, as will be shown later).

9.   The cavity need not be spherical, but can have any shape for which the volume is equal to $4\pi a^3/3$, and which presents a sharp change of cross section at the aperture. Similarly, the aperture can be square rather than circular, if the same area is maintained.

10.   The analysis does not consider interactions between adjacent resonators tuned to the same frequency, and applies only when the separation between individual resonators tuned to the same frequency is $\lambda_o/2$ or more.

FIGURE 12.6a.4

Relation between the resonance frequency and the resonator dimensions, for air at room temperature. The broken lines give the resonance frequency F_o, in cps, as a function of $k_o a$, for various values of cavity radius a. The solid curves, which represent Eq. (12.6a.6) for the case $\beta = 0.9$, relate r_o/a to $k_o a$ for various values of t/r_o. Aperture thickness, t; aperture radius, r_o; $k_o = 2\pi f_o/c$; c is the speed of sound. From Ingard 6a.1/.

F₀ IN CPS
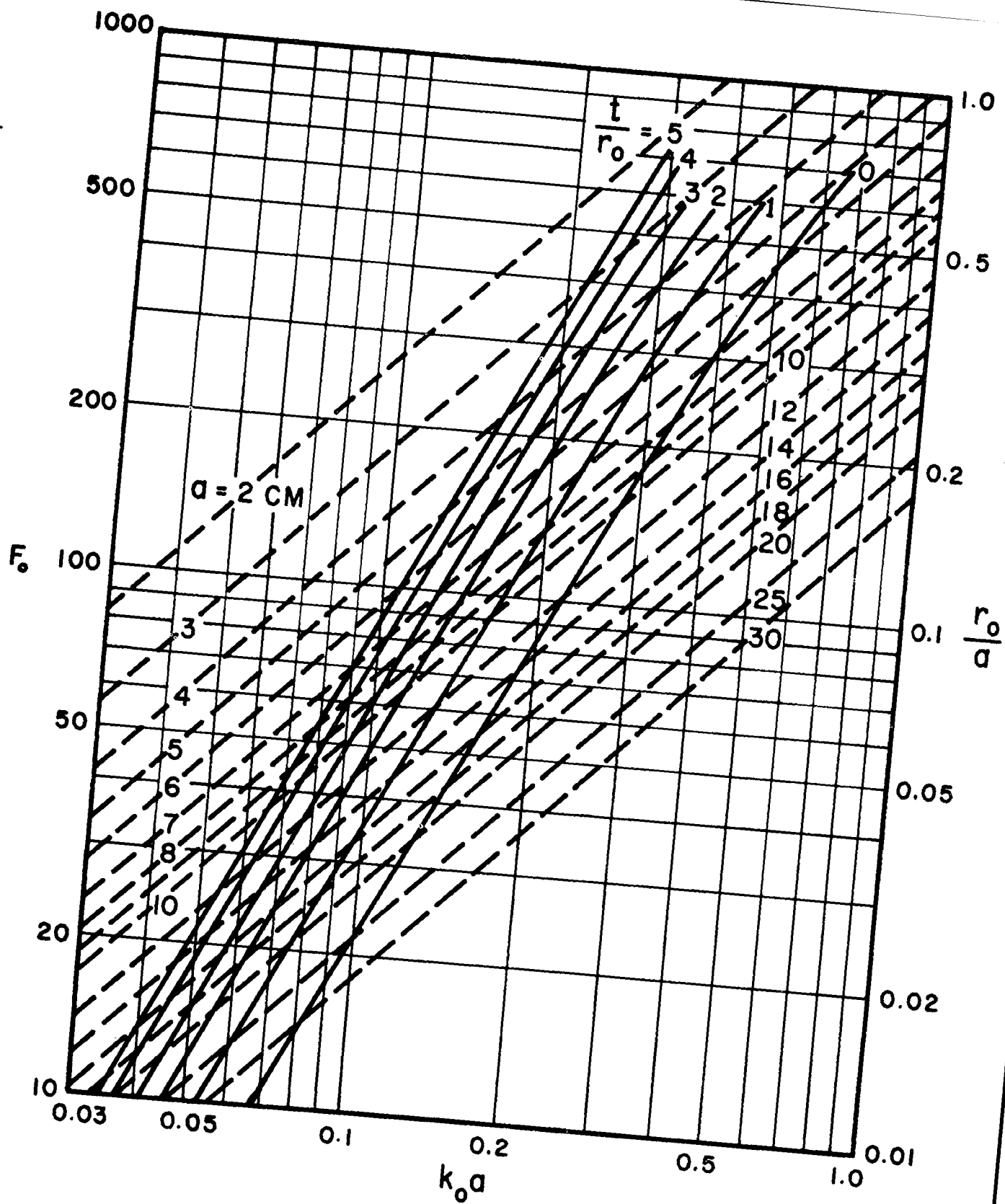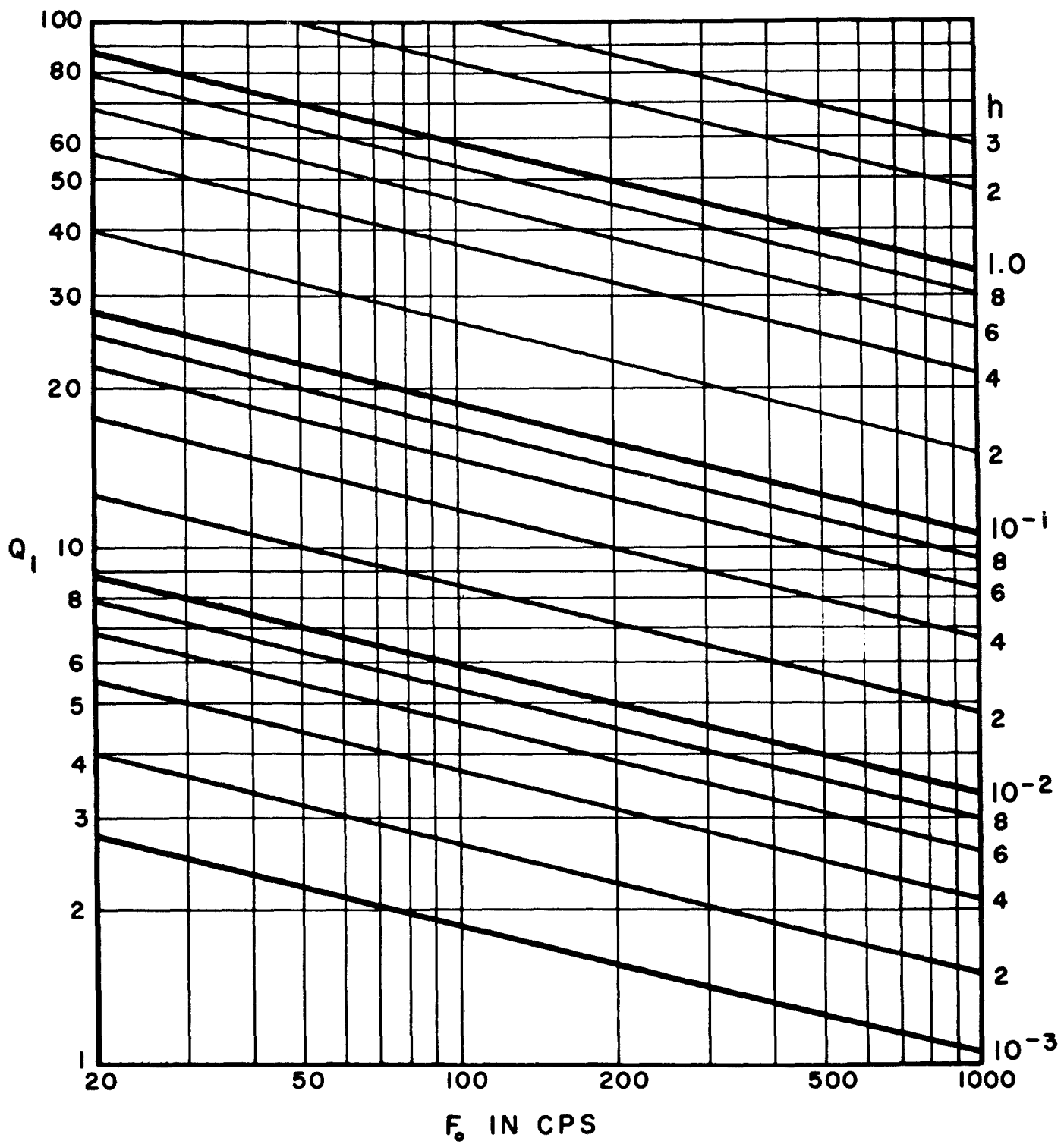
The case of a large area continuously covered by resonators tuned to the same frequency is treated in Sec. 12.1, under the topic of perforated facings for acoustical materials.

11. Adjacent resonators can be considered non-interacting when the difference in the resonance frequencies is greater than either of the bandwidths. When this restriction is observed, the analysis applies to banks of adjacent resonators which are "stagger-tuned" to cover a wide band of frequencies.

12. When short-neck resonators are used in an optimum design, as is necessary to secure large bandwidth, the bandwidth is proportional to the resonator volume. Therefore, the volume occupied by a "stagger-tuned" array for a given frequency band is a constant for optimum design, no matter whether, say, n resonators are used with one set of Q values, of 2n resonators are used with individual Q's twice as large.

Simplified Design for Short-Neck Resonators. It is evident from the preceding list of design considerations that resonators intended for large bandwidths represent a special case in which the neck is very short, or $t/r_0 \simeq 0$. The design procedure can be greatly shortened for this condition. The simplified relations for the short-neck resonator are given below, with numerical coefficients given for the case of room temperature air and $\beta = 0.9$. These relations represent optimum-design combinations; that is, combinations which represent maximum possible resonance absorption and maximum possible Q for a given resonator opening at a given frequency.

The optimum volume, in terms of the optimum Q and the frequency of resonance, is

$$V_1 = \frac{3.53 \times 10^7}{\langle 2 \rangle \, Q_1 \, f_0^{\,3}}$$

(12.6a.24)

FIGURE 12.6a.5

The Q value, Q_1, obtained in an optimum resonator design when the frequency of resonance in cps, F_0, and the hole parameter, h, are given. Represents Eq. (12.8a.19) for air at room temperature. From Ingard 6a.1/.

Here V_1 is in ft^3, and f_o in cps. This relation is derived by combining Eqs. (12.6a.17) and (12.6a.19). The required aperture radius is

$$r_o = 1.90 \times 10^{-4} \, f_o^{\,2} \, V_1 \qquad\qquad (12.6a.25)$$

where r_o is in inches, f_o is in cps, and V_1 is in ft^3. This relation follows from Eq. (12.6a.6). Using Eq. (12.6a.24), the radius (in inches) can also be expressed as

$$r_o = 6.70 \times 10^3 / f_o Q_1 \, \langle 2 \rangle \qquad\qquad (12.6a.26)$$

While the value of h, the hole parameter, is not required for the present calculations, it is helpful to be able to compute this quantity in order to refer back to the more extensive design charts. From Eq. (12.6a.19), the value of h for the present special conditions is

$$h = \langle 2 \rangle \, 2.82 \times 10^{-5} \, \sqrt{f_o} \; Q_1^{\,2} \qquad\qquad (12.6a.27)$$

where f_o is in cps.

The required flow resistance of the screen of cloth in the aperture is found by combining (12.6a.27) with (12.6a.8), and making use of the definition of ϵ . The required added flow resistance in rayls is given by

$$R' = \frac{191}{\langle 2 \rangle \, Q^2} - \left(3.26 \times 10^{-3} \right) \sqrt{f_o} \qquad\qquad (12.6a.28)$$

The maximum allowable volume for a resonator representing an optimum combination of value is set by the condition $(r_o/a_1) < 0.3$. The value of this maximum allowable volume is found by writing Eq. (12.6a.25) in the form of a relation between r_o and a_1, imposing the required

---

FIGURE 12.6a.6

The reverberation time in seconds, T_1, obtained in an optimum resonator design when the frequency of resonance in cps, F_o, and the hole parameter, h, are given. This represents Eq. (12.6a.20) for air at room temperature. From Ingard 6a.1/.

F₀ IN CPS

284
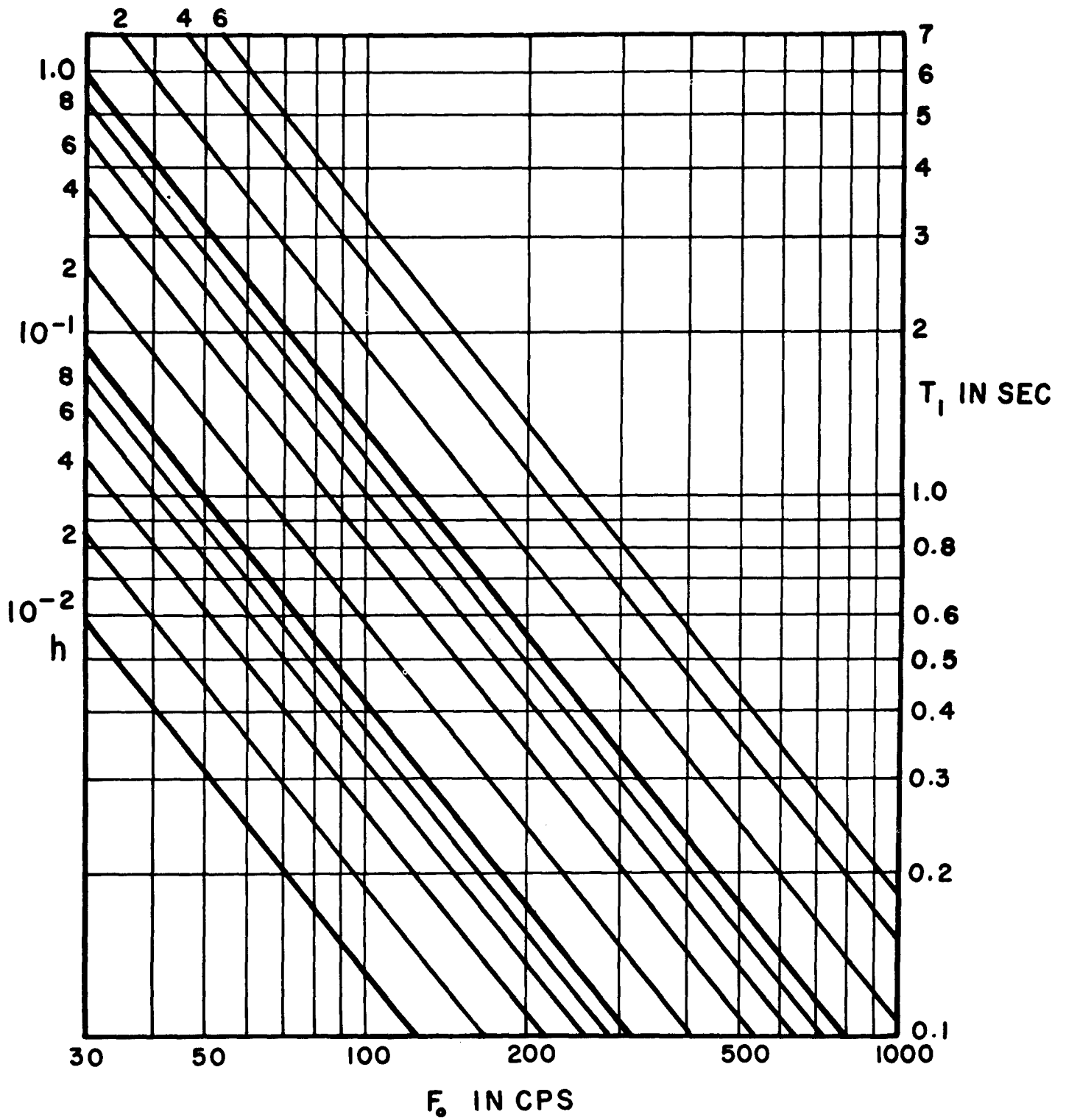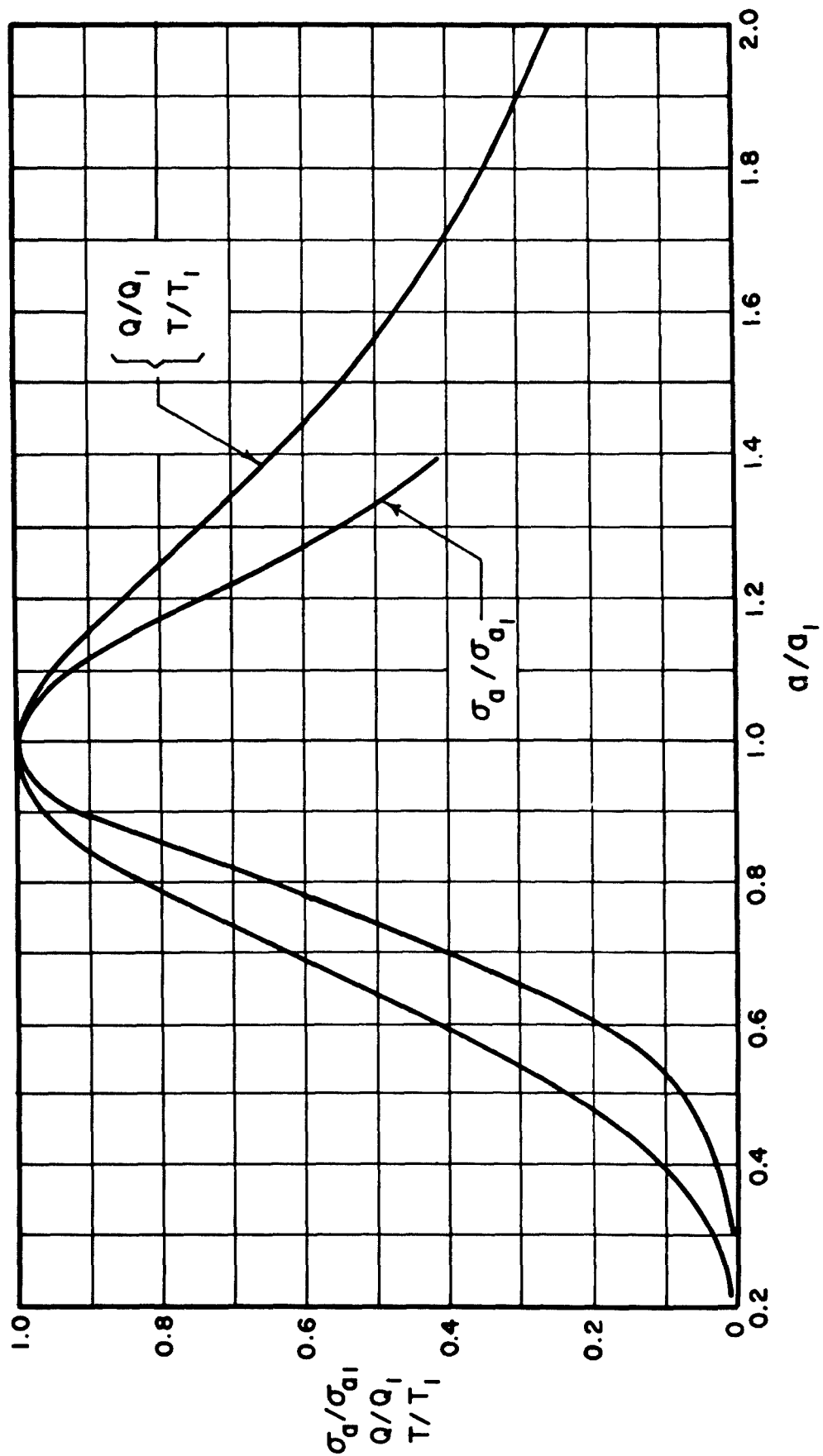
conditions, and then finding the volume from the resulting value for a_1. The resulting restriction on the volume is

$$V < \frac{1.4 \times 10^6}{f_o^3} \ \text{ft}^3 \qquad (12.6a.29)$$

The minimum Q which can be obtained with optimum design conditions is obtained in a resonator of maximum volume, and is found by combining (12.6a.29) and (12.6a.24). This minimum value of Q_1 is approximately $25/\langle 2 \rangle$. Correspondingly, the minimum reverberation time in optimum designs is approximately

$$T_{1 \ min} = 55/\langle 2 \rangle f_o \ \text{sec.} \qquad (12.6a.30)$$

Finally, the procedure for obtaining the optimum design of short-neck resonators can be summarized as follows: decide upon the desired resonance frequency. Then choose a resonator volume not exceeding the limit given by Eq.(12.6a.29), or choose a Q not less than $25/\langle 2 \rangle$. The remaining design quantities can then be found directly from the preceding equations if the resonator operates in air at room temperature.

The numerical coefficients, and the limiting values of the volume and the Q, will be different if other values of the density and the viscosity of the gas are used, and it will be necessary in that event to go to the basic equations given previously in this section.

FIGURE 12.6a.7

The relative effects upon the resonance absorption cross section, σ_{ao}, the reverberation time, T, and the Q, when a departure is made from optimum resonator design. It is assumed that the resonance frequency f_o and the hole parameter h retain the values for which the optimum cavity radius a_1 applies, but that the cavity radius has been changed arbitrarily from a_1 to some value a, and a corresponding change made in the aperture radius. From Ingard 6a.1/.

Effects of Non-linearity. The internal resistance of
the resonator includes a non-linear contribution which be-
comes important when the resonator is exposed to large
incident sound pressures, as was found in Sec. 12.6 in
connection with the design of a resonator attached to a duct.
The effect of non-linearity may become significant when the
SPL of the incident signal exceeds 80 to 90 db, but in
large, low-frequency resonators this threshold may be much
higher. The effect of the non-linear resistance is to de-
crease the resonance absorption and the Q of the system.
To include the non-linear resistance in the basic equations
would lead to results so cumbersome as not to be highly
useful. Therefore, only special aspects of the problem
will be considered.

In the general case, the non-linear resistance depends
upon the orifice thickness, the particle velocity, and the
particle displacement. The effect of frequency is
apparently not great, but this question has not been ex-
plored extensively. Non-linear resistance data are experi-
mental, because no general theory has been given yet. For
the present purposes, an empirical relation 6a.1/expressed
by Eq. (12.6a.31) will be used for the non-linear resistance.
This relation is more accurate over a wide range of condi-
tions than the one used in Sec. 12.6, although both formulas
lead to approximately the same value of sound pressure at
which the response of the resonator is seriously affected
by non-linear resistance. Only the effect of particle velo-
city is shown, since this is the variable of major importance
in the non-linear resistance unless the particle displace-
ment amplitude exceeds the orifice thickness. The non-linear
acoustic resistance is

$$R_{NL} = 1.36 \times 10^{-5} \quad U^{1.7}/A^{2.7} \qquad (12.6a.31)$$

where U is the rms volume velocity in cm^3/sec and A is the
aperture area in cm^2.

The effects of the added resistance R_{NL} upon the Q and
the peak absorption of a resonator designed to meet optimum
conditions in the absence of the non-linear resistance are
easily expressed. The total resonator resistance is $R_i + R_r$;
in the optimum design, this is simply $2R_r$. When non-linear

effects are present, the total resistance is $2R_r + R_{NL}$. Thus the Q, which is inversely proportional to resistance, is changed according to the relation

$$\frac{Q_{NL}}{Q_1} = \frac{2R_r}{2R_r + R_{NL}} \qquad (12.6a.32)$$

The effect upon the resonance-frequency absorption cross section is found by inserting the appropriate resistance values into (12.6a.2). It is convenient to express the result in terms of the change in the Q, by using (12.6a.32). This leads to the relation

$$\frac{\sigma_{aoNL}}{\sigma_{al}} = \frac{Q_{NL}}{Q_1} \qquad (2 - \frac{Q_{NL}}{Q_1}) \qquad (12.6a.33)$$

The sound pressure required to bring the Q down to the value Q_{NL} will be calculated in the special case where the resonator represents an optimum design combination characterized by Q_1 for small sound pressures. Because of the cumbersome manner in which the nonlinear resistance enters into the resonator equations, the procedure to be followed in this and other related calculations is to solve the non-linear resistance expression for the volume velocity, and to work back from this to find the pressure. The procedure is shown in sufficient detail to suggest a general method of approach. The volume velocity is

$$U = (R_{NL} \, A^{2.7}/1.36 \times 10^{-5})^{1/1.7}$$

The quantity R_{NL} will be replaced by its value in terms of R_r, from Eq. (12.6a.32), which is

$$R_{NL} = 2R_r \, [(\frac{Q_1}{Q_{NL}}) - 1]$$

The pressure is $p = UR_{total} = U(2R_r + R_{NL})$, which can be expressed as

$$p = 2R_r (Q_1/Q_{NL})U$$

The radiation resistance is $R_r = \langle 2 \rangle \; 2\pi\rho f_o^2/c$. When this sequence of calculations is combined and expressed in numerical values for air at room temperature, the result is

$$p = 3.0(6.8 \times 10^{-6})(r_o f_o)^{3.2} \frac{Q_1}{Q_{NL}} \left(\frac{Q_1}{Q_{NL}} - 1\right)^{0.59} \text{ rms dyne/cm}^2$$

$$(12.6a.34)$$

where r_o is the aperture radius in inches. For example, if a resonator is designed for optimum small-signal operation in open space at 55 cps, with an aperture radius of 4.7 inches, Eq. (12.6a.34) indicates that the pressure which will reduce the Q to $Q_1/2$ is approximately 600 dyne/cm^2, corresponding to a sound pressure level of 130 db (re 0.0002 dyne/cm^2). Furthermore, according to (12.6a.33), the resonance absorption is reduced to 0.75 of the small-signal value.

The non-linear behavior of a screen or cloth in the orifice may be different from that of the orifice itself, and may become important at smaller sound pressures. For this reason, the result above is most accurate when the orifice contains no additional resistive material.

Another special non-linear resonator problem which can be treated easily is as follows: given the sound pressure level at which a resonator with no added resistance material is to represent an optimum design, find the effective value of ϵ (which now represents the added resistance due to non-linearity rather than that due to cloth or screen), so that the optimum design can be computed with the charts already given. This problem can be solved by a procedure similar to the one used in the preceding case, but the resulting equations are much less convenient for direct calculation. Therefore the results are expressed in chart form, in Fig. 12.6a.8. The results shown apply to a

frequency of 220 cps, but are sufficiently accurate for all audio frequencies below 500 cps. Experience in the use of this chart will show that the resonator volume for optimum design increases with increasing sound pressure, so that there is always some sound pressure level above which an optimum design is not practical.

The non-linear resistance is less important in relation to the other resistances and causes less reduction in absorption, in those resonators which are designed for broad-band operation. Those are the maximum-volume, large-aperture resonators. Therefore, when the sound pressure is so large that an optimum design is impossible, the greatest absorption possible under the circumstances is obtained by using a short-neck resonator of maximum allowable volume. The absorption under these conditions can be calculated by making successive approximations until a value of volume velocity is found which is consistent both with the driving pressure and with the non-linear resistance which was assumed in arriving at the volume velocity.

The driving pressure, p, is equal to twice the incident-wave pressure in the case of the resonator in a large wall.

All relations derived for non-linear effects in this discussion have applied to frequencies in the vicinity of resonance. The non-linear effect is much less important at frequencies outside the normal bandwidth region.

The End-Correction Factor in Special Cases. The value of the end-correction factor β has been computed for a number of cases in which the aperture and the cavity cross section have simple shapes 6a.1/. The total value of β for a given aperture is the sum of the values for its two ends. The value β_e for one end of the aperture is given by the relation

$$\beta_e = 0.5 - 0.625\,\xi$$

$$(\xi \quad < 0.4) \qquad\qquad (12.6a.35)$$

where the variable ξ is defined for the following cases:
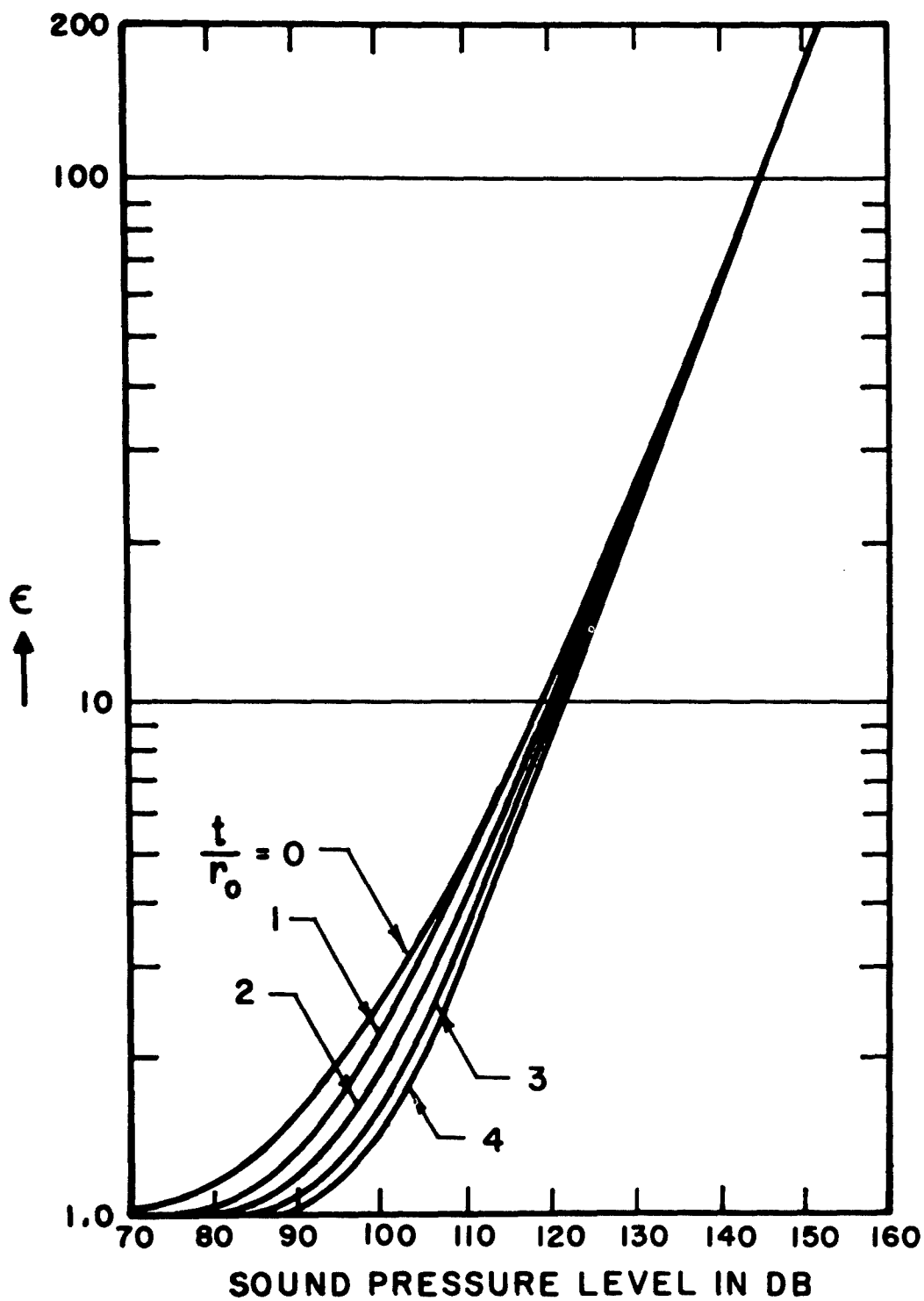
Concentric circular hole of radius r_0 opening
into circular tube of radius R, $\xi = r_0/R$.

Concentric circular hole of radius r_0 opening
into square tube of side 2a, $\xi = r_0/a$.

Concentric square hole of side $2a_1$ opening into
square tube of side 2a, $\xi = a_1/a$.

Circular or square hole opening in large plane
wall, $\xi = 0$.

For example, for a circular hole of radius 3 in. which
opens on one side in a large wall and on the other side into
a concentric circular tube of radius 10 in.,

$$\beta = [0.5-0.625(0)] + [0.5-0.625(3/10)] = 0.5 + 0.31 = 0.81$$

Temperature Effects. The temperature coefficient of
the frequency of resonance is equal to that of the speed of
sound. Thus, f_0 is proportional to the square root of the
absolute temperature, so that under ordinary conditions
the frequency of resonance increases approximately one per-
cent for a temperature increase of 10°F. It is easily
possible to design a resonator having sufficiently high Q
(50 or more) that a one percent frequency change will reduce
the absorption at constant frequency to one-half. Thus it
is desirable to design for the smallest optimum-design Q
when a single resonator must absorb a constant frequency

FIGURE 12.6a.8

The effect of nonlinear resistance in an optimum-design resonator,
for air at room temperature. Values are derived for 220 cps, but
may be used for audio frequencies below 500 cps. It is assumed
that no extra flow resistance element has been added to the aper-
ture. To use the chart, determine the expected sound pressure
level and the expected ratio t/r_0 of aperture thickness to aper-
ture radius, and then find the resistance-increase parameter
from the chart. Complete an optimum resonator design as for small
signals, with this value of $\in$ as a starting point. The optimum
design performance will then be realized when the resonator is
exposed to the sound pressure level originally assumed, rather
than under small-signal conditions. From Ingard 6a.1/.

under conditions of fluctuating temperature. This diffi-
culty is not pronounced in the case of a stagger-tuned
array of resonators, since all frequencies of resonance
are affected by the same factor when the temperature changes.

Practical Tuning of Resonators. The approximations
made in calculating the frequency of resonance, or tolerances
in construction, may result in serious mistuning of a high-
Q resonator which is intended to operate at a specific
frequency. The most reliable solution to the tuning pro-
blem is to adjust the resonator to the proper frequency after
installation. The adjustment may be performed by varying
either the volume or the area of the opening. An indication
of proper adjustment may be obtained by use of a sound level
meter connected to a pressure microphone located outside
the resonator next to the resonator opening. When the
resonator is exposed to constant intensity sound of the fre-
quency that one wishes to absorb, the resonator is tuned by
adjusting the resonator variable for a minimum sound level
meter reading compared to the initial sound pressure level.

Another source of tuning error is the non-linear
contribution to the acoustic mass, which becomes important
at high signal levels. This non-linear effect is generally
less important than the non-linear resistance and hence has
not been considered in the analysis. Provision for tuning
adjustment is particularly desirable to compensate for this
effect where strong signals are expected.

Significance of Reverberation Time. When a resonator is
used as a sound absorber in a room intended for listening to
music or speech, the reverberation time of the resonator
should be less than that of the room at the frequency of
resonance, in order to avoid a localized "hold over" follow-
ing transient signals. This requirement on the reverbera-
tion time is ordinarily not difficult to satisfy. For
example, stagger-tuned resonator arrays have been successfully
used to provide low-frequency absorption in small radio
studios.

Numerical Examples of Resonator Design. As a first
example, it will be supposed that an optimum-design, wall-
mounted resonator is required to operate at 55 cps, with a
bandwidth of 2.2 cps.

Since the Q is relatively low (25), it will be desirable to use the simplified design procedure for the short-neck resonator. The design is possible, since a Q as low as 13 can be obtained with a wall-mounted resonator.

From Eq. (12.6a.24), the required volume is 4.24 ft^3.

From Eq. (12.6a.25), the aperture radius is 2.44 in.

From Eq. (12.6a.28), the added flow resistance must be 0.15 rayls.

The reverberation time is 2.19 Q_1/f_o, or 1.0 sec.

From Eq. (12.6a.34), the driving sound pressure at which the Q is halved is 110 dynes/cm^2, corresponding to a sound pressure of 55 dynes/cm^2 in the wave incident on the wall, a sound pressure level of 109 db. This is also the incident sound pressure at which the center-frequency absorption is reduced to 75 percent of the small-signal value due to non-linear operation according to Eq. (12.6a.33).

The maximum small-signal absorption ($\lambda_o{}^2/2\pi$) is 64 sabins at a wavelength of 20 ft.

As a second example, suppose that it is desired to determine the dimensions of a short-neck resonator, with no added resistance in the aperture, which shall represent an optimum design at 60 cps when used in space where the incident SPL is 110 db. The initial step is to consult Fig. 12.6a.8, according to which $\epsilon = 4.9$ under the given conditions. The remaining steps are carried out according to the "Procedure for optimum design calculation", given following Eq. (12.6a.22).

From Fig. 12.6a.2, h = 0.18

From Fig. 12.6a.3, a_1 = 34 cm.

From Fig. 12.6a.4, $k_o a_1$ = 0.39

From Fig. 12.6a.4, r_o/a = 0.29, so that r_o = 9.9 cm.

From Eq. (12.6a.13), F = 1.34.

The maximum absorption cross section
is 1.35 $\lambda_o^2/4\pi$ = 37 sabins.

From Fig. 12.6a.5, Q_1 = 29.

References for Sec. 12.6a

6a.1 Ingard, Uno, "On the Theory and Design of
      Acoustic Resonators", J. Acous. Soc. Am.
      25 1037 (1953).

12.9 Acoustical Shielding Properties of Walls and Structures

A common problem is that of using a wall or building to obtain acoustic shielding from a noise source. This type of solution is of value when the noise source is movable or where covering it completely with a muffling structure would interfere with the operation of the device. For example, annoyance to nearby residences due to the noise of large, outdoor power substation transformers can sometimes be reduced by partially enclosing them by walls. Or engine run-ups in airports near residential areas can be made less annoying if hanger structures are suitably placed to provide acoustical shielding.

General Design Procedure. Data showing the noise reduction provided by walls have been reported by Fehr and by Hayhurst 9.1,9.2/. The chart presented by Fehr is based on the Fresnel diffraction of a wave from a line source parallel to an infinitely long edge. As a result of field measurements, several modifications to the Fehr formula have been made. In addition, several factors which Fehr has not considered but which enter into the practical acoustical problem such as a finite wall, atmospheric turbulence and ground attenuation are also discussed.

Figure 12.9.1 shows the geometrical situation being considered. The sound source is at a distance R on the ground behind a wall or structure of height H. At a distance D on the other side of the wall, also on the ground is the point where the sound level is to be calculated.

One calculates the parameter X given by

$$X = 2[R(\sqrt{1 + (H/R)^2}-1) + D(\sqrt{1 + (H/D)^2}-1)]/\lambda[1 + (H/R)^2].$$

$$(12.9.1)$$

For the common situation where D >> R and R ⩾ H,

$$X \simeq H^2/\lambda R \qquad\qquad (12.9.2)$$

where λ is the wavelength of sound in air which for a frequency f (in cps) is 1120/f feet. As one expects, the shielding effect depends on frequency. At low frequencies, the

diffraction around the obstacle leads to relatively high sound levels at D while for high frequencies the "beaming" tendency causes D to lie in an acoustic shadow zone.

Figure 12.9.2 gives the noise reduction (NR) in decibels for a given value of X. The line is a plot of the equation

$$(NR) = 10 \log 20X \qquad (12.9.3)$$

Factors Modifying Shielding Noise Reduction. The value of NR calculated from Eq. (12.9.3) or Fig. 12.9.2 would actually be measured if the source were on the ground, the ground presented an infinitely high impedance and the atmosphere were a quiescent, homogeneous medium. As pointed out in Sec. 12.8, the presence of wind and temperature gradients in the atmosphere can lead to the deflection of sound upward or downward. In the first case, there is an acoustical shadow zone formed, while in the second, sound energy originally traveling upward is deflected down. For a quantitative discussion of these effects, the reader is referred to the work of Ingard and Pridmore-Brown 9.3, 9.4/ and Stevens and Bolt 9.5/. In the following sections, we consider
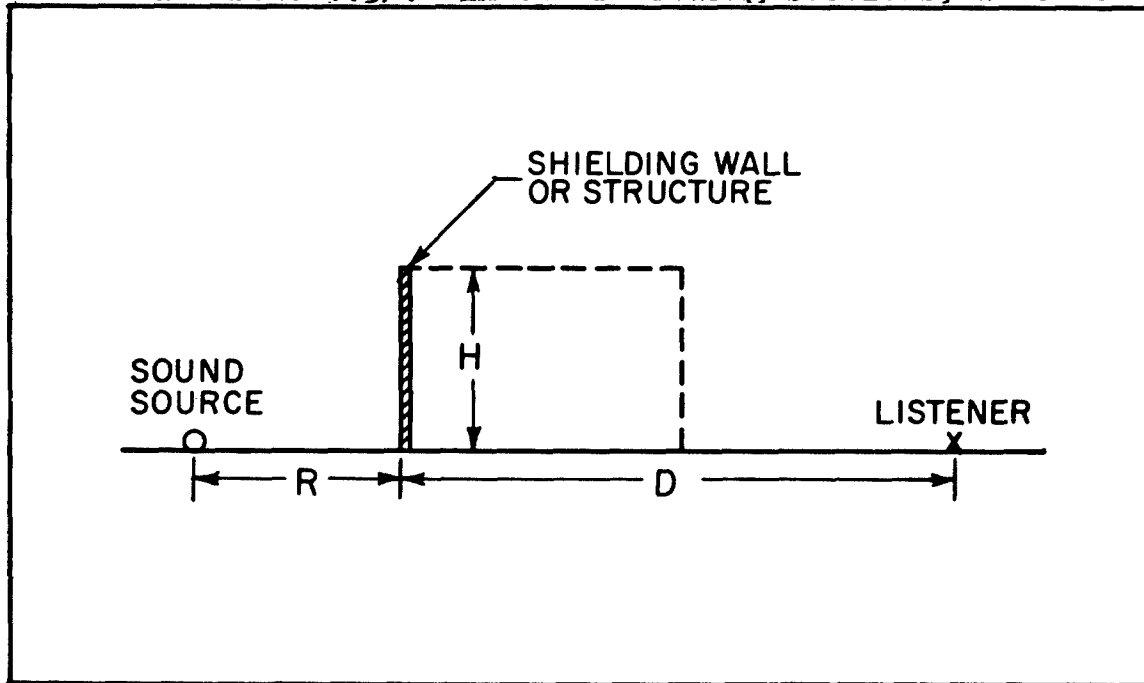

FIGURE 12.9.1

Sketch showing geometrical arrangement considered. A sound source is on the ground at a distance R behind a shielding wall or structure of height H. The listener is on the other side of the wall or obstacle at a distance D. For a thick structure, D is measured from the side nearest the sound source.

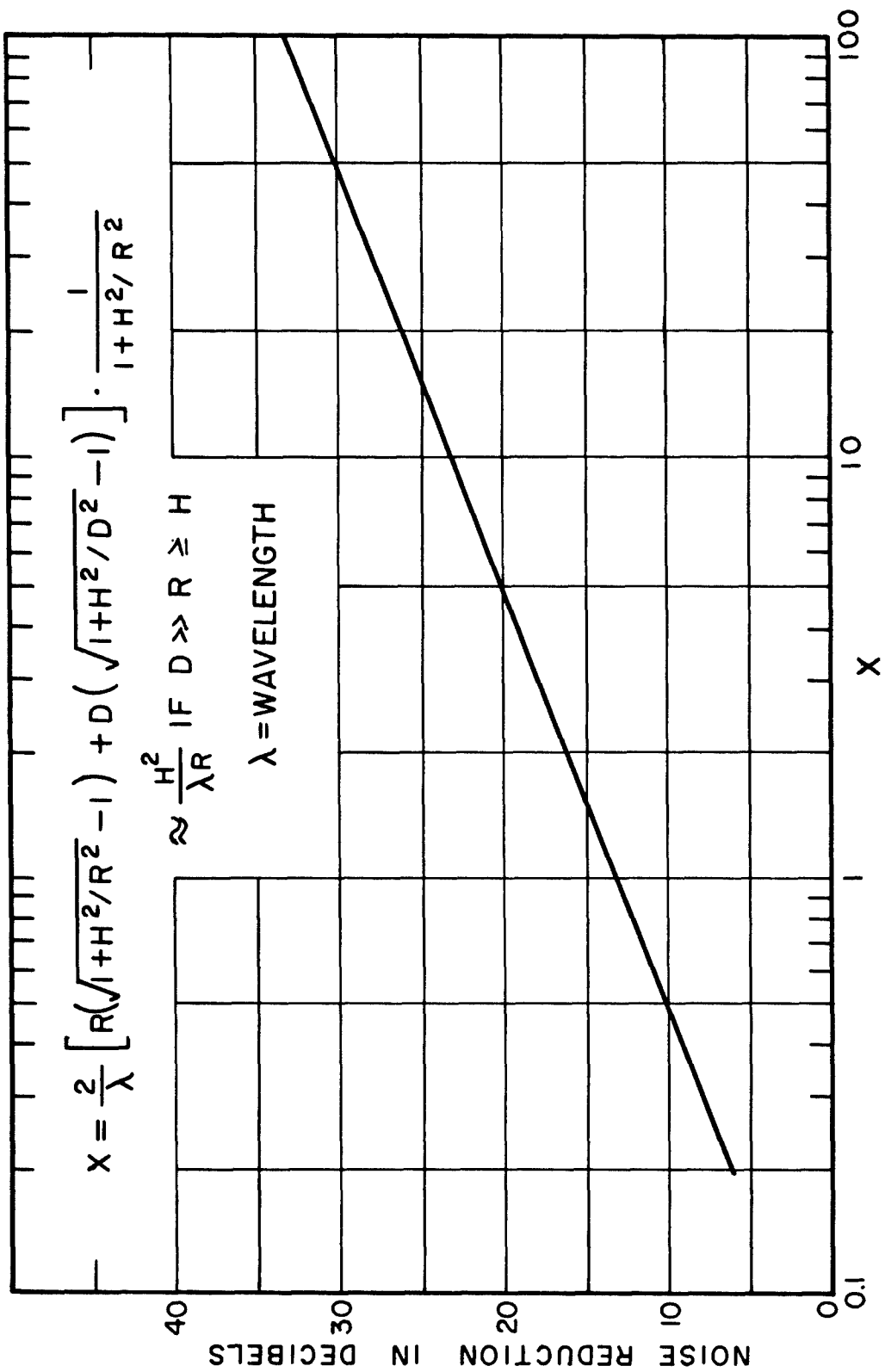the modifications necessary to account for

1. the sound source not being on the ground

2. absorption by the ground

3. atmospheric turbulence

4. "flanking" around the side of a structure

1. Consider the situation shown in Fig. 12.9.3 where a sound source is located some height h above the ground and at a distance R from a shielding wall or structure. Ray A shows the direct path from the source to the obstacle. For very high frequencies, this ray also marks the edge of the shadow zone. Any sound energy found below Ray A on the receiving side of the shield must be there because of diffraction, by virtue of the wave nature of sound. For a certain frequency ν_1 the distance SO along path B is longer than that along path A by $\lambda/2$. The two waves then destructively interfere, causing higher shielding than would otherwise be the case. For this to occur

$$\nu_1 = \frac{c/2}{[(H + h)^2 + R^2]^{1/2} - [(H - h)^2 + R^2]^{1/2}}$$

(12.9.4)

When the path length difference between the direct and reflected ray is one wavelength, there will be pressure doubling at point O. Consequently the sound pressure will be 6 db higher and there will be a minimum in the shielding effect. This second case will occur at a frequency ν_2 given by $\nu_2 = 2\nu_1$. When (H+h) and (H - h) << R, we find for ν_1

$$\nu_1 = cR/4Hh$$

(12.9.5)

$$x = \frac{2}{\lambda}\left[R\left(\sqrt{1+H^2/R^2}-1\right)+D\left(\sqrt{1+H^2/D^2}-1\right)\right]\cdot\frac{1}{1+H^2/R^2}$$

$$\approx \frac{H^2}{\lambda R} \quad \text{IF } D \gg R \gtrapprox H$$

$\lambda = $ WAVELENGTH

NOISE REDUCTION IN DECIBELS

2. Now consider the effect of the absorption of sound due to the finite acoustic impedance of the ground. In the absence of the shield, sound would travel from the source to the receiver with an attenuation due to inverse square spreading (6 db per distance doubling) plus some additional ground attenuation. However, when an obstacle is present, the sound which reaches the receiver has traveled over the obstacle and so has suffered less ground attenuation. Therefore, a measurement of the sound level with and without the obstacle should show somewhat less shielding than diffraction theory (which assumes infinite ground impedance) would predict. Adding the obstacle has introduced shielding but has prevented the terrain attenuation from being as great as when the ground was fully exposed.

To correct this effect, one must know the ground attenuation for the type of terrain involved (concrete, bare earth, low or high grass, etc.). Then plot the attenuation expected for the distance R + D as a function of frequency. On the basis of this, estimate the expected terrain attenuation considering the height of the structure and/or the fraction of the total path length R + D occupied by the shielding obstacle. Such a curve for the special case of high grassy terrain is shown in Fig. 12.9.4. The estimate of the percent of the terrain attenuation which should be taken when a shielding structure is in place is, of course, somewhat arbitrary. However, it is important to make some estimate of the effect in the frequency region where it is important, even if the magnitude of the correction is doubtful.

3. Next consider the effect of atmosphere turbulence. So far, it has been assumed that the air is still and that

---

FIGURE 12.9.2

Noise reduction (NR) in decibels due to a shielding structure. To find the shielding for a wavelength λ for given values of R, H and D, calculate X by Eq. (12.9.1) or (12.9.2) and read the (NR) from this chart. This value of (NR) must be corrected for the height of the source above the ground, terrain attenuation and turbulent scattering in the atmosphere, as discussed in the following sections.

there is no turbulence. For wind velocities less than 5 mph, this is approximately true although even in "still" air, there is a turbulent layer of air about 100-300 ft thick at the surface of the earth. Therefore, there will always be some sound scattered down into the region bounded at the top by Ray A of Fig. 12.9.3. But since the amount of turbulence increases with wind velocity, it is expected that the scattering effect, and thus the deviation from the noise reduction predicted from Fig. 12.9.2 would increase with wind velocity. This effect should be relatively independent of wind direction as long as the turbulence is roughly isotropic.

While the amount of turbulent scattering is independent of wind direction, it must be remembered that except for the case of a crosswind, the wind may create a shadow zone. The presence of a shadow zone will, of course, modify the shielding prediction. The reader is again referred to Refs. 9.3-9.5.
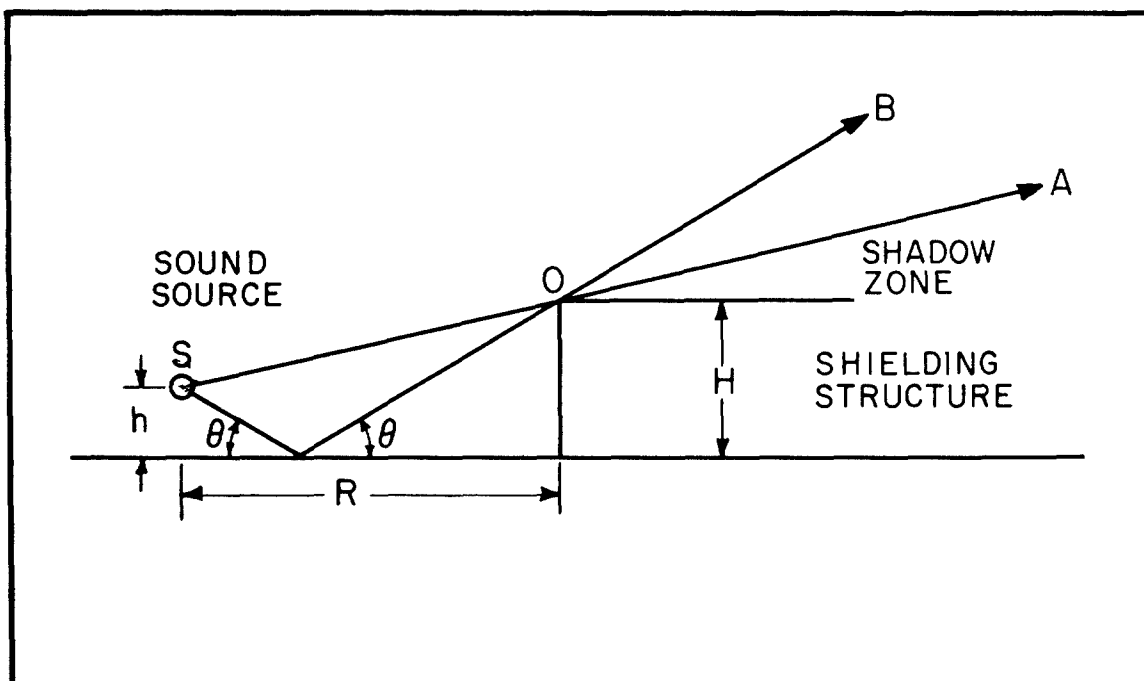
FIGURE 12.9.3

Geometric illustration of the effect of having the source above the ground. Frequency-dependent interference effects will be observed due to the two possible paths from the sound source to the shielding structure.

Figure 12.9.5 shows approximate corrections to the expected noise reduction which were found from a set of field measurements. The curves give the correction to be subtracted from the predicted noise reduction to account for turbulent scattering.

4. The last point, flanking around an obstacle due to its finite length, can best be illustrated by a set of measurements taken with a sound source located at a point R = 50 ft and 50 ft from the edge of a structure 40 ft high and 200 ft deep. Figure 12.9.6 shows measurements in four frequency regions. From these polar plots, it can be seen that the maximum shielding effect is not obtained unless the receiving point is on the 0° line, or directly opposite the source. The 45° lines show the geometric "shadow". Near this line, the shielding is quite small compared to the calculated (maximum) value. In general, a good idea is to have the distance from the sound source to the edge of the shield at least twice the distance R. If the shield has "wings" such as to enclose the sound source on more than one side, this precaution will, of course, be unnecessary.

Numerical Example. Consider the following case. We wish to calculate the shielding at a distance of 400 ft of a structure 40 ft high along the 0° line. There is a cross-wind whose speed is 10 mph, the ground is covered by long grass (this is the type of ground for which Fig. 12.9.4 was drawn) and the sound source is 50 ft from the wall and well back from the edge of the structure. Table 12.9.1 shows the calculations for octave bands (carried out for the geometric mean frequency of the band limits). Then R = 50, H = 40, D = 400 ft. Consider the sound source to be on the ground.

From the approximate Eq. (12.9.2), one can see that the shielding increases with frequency and with the wall height, but decreases as the sound source is moved back from the wall (R increasing). The shielding also decreases as the listener moves back from the wall (D increasing). Atmospheric turbulence and the effect of ground absorption decrease the shielding from what diffraction theory would predict.
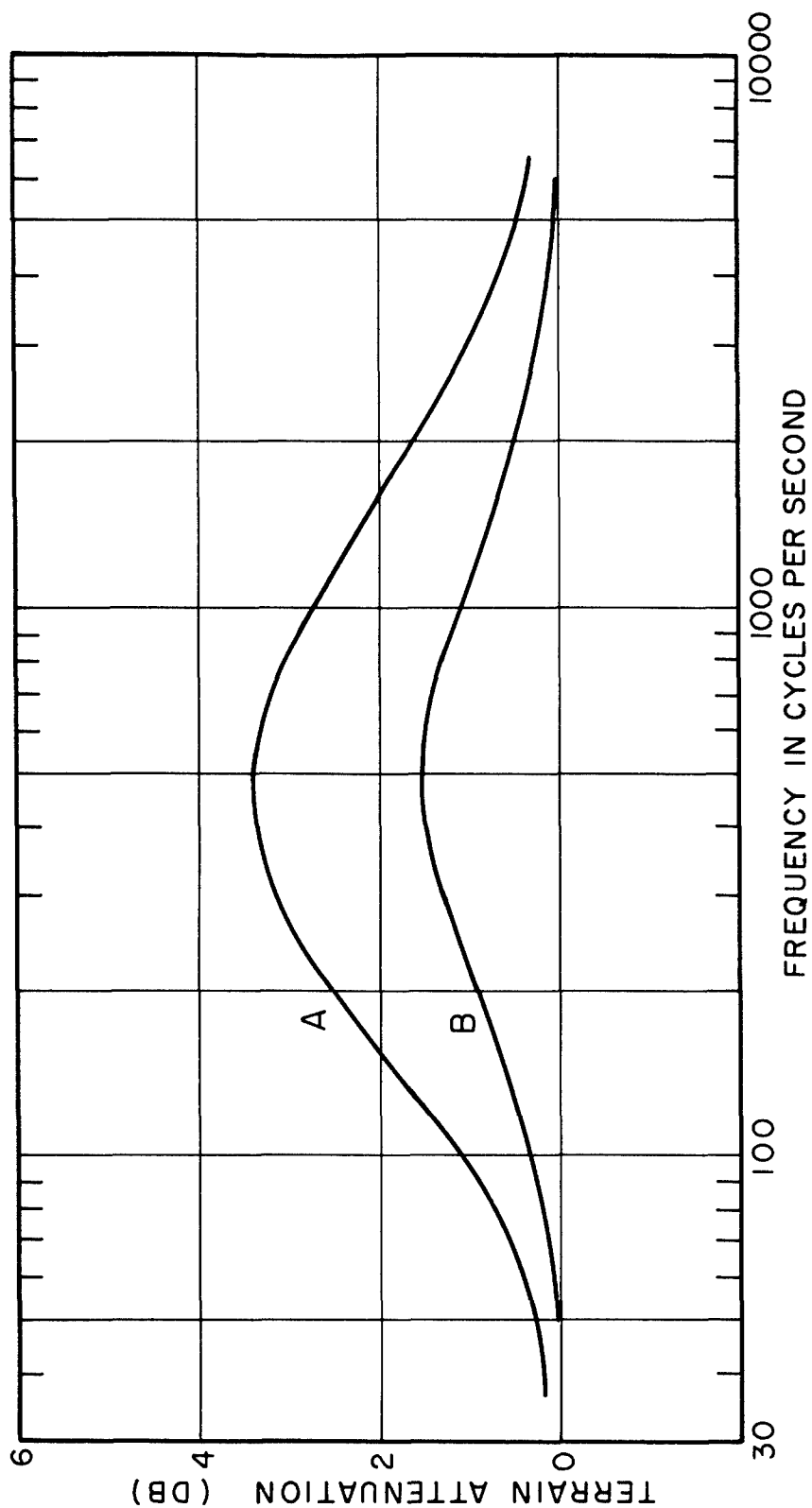
FREQUENCY IN CYCLES PER SECOND

10000

1000

100

30

TERRAIN ATTENUATION (DB)

6

4

2

0

A

B

TABLE 12.9.1

Frequency Band cps	Geometric Mean Frequency cps	X from Eq. (12.9.1) or (12.9.2)	(NR) from Fig. 12.9.2 db	Ground Absorption Correction db	Turbulence Correction db	Total Correction db	Corrected NR db
20-75	39	0.60	11	0	0	0	11
75-150	106	1.6	15	-0.7	0	-0.7	14
150-300	212	3.4	18	-1.5	0	-1.5	16
300-600	424	6.6	22	-1.7	-1	-2.7	19
600-1200	848	13.1	24	-1.4	-3	-4.4	19
1200-2400	1700	26.4	27	-1.1	-5.5	-6.6	20
2400-4800	3490	54.1	30	-0.6	-9	-9.6	20
4800-10000	6930	107	33	0	-12	-12	21

FIGURE 12.9.4

Illustration of the method of correcting the NR found from Fig.12.9.2 for the effects of ground attenuation. Curve A shows the absorption (in excess of inverse-square spreading) of 450 ft of grassy terrain. Curbe B is the estimated ground attenuation when the shielding structure is in place, and is obtained from Curve A by taking a certain fraction of the values for the unobstructed case. For the dimensions used in the numerical example, Curve B = (Curve A)/2.
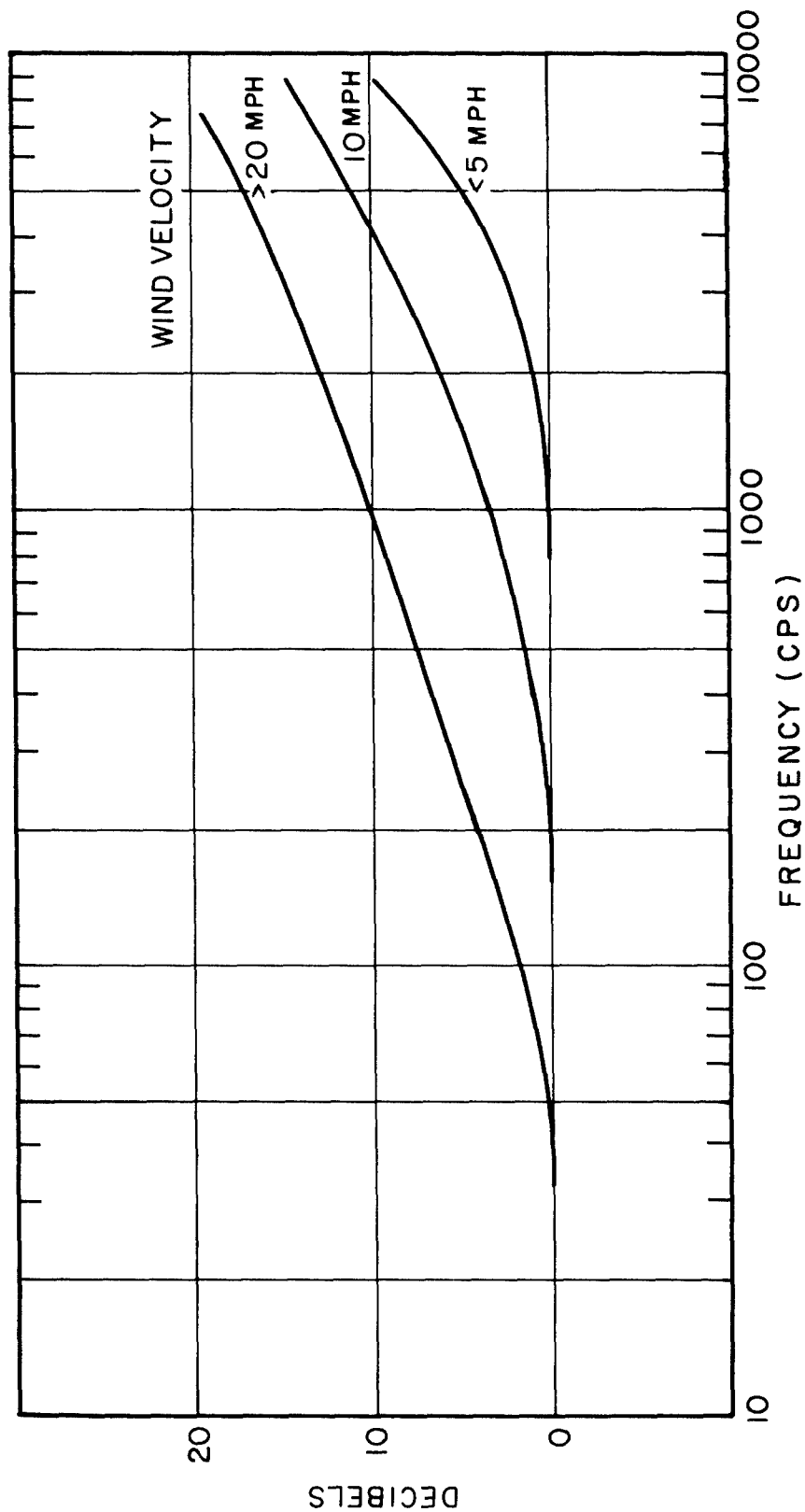
FIGURE 12.9.5

Correction to (NR) found from Fig. 12.9.2 due to scattering by atmospheric turbulence. The value given is to be subtracted from the ideal (NR) found from Fig. 12.9.2. Since the amount of atmospheric turbulence depends on the wind velocity, three curves are given, for wind velocities less than 5 mph, equal to 10 mph or greater than 20 mph. Values for intermediate cases can be obtained by interpolating between the curves given.

50 – 100 CPS

20 DB

10 DB

HANGAR

SOURCE

O DB

125 – 320 CPS

20 DB

10 DB

HANGAR

SOURCE

O DB

400 – 1000 CPS

20 DB

10 DB

HANGAR

SOURCE

O DB
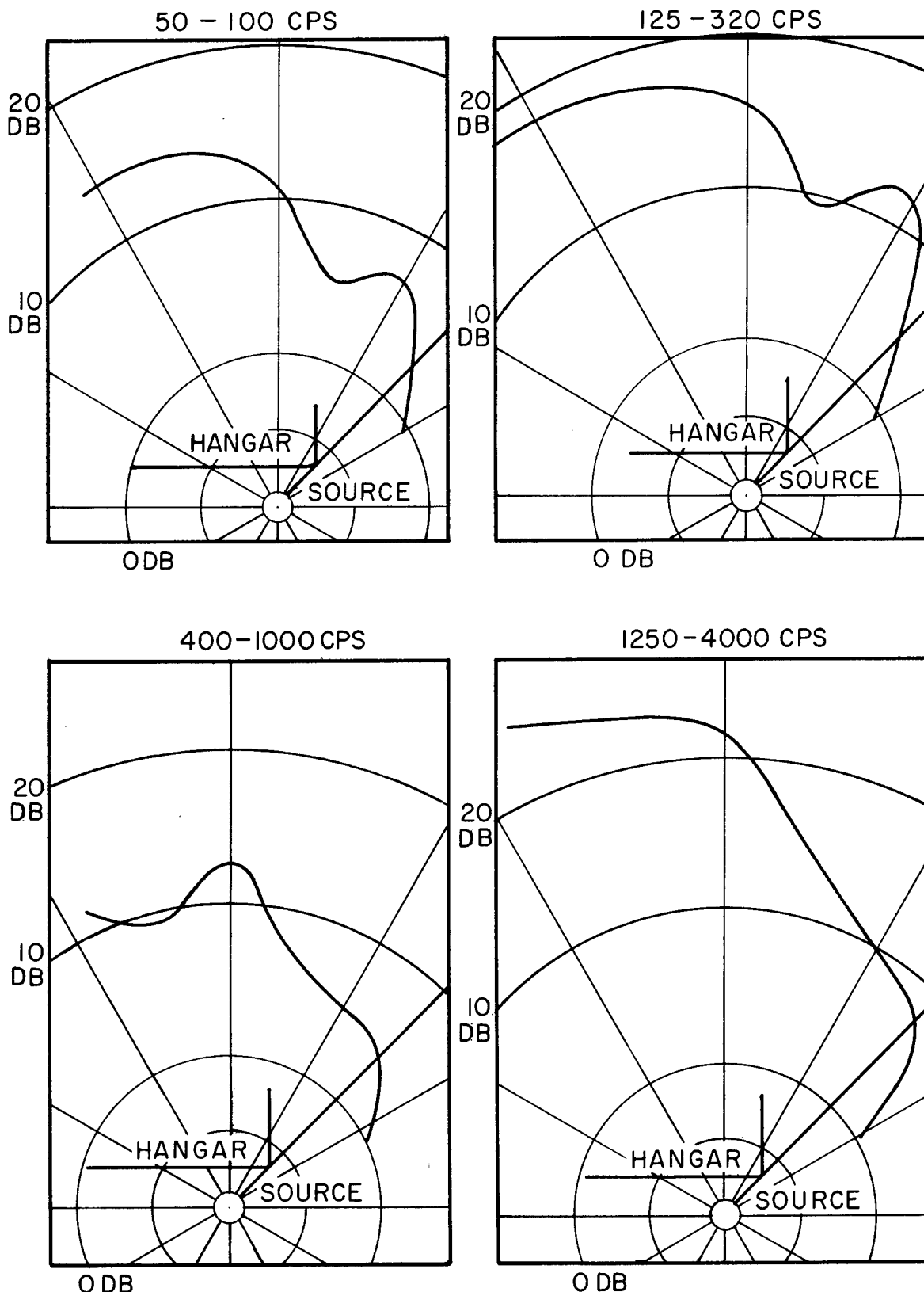
1250 – 4000 CPS

20 DB

10 DB

HANGAR

SOURCE

O DB

FIGURE 12.9.6

These curves show the average measured attenuation in four frequency ranges when the source is located close to the edge of an airplane hangar. The attenuation is shown at various angles with respect to the edge of the geometrical shadow created by the hangar (marked by the heavy line at 45°).

References

(9.1)   Fehr, R. O. "The Reduction of Industrial Machine Noise" Proc. Second Annual National Noise Abatement Symposium, Technology Center, Chicago 16, Illinois 5 Oct. 1951

(9.2)   Hayhurst, J. D. "Acoustic Screening by an Experimental Running-Up Pen" J. Roy. Aero. Soc. 57 3-11 (1953)

(9.3)   Ingard, U. "The Physics of Outdoor Sound" Proc. Fourth Annual National Noise Abatement Symposium, Technology Center, Chicago 16, Illinois 23-24 Oct. 1953

Ingard, U. "Review of the Influence of Meteorological Conditions on Sound Propagation" J. Acoust. Soc. Am., 25 405-11 (1953)

(9.4)   Pridmore-Brown, D. and U. Ingard "Sound Propagation into the Shadow Zone in a Temperature-Stratified Atmosphere Above a Plane Boundary" J. Acoust. Soc. Am. 27 36-42 (1955)

(9.5)   Stevens, K.N. and R. H. Bolt "On the Shielding of Noise Outdoors" paper presented at Forty-Seventh meeting of the Acoustical Society of America 23-26 June 1954

Page

vii   line (17) for wrapping   read wrappings

viii   line (6)   for temperatures   read temperature

viii   add Sec. 15 "Attenuation of Sound Within Piping"

xi   title Fig. 3.4   read $Q > 1$

xi   title Fig. 3.5   read $Q < 1$

xii   title Fig. 6.4   for of   read between

18   line (8)   for sound pressure read sound pressure level

20   line (5)   for result   read results

23   line (5) of text for median   read medians

29   line (7)   for .7%   read 0.8%

46   the remark made in connection with Fig. 2.9 is true
        only in the limit of low frequencies

63   line (22)   write to
                        National Noise Abatement Council
                        9 Rockefeller Plaza
                        New York, N. Y.

64   add   Noise Control
                        57 East 55th Street
                        New York 22, N. Y.

        A bi-monthly journal published by the
        Acoustical Society of America, directed to the
        reader with practical noise problems. In addi-
        tion to technical information, this magazine
        presents discussions of the legal aspects of
        noise control and pertinent news items concerning
        noise problems.

98   line (35)   read Fig. 4.1

Page

123   read Eq. (5.2a)

$$W = [5.70] \frac{S^3(T - T_a)^3}{T} [\frac{A}{286}] P$$

123   line (11)   for T_o read T_a

135   Caption Fig. 6.2   read $\nu L/U$

149   line (29) for centrifugal   read   axial-flow

257   line (4)   for $k_o t$ read $k_o t_1$

268   see Fig. 12.1.9 for a more complete figure,
        with all materials identified

279   lines (1) - (6) of text read:

        The action of the bend may be explained
        qualitatively by the statement that
        incoming sound waves travel across the bend
        to strike the absorbent lining, where a large
        portion of the energy may be absorbed. A
        smaller portion of the energy, reflected back
        toward the source, is partially absorbed upon
        again traversing the incoming duct section.

342   ref. (22) for Reference (10) read Reference (8)